Variations on PIGS: Non-standard approaches for imaginary-time path integrals

by

Dmitri Iouchtchenko

A thesis
presented to the University of Waterloo
in fulfilment of the
thesis requirement for the degree of
Master of Science
in
Chemistry

Waterloo, Ontario, Canada, 2015

© Dmitri Iouchtchenko 2015

I hereby declare that I am the sole author of this thesis. This is a true copy of the thesis, including any required final revisions, as accepted by my examiners.

I understand that my thesis may be made electronically available to the public.

Abstract

The second Rényi entropy has been used as a measure of entanglement in various model systems, including those on a lattice and in the continuum. The present work focuses on extending the existing ideas to measurement of entanglement in physically relevant systems, such as molecular clusters. We show that using the simple estimator with the regular Path Integral Ground State (PIGS) distribution is not effective, but a superior estimator exists so long as one has access to other configuration sectors. To this end, we implement the ability to explore different sectors in the Molecular Modelling Toolkit (MMTK) and use it to obtain the entanglement entropy for a test system of coupled harmonic oscillators.

The Semiclassical Initial Value Representation (SC-IVR) method for real-time dynamics using the Herman–Kluk propagator is known to be an effective semiclassical method. In the present work, we combine this approximate real-time propagator with exact and approximate ground state wavefunctions in order to find ground state survival amplitudes. The necessary integrals are first performed numerically on a grid (which is feasible for only low-dimensional systems) and then stochastically using MMTK (which has applicability to high-dimensional systems). The stochastic approach is used to compare two estimators, and it is again demonstrated that better results are obtained in a specialized configuration sector.

Acknowledgements

I am extremely grateful to Pierre-Nicholas Roy for being an excellent supervisor. The comments and suggestions from my committee, consisting of Marcel Nooijen and Roger Melko, have been a useful part of my learning process.

The Theoretical Chemistry group at the University of Waterloo is a superb group of people, and they have made my last two years nothing if not fun and rewarding.

The many discussions with Chris Herdman about the details of Path Integral Monte Carlo, entanglement entropy, and the coupled harmonic oscillator system have been very valuable.

I am ~~thankful~~ indebted to Shirley Wong for thoroughly proofreading this entire thesis.

Finally, this thesis would be impossible (or at least entirely different) without MMTK and its support for path integrals. Many thanks to Konrad Hinsen, Chris Ing, and Steve Constable!

Dear parents,

This is all your fault.

Thank you!

Contents

List of abbreviations **xiii**

List of figures **xv**

List of tables **xvii**

Summary of results **xix**

Notation **xxi**

1 Introduction **1**
- 1.1 Molecular clusters . . . 1
- 1.2 Path integral ground state . . . 2
- 1.3 Configuration space sectors . . . 5
- 1.4 Graphical notation . . . 6
- 1.5 Thesis outline . . . 7

2 Rényi entropy for particle entanglement **9**
- 2.1 Estimators . . . 11
- 2.2 Implementation details . . . 15
  - 2.2.1 Simulated link . . . 17
  - 2.2.2 Momentum distribution . . . 18
- 2.3 Model system . . . 21
  - 2.3.1 Primitive estimator . . . 21
  - 2.3.2 Minimal estimator . . . 28

3 Semiclassical IVR with PIGS **35**
- 3.1 Numerical integration . . . 38
  - 3.1.1 Harmonic oscillator . . . 43
  - 3.1.2 Double well . . . 43
- 3.2 Stochastic integration . . . 58
  - 3.2.1 Harmonic oscillator . . . 60

4 Conclusion **65**
- 4.1 Summary . . . 65
- 4.2 Future work . . . 65
  - 4.2.1 Entanglement entropy . . . 65
  - 4.2.2 Real-time correlation functions . . . 66

5 Bonus content **67**

5.1 Integration of radial distribution 67

  5.1.1 Spherical volume 67

  5.1.2 Periodic volume 72

5.2 PILE with odd P 78

A Useful formulas **81**

A.1 Momentum-position change of basis 81

A.2 Gaussian integrals 82

A.3 Simple recurrence relation 84

A.4 Roots of unity 85

A.5 Cosine series 86

A.6 Exponential derivative operator 86

B Discrete cosine transform **89**

B.1 DCT normalization in FFTW 89

B.2 DCT via FFT 90

C Coupled harmonic oscillators **93**

C.1 Exact ground state wavefunction 93

C.2 Exact Rényi entropy 95

C.3 Energy convergence studies 96

D Solutions to exercises **99**

E Custom software **117**

F Code listings **119**

References **123**

List of abbreviations

DCT	Discrete Cosine Transform
DFT	Discrete Fourier Transform
FFT	Fast Fourier Transform
FFTW	Fastest Fourier Transform in the West
HK	Herman–Kluk
LePIGS	Langevin equation Path Integral Ground State
MMTK	Molecular Modelling Toolkit
PIGS	Path Integral Ground State
PILE	Path Integral Langevin Equation
PIMC	Path Integral Monte Carlo
PIMD	Path Integral Molecular Dynamics
SC-IVR	Semiclassical Initial Value Representation

List of figures

1.1 Examples of paths used in path integral simulations 4
1.2 Examples of path diagrams 8

2.1 Example particle partition 11
2.2 Graphical notation for Rényi entropy 12
2.3 Untwisting of permuted paths 15
2.4 Broken path middle bead distribution 19
2.5 Broken path momentum distribution 22
2.6 Error convergence for primitive estimator 24
2.7 Friction optimization for primitive estimator 25
2.8 Distribution of traces for primitive estimator 26
2.9 Convergence of entropy with primitive estimator 27
2.10 Error convergence for minimal estimator 29
2.11 Friction optimization for minimal estimator 30
2.12 Distribution of components for minimal estimator 31
2.13 Convergence of entropy with minimal estimator 32
2.14 Results for minimal estimator 33

3.1 Example classical trajectories for harmonic oscillator 40
3.2 Example HK prefactors for harmonic oscillator 41
3.3 HK prefactors with incorrect square root branch 42
3.4 Harmonic oscillator survival amplitude convergence with position grids 44
3.5 Harmonic oscillator survival amplitude convergence with position grids *(continued)* 45
3.6 Harmonic oscillator survival amplitude divergence with momentum grid 46
3.7 Aliasing of integrand in momentum space 47
3.8 Harmonic oscillator survival amplitude with converged parameters 48
3.9 Harmonic oscillator survival amplitude with unconverged parameters 49
3.10 Double well survival amplitude convergence with position grids 50
3.11 Double well survival amplitude convergence with position grids *(continued)* 51
3.12 Double well survival amplitude with poor parameters 52
3.13 Double well survival amplitude with improved parameters 53
3.14 Time evolution of integrand for harmonic oscillator 54
3.15 Time evolution of integrand for harmonic oscillator *(continued)* 55
3.16 Time evolution of integrand for double well 56
3.17 Time evolution of integrand for double well *(continued)* 57
3.18 Graphical notation for survival amplitude 59
3.19 Harmonic oscillator survival amplitude with added Gaussian weight 61

3.20 Harmonic oscillator survival amplitude using primitive estimator 62
3.21 Harmonic oscillator survival amplitude using primitive estimator (exact sampling) 63
3.22 Harmonic oscillator survival amplitude using minimal estimator 64

5.1 Reduction of spherical volume problem 69
5.2 Representative spherical shells 74
5.3 Dimensionless piecewise Jacobian for integration in periodic boundary conditions . 77

C.1 Convergence of energy for coupled oscillators 97

D.1 PIGS normal mode frequency distribution 108

List of tables

1 Definitions of common symbols xxi

2.1 Selected parameters for coupled harmonic oscillators 23

3.1 Selected parameters for harmonic oscillator (numerical) 43
3.2 Selected parameters for double well (numerical) 46
3.3 Improved parameters for double well (numerical) 46
3.4 Selected parameters for harmonic oscillator (stochastic) 60

Summary of results

Harmonic oscillator momentum distribution . . . . fig. 2.5 on page 22
Convergence of Rényi entropy to within statistical error . . . . . . fig. 2.14a on page 33
Rényi entropy for various coupling strengths in model system . . . fig. 2.14b on page 33

Harmonic oscillator ground state survival amplitude (numerical) . . . fig. 3.8 on page 48
Double well ground state survival amplitude (numerical) . . . . fig. 3.13 on page 53
Harmonic oscillator ground state survival amplitude (stochastic) . . . fig. 3.22 on page 64

Effective Jacobian for integration in a spherical volume . . . . eq. (5.31) on page 71
Effective Jacobian for integration in a periodic volume . . . . eq. (5.61) on page 76
Normal mode transformation for PILE with odd P . . . . eq. (5.71) on page 79

Notation

In this work, symbols for scalars are italic (x), while symbols for vectors are bold ($\mathbf{x}$). A matrix denoted by $\underline{\mathbf{X}}$ has matrix elements $x_{i,j}$. Unless otherwise specified, vectors and matrices are zero-indexed (*i.e.* the first element of $\mathbf{x}$ is x_0). Operators are dressed in hats, whether they are scalar ($\hat{x}$) or vector ($\hat{\mathbf{x}}$) operators. The identity matrix and operator are $\underline{\mathbf{1}}$ and $\hat{1}$. Table 1 lists some of the more commonly used symbols.

Symbol	Definition
D	Number of spatial dimensions
N	Number of particles
P	Number of beads per particle
ℓ	Number of links per particle
F	Number of degrees of freedom
M	Index of middle bead
$\mathbf{p}$	Momentum vector
$\mathbf{q}$	Coordinate vector

Table 1: Definitions of common symbols used within this document.

To avoid ambiguity between indexing of particles and beads within a vector, we use the following notation whenever beads are involved:

- jth bead of ith particle: $\mathbf{x}_i^{(j)} = \begin{pmatrix} x_{i,0}^{(j)} & x_{i,1}^{(j)} & \cdots & x_{i,D-1}^{(j)} \end{pmatrix}$;
- jth bead of all particles: $\mathbf{x}^{(j)} = \begin{pmatrix} \mathbf{x}_0^{(j)} & \mathbf{x}_1^{(j)} & \cdots & \mathbf{x}_{N-1}^{(j)} \end{pmatrix}$;
- all beads of ith particle: $\mathbf{x}_i = \begin{pmatrix} \mathbf{x}_i^{(0)} & \mathbf{x}_i^{(1)} & \cdots & \mathbf{x}_i^{(P-1)} \end{pmatrix}$; and
- all beads of all particles: $\mathbf{x} = \begin{pmatrix} \mathbf{x}_0 & \mathbf{x}_1 & \cdots & \mathbf{x}_{N-1} \end{pmatrix} = \begin{pmatrix} \mathbf{x}^{(0)} & \mathbf{x}^{(1)} & \cdots & \mathbf{x}^{(P-1)} \end{pmatrix}$.

The bead notation is also borrowed for indexing normal modes, but there is no contention as the two are mutually exclusive. Additionally, the following labels are used to narrow the meaning of the above symbols:

- partition A: $\mathbf{x}_A$; and
- replica λ: $\mathbf{x}^{[\lambda]}$.

When these are in use, $\mathbf{x}$ may refer to all the degrees of freedom across all the replicas if this is obvious from context.

Unless otherwise specified, any integral without explicit limits of integration is a definite integral whose domain of integration is the entire space on which the variable of integration is defined. For example, if $\mathbf{q}$ is a three-dimensional position, then we implicitly have

$$\int \mathrm{d}\mathbf{q}\, f(\mathbf{q}) = \int\limits_{\text{all space}} \mathrm{d}\mathbf{q}\, f(\mathbf{q}) = \int_{-\infty}^{\infty} \mathrm{d}x \int_{-\infty}^{\infty} \mathrm{d}y \int_{-\infty}^{\infty} \mathrm{d}z\, f(x, y, z). \tag{1}$$

On occasion color is used in mathematical expressions to draw the eye to particularly important or subtle details, such as in

$$2 + 2 \neq 5. \tag{2}$$

This has no bearing on the meaning of the expressions. Regretfully, color is used in many of the plots and *is* important to their interpretation. Apologies to those with colorblindness or a monochrome copy of this work.

The graphical notation for expressions like 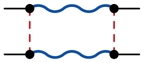 is described in detail in section 1.4 on page 6.

Values of some quantities may be given in kelvin or reciprocal kelvin, as in $\omega = 1\,\mathrm{K}$ or $\beta = 1\,\mathrm{K}^{-1}$. This is to be understood as a shorthand omitting the k_B and $\hbar$ necessary to have the appropriate dimension for the given quantity.

The imaginary unit is written as i, even though i is sometimes used as a variable (typically an index). It is always evident from context when i refers to the imaginary unit (as in $i/\hbar$) and when it refers to a variable (as in q_i). The real part of a complex number x is given by $\Re(x)$ and the imaginary part by $\Im(x)$.

Chapter 1

Introduction

1.1 Molecular clusters

It has now been nearly a century since the discovery of superfluidity in liquid helium, and over that time the phenomenon has been extensively studied both experimentally and theoretically [Bal07]. However, it is only much more recently that studies of low-temperature helium clusters, rather than of bulk helium, have been performed. While in bulk liquids one can directly observe manifestations of superfluidity (one only needs to search YouTube for "superfluid helium"), the microscopic nature of molecular clusters makes it more difficult to detect their superfluidity. After all, even asking whether a cluster is solid or liquid is itself not a well-defined question. These are states of bulk materials, which do not suffer from finite-size effects. Molecular clusters are instead described by the nebulous terms "solid-like" and "liquid-like" [CR08].

The Andronikashvili experiment from 1946 used an ingenious method to study the behaviour of superfluid helium [GTV98]. It involved placing a probe of rotating disks in a container of helium and observing its effective moment of inertia as the helium was cooled below its superfluid transition temperature. One would typically expect the moment of inertia to increase as a liquid is cooled, since greater viscosity should lead to greater drag. For superfluid helium, the opposite was the case: the moment of inertia decreased, meaning that there was less drag on the probe, an indication of superfluidity.

More recently, a microscopic version of the Andronikashvili experiment was performed, using small helium droplets with OCS acting as a molecular rotational probe [GTV98]. It was observed that the OCS IR spectrum had broad peaks when placed in pure ^{3}He droplets, but that the peaks became sharper with the addition of ^{4}He to the droplets, revealing rotational structure. These sharp peaks are an indication that the OCS probe is rotating nearly freely in the droplets containing sufficient amounts of ^{4}He. Thus, it turns out that finite-sized clusters may also exhibit superfluid effects and there is a way of quantifying these effects experimentally.

Although no bulk materials other than helium are currently known to act as superfluids, there is evidence that *para*-H_2 clusters can also display superfluidity [GST00]. These findings are confirmed by several recent theoretical studies [LLR10, RJL12, ZLR12, ZGC13]. Additionally, it has been suggested that some *para*-H_2 clusters have structure in their radial density and may be referred to as "supersolid" [SCK91].

Thus, ^{4}He and *para*-H$_2$ clusters are reasonably good test subjects for probing superfluidity and related properties. Although we do not simulate such clusters in the present work, they are the main motivation behind the methods which are implemented and tested. We hope to apply the presented theory and software to molecular clusters in the near future.

1.2 Path integral ground state

Quantum many-body problems are in general impossible to approach in a direct fashion [Tuc10, pp. 391-392]. This is due to the "curse of dimensionality," which implies that the memory and computational effort needed to perform a calculation scale exponentially with the number of degrees of freedom. For a cluster of only 16 point particles in 3 dimensions (48 degrees of freedom), a grid of just 2 points in each spatial direction (which is so small as to be utterly useless) would require on the order of terabytes to represent a single state vector. There are various tricks involving more sophisticated representations, which allow either the reduction of necessary degrees of freedom (by some clever choice of coordinates) or of the number of points used to represent each degree of freedom (by some clever choice of basis set), but these only offer a limited improvement to the problem. One of more effective ways to get around the curse is to use statistical methods, such as those based on the path integral formulation of quantum mechanics.

The Path Integral Ground State (PIGS) method is a variational method, involving the propagation of a trial function $|\psi_\mathrm{T}\rangle$ by the Boltzmann operator $e^{-\beta\hat{H}}$ to project out the ground state of a Hamiltonian $\hat{H}$ in the $\beta \to \infty$ limit [SSM00]. In the present work, we use only Hamiltonians for itinerant particles in Cartesian coordinates:

$$\hat{H} = \left[\sum_{n=0}^{N-1} \frac{|\hat{\mathbf{p}}_n|^2}{2m_n}\right] + V(\hat{\mathbf{q}}). \tag{1.1}$$

Exercise 1.1 PIGS limit

Consider a Hamiltonian $\hat{H}$ with a non-degenerate ground state $|0\rangle$: $\hat{H}\,|0\rangle = E_0\,|0\rangle$. Show that when $\langle\psi_\mathrm{T}|0\rangle \neq 0$,

$$|0\rangle \propto \lim_{\beta\to\infty} e^{-\beta\hat{H}}\,|\psi_\mathrm{T}\rangle\,. \tag{1.2}$$

Solution on page 99.

Our convention will be to propagate the trial function by $\beta/2$, giving the following (unnormalized) approximation to the ground state:

$$|0\rangle_\beta = e^{-\frac{\beta}{2}\hat{H}}\,|\psi_\mathrm{T}\rangle \approx |0\rangle\,. \tag{1.3}$$

The outer product of this with itself gives us an approximate ground state density operator

$$\hat{\varrho}_\beta = |0\rangle_\beta\langle 0|\,, \tag{1.4}$$

which approaches (up to normalization) the true ground state density operator $\hat{\varrho}$ as $\beta \to \infty$. From this, we get the approximate ground state pseudo partition function

$$Z_\beta = \mathrm{Tr}\, \hat{\varrho}_\beta = \langle \psi_\mathrm{T} | e^{-\beta \hat{H}} | \psi_\mathrm{T} \rangle \,. \tag{1.5}$$

Although the trace of a normalized density operator is trivially unity, Z_β is an arbitrary constant and we must be careful to explicitly normalize any expectation values:

$$\langle \hat{A} \rangle_{\hat{\varrho}_\beta} = \frac{\mathrm{Tr}\, \hat{\varrho}_\beta \hat{A}}{\mathrm{Tr}\, \hat{\varrho}_\beta}. \tag{1.6}$$

Exercise 1.2 PIGS classical isomorphism

Show that Z_β can be approximated arbitrarily well by the partition function of a classical system of open-chain polymers. Also show that this classical system can be used to find expectation values of quantum properties.

Hint: Chapter 12 of ref. [Tuc10] provides a detailed derivation for finite-temperature systems and the resulting cyclic polymers.

Solution on page 99.

Thanks to the isomorphism between quantum and classical statistical mechanics (originally introduced in ref. [CW81]), it is possible to side-step the dreaded “curse of dimensionality” and run purely classical simulations for quantum systems. The classical simulations consist of many copies of the quantum system coupled by harmonic springs, as depicted in fig. 1.1.

The family of methods that make use of this isomorphism is known as Path Integral Molecular Dynamics (PIMD) [Tuc10, pp. 471,479].‡ In order to use these methods to sample from the canonical distribution, one needs to have thermostatted equations of motion describing the evolution of the classical system. While this is in principle a solved problem (there are several well-known thermostat algorithms for simulating the canonical ensemble, such as Andersen and Nose–Hoover chains), many approaches suffer from issues including not sampling the correct ensemble and inefficient sampling [BP07, CPM10]. In order to avoid these issues, the Path Integral Langevin Equation (PILE) method makes use of a transformation to normal modes and a Langevin dynamics thermostat [CPM10].

Since the PILE is applicable only to finite-temperature quantum systems (which feature closed paths), it is necessary to modify it for the open paths of PIGS. This was done in ref. [CSI13], which introduced the Langevin equation Path Integral Ground State (LePIGS) method. This method is a variant of the PILE and offers a way to efficiently simulate classical systems of polymers corresponding to approximate PIGS ground states. Both the PILE and LePIGS are implemented in the Molecular Modelling Toolkit (MMTK) [Hin00].§ Since MMTK is the tool of choice in the present work, in an effort to be consistent with it (and in contrast with ref. [CPM10]), we use the conventions that the reciprocal temperature of the simulation is β and the fictitious masses are $m_n^\star = m_n/\ell$.

---

‡ As opposed to Path Integral Monte Carlo (PIMC) methods, which use rejection sampling to sample from the canonical distribution.

§ `http://dirac.cnrs-orleans.fr/MMTK/`

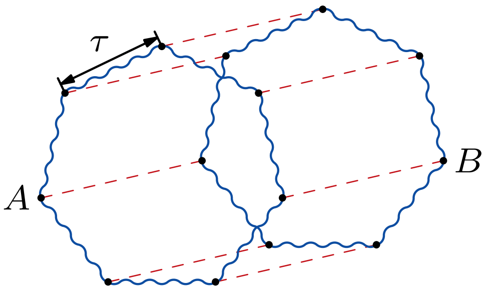

(a) Closed (cyclic) paths for a finite temperature PIMD simulation using the PILE.

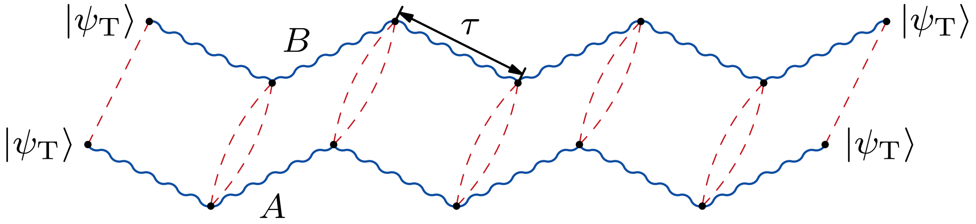
$|\psi_{\mathrm{T}}\rangle$
$|\psi_{\mathrm{T}}\rangle$
B
τ
$|\psi_{\mathrm{T}}\rangle$
$|\psi_{\mathrm{T}}\rangle$
A

(b) Open paths for a PIGS simulation using LePIGS. The $|\psi_{\mathrm{T}}\rangle$ signify the action of the trial function on the end beads.

Figure 1.1: Examples of paths used in path integral simulations with the PILE and LePIGS integrators. In both cases, there are two particles A and B made up of seven beads each. The beads interact via the "kinetic" springs (shown as blue wavy lines) and the scaled quantum potential (shown as red dashed lines). The segments labelled τ correspond to propagation in imaginary time by τ.

Exercise 1.3 PIGS normal mode transformation

Transform the PIGS "free particle" (*i.e.* $\hat{V} = 0$) classical polymers of eq. (D.22) to the normal mode representation of independent oscillators.

Solution on page 103.

Exercise 1.4 LePIGS algorithm

Using the Langevin dynamics equations of motion, derive the LePIGS algorithm.

Solution on page 109.

Using LePIGS, we are able to stochastically evaluate integrals of the form

$$\frac{\int \mathrm{d}\mathbf{q}\, \psi_{\mathrm{T}}(\mathbf{q}^{(0)}) \left[\prod_{j=0}^{P-2} \exp\left[-\frac{m}{2\hbar^2\tau}\left|\mathbf{q}^{(j)} - \mathbf{q}^{(j+1)}\right|^2 - \frac{\tau}{2}\left(V(\mathbf{q}^{(j)}) + V(\mathbf{q}^{(j+1)})\right)\right]\right] \psi_{\mathrm{T}}(\mathbf{q}^{(P-1)}) A(\mathbf{q})}{\int \mathrm{d}\mathbf{q}\, \psi_{\mathrm{T}}(\mathbf{q}^{(0)}) \left[\prod_{j=0}^{P-2} \exp\left[-\frac{m}{2\hbar^2\tau}\left|\mathbf{q}^{(j)} - \mathbf{q}^{(j+1)}\right|^2 - \frac{\tau}{2}\left(V(\mathbf{q}^{(j)}) + V(\mathbf{q}^{(j+1)})\right)\right]\right] \psi_{\mathrm{T}}(\mathbf{q}^{(P-1)})} \tag{1.7}$$

for any function $A(\mathbf{q})$. For ground state expectation values of operators that are diagonal in the position representation, this function depends only on the position of the middle beads. We may write eq. (1.7) in a more compact form as

$$\langle A \rangle = \frac{\int \mathrm{d}\mathbf{q}\, \pi(\mathbf{q}) A(\mathbf{q})}{\int \mathrm{d}\mathbf{q}\, \pi(\mathbf{q})}, \tag{1.8}$$

where $\pi(\mathbf{q})$ is the distribution and $A(\mathbf{q})$ is the estimator.

1.3 Configuration space sectors

The integrals in eq. (1.8) are over all space for each degree of freedom, so it may be tempting to call the space of all possible spatial configurations of the polymers the "configuration space," but we will find that this is too restrictive for our goals. In conventional PIMC and PIMD, the configuration space is restricted to such configurations (typically referred to as *diagonal* or Z), which are sufficient for physical quantities that are diagonal in the position representation [BPS06]. Inspired by the worm algorithm, we will embrace the notion of an extended configuration space, which is separated into disjoint *sectors* [BPS06, PST98]. The aforementioned Z configurations reside in the Z-sector.

A sector contains all the spatial configurations of a particular set of classical polymers, which is defined by the number of beads in the classical system as well as the way in which they are connected. For example, the addition of an additional polymer (or even of a single bead) implies the discrete transition to another sector. This sort of action is necessary for the sampling of a grand-canonical ensemble (for example to obtain chemical potentials) [HRD14], but will not be pursued in the present work. We will focus instead on the removal of elements from the sampling distribution. For example, consider the Z-sector distribution from eq. (1.8):

$$\pi(\mathbf{q}) = \psi_{\mathrm{T}}(\mathbf{q}^{(0)}) \left[\prod_{j=0}^{P-2} \exp\left[-\frac{m}{2\hbar^2\tau} \left| \mathbf{q}^{(j)} - \mathbf{q}^{(j+1)} \right|^2 - \frac{\tau}{2} \left(V(\mathbf{q}^{(j)}) + V(\mathbf{q}^{(j+1)}) \right) \right] \right] \psi_{\mathrm{T}}(\mathbf{q}^{(P-1)}). \tag{1.9}$$

We may choose to remove the link between beads $M-1$ and M (where $M = \ell/2$ is the index of the middle bead), which would lead to the following distribution in a different sector:

$$\begin{aligned} \pi(\mathbf{q}) = \psi_{\mathrm{T}}(\mathbf{q}^{(0)}) & \left[\prod_{j=0}^{\color{red}{M-2}} \exp\left[-\frac{m}{2\hbar^2\tau} \left| \mathbf{q}^{(j)} - \mathbf{q}^{(j+1)} \right|^2 - \frac{\tau}{2} \left(V(\mathbf{q}^{(j)}) + V(\mathbf{q}^{(j+1)}) \right) \right] \right] \\ \times & \left[\prod_{j=\color{red}{M}}^{P-2} \exp\left[-\frac{m}{2\hbar^2\tau} \left| \mathbf{q}^{(j)} - \mathbf{q}^{(j+1)} \right|^2 - \frac{\tau}{2} \left(V(\mathbf{q}^{(j)}) + V(\mathbf{q}^{(j+1)}) \right) \right] \right] \psi_{\mathrm{T}}(\mathbf{q}^{(P-1)}). \end{aligned} \tag{1.10}$$

Note that this removal involves both the "kinetic" spring potential between the beads and the corresponding halves of the quantum potential. We may perform a more surgical removal and only take out the spring, leading to another distribution in another sector:

$$\begin{aligned}\pi(\mathbf{q}) = \psi_{\mathrm{T}}(\mathbf{q}^{(0)}) &\left[\prod_{j=0}^{M-2} \exp\left[-\frac{m}{2\hbar^2\tau}\left|\mathbf{q}^{(j)} - \mathbf{q}^{(j+1)}\right|^2 - \frac{\tau}{2}\left(V(\mathbf{q}^{(j)}) + V(\mathbf{q}^{(j+1)})\right)\right]\right] \\ &\times \exp\left[-\frac{\tau}{2}\left(V(\mathbf{q}^{(M-1)}) + V(\mathbf{q}^{(M)})\right)\right] \\ &\times \left[\prod_{j=M}^{P-2} \exp\left[-\frac{m}{2\hbar^2\tau}\left|\mathbf{q}^{(j)} - \mathbf{q}^{(j+1)}\right|^2 - \frac{\tau}{2}\left(V(\mathbf{q}^{(j)}) + V(\mathbf{q}^{(j+1)})\right)\right]\right] \psi_{\mathrm{T}}(\mathbf{q}^{(P-1)}).\end{aligned} \tag{1.11}$$

An entire simulation may be done in a single sector (Z or otherwise), in which case the equations of motion may need to be tweaked, but it is still a straightforward simulation of *some* classical canonical ensemble. The more interesting case is when the sector is changed during the course of a simulation. This possibility is not considered in the present work, but it is necessary in order to implement the worm algorithm [BPS06], sampling of the grand-canonical ensemble [HRD14], and efficient sampling for particle entanglement [HIR14].

1.4 Graphical notation

> Admire the power of the Dirac notation!
>
> *Modern Quantum Mechanics*
> Jun John Sakurai

Like every useful notation, Dirac's kets (and their dual bras) form a powerful abstraction over the underlying machinery. In the case of the kets, not only is there less clutter for common activities, like taking inner products of elements of the Hilbert space,

$$\langle\varphi|\psi\rangle = \int \mathrm{d}x\, \varphi^*(x)\psi(x), \tag{1.12}$$

but there are conceptual advantages. Kets are not tied to any basis, allowing us to think in more abstract terms. They can also represent objects which cannot even exist in Hilbert space (such as the delta-function-normalized position basis states $|q\rangle$), and which would normally require the theory of distributions and a rigged Hilbert space to account for rigorously [De05].

However, even Dirac notation can become tedious and opaque if one accumulates sufficiently many bras and kets, as tends to happen with path integrals. If the bras, kets, and operators are further expanded, one obtains inscrutable expressions, such as those in eqs. (1.9) to (1.11). It is therefore beneficial to introduce a graphical notation for representing paths, especially when the goal is to manipulate and discuss the structure of the paths at the level of beads and springs.

The elements in which we're interested are the beads themselves, the "kinetic" spring links between them, and the interaction terms due to the quantum potential. The beads, being point particles, are naturally represented as points in a schematic drawing. The springs connect beads and can be represented as wavy curves between the points. The basic unit of interaction is half of a single term, since each link contributes half of the interactions on either side. Additionally, interactions may either involve multiple particles or a single particle; the former are referred to as N-*body* interactions and the latter are referred to as *central* or *trapping* interactions. In either case, we use dashed segments to represent such interactions.

The easiest way to understand this notation is to see a concrete example. Let us consider a system of two particles A and B, each of which experiences a central potential of some sort ($\hat{V}_A$ and $\hat{V}_B$). Additionally, they interact with a coupling potential ($\hat{V}_{AB}$). We shall encounter a model system like this very shortly. The distribution from eq. (1.9) for our simple system may be represented visually as in fig. 1.2a. The trial function is not displayed in the diagrams, as its presence (or absence) should be straightforward to describe in words.

Since we are often not interested in the central interactions, they may be omitted from the diagram, as in fig. 1.2b. So far these diagrams have not been particularly eventful, but we can start to see how they may be useful if we represent the distributions from eqs. (1.10) and (1.11), which are shown in figs. 1.2c and 1.2d. Despite the elision of many irrelevant beads (namely those between 1 and $M-1$ and those between $M+1$ and $P-2$), these diagrams still display information that is not relevant to what we are trying to show: how the paths are affected around beads $M-1$ and M. Of course, if we are careful to specify which beads we wish to focus on (in this case $M-1$ and M), we may disregard everything else, as in figs. 1.2e to 1.2g. In these diagrams, the tails on the left and right signify that we wish to refer to the rest of the paths as well. Sometimes we want to refer only to a particular segment of the path, in which case these tails are omitted, as in fig. 1.2h.

The reader may understandably be bored at this point, as there has not been anything so far resembling a "graphical notation," merely diagrams presented in a figure on a separate page. That is far from convenient and only marginally useful! However, these diagrams can be inserted in an intuitive way into mathematical statements:

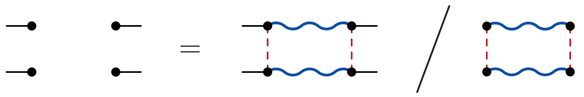

(1.13a)

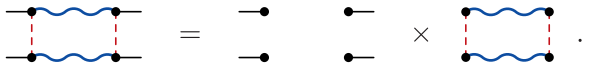

(1.13b)

These two equations show the removal (and reinsertion) of a full link.

1.5 Thesis outline

In the present work, we are concerned with two fundamental aspects of quantum mechanics: entanglement and time evolution. For the former, we look at the Rényi entropy as a measure of entanglement in quantum systems in chapter 2. Specifically, we implement a method for obtaining particle entanglement in molecular systems. For the latter, we investigate a novel approach to semiclassical IVR for real-time correlation functions in chapter 3. The novelty involves using stochastic sampling of ground state wavefunctions in order to find ground-state correlation functions. In chapter 4, we summarize the results and provide a brief outlook on future work. Finally, chapter 5 contains some miscellaneous results that are not directly related to the rest of the thesis.

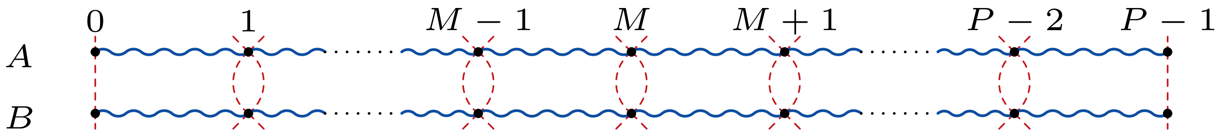

(a) Two interacting quantum particles depicted as classical polymers (paths) composed of P beads, showing the springs (blue, wavy) and potentials (red, dashed) connecting the beads. The end beads experience only half of the regular potential, but they also feel a potential due to the trial function, which is not displayed here. The letters along the left are the particle labels and the numbers along the top are the bead indices. Most beads have been elided, as indicated by the $\cdots$, implying that their presence would add nothing of interest to the diagram.

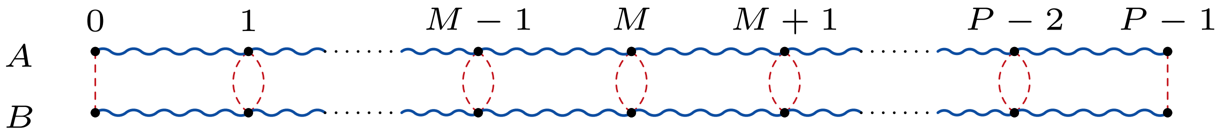

(b) The same situation as in **(a)**, but with the central potentials omitted, resulting in a cleaner diagram.

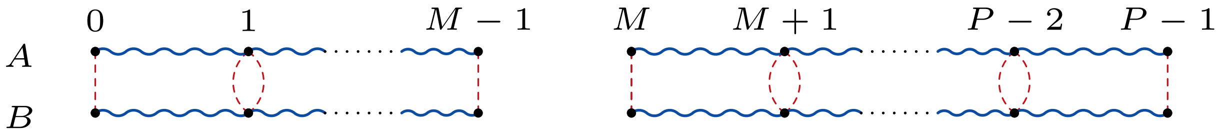

(c) A similar situation to the one in **(b)**, but without the link between beads $M-1$ and M.

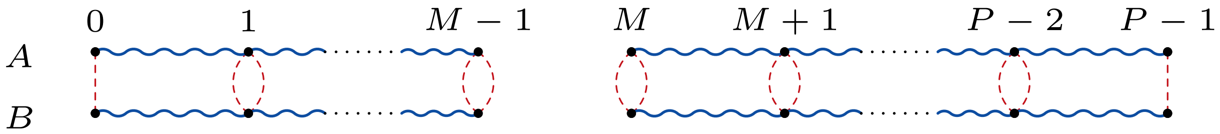

(d) A similar situation to the one in **(b)**, but without the kinetic springs between beads $M-1$ and M.

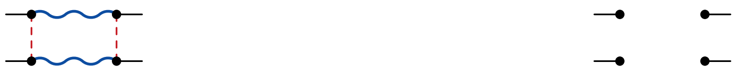

(e) A more compact version of **(b)**, focused on the link between $M-1$ and M.

(f) A more compact version of **(c)**, focused on the link between $M-1$ and M.

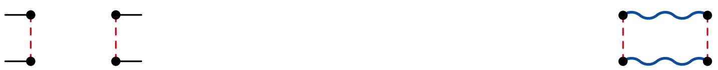

(g) A more compact version of **(d)**, focused on the link between $M-1$ and M.

(h) The missing link from **(c)** and **(f)**, showing only beads $M-1$ and M.

Figure 1.2: Examples of path diagrams, showing the distillation of the compact graphical notation.

Chapter 2

Rényi entropy for particle entanglement

Entropy is a well-known fundamental concept in both thermodynamics and information theory. In the former, it appears as the Gibbs entropy, [McQ76, p. 48]

$$S_{\mathrm{G}} = -k_{\mathrm{B}} \sum_n p_n \log p_n, \tag{2.1}$$

and in the latter as the Shannon entropy, [Sha48]

$$S_{\mathrm{S}} = -\sum_n p_n \log p_n. \tag{2.2}$$

In both cases, the sum is over all possible states, and p_n is the probability of being in a given state, whether it is a microstate of the system or an output symbol on a channel. Found in quantum mechanics as a connection between the two is the von Neumann entropy, [Wil13, p. 253]

$$S_{\mathrm{vN}} = -\operatorname{Tr} \hat{\varrho} \log \hat{\varrho}. \tag{2.3}$$

In a basis which diagonalizes $\hat{\varrho}$, we find

$$S_{\mathrm{vN}} = -\sum_n \varrho_n \log \varrho_n, \tag{2.4}$$

which is exactly analogous to the above entropies, since the interpretation of the diagonal elements of the density matrix is the probability of being in the corresponding basis states [Wil13, p. 102]. The von Neumann entropy provides a measure of the *purity* of a state: how *pure* or *mixed* the state is. This makes intuitive sense: it assigns a number to the uncertainty about which pure state one actually holds if one only has a mixed state description of it [Wil13, p. 254]. Any pure state naturally has zero entropy, while maximally-mixed states have the largest possible entropy for systems of that Hilbert space dimension [Wil13, p. 255].

Some quantum states may be written as tensor products of other states:

$$|\psi_{AB}\rangle = |\psi_A\rangle \otimes |\psi_B\rangle \tag{2.5a}$$
$$\hat{\varrho}_{AB} = \hat{\varrho}_A \otimes \hat{\varrho}_B. \tag{2.5b}$$

Here A and B describe some disjoint sets of degrees of freedom of the system, and it is possible to perform the trace over one set to produce exactly the state for the subsystem containing the remaining degrees of freedom:

$$\mathrm{Tr}_B\, \hat{\varrho}_{AB} = \mathrm{Tr}_B\left(\hat{\varrho}_A \otimes \hat{\varrho}_B\right) = \mathrm{Tr}_B\, \hat{\varrho}_A \otimes \mathrm{Tr}_B\, \hat{\varrho}_B = \hat{\varrho}_A. \tag{2.6}$$

Such states are known as *product states*. Importantly, not all states have this property. Those which are not product states are called *entangled* and they cannot be written in the form of eq. (2.5) [Wil13, p. 83].[‡] Unlike for product states, for entangled states,

$$\hat{\varrho}_{AB} \neq \mathrm{Tr}_B\left(\hat{\varrho}_{AB}\right) \otimes \mathrm{Tr}_A\left(\hat{\varrho}_{AB}\right). \tag{2.7}$$

The best-known entangled states are the four so-called "Bell states" involving the eigenstates $|0\rangle$ and $|1\rangle$ of a two-level system [Wil13, p. 88]. One of the Bell states is provided here as a simple example:[§]

$$|\Psi^-\rangle = \frac{1}{\sqrt{2}}\left(|0\rangle_A |1\rangle_B - |1\rangle_A |0\rangle_B\right) = \frac{1}{\sqrt{2}}\left(|01\rangle - |10\rangle\right). \tag{2.8}$$

This state has the density matrix (in the $\{|00\rangle, |01\rangle, |10\rangle, |11\rangle\}$ basis)

$$\varrho_{AB} = \frac{1}{2}\begin{pmatrix} 0 & 0 & 0 & 0 \\ 0 & 1 & -1 & 0 \\ 0 & -1 & 1 & 0 \\ 0 & 0 & 0 & 0 \end{pmatrix}. \tag{2.9}$$

In this example, taking the trace over B results in the *reduced state*

$$\hat{\varrho}_A = \mathrm{Tr}_B\, \hat{\varrho}_{AB} = \frac{1}{2}\left(|0\rangle\langle 0| + |1\rangle\langle 1|\right), \tag{2.10}$$

which is the maximally mixed two-level state. That is, we learn absolutely nothing about the part of the state in A if we ignore the information we have about the part of the state in B. Additionally, even though we started with a pure state, which can be written as a sum of kets, the result is a mixed state, which cannot.

Since the von Neumann entropy can be used as a measure of the "mixedness" of a state, we can use the von Neumann entropy of the reduced state as a measure of the entanglement of the original state [Sch95, VPR97]. For example, since the von Neumann entropy of pure states is zero, and the partial trace of a pure product state results in a pure state, the von Neumann entanglement entropy of any pure product state is zero. On the other hand, the von Neumann entropy of the state in eq. (2.10) is

$$S_{\mathrm{vN}}(\hat{\varrho}_A) = -\left(\frac{1}{2}\log\frac{1}{2} + \frac{1}{2}\log\frac{1}{2}\right) = \log 2, \tag{2.11}$$

which is the maximum possible von Neumann entropy for a two-level state [Wil13, p. 255].

[‡] In the case of mixed states, there is the third category of *separable states* [Wil13, p. 114], but these are not relevant for the present work.

[§] We omit the "⊗" symbol when the tensor product operation is implied by adjacent kets.

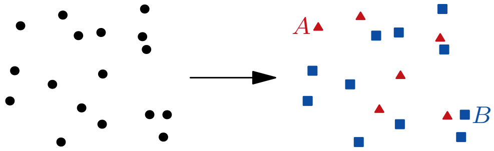

Figure 2.1: Example particle partition used to investigate the particle entanglement between A and B.

While the above discussion is focused on a pair of two-level systems, the ideas are general and apply to any system with at least two degrees of freedom. In the case of an N-body system, we may partition the set of N particles into disjoint subsets of N_A and N_B particles, as in fig. 2.1. We refer to this as a *particle partition* and the quantity in question will be *particle entanglement*; other possibilities, such as partitioning space, will not be considered in the present work. If our description of the system is in Cartesian coordinates $\mathbf{q}$, we may split these into $\mathbf{q}_A$ and $\mathbf{q}_B$, where the former contains the coordinates for the particles in A and the latter for the particles in B. Our density matrix[‡] can then be written as $\varrho(\mathbf{q}_A, \mathbf{q}_B; \mathbf{q}'_A, \mathbf{q}'_B)$ and we may perform the partial trace as

$$\varrho_A(\mathbf{q}_A; \mathbf{q}'_A) = \int \mathrm{d}\mathbf{q}_B \, \varrho(\mathbf{q}_A, \mathbf{q}_B; \mathbf{q}'_A, \mathbf{q}_B). \tag{2.12}$$

Thus, we have (at least in principle) a prescription for finding the von Neumann entropy for particle entanglement of any N-body system.[§] We just need to have access to the density matrix of the state of interest, but quantum mechanics rarely yields to such demands. Thus, we must search for another method of measuring the entanglement of a state. Conveniently, there is a generalization of the Shannon and von Neumann entropies, named the *Rényi entropy* [HIR14, Ren61]:

$$S_\alpha = \frac{1}{1-\alpha} \log \left(\mathrm{Tr}\, \hat{\varrho}_A^\alpha \right) \tag{2.13}$$

for $\alpha \geq 0$. It is a generalization in the sense that $S_\alpha \to S_{\mathrm{vN}}$ as $\alpha \to 1$ and was originally obtained by Rényi by relaxing the subadditivty requirement of Shannon (that the joint entropy must not exceed the sum of the individual entropies) [Sha48, Ren61]. As we will see shortly, this measure of entropy can be used with existing methods of quantum statistical mechanics (as described in chapter 1) to get around the need to obtain $\hat{\varrho}$ explicitly.

2.1 Estimators

Although there are infinitely many Rényi entropies S_α, in the present work we are only interested in the *second Rényi entropy*

$$S_2 = -\log \left(\mathrm{Tr}\, \hat{\varrho}_A^2 \right), \tag{2.14}$$

and the associated quantity $\mathrm{Tr}\, \hat{\varrho}_A^2$ to which we shall refer simply as *the trace*. This particular measure of entropy has been used for studying entanglement of lattice systems [HGK10, SMP12]

[‡] It is not strictly a matrix, since we are in the continuous position basis, but we can't be blamed for listening to Dirac in ref. [Dir81, pp. 69-70]!

[§] Since we are usually interested in systems of *indistinguishable* particles, we must also be careful to preserve permutation symmetry when identical particles are split between A and B.

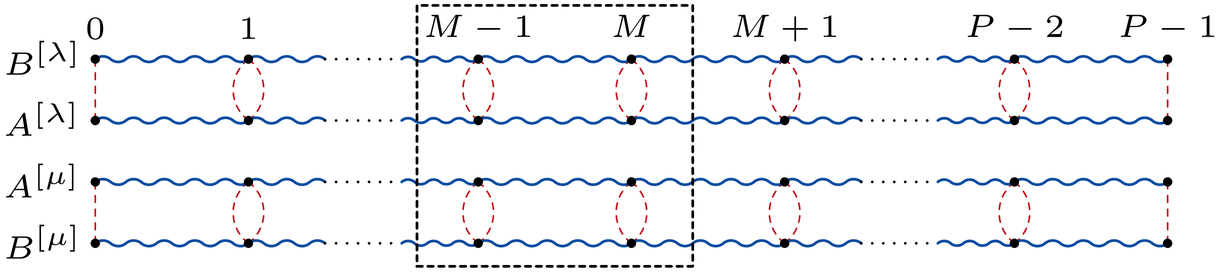

Figure 2.2: Details of the graphical notation used for the Rényi entropy. Dashed box indicates the region of interest. Note that we have grouped all paths for a single partition (A or B) into a single effective path for the diagram. As a consequence, the potential interactions *within* a partition are not displayed (which is fine, because they are not relevant). Additionally, for system λ the path for partition B appears at the top.

and more recently in the continuum [HIR14, HRM14]. To demonstrate why it is appealing in practice, we will make use of the *replica trick*, which involves multiple copies of the system [HGK10]. We start with the exact ground state density operator

$$\hat{\varrho} = |0\rangle\langle 0| \tag{2.15}$$

and perform a partial trace over the degrees of freedom in partition B,[‡] leaving us with the reduced density operator for partition A

$$\hat{\varrho}_A = \operatorname{Tr}_B \hat{\varrho}. \tag{2.16}$$

If we square and trace this, we obtain the trace from eq. (2.14). We may perform these operations explicitly in the position representation:

$$\varrho(\mathbf{q}_A, \mathbf{q}_B; \mathbf{q}'_A, \mathbf{q}'_B) = \langle \mathbf{q}_A \mathbf{q}_B | 0\rangle \, \langle 0 | \mathbf{q}'_A \mathbf{q}'_B \rangle \tag{2.17a}$$

$$\varrho_A(\mathbf{q}_A; \mathbf{q}'_A) = \int \mathrm{d}\mathbf{q}_B \; \langle \mathbf{q}_A \mathbf{q}_B | 0\rangle \, \langle 0 | \mathbf{q}'_A \mathbf{q}_B \rangle \tag{2.17b}$$

$$\varrho_A^2(\mathbf{q}_A; \mathbf{q}''_A) = \iiint \mathrm{d}\mathbf{q}'_A \, \mathrm{d}\mathbf{q}_B \, \mathrm{d}\mathbf{q}'_B \; \langle \mathbf{q}_A \mathbf{q}_B | 0\rangle \, \langle 0 | \mathbf{q}'_A \mathbf{q}_B \rangle \, \langle \mathbf{q}'_A \mathbf{q}'_B | 0\rangle \, \langle 0 | \mathbf{q}''_A \mathbf{q}'_B \rangle \tag{2.17c}$$

$$\operatorname{Tr} \hat{\varrho}_A^2 = \iiiint \mathrm{d}\mathbf{q}_A \, \mathrm{d}\mathbf{q}'_A \, \mathrm{d}\mathbf{q}_B \, \mathrm{d}\mathbf{q}'_B \; \langle \mathbf{q}_A \mathbf{q}_B | 0\rangle \, \langle 0 | \mathbf{q}'_A \mathbf{q}_B \rangle \, \langle \mathbf{q}'_A \mathbf{q}'_B | 0\rangle \, \langle 0 | \mathbf{q}_A \mathbf{q}'_B \rangle \tag{2.17d}$$

$$= \iiiint \mathrm{d}\mathbf{q}_A^{[\lambda]} \, \mathrm{d}\mathbf{q}_B^{[\lambda]} \, \mathrm{d}\mathbf{q}_A^{[\mu]} \, \mathrm{d}\mathbf{q}_B^{[\mu]} \; \langle 0 | \mathbf{q}_A^{[\mu]} \mathbf{q}_B^{[\lambda]} \rangle \, \langle \mathbf{q}_A^{[\lambda]} \mathbf{q}_B^{[\lambda]} | 0\rangle \, \langle 0 | \mathbf{q}_A^{[\lambda]} \mathbf{q}_B^{[\mu]} \rangle \, \langle \mathbf{q}_A^{[\mu]} \mathbf{q}_B^{[\mu]} | 0\rangle \, . \tag{2.17e}$$

The final step is nothing more than a reordering and relabelling of the various pieces.[§] If we replace the exact ground state $|0\rangle$ by the approximate PIGS ground state $|0\rangle_\beta$ and expand it into beads and links (see chapter 1 for details), eq. (2.17e) resembles integrals over two paths, but with some of the indices permuted.

Before we really dig into the expression for the trace, let us first consider a simpler one:

$$Z^2 = \iiiint \mathrm{d}\mathbf{q}_A^{[\lambda]} \, \mathrm{d}\mathbf{q}_B^{[\lambda]} \, \mathrm{d}\mathbf{q}_A^{[\mu]} \, \mathrm{d}\mathbf{q}_B^{[\mu]} \; {}_\beta\langle 0 | \mathbf{q}_A^{[\lambda]} \mathbf{q}_B^{[\lambda]} \rangle \, \langle \mathbf{q}_A^{[\lambda]} \mathbf{q}_B^{[\lambda]} | 0\rangle_\beta \, {}_\beta\langle 0 | \mathbf{q}_A^{[\mu]} \mathbf{q}_B^{[\mu]} \rangle \, \langle \mathbf{q}_A^{[\mu]} \mathbf{q}_B^{[\mu]} | 0\rangle_\beta \, . \tag{2.18}$$

[‡] Technically, one partitions a set into subsets, but we will be sloppy with our terminology and refer to the subsets as "partitions" themselves.

[§] We introduce extra noise into our expressions with the $\mathbf{q}^{[x]}$ labels, but they allow us to talk about the replicas using reasonable names instead of "unprimed" and "primed."

Here we have taken paths for two independent replicas of the system (λ and μ), multiplied them together, and integrated over all the positions. We can write this using the graphical notation as

$$Z^2 = \int \mathrm{d}\mathbf{q}$$

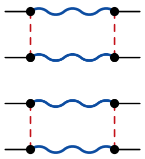

$$. \qquad (2.19)$$

The particulars of the graphical notation in this chapter are outlined in fig. 2.2. What is important to notice here is that, as the diagram alludes, the integrals are obviously separable. On the other hand, we may express the trace from eq. (2.17e) as

$$\mathrm{Tr}\,\hat{\varrho}_A^2 \propto \int \mathrm{d}\mathbf{q}$$

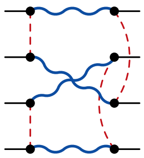

$$, \qquad (2.20)$$

and it is clear that we cannot view this as a product of integrals. We have been careful to claim that these quantities are not equal, but only proportional. This is because when we substitute $|0\rangle_\beta$ for $|0\rangle$ we must take into account the normalization, which amounts to $1/Z^2$, leading to the ratio

$$\mathrm{Tr}\,\hat{\varrho}_A^2 = \int \mathrm{d}\mathbf{q}$$

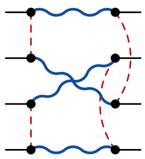

$$\Big/ \int \mathrm{d}\mathbf{q}$$

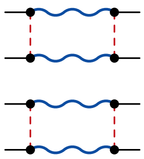

$$. \qquad (2.21)$$

As the astute reader has noticed, this is equivalent in form to eq. (1.8) on page 5, with the distribution composed of two replicas of the system, and the estimator function

$$\mathcal{N}_\mathrm{P} =$$

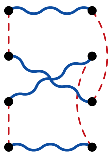

$$\Big/$$

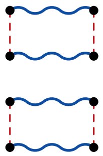

$$=$$

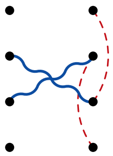

$$\Big/$$

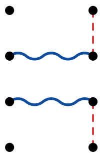

$$. \qquad (2.22)$$

We will refer to $\mathcal{N}_\mathrm{P}$ as the *primitive estimator of the trace*. Now that the brunt of the work has been done, we may write the result down using conventional notation:

$$\begin{aligned}\mathcal{N}_\mathrm{P} = \exp&\left[-\sum_{i\in A}\frac{m_i}{2\hbar^2\tau}\left(\left|\mathbf{q}_i^{(M-1)[\lambda]} - \mathbf{q}_i^{(M)[\mu]}\right|^2 + \left|\mathbf{q}_i^{(M-1)[\mu]} - \mathbf{q}_i^{(M)[\lambda]}\right|^2\right)\right] \\ \times \exp&\left[+\sum_{i\in A}\frac{m_i}{2\hbar^2\tau}\left(\left|\mathbf{q}_i^{(M-1)[\lambda]} - \mathbf{q}_i^{(M)[\lambda]}\right|^2 + \left|\mathbf{q}_i^{(M-1)[\mu]} - \mathbf{q}_i^{(M)[\mu]}\right|^2\right)\right] \\ \times \exp&\left[-\frac{\tau}{2}\left(V_{AB}(\mathbf{q}_A^{(M)[\lambda]}, \mathbf{q}_B^{(M)[\mu]}) + V_{AB}(\mathbf{q}_A^{(M)[\mu]}, \mathbf{q}_B^{(M)[\lambda]})\right)\right] \\ \times \exp&\left[+\frac{\tau}{2}\left(V_{AB}(\mathbf{q}_A^{(M)[\lambda]}, \mathbf{q}_B^{(M)[\lambda]}) + V_{AB}(\mathbf{q}_A^{(M)[\mu]}, \mathbf{q}_B^{(M)[\mu]})\right)\right],\end{aligned} \qquad (2.23)$$

where $V_{AB}(\mathbf{q}_A, \mathbf{q}_B)$ is the sum of all potentials that act on particles in *both* partitions.[‡] Thus, if we can sample path configurations for the two-replica system, all we need to do is average the estimator over those configurations to obtain an estimate of the trace, from which we may obtain S_2.

We can generalize this approach by making the observation that

$$\langle \mathcal{N} \rangle_\pi = \frac{\int \mathrm{d}\mathbf{q}\, \pi(\mathbf{q}) \mathcal{N}(\mathbf{q})}{\int \mathrm{d}\mathbf{q}\, \pi(\mathbf{q})} = \frac{\int \mathrm{d}\mathbf{q}\, \pi'(\mathbf{q}) \mathcal{N}'(\mathbf{q})}{\int \mathrm{d}\mathbf{q}\, \pi'(\mathbf{q}) \mathcal{D}'(\mathbf{q})} = \frac{\int \mathrm{d}\mathbf{q}\, \pi'(\mathbf{q}) \mathcal{N}'(\mathbf{q})}{\int \mathrm{d}\mathbf{q}\, \pi'(\mathbf{q})} \frac{\int \mathrm{d}\mathbf{q}\, \pi'(\mathbf{q})}{\int \mathrm{d}\mathbf{q}\, \pi'(\mathbf{q}) \mathcal{D}'(\mathbf{q})} = \frac{\langle \mathcal{N}' \rangle_{\pi'}}{\langle \mathcal{D}' \rangle_{\pi'}} \tag{2.24}$$

for a suitably chosen distribution $\pi'(\mathbf{q})$ and estimators $\mathcal{N}'(\mathbf{q})$ and $\mathcal{D}'(\mathbf{q})$. Obviously, we may choose anything whatsoever for $\pi'(\mathbf{q})$ and offload the details onto the estimators by dividing out the unnecessary bits and multiplying in the required ones, but most arbitrary distributions would not be very sensible. One natural approach is to choose a distribution which requires nothing to be divided out, and only the minimal amount to be multiplied in. In our case, this results in the distribution

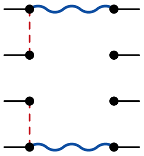

(2.25)

and the estimators

$\mathcal{N}_\mathrm{M} =$ 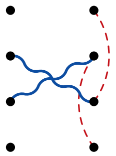 $\mathcal{D}_\mathrm{M} =$ 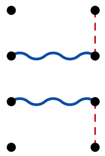 . (2.26)

We will refer to the ratio estimator $\langle \mathcal{N}_\mathrm{M} \rangle / \langle \mathcal{D}_\mathrm{M} \rangle$ as the *minimal estimator of the trace*. As we might expect from eq. (2.24),

$$\mathcal{N}_\mathrm{P} = \frac{\mathcal{N}_\mathrm{M}}{\mathcal{D}_\mathrm{M}}. \tag{2.27}$$

It seems that there is inherent asymmetry in reconnecting the paths on the "left" side (*i.e.* between beads $M-1$ and M), and that it would be better to use an even number of beads so that there is a middle link. However, if we allow ourselves the use of perspective in our diagrams, we can show that this is not necessary. In fig. 2.3a, we see that the paths corresponding to eq. (2.20) cross on one side when drawn in the usual way. However, in fig. 2.3b, we see the same paths without any asymmetry between the left and right sides. When viewed in this way, it instead seems that the middle bead is special, but none of the links are privileged.

[‡] When the system has only pairwise interactions, this is straightforward: if an interaction affects one particle in A and one in B, it should be included. In the general case, where interactions may include more than two particles, the requirement may become more clear if inverted: $V_{AB}(\mathbf{q}_A, \mathbf{q}_B)$ is the sum of all potentials that are *not* restricted to particles in only one partition.

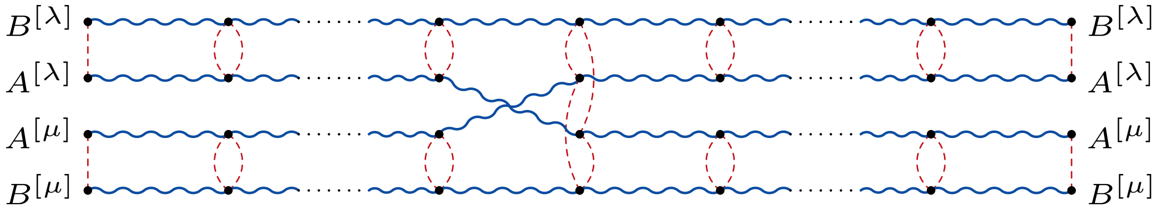

(a) Twisted permuted paths.

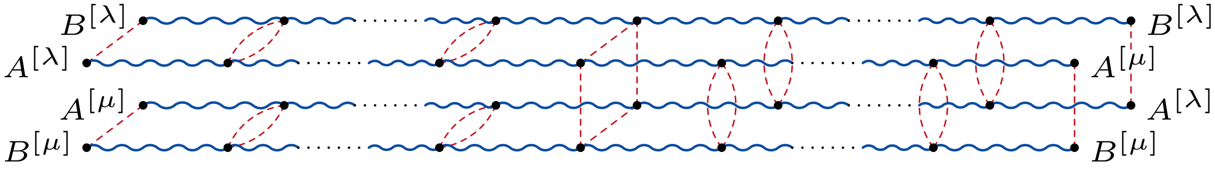

(b) Untwisted permuted paths.

Figure 2.3: Untwisting of permuted paths for the trace. The symmetry that is plainly visible in **(b)** is not evident in **(a)**.

2.2 Implementation details

Our tool of choice in the present work is MMTK, which contains an implementation of LePIGS.[‡] Prior to this work, the implementation was implicitly targeted at Z-sector simulations. However, in order to use the minimal estimator of the trace, we are required to sample from a different sector. This required ensuring that the LePIGS algorithm works outside the Z-sector and making the appropriate changes to MMTK.

The three distinct parts of the LePIGS procedure are:

- propagate free particles in normal modes;
- apply force fields to Cartesian momenta; and
- thermostat normal modes.

Implicit in these is the conversion between Cartesian coordinates and normal modes. The conversion itself works for paths of any length and is independent of the force fields, so it is not problematic.

The same is true for the free particle propagation: once we have converted the coordinates to normal modes, the equations of motion are the same for all paths. The only subtleties involved have to do with masses and frequencies, but these are simple to deal with. The effective masses of the normal modes are the same as those of the beads ($m_n^\star$), so we do not need to do anything to them even if we change sectors. The frequencies ω_k depend on τ (the "length" of each link) and P (the number of beads in the path). The former is unchanged between the sectors we are considering, but the latter is a property of the paths that is now allowed to change.

Application of the force fields is similarly straightforward: some of the forces may be scaled or missing entirely, so the changes to the momenta will be modified accordingly.

Thermostatting of the normal modes is potentially tricky, due to the appearance of β, which starts out as the imaginary-time propagation length in the derivation. Since some of the paths may change length, it may be tempting to adjust the value of β for each path to account for the varying length. However, that would be incorrect, because the β which appears in the thermostat is related to the temperature of the simulation and is a global property. Indeed, it is the same β which appears in the exponent of eq. (D.23) on page 103, and it is not affected by anything we might do to the connectivity of paths or scaling of potentials inside H_{cl}.

[‡] As of this writing, the implementation in question has not been pushed upstream to `https://bitbucket.org/khinsen/mmtk`. There are plans to rectify this in the near future.

Thus, to implement transitions to the sectors of interest, there were three requirements which had to be satisfied by MMTK:

- it must be possible to scale the force fields arbitrarily;
- the integrator must deal with paths, rather than particles; and
- there must be a convenient mechanism for changing the force field scaling and path connectivity.

In order for the force fields to be scalable, it was necessary to add the function pointer field `scale_func` to the `PyFFEnergyTermObject` struct. This function takes the new scaling value and is responsible for updating the force field to effect the change. To declare that it has support for this mechanism, a force field must override `supportsDynamicScaling` to return `True`. Pure Python force fields, which do not have direct access to the fields of `PyFFEnergyTermObject`, should implement a `setScaling` method; it is assigned automatically in the `PyEnergyTerm` Cython class from which all pure Python force field terms inherit. The built-in restraint force fields, such as `HarmonicDistanceRestraint`, were modified to support this scaling; these modifications involve scaling the energy, gradients, and force constants by the required amount.

In order for the integrator to deal with paths explicitly (rather than with particles, which only map to paths exactly in the Z-sector), it was necessary to make some subtle changes. When calculating ω_ℓ (see eq. (D.16) on page 102) in `propagateOscillators`, `springEnergyNormalModes`, and `applyThermostat`, it would no longer be correct to determine τ as β/ℓ (since the effective β of each path would change with ℓ, while τ remains constant), so a particular value of τ is assigned to each path, and this value does not change even as the paths are broken and recombined. On the other hand, it was important *not* to change the β which appears in the random force component of `applyThermostat`, as this has to do with the "physical" temperature of the simulation, not the length of the path.

To keep track of the connectivity of the paths, the global array `connectivity` was introduced, alongside the existing `bead_data`. This array consists of three columns and as many rows as there are beads in the simulation; the beads of a single path are stored in contiguous rows of the array. Each of the three columns stores a different kind of information about the beads:

0. the index of the bead in the universe, which acts as a pointer into the existing data structures;
1. the positive length of the path (used as a sentinel to signal the first bead of a path) *or* the negative offset to the beginning of the path; and
2. a flag indicating whether the path is closed (as in finite temperature simulations) or open (as in ground state simulations).

Two additional consequences of this new array were the ability to combine the finite temperature and ground state integrators, reducing code duplication, and the ability to open and close paths during a simulation. This connectivity data may be written to the output trajectory file and analyzed later. The ability to view the connectivity as it changed during a simulation was added to the `tviewer` application which is included with MMTK.

In order to abstract away the above details for the end user, the Cython class `PIReconnector` was provided. If a class inheriting from `PIReconnector` is given to the path integral integrator, its `step` method is called at the end of each integrator step, allowing the user to manipulate the simulation. For convenience, the following methods are provided in `PIReconnector`:

- `getScaling(self, Py_ssize_t t)` to get the scaling of a force field term;
- `setScaling(self, Py_ssize_t t, double x)` to set the scaling of a force field term;
- `openPath(self, Py_ssize_t p)` to open a closed path (*i.e.* cyclic to linear);
- `closePath(self, Py_ssize_t p)` to close an open path (*i.e.* linear to cyclic);
- `breakPath(self, Py_ssize_t p)` to break a single path into two paths; and
- `joinPaths(self, Py_ssize_t p1, Py_ssize_t p2)` to join two paths into a single path.

The four methods for operating on paths allow the user to achieve any connectivity with the restriction that a single bead may be connected via no more than two links. Additionally, because one can manipulate the connectivity during the simulation, it is possible to perform the sort of updates discussed in ref. [HIR14] which are necessary to preserve permutation symmetry with broken paths. Although the idea is not pursued in the present work, the above methods in principle also allow for sampling of the grand canonical ensemble via the worm algorithm: previously "hidden" beads may be added to the simulation from a reservoir by joining them to a path and turning on their force field terms.

2.2.1 Simulated link

One simple test for the implementation of broken paths is to break an open PIGS path into two parts and add a force field between the new free ends that simulates the removed link. This should allow us to sample from an identical ensemble, so the distribution of all bead positions (including the middle bead) should be unchanged. Since we know what the middle bead distribution should be for a harmonic oscillator, we perform this test for a single particle in a harmonic trap and compare to the exact distribution.

The Hamiltonian of the one-dimensional harmonic oscillator with mass m and angular frequency ω is

$$\hat{H} = \frac{\hat{p}^2}{2m} + \frac{1}{2} m\omega^2 \hat{q}^2, \tag{2.28}$$

so its ground state wavefunction is [Mes99, pp. 440-441,492]

$$\psi_0(q) = \left(\frac{m\omega}{\pi\hbar}\right)^{\frac{1}{4}} e^{-\frac{m\omega}{2\hbar} q^2} \tag{2.29}$$

and the corresponding diagonal density is

$$\varrho(q) = \left|\psi_0(q)\right|^2 = \left(\frac{m\omega}{\pi\hbar}\right)^{\frac{1}{2}} e^{-\frac{m\omega}{\hbar} q^2}. \tag{2.30}$$

This is what we expect to see for the middle bead distribution when we have converged in both the $\beta \to \infty$ and $\tau \to 0$ limits. We will remove the link from bead $M-1$ to bead M (where M, as usual, is the index of the middle bead), which corresponds to dividing

$$\exp\left[-\frac{m}{2\hbar^2\tau}\left(q^{(M-1)} - q^{(M)}\right)^2\right] \tag{2.31}$$

out of the distribution. In order to reinsert this in the form of a force field, we use the same approach as for trial functions in ref. [SCI14]. The potential $V(\mathbf{q})$ for a force field enters the distribution as

$$e^{-\tau V(\mathbf{q})}, \tag{2.32}$$

so the potential we require is the harmonic distance restraint

$$V(q^{(M-1)}, q^{(M)}) = \frac{m}{2\hbar^2\tau^2}\left(q^{(M-1)} - q^{(M)}\right)^2. \tag{2.33}$$

We choose the mass m to be that of a single electron and the angular frequency to be $\omega = 1\,\mathrm{K}$. With the parameters $\beta = 8\,\mathrm{K}^{-1}$, $\ell = 256$, $\tau = 3.125 \times 10^{-2}\,\mathrm{K}^{-1}$, $\Delta t = 0.1\,\mathrm{ps}$, $\gamma^{(0)} = 0.1\,\mathrm{ps}^{-1}$, and 10^6 steps, we get the distribution in fig. 2.4a when we sample regularly. If we remove the link, we instead get the distribution in fig. 2.4b, which, as expected, does not match the "exact" value. The actual test is, of course, to simulate the link using an explicit harmonic distance restraint, as in fig. 2.4c, where we see that the distribution is restored.

2.2.2 Momentum distribution

Another way to check that the implementation works correctly is to look at the harmonic oscillator momentum distribution. We will consider the same system as in section 2.2.1, but we will actually use the broken path to our advantage. The momentum distribution, like the position distribution in eq. (2.30), is the square of the magnitude of the wavefunction, but in the momentum representation. The momentum representation of a wavefunction may be obtained by the Fourier transform of the position representation [Cep95], so we obtain (by eq. (A.17) on page 83)

$$\psi_0(p) = \frac{1}{\sqrt{2\pi\hbar}}\int \mathrm{d}q\, e^{-\frac{i}{\hbar}pq}\psi_0(q) = \left(\frac{m\omega}{4\pi^3\hbar^3}\right)^{\frac{1}{4}}\int \mathrm{d}q\, e^{-\frac{m\omega}{2\hbar}q^2 - \frac{i}{\hbar}pq} = \left(\frac{1}{\pi\hbar m\omega}\right)^{\frac{1}{4}} e^{-\frac{1}{2\hbar m\omega}p^2} \tag{2.34a}$$

$$\varrho(p) = \left|\psi_0(p)\right|^2 = \left(\frac{1}{\pi\hbar m\omega}\right)^{\frac{1}{2}} e^{-\frac{1}{\hbar m\omega}p^2}. \tag{2.34b}$$

Both of the densities so far described are *diagonal* and may be expressed in terms of the more general *off-diagonal* densities

$$\varrho(q) = \varrho(q;q) = \langle q|\hat{\varrho}|q\rangle \tag{2.35a}$$

$$\varrho(p) = \varrho(p;p) = \langle p|\hat{\varrho}|p\rangle. \tag{2.35b}$$

The translation operator [Mes99, p. 651]

$$\hat{T}(x) = \exp\left[-\frac{i}{\hbar}x\hat{p}\right] \tag{2.36}$$

has the action [Mes99, p. 650]

$$\hat{T}(x)\,|q\rangle = |q+x\rangle, \tag{2.37}$$

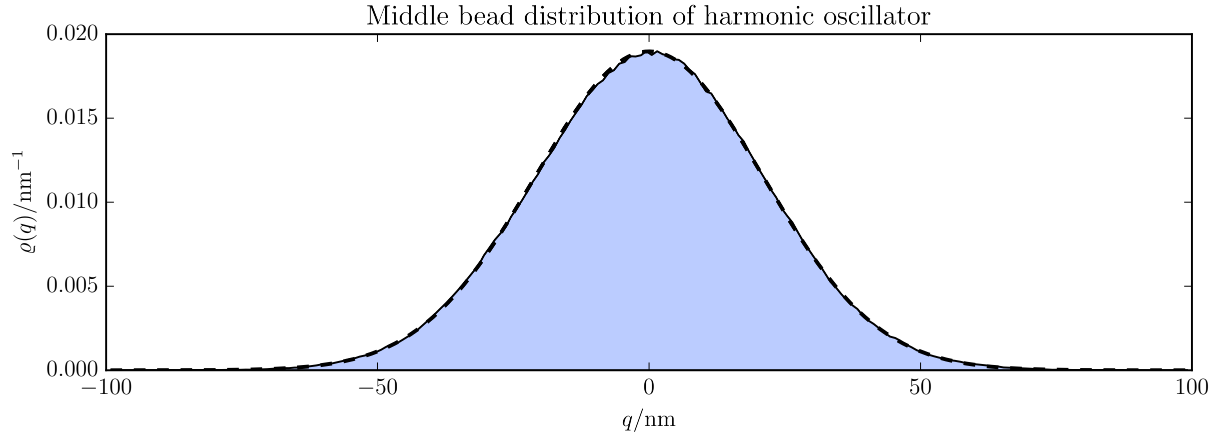

(a) Sampling a regular PIGS path in a harmonic trapping potential.

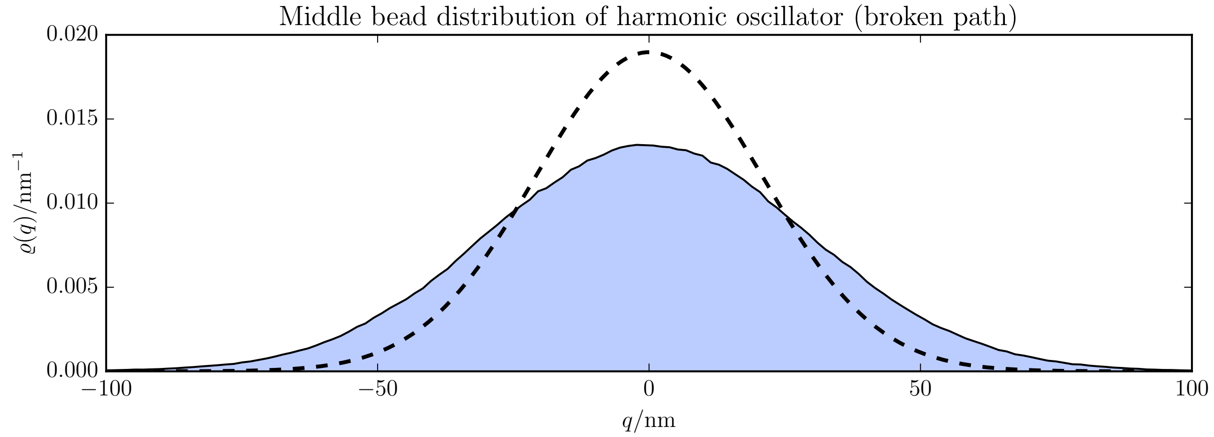

(b) Sampling a broken PIGS path in a harmonic trapping potential. The break is between the middle bead (whose distribution is displayed) and an adjacent bead.

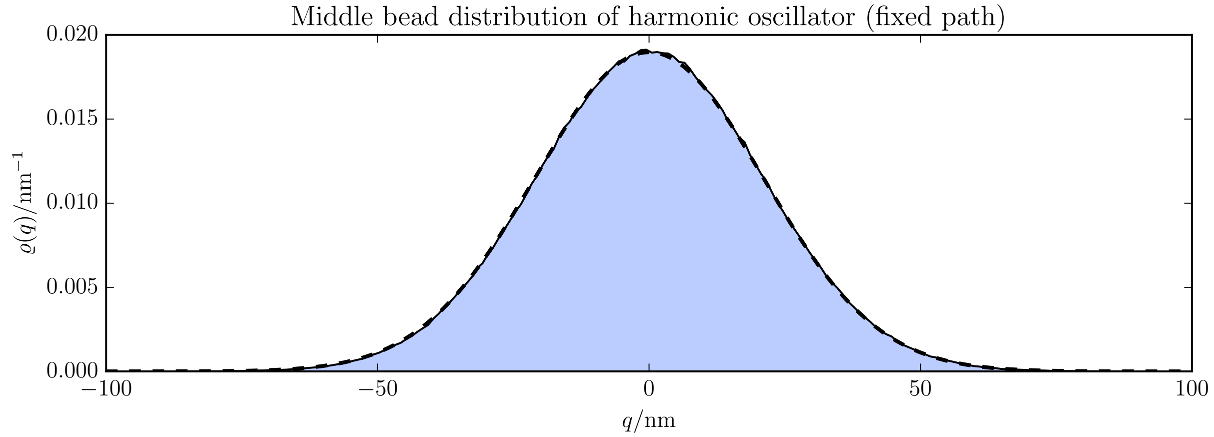

(c) Sampling a fixed PIGS path in a harmonic trapping potential. The break in the path is filled with an explicit harmonic distance restraint.

Figure 2.4: Middle bead distribution of a harmonic oscillator in various path configurations. Dashed curves are the exact harmonic oscillator ground state density.

where $|q\rangle$ is a position state ket and $\hat{p}$ is the momentum operator along the same direction as q. Applying the Fourier transform to the momentum distribution, since the trace is independent of basis, we find

$$\begin{aligned}
\mathcal{F}[\varrho(p)](\delta q) &= \frac{1}{\sqrt{2\pi\hbar}} \int \mathrm{d}p \, \exp\left[-\frac{i}{\hbar}p(\delta q)\right] \varrho(p) && \text{(2.38a)} \\
&= \frac{1}{\sqrt{2\pi\hbar}} \int \mathrm{d}p \, \langle p|\hat{\varrho}\hat{T}(\delta q)|p\rangle && \text{(2.38b)} \\
&= \frac{1}{\sqrt{2\pi\hbar}} \operatorname{Tr}\left[\hat{\varrho}\hat{T}(\delta q)\right] && \text{(2.38c)} \\
&= \frac{1}{\sqrt{2\pi\hbar}} \int \mathrm{d}q \, \langle q|\hat{\varrho}\hat{T}(\delta q)|q\rangle && \text{(2.38d)} \\
&= \frac{1}{\sqrt{2\pi\hbar}} \int \mathrm{d}q \, \varrho(q, q+\delta q). && \text{(2.38e)}
\end{aligned}$$

We define the quantity

$$\varrho(\delta q) = \int \mathrm{d}q \, \varrho(q, q+\delta q), \tag{2.39}$$

which is dimensionless, unlike the densities we have seen so far, and normalized so that $\varrho(\delta q = 0) = 1$. For a harmonic oscillator, it is given by

$$\varrho(\delta q) = \left(\frac{1}{\pi\hbar m\omega}\right)^{\frac{1}{2}} \int \mathrm{d}p \, e^{-\frac{1}{\hbar m\omega}p^2 - \frac{i}{\hbar}p(\delta q)} = e^{-\frac{m\omega}{4}(\delta q)^2}. \tag{2.40}$$

It is clear that we may recover the momentum distribution from this quantity via the inverse Fourier transform:

$$\varrho(p) = \frac{1}{\sqrt{2\pi\hbar}} \mathcal{F}^{-1}[\varrho(\delta q)](p). \tag{2.41}$$

In order to figure out how to estimate $\varrho(\delta q)$, we write it in the more suggestive form

$$\varrho(\delta q) = \int \mathrm{d}q \, \langle 0|q+\delta q\rangle \langle q|0\rangle \,. \tag{2.42}$$

If we were to expand each ground state $|0\rangle$ into half of a PIGS path, we would see that the halves only meet in the $\delta q = 0$ case. Indeed, we may write this as

$\varrho(\delta q) = \int \mathrm{d}q$ 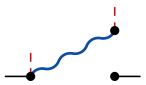 $\Big/ \int \mathrm{d}q$ 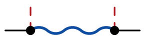 . (2.43)

We have been careful to include the central potential in the diagrams, as it is important for this problem. The separation between the "real" and "virtual" beads at M is, of course, δq:

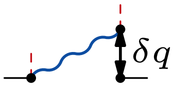

. (2.44)

We may therefore estimate $\varrho(\delta q)$ by sampling from the broken distribution

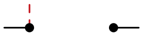

(2.45)

and using the ratio estimator

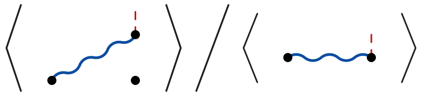

, (2.46)

thereby testing the broken path implementation in MMTK. Note that unlike the estimators we've encountered so far, which have not depended on any parameters, this estimator is a function of δq.

For the simulation, we used the same parameters as in section 2.2.1, with the exception that configurations are sampled every 1 ps rather than every 0.1 ps. The results for $\varrho(\delta q)$ and $\varrho(p)$ for the harmonic oscillator system are shown in fig. 2.5. While the raw estimator output differs slightly from the expected curve, the Fourier transform provides a sufficient amount of smoothing that the obtained momentum distribution is indistinguishable from the expected one.

2.3 Model system

As our benchmark system for calculating the Rényi entropy, we use what is arguably the simplest non-trivial system for which particle entanglement can be defined: two harmonically-coupled harmonic oscillators. This system is described in detail (including analytic solutions) in appendix C on page 93. We consider the one-dimensional variant of the problem, with the Hamiltonian

$$\hat{H} = \frac{\hat{p}_A^2}{2m} + \frac{\hat{p}_B^2}{2m} + \frac{1}{2} m\omega_0^2(\hat{q}_A^2 + \hat{q}_B^2) + \frac{1}{2} m\omega_{\text{int}}^2(\hat{q}_A - \hat{q}_B)^2. \tag{2.47}$$

We choose the parameters $m = m_\text{e}$ (mass of an electron) and $\omega_0 = 1\,\text{K}$; we vary the coupling strength ω_int in order to vary the entanglement of the system. These parameters are chosen specifically so that we can replicate the results of ref. [HIR14] using a molecular dynamics approach (instead of using Monte Carlo). This system lends itself to a natural particle partitioning: one partition containing solely particle A and the other B.

We must optimize the usual parameters for this system: β, τ, Δt, and $\gamma^{(0)}$. In order to be able to use a smaller value for β (and therefore fewer beads, leading to shorter simulation times), we use a trial function that is very similar to the exact ground state. Specifically, we use eq. (C.13) on page 94, but we scale the mass down to $m/2$, making it closer to a uniform trial function. This trial function is also used for the energy convergence study in appendix C.3 on page 96. Unless otherwise specified, the parameter values from table 2.1 are used for this model system.

2.3.1 Primitive estimator

Because we expect the two estimators introduced in section 2.1 to behave differently, we perform separate convergence studies. We first look at the primitive estimator, defined in eq. (2.22) on page 13, which requires us to use the regular sampling distribution. This estimator is a ratio of two

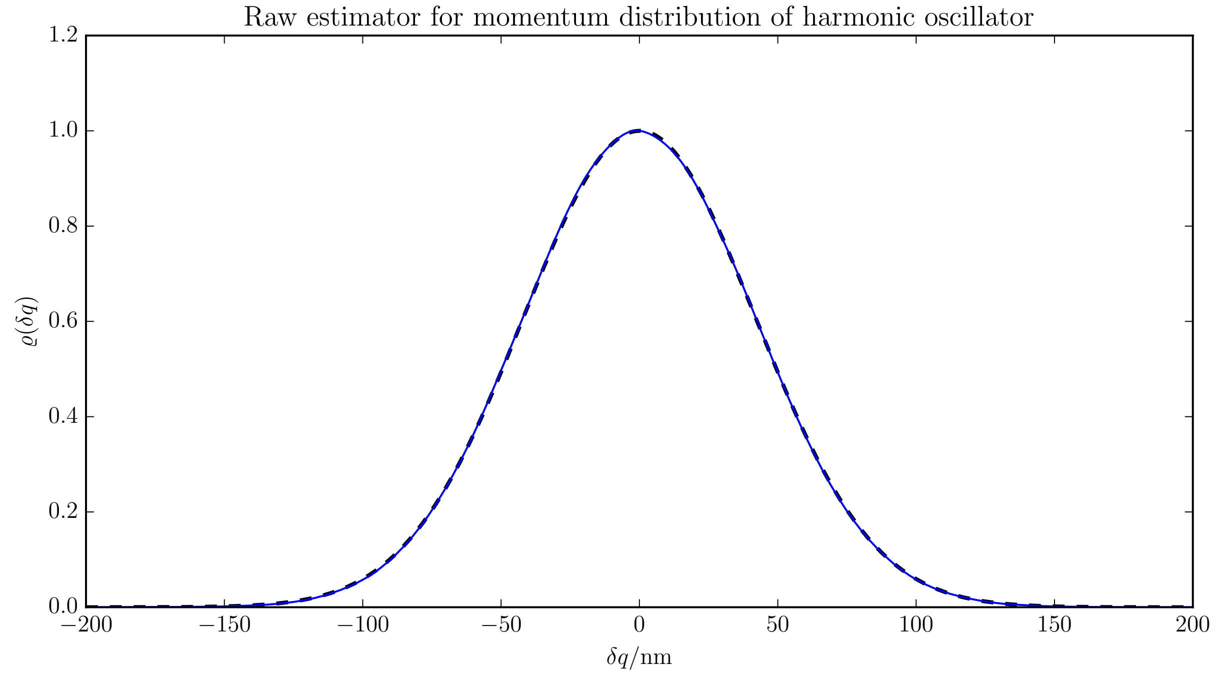

(a) The quantity from eq. (2.39) for a harmonic oscillator.

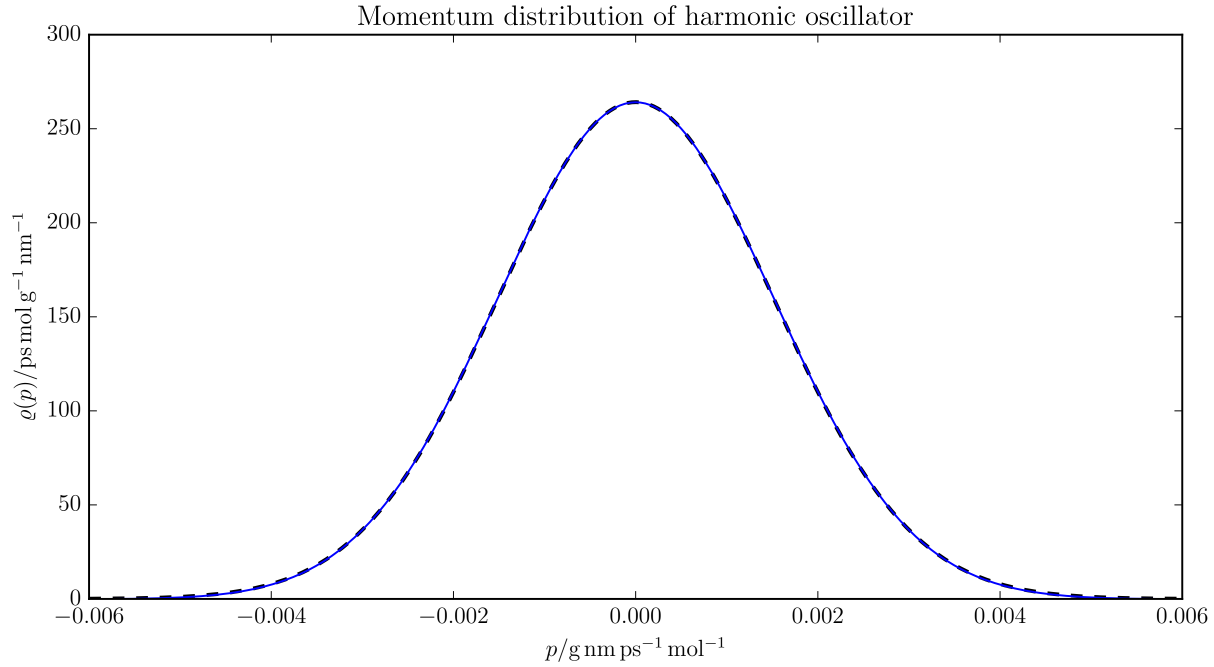

(b) Momentum distribution of a harmonic oscillator, obtained as the Fourier transform of the function in **(a)**.

Figure 2.5: Momentum distribution of a harmonic oscillator (including the unprocessed estimator results). Dashed curves are exact harmonic oscillator results.

$\omega_{\text{int}}/\omega_0$	β/K^{-1}	τ/K^{-1}	P	$\Delta t/\text{ps}$	$\gamma^{(0)}/\text{ps}^{-1}$
0	3.0	0.25	13	0.5	0.1
1	3.5	0.125	29	0.5	0.1
2	4.0	0.1	41	0.25	0.1
4	4.5	0.05	91	0.2	0.1
8	5.0	0.025	201	0.1	0.1

Table 2.1: Selected parameters for the model system of coupled harmonic oscillators.

quantities, both of which become exponentially small with decreasing τ. This makes it challenging to sample well and is at odds with the need to decrease τ to minimize the error due to the Trotter factorization. Consequently, the results are not good, but are provided for comparison with the minimal estimator.

We start our optimization with the friction. Since the goal when optimizing friction is to increase the efficiency of sampling, this should be reflected by a smaller standard error of the mean. To estimate the error, we use the binning analysis described in ref. [AT10] for frictions spanning several orders of magnitude. To get a feel for the effects of friction on the error, we look at fig. 2.6. All the curves in both plots plateau, which gives the illusion that the simulations are long enough for the error to converge. However, even though the two plots were generated using simulations with the same parameters, they are drastically different.

We might hope for a more useful landscape if we look from a different perspective, as in fig. 2.7, but almost no insights are to be had from these plots either. We may make one minor observation: in fig. 2.7a, we see that the curves for large τ (few beads, not yet converged) are better behaved than the others. Those curves are not useful, but they do foreshadow the poor behaviour we expect to see when we try to converge the entropy by decreasing τ. This is confirmed in fig. 2.7b, where the curve corresponding to the system with no coupling is the only one that looks reasonable, and it happens to be the one with the largest τ value.

Undeterred, we choose an arbitrary friction of $0.1\,\text{ps}^{-1}$ and press on. At this point, it would be nice to see an example of how the values we sample are distributed. This is shown in fig. 2.8, and the distribution doesn't look good: there are sporadic large values, which are difficult to sample.

The curious reader may very well want to know what happens if we use this estimator to estimate the second Rényi entropy. As expected, the results are not particularly impressive. There is not much to be gained by examining figs. 2.9a and 2.9c, but fig. 2.9b holds some explanations for us. We can see that there is no hope of converging with β or Δt, because we cannot choose a τ that is sufficiently small. When we try to do so, we tend to underestimate the trace, leading us to overestimate the entropy. Having seen the distribution, we should not be surprised by the small error bars on points that are too high: in those cases, we underestimate the trace by not sampling enough of the large outliers, so we don't even realize that we've underestimated it.

The reader should not be discouraged at this point, as the primitive estimator at small τ is expected to behave poorly. It is difficult to expect anything reasonable from a distribution such as that in fig. 2.8, where the spread of values spans many orders of magnitude.

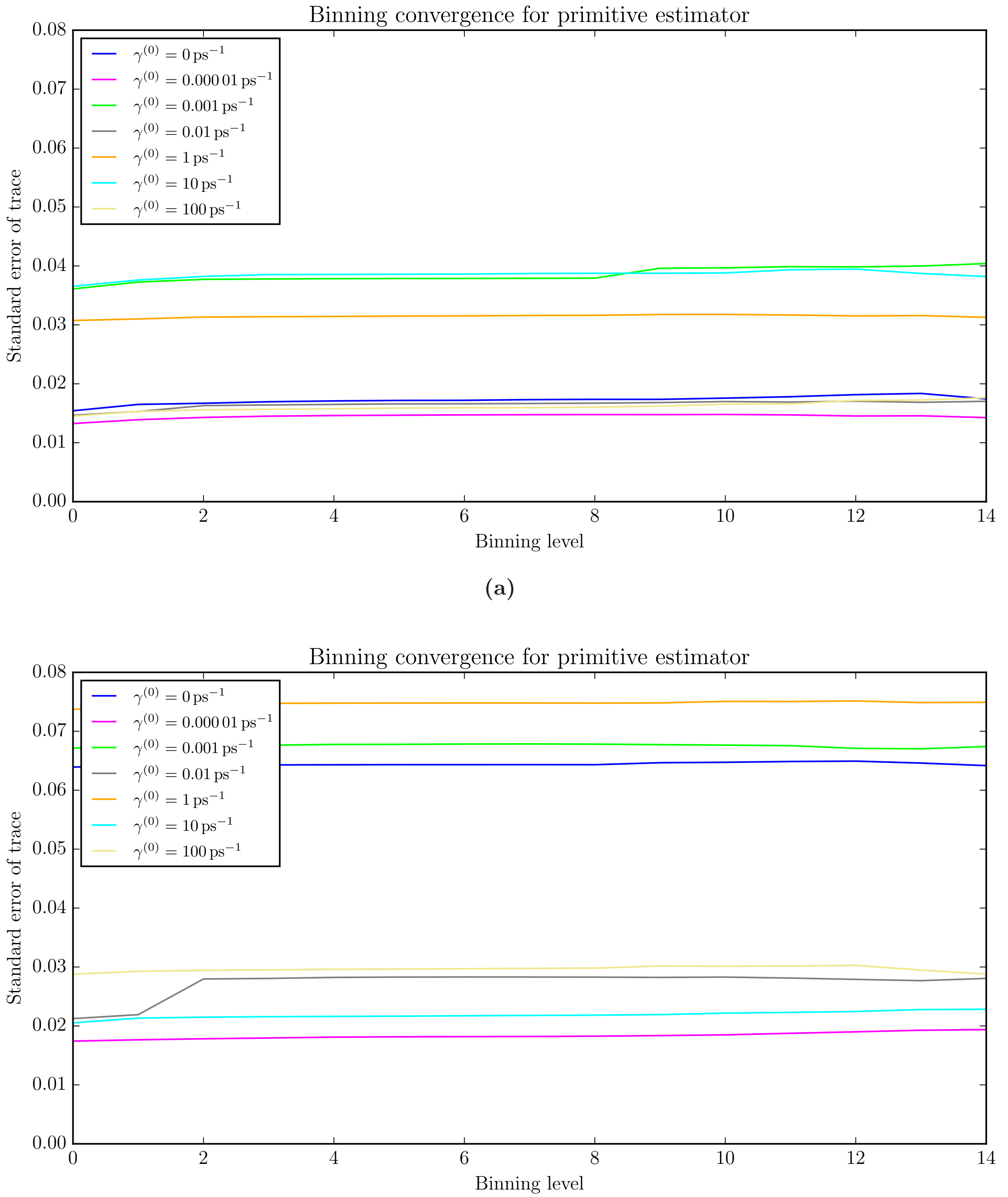

(a)

(b)

Figure 2.6: Convergence of error with binning level for different frictions using the primitive estimator. $\omega_{\mathrm{int}} = 4\,\mathrm{K}$, 10^6 steps. The two plots show results from different simulations using identical parameters.

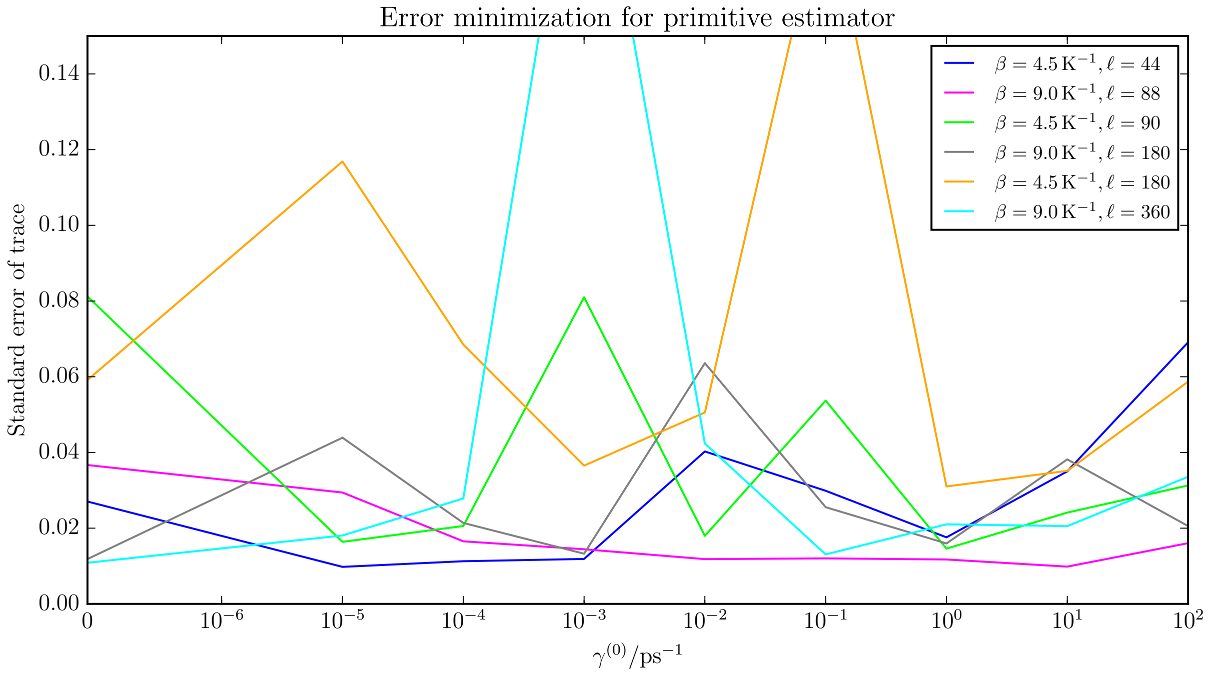

(a) Minimization of error with friction for different values of β and ℓ. $\omega_{\text{int}} = 4\,\mathrm{K}$.

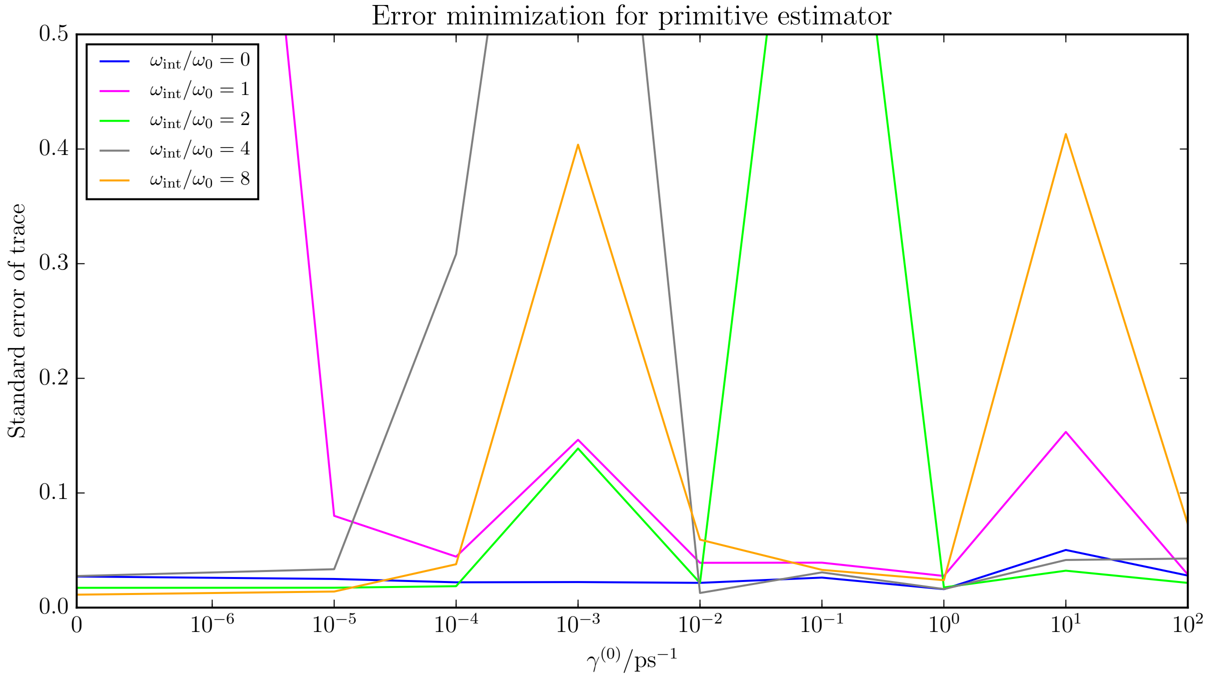

(b) Minimization of error with friction for different values of ω_{int}.

Figure 2.7: Friction optimization for the primitive estimator with different parameter sets. 10^6 steps. Some of the large magnitude values have been cut off to emphasize the smaller values.

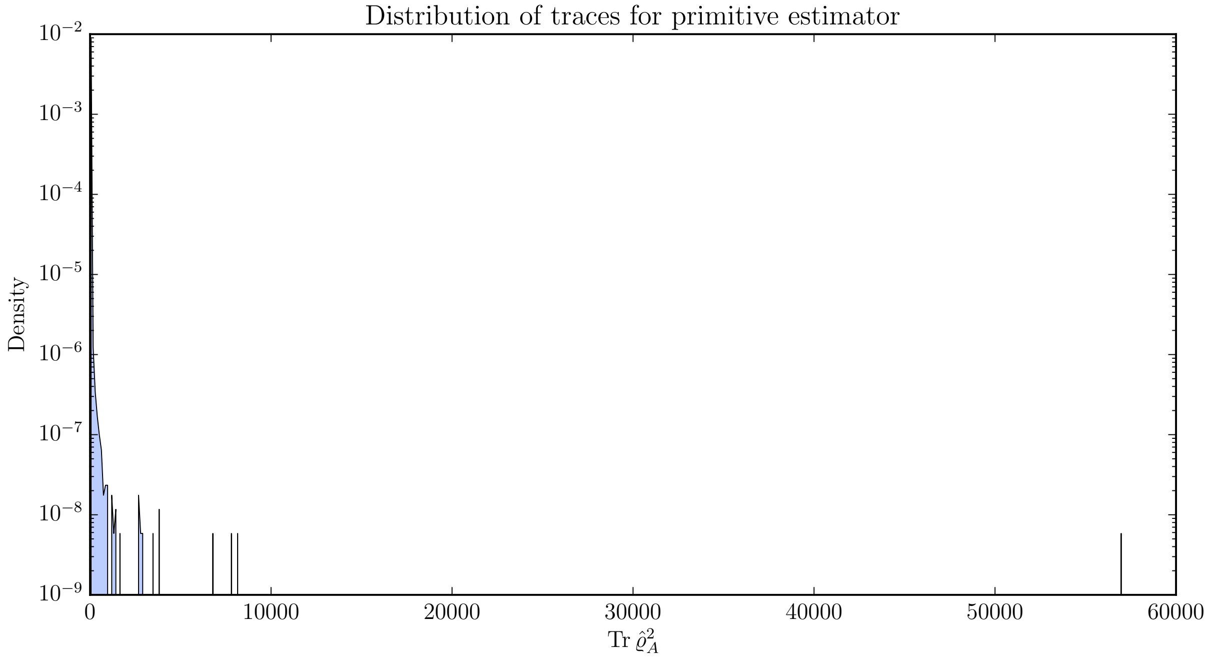

(a) Distribution of all traces in a 10^6 step simulation. Note the outlier to the extreme right, causing the loss of detail on the left.

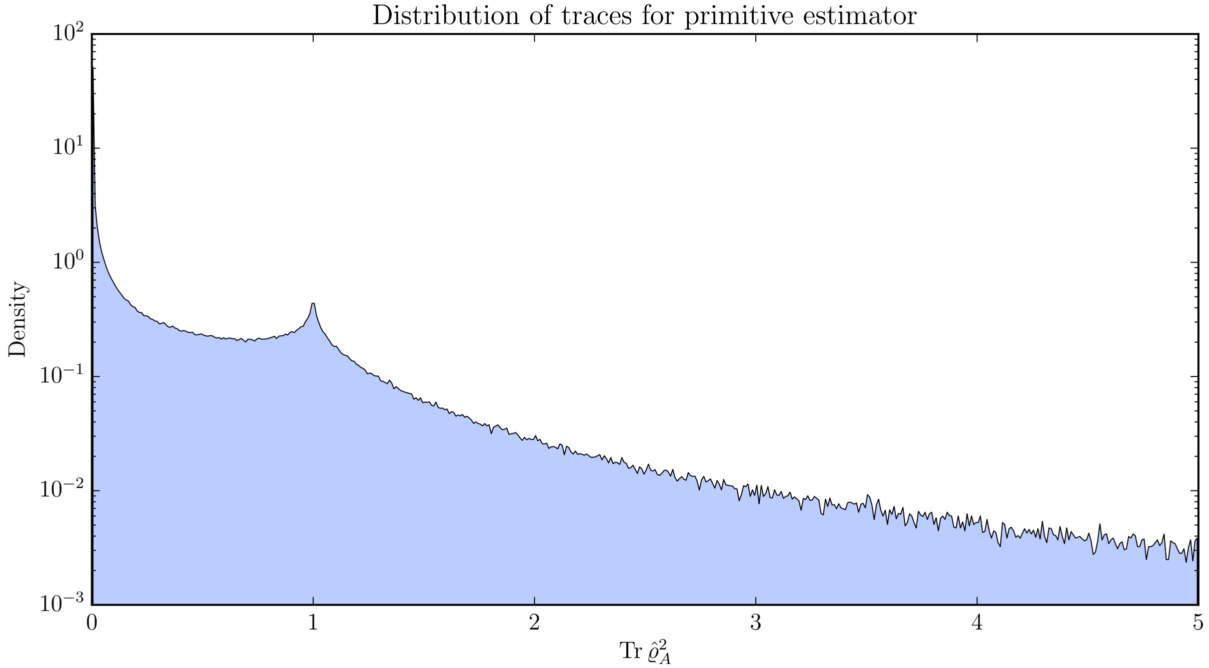

(b) Distribution of only those traces in a 10^6 step simulation that fell below a cutoff value.

Figure 2.8: Distribution of traces for the primitive estimator. The logarithmic scale on the y-axis is necessary to make anything other than the first few bins visible.

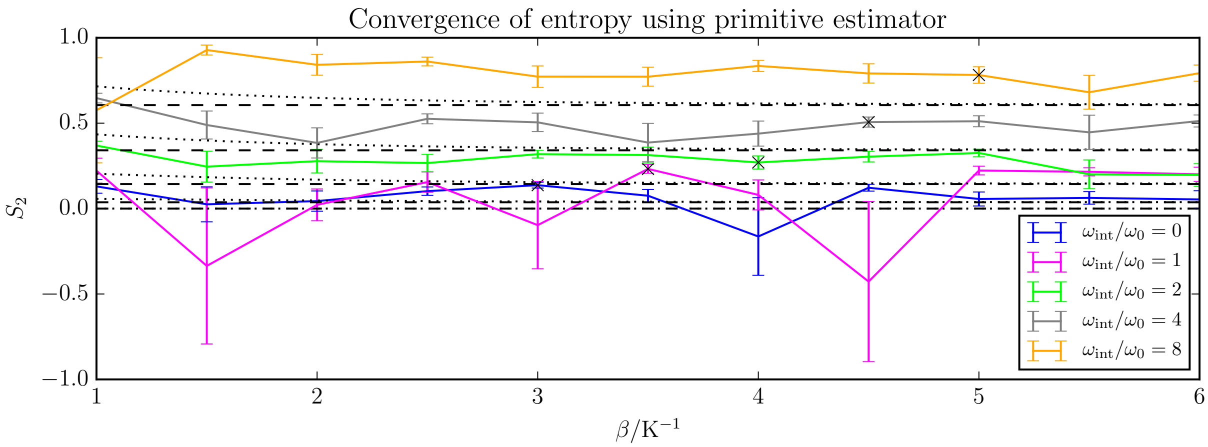

(a) Convergence of the entropy with β.

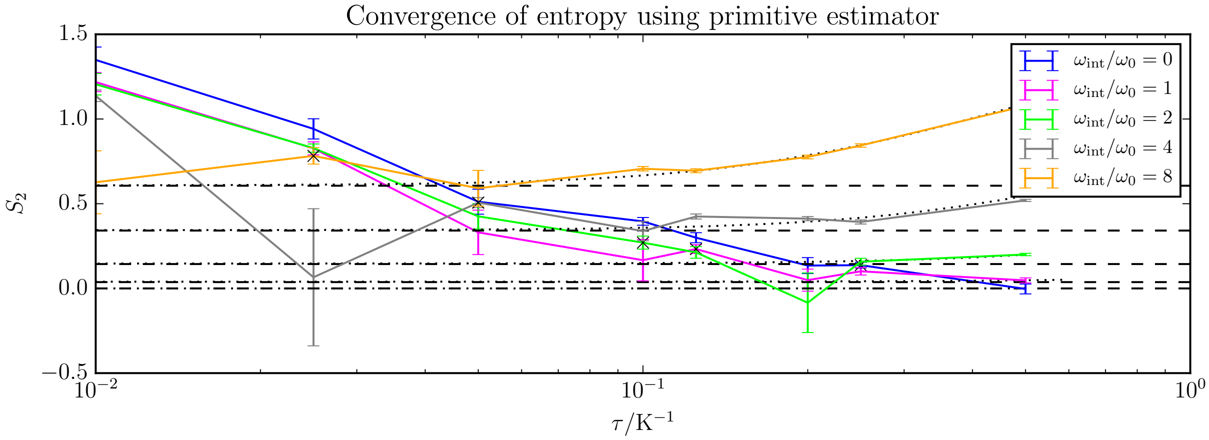

(b) Convergence of the entropy with τ.

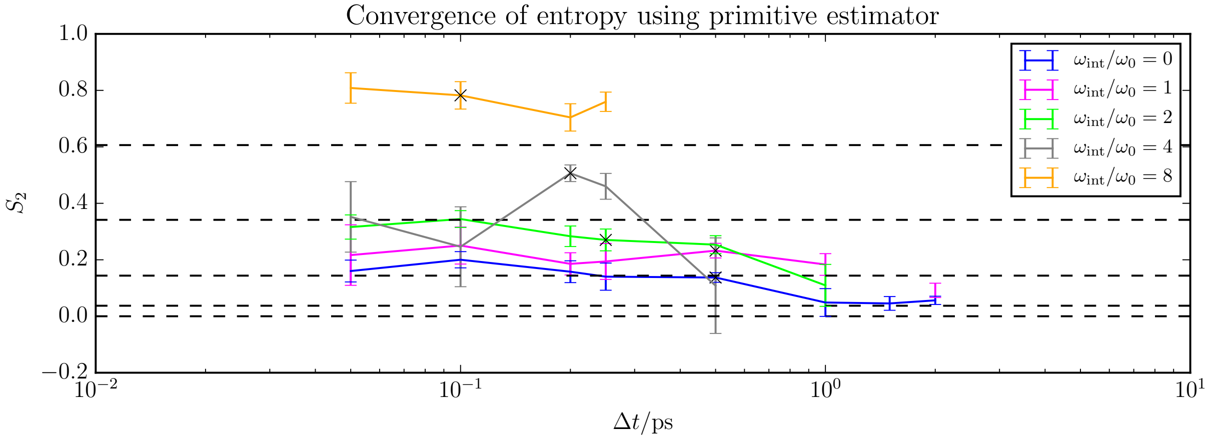

(c) Convergence of the entropy with Δt.

Figure 2.9: Unsuccessful convergence of the second Rényi entropy of the coupled oscillators with β, τ, and Δt using the primitive estimator. 10^6 steps. Dashed lines indicate the exact answer; dotted curves are the expected convergence obtained from a direct numerical method; crosses mark the values in table 2.1 on page 23.

2.3.2 Minimal estimator

For the minimal estimator, we perform the same analyses as above. We again start by optimizing the friction. Judging from fig. 2.10, we have enough steps in the simulation for the error to converge. Looking at fig. 2.11, we see reasonable behaviour whether we have large or small τ. More importantly, there is a clear minimum in the error at $\gamma^{(0)} = 0.1\,\mathrm{ps}^{-1}$ for all coupling strengths, which is rather convenient.

Having settled on a centroid friction, we look at the distribution of values for the numerator and denominator components in fig. 2.12 and we see pleasant shapes that only extend as far as unity. This means that we avoid the issue of arbitrarily large outliers that we saw with the primitive estimator. Thus, we are able to make the well-behaved convergence plots in fig. 2.13.

As shown in fig. 2.14a, by increasing the number of steps (and therefore the time required to run the simulation), we are able to reduce the error bars to the same magnitude as the residual systematic error. The largest relative error is about $0.3\,\%$.

Finally, now that we know that the minimal estimator works well for the second Rényi entropy, we apply it to a range of coupling strengths. The results are shown in fig. 2.14b.

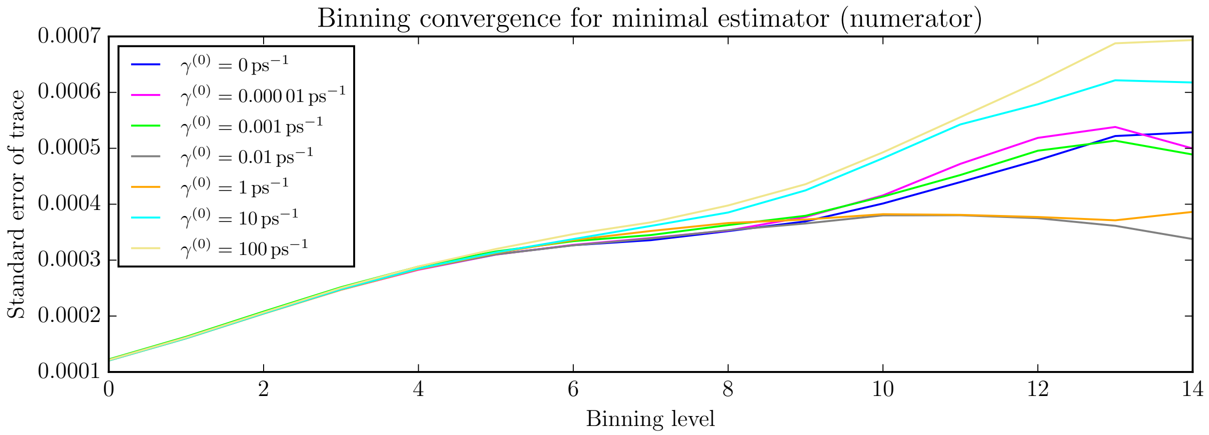

(a) Error in the numerator component.

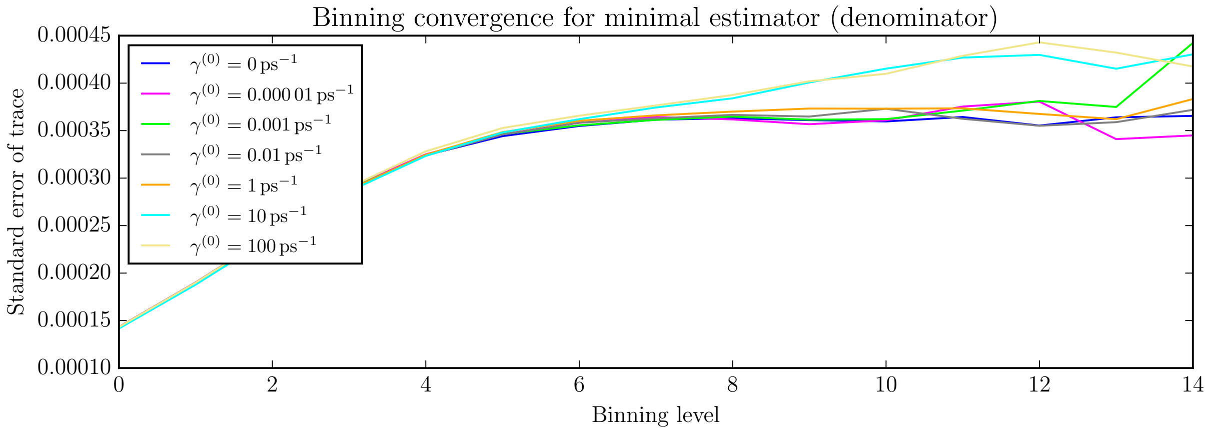

(b) Error in the denominator component.

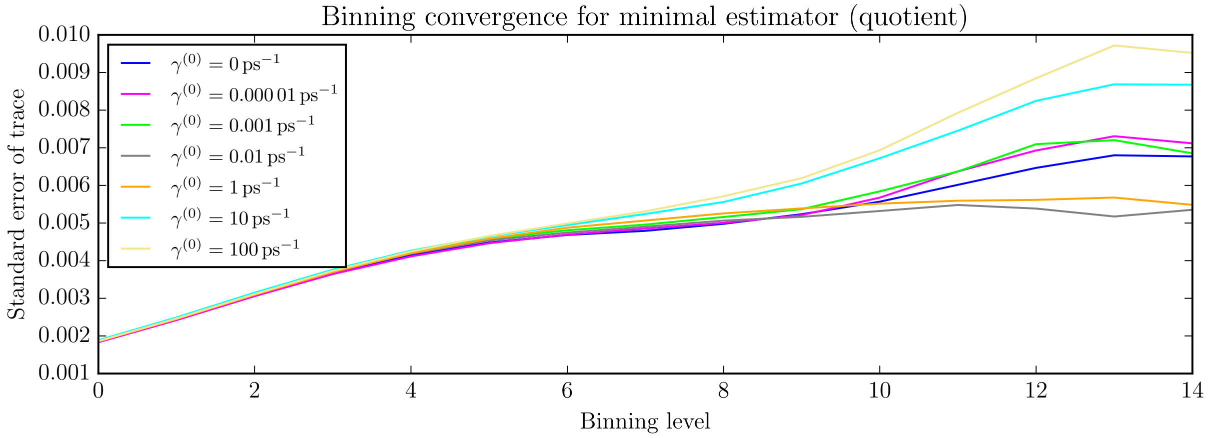

(c) Error in the quotient.

Figure 2.10: Convergence of error with binning level for different frictions using the minimal estimator. $\omega_{\text{int}} = 4\,\mathrm{K}$, 10^6 steps.

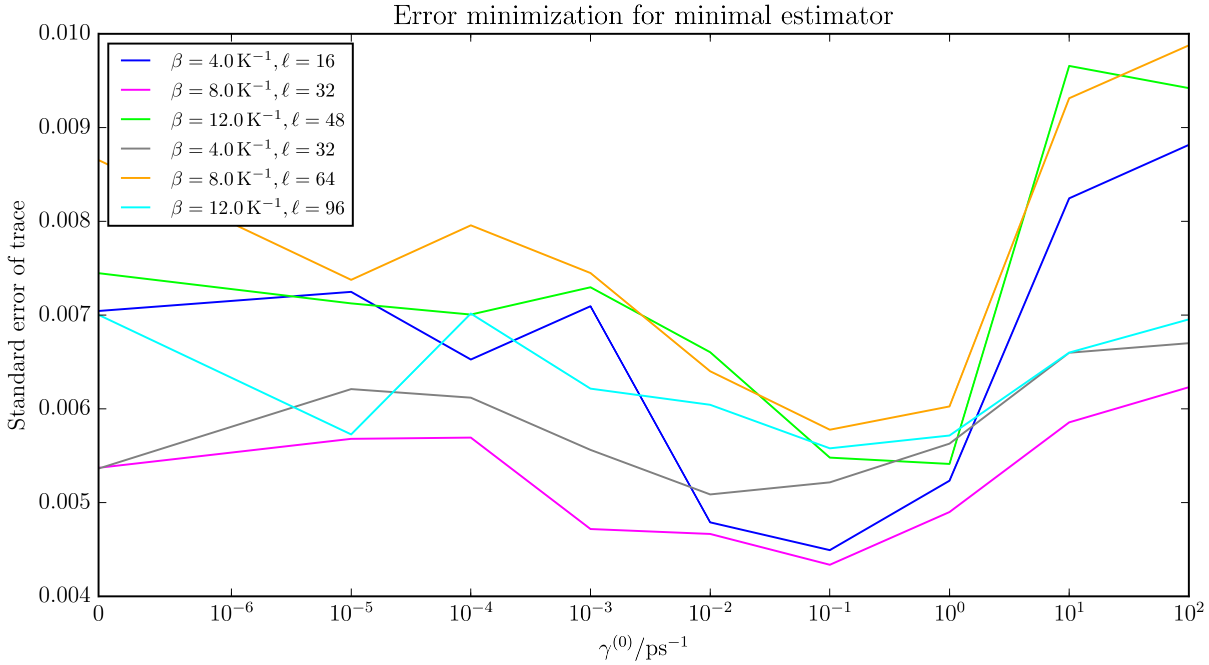

(a) Minimization of error with friction for different values of β and ℓ. $\omega_{\mathrm{int}} = 4\,\mathrm{K}$.

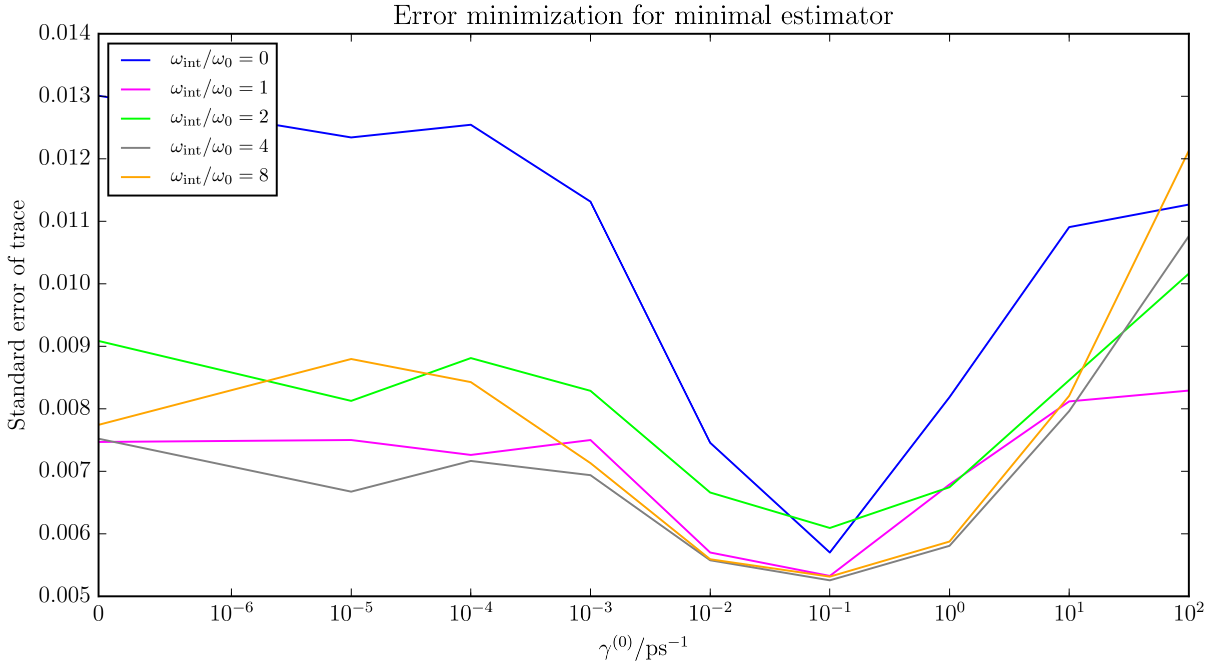

(b) Minimization of error with friction for different values of ω_{int}.

Figure 2.11: Friction optimization for the minimal estimator with different parameter sets. 10^6 steps.

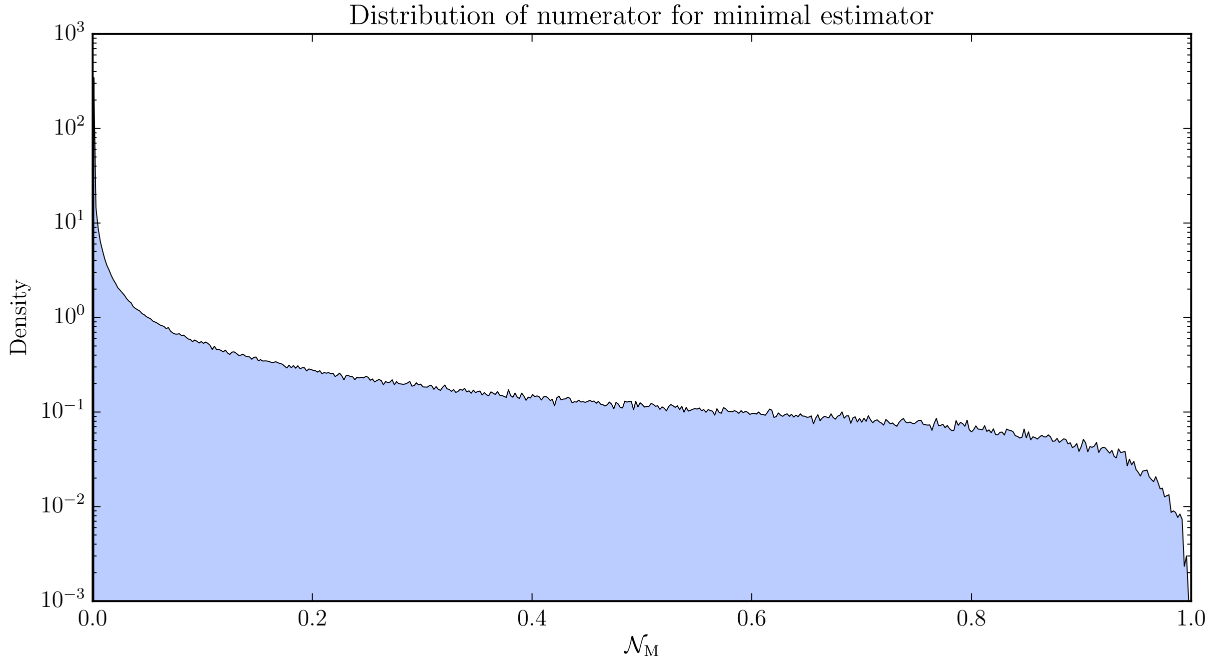

(a) Distribution of the numerator estimator in a 10^6 step simulation.

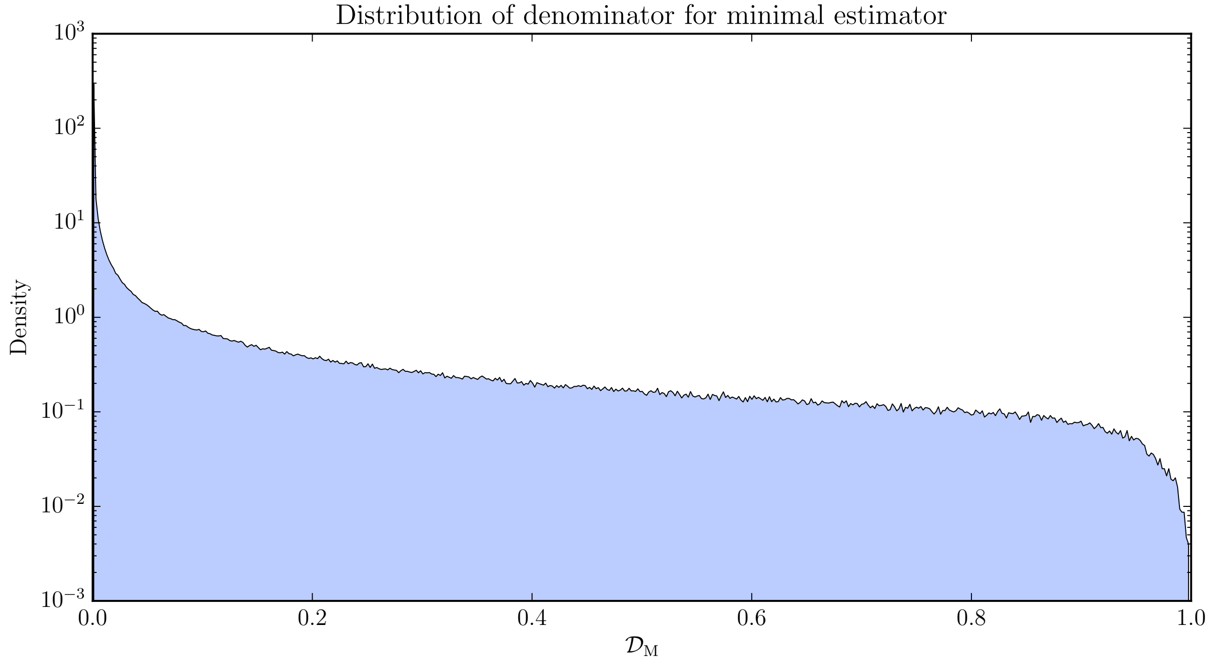

(b) Distribution of the denominator estimator in a 10^6 step simulation.

Figure 2.12: Distribution of numerator and denominator components for the minimal estimator. The logarithmic scale on the y-axis is necessary to make anything other than the first few bins visible.

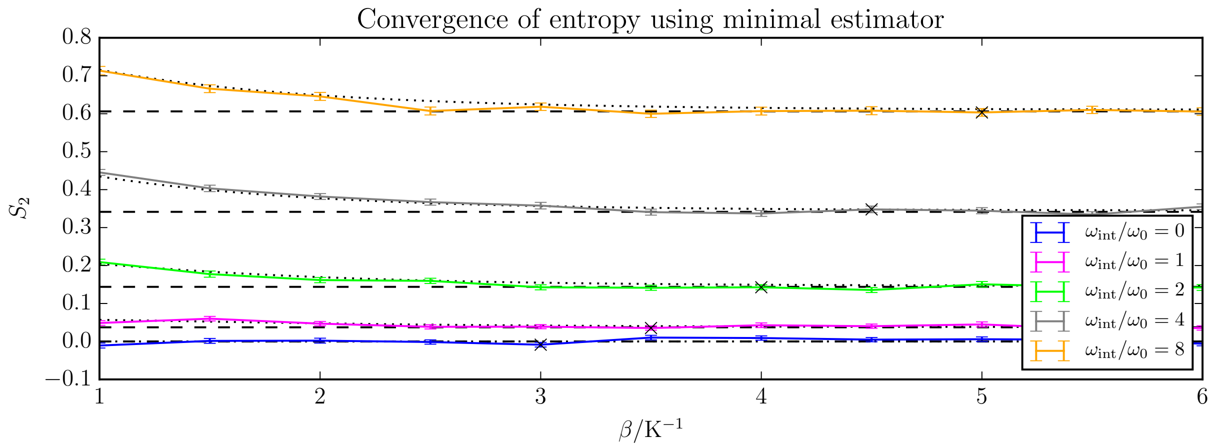

(a) Convergence of the entropy with β.

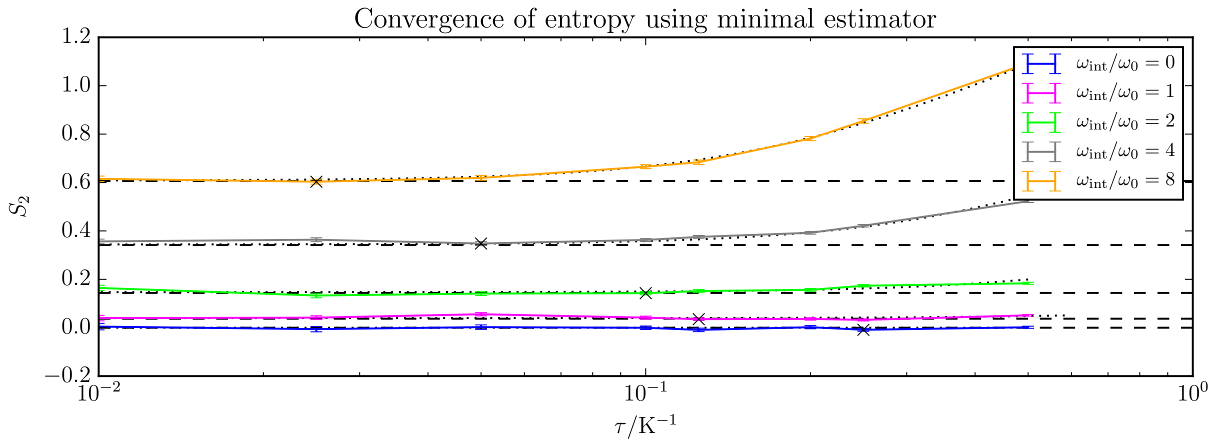

(b) Convergence of the entropy with τ.

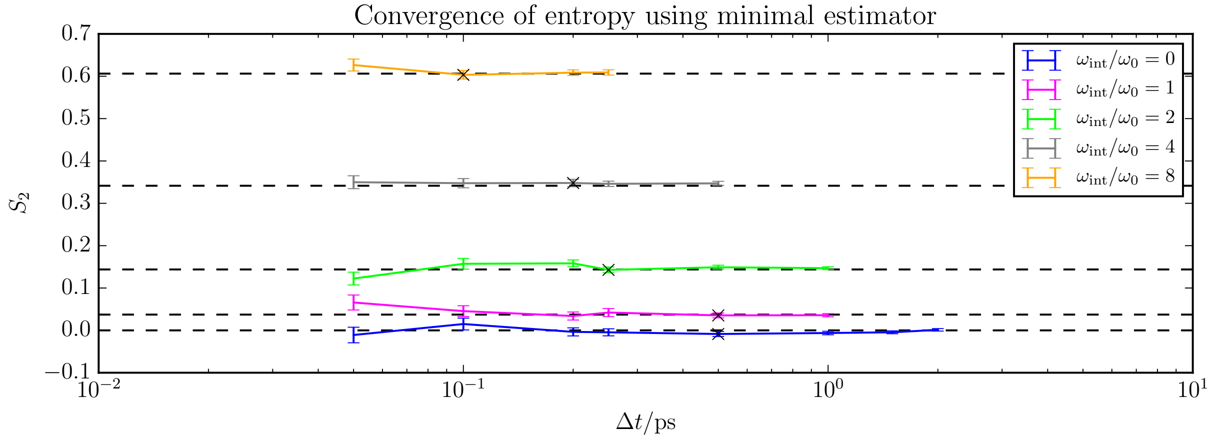

(c) Convergence of the entropy with Δt.

Figure 2.13: Successful convergence of the second Rényi entropy of the coupled oscillators with β, τ, and Δt using the minimal estimator. 10^6 steps. Dashed lines indicate the exact answer; dotted curves are the expected convergence obtained from a direct numerical method; crosses mark the values in table 2.1 on page 23.

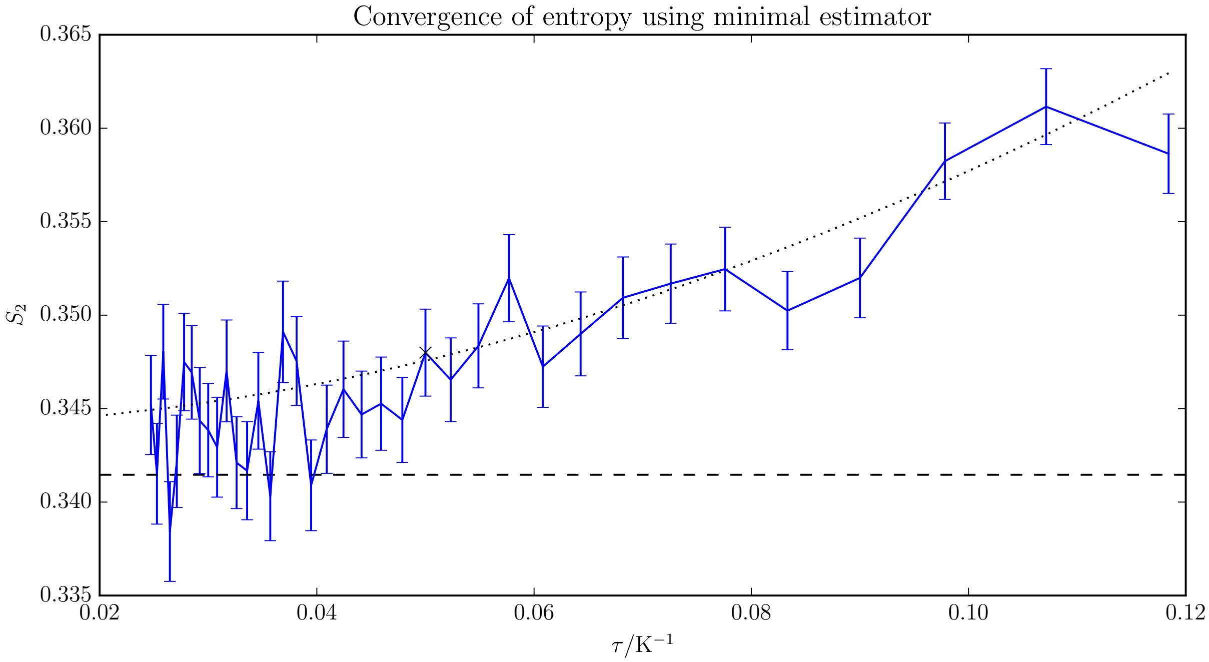

(a) Reasonably converged entanglement entropy. $\omega_{\text{int}} = 4\,\mathrm{K}$.

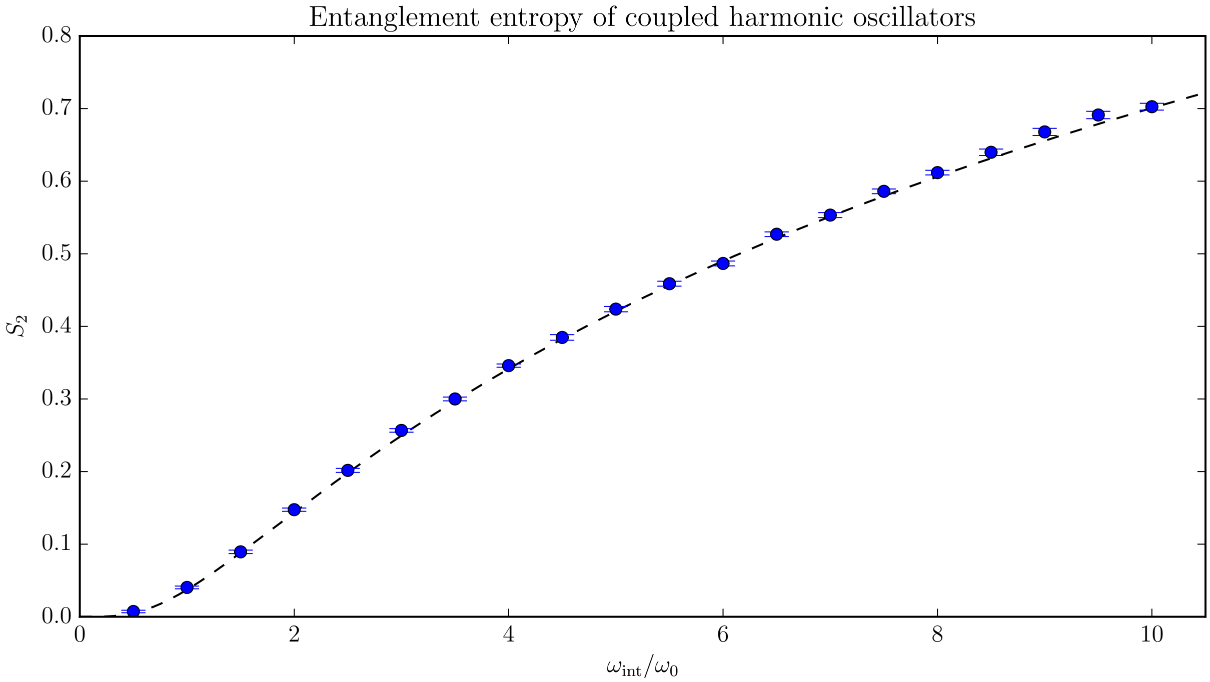

(b) Entanglement entropy for various coupling strengths. The error bars look peculiar because they are smaller than the symbols.

Figure 2.14: Detailed results for the minimal estimator. 10^7 steps. Dashed lines indicate the exact answer; dotted curves are the expected convergence obtained from a direct numerical method; crosses mark the values in table 2.1 on page 23.

Chapter 3

Semiclassical IVR with PIGS

Real-time correlation functions are of particular interest in chemistry, because they relate to experimental observables. For example, the spectrum (*i.e.* the Fourier transform) of the dipole-dipole correlation function of a molecule is proportional to the electromagnetic spectrum of that molecule [Zwa01, pp. 12,56],[McQ76, p. 473]. The ability to computationally generate spectra for molecules in various chemical environments, such as clusters, could help with the identification of existing compounds and the synthesis of novel ones.

The time evolution of a quantum mechanical system is well-known and is described in the Schrödinger picture by the time-dependent Schrödinger equation [Dir81, p. 111]

$$\frac{\partial}{\partial t}\left|\psi(t)\right\rangle = -\frac{i}{\hbar}\hat{H}\left|\psi(t)\right\rangle. \tag{3.1}$$

Starting from an initial state $\left|\psi\right\rangle$, this has the formal solution

$$\left|\psi(t)\right\rangle = e^{-\frac{i\hat{H}t}{\hbar}}\left|\psi\right\rangle. \tag{3.2}$$

We will refer to the operator

$$\hat{U}(t) = e^{-\frac{i\hat{H}t}{\hbar}} \tag{3.3}$$

as the *real-time propagator*. We find it convenient to work in the Heisenberg picture, where we propagate the operators through time, rather than the wavefunctions. Since we wish to preserve expectation values, for any operator $\hat{O}$, it must be that

$$\langle\psi(t)|\hat{O}|\psi(t)\rangle = \langle\psi|\hat{U}^\dagger(t)\hat{O}\hat{U}(t)|\psi\rangle = \langle\psi|\hat{O}(t)|\psi\rangle, \tag{3.4}$$

which gives us the usual definition for the time dependence of an operator, [Mes99, p. 315]

$$\hat{O}(t) = \hat{U}^\dagger(t)\hat{O}\hat{U}(t) = e^{\frac{i\hat{H}t}{\hbar}}\hat{O}e^{-\frac{i\hat{H}t}{\hbar}}. \tag{3.5}$$

The correlation functions in which we are interested have the general form

$$C_{\hat{A}\hat{B}}(t) = \langle\hat{A}(t)\hat{B}\rangle = \frac{\mathrm{Tr}\,\hat{\varrho}\hat{A}(t)\hat{B}}{\mathrm{Tr}\,\hat{\varrho}}, \tag{3.6}$$

for a density operator $\hat{\varrho}$ and some operators $\hat{A}$ and $\hat{B}$. In the case that the state is a normalized ground state $|0\rangle$ with energy E_0, we may write this as

$$C_{\hat{A}\hat{B}}(t) = \langle 0|\hat{A}(t)\hat{B}|0\rangle = \langle 0|e^{\frac{i\hat{H}t}{\hbar}}\hat{A}e^{-\frac{i\hat{H}t}{\hbar}}\hat{B}|0\rangle = e^{\frac{iE_0t}{\hbar}}\langle 0|\hat{A}\hat{U}(t)\hat{B}|0\rangle\,. \tag{3.7}$$

At $t = 0$, this is simply the ground state expectation value of $\hat{A}\hat{B}$. However, at later times, we must take into account the real-time propagator $\hat{U}(t)$; to do this exactly is as difficult as diagonalizing $\hat{H}$, which is essentially impossible for interesting problems.

Consider a particle of mass m in a potential $\hat{V}$.[‡] One approximation to the real-time propagator is given by the Herman–Kluk (HK) propagator [Mil02]

$$\hat{U}^{\mathrm{HK}}(t) = \frac{1}{2\pi\hbar}\iint \mathrm{d}p\,\mathrm{d}q\,R_t^{p,q}e^{\frac{i}{\hbar}S_t^{p,q}}\,|p_t^{p,q}\,q_t^{p,q}\rangle\langle p\,q|\,, \tag{3.8}$$

where $p_t^{p,q}$ and $q_t^{p,q}$ are phase space variables for classical trajectories, p and q are the initial conditions for those trajectories, $|p\,q\rangle$ is a coherent state[§] of reciprocal width γ,

$$R_t^{p,q} = \sqrt{\frac{1}{2}\left(\frac{\partial p_t^{p,q}}{\partial p} + \frac{\partial q_t^{p,q}}{\partial q} + \frac{i}{\hbar\gamma}\frac{\partial p_t^{p,q}}{\partial q} - i\hbar\gamma\frac{\partial q_t^{p,q}}{\partial p}\right)} \tag{3.9}$$

is the HK prefactor,

$$S_t^{p,q} = \int_0^t \mathrm{d}\tau\,(p_\tau^{p,q}\dot{q}_\tau^{p,q} - H^{p,q}) = \frac{1}{m}\int_0^t \mathrm{d}\tau\,(p_\tau^{p,q})^2 - tH^{p,q} \tag{3.10}$$

is the classical action, and

$$H^{p,q} = \frac{p^2}{2m} + V(q) \tag{3.11}$$

is the classical Hamiltonian (total energy) for the given initial conditions. This approximation is a *semiclassical* one, because it relies on the combination of classical trajectories to produce time evolution that takes into account quantum effects, such as interference [GGT00, TWM01]. Unlike other semiclassical methods, this one does not suffer from the root search problem, because it is an initial value method; it is part of a family of methods known as Semiclassical Initial Value Representation (SC-IVR) [GGT00]. At $t = 0$, it is exact:

$$\hat{U}^{\mathrm{HK}}(t=0) = \frac{1}{2\pi\hbar}\iint \mathrm{d}p\,\mathrm{d}q\;|p\,q\rangle\langle p\,q| = \hat{1} = \hat{U}(t=0). \tag{3.12}$$

At later times, we need to obtain the aforementioned quantities from classical trajectories. For all but the most trivial of problems, this will need to be done by numerical integration of the equations of motion with a time step $\Delta t^\star$.

[‡] In this chapter, we look at only the one-dimensional problem, but all the ideas are applicable to any number of degrees of freedom with some modifications. Among other things, the scaling factor in the coherent state resolution of the identity is changed to $(2\pi\hbar)^{-F}$ for F degrees of freedom, γ is turned into a matrix, and the HK prefactor is generalized to be in the form of the determinant of a matrix.

[§] An introduction to coherent states may be found in ref. [Sch96, pp. 242-245] and a thorough summary of their properties is available in ref. [GZ04, pp. 99-106].

For simplicity, we will consider $\hat{A} = \hat{B} = \hat{1}$, in which case the correlation function is trivially unity at all times:

$$C_{\hat{1}\hat{1}}(t) = e^{\frac{iE_0 t}{\hbar}} \langle 0|\hat{U}(t)|0\rangle = 1. \tag{3.13}$$

This may appear to be useless, but it contains a quantity known as the *survival amplitude* [IR07]

$$S_\psi(t) = \langle\psi|\hat{U}(t)|\psi\rangle = \langle\psi|\psi(t)\rangle\,, \tag{3.14}$$

which is the overlap of a wavefunction with itself at a later time. The survival amplitude retains nearly all the difficulty associated with correlation functions, since it still contains the real-time propagator.

In order to verify our methods, we wish to look at the ground state survival amplitude

$$S_0(t) = \langle 0|\hat{U}(t)|0\rangle = e^{-\frac{iE_0 t}{\hbar}} = \cos(\omega_0 t) - i\sin(\omega_0 t) \tag{3.15}$$

for model systems, where $\omega_0 = E_0/\hbar$ may also be determined by other means. Our method of choice for finding the ground state is PIGS in the position representation, so we have some access to $\langle q|0\rangle$, but not to $\langle p\, q|0\rangle$. However, the HK propagator is explicitly in the coherent state representation. We may try to get around the difference in representations by inserting a resolution of the identity in the position representation, as in

$$\begin{aligned}\langle p\, q|0\rangle &= \int \mathrm{d}q'\ \langle p\, q|q'\rangle\,\langle q'|0\rangle &\text{(3.16a)}\\ &= \int \mathrm{d}q'\ \exp\left[-\frac{\gamma}{2}(q'-q)^2 - \frac{i}{\hbar}p(q'-q)\right]\langle q'|0\rangle\,. &\text{(3.16b)}\end{aligned}$$

When we try to use this with the HK propagator to obtain the ground state survival amplitude, we get

$$\begin{aligned}S_0^{\mathrm{HK}}(t) &= \langle 0|\hat{U}^{\mathrm{HK}}(t)|0\rangle &\text{(3.17a)}\\ &= \frac{1}{2\pi\hbar}\iint \mathrm{d}p\,\mathrm{d}q\, R_t^{p,q} e^{\frac{i}{\hbar}S_t^{p,q}}\,\langle 0|p_t^{p,q}\, q_t^{p,q}\rangle\,\langle p\, q|0\rangle &\text{(3.17b)}\\ &= \frac{1}{2\pi\hbar}\iiiint \mathrm{d}p\,\mathrm{d}q_{\mathrm{L}}\,\mathrm{d}q\,\mathrm{d}q_{\mathrm{R}}\, R_t^{p,q} e^{\frac{i}{\hbar}S_t^{p,q}}\,\langle 0|q_{\mathrm{L}}\rangle\,\langle q_{\mathrm{L}}|p_t^{p,q}\, q_t^{p,q}\rangle\,\langle p\, q|q_{\mathrm{R}}\rangle\,\langle q_{\mathrm{R}}|0\rangle &\text{(3.17c)}\\ &= \frac{1}{2\pi\hbar}\iiiint \mathrm{d}p\,\mathrm{d}q_{\mathrm{L}}\,\mathrm{d}q\,\mathrm{d}q_{\mathrm{R}}\, R_t^{p,q}\,\langle 0|q_{\mathrm{L}}\rangle\,\langle q_{\mathrm{R}}|0\rangle \exp\left[-\frac{\gamma}{2}\left((q_{\mathrm{L}} - q_t^{p,q})^2 + (q_{\mathrm{R}} - q)^2\right)\right]\\ &\qquad\times \exp\left[\frac{i}{\hbar}\left(S_t^{p,q} + p_t^{p,q}(q_{\mathrm{L}} - q_t^{p,q}) - p(q_{\mathrm{R}} - q)\right)\right]. &\text{(3.17d)}\end{aligned}$$

Naturally, one cannot hope to perform this integration analytically. Should we try to use another method, we are faced with the fact that all the integrals are from $-\infty$ to ∞. For the position coordinates, we at least have some hope of narrowing this range down thanks to the exponential decay of the ground state wavefunctions and the Gaussian from the coherent states. For the momentum coordinate, however, there is no such possibility; instead, we will be forced to explore other ideas.

3.1 Numerical integration

Since we are working in only one spatial dimension, the integrals in eq. (3.17d) may be performed on a grid. We begin with the assumption that we have four evenly-spaced grids whose elements are p_i, q_j, q_k, q_ℓ (corresponding to p, q_{L}, q, and q_{R}) and whose spacings are, respectively, Δp, $\Delta q^\star$, Δq, $\Delta q^\star$.[‡] These grids are symmetric about zero and extend in each direction to $p_{\max}$, $q^\star_{\max}$, $q_{\max}$, $q^\star_{\max}$. We may then approximate the integrals in eq. (3.17d) by sums:

$$S_0^{\mathrm{HK}}(t) \approx \frac{\Delta p (\Delta q^\star)^2 \Delta q}{2\pi\hbar} \sum_{i,j,k,\ell} R_t^{p_i,q_k} \langle 0|q_j\rangle \langle q_\ell|0\rangle \exp\left[-\frac{\gamma}{2}\left((q_j - q_t^{p_i,q_k})^2 + (q_\ell - q_k)^2\right)\right]$$
$$\times \exp\left[\frac{i}{\hbar}\left(S_t^{p_i,q_k} + p_t^{p_i,q_k}(q_j - q_t^{p_i,q_k}) - p_i(q_\ell - q_k)\right)\right]. \tag{3.18}$$

For brevity, we introduce

$$C = \frac{\Delta p (\Delta q^\star)^2 \Delta q}{2\pi\hbar} \qquad w^j = \langle q_j|0\rangle \tag{3.19a}$$
$$R_t^{i,k} = R_t^{p_i,q_k} \qquad S_t^{i,k} = S_t^{p_i,q_k} \tag{3.19b}$$
$$p_t^{i,k} = p_t^{p_i,q_k} \qquad q_t^{i,k} = q_t^{p_i,q_k}, \tag{3.19c}$$

which lets us write

$$S_{0,t}^{\mathrm{HK}} = C \sum_{i,j,k,\ell} R_t^{i,k} w^j w^\ell \exp\left[-\frac{\gamma}{2}\left((q_j - q_t^{i,k})^2 + (q_\ell - q_k)^2\right)\right]$$
$$\times \exp\left[\frac{i}{\hbar}\left(S_t^{i,k} + p_t^{i,k}(q_j - q_t^{i,k}) - p_i(q_\ell - q_k)\right)\right]. \tag{3.20}$$

We refer to the 4-tuple $T_t^{i,k} = \left(p_t^{i,k}, q_t^{i,k}, R_t^{i,k}, S_t^{i,k}\right)$ as the *classical trajectory* with initial conditions p_i, q_i.

As mentioned earlier, we do not have as obvious a guideline for setting up our momentum grid as we do for the position grids. Taking a hint from the Fourier-transform-like form of the p contribution in eq. (3.20), we choose the p_i grid to be the momentum space grid corresponding to a position grid, but it is not immediately clear which position grid to use. If we look only at the initial time, we see

$$S_{0,t=0}^{\mathrm{HK}} = C \sum_{i,j,k,\ell} w^j w^\ell \exp\left[-\frac{\gamma}{2}\left((q_j - q_k)^2 + (q_\ell - q_k)^2\right) + \frac{i}{\hbar} p_i (q_j - q_\ell)\right], \tag{3.21}$$

which suggests that the position grid to use should be the $\{q^\star_{\max}, \Delta q^\star\}$ grid.[§] This results in [FBK96]

$$p_{\max} = \frac{\pi\hbar}{\Delta q^\star}. \tag{3.22}$$

We will see later what happens if we neglect this and go farther out in momentum space.

[‡] Since the wavefunction must be evaluated at q_j and q_ℓ, we require that these grids be identical to keep things simple.

[§] Technically, the range of possible values for the difference of the grid elements is twice the range for the grid itself, but the spacing remains the same, and that is what we care about here.

Given the ground state wavefunction on the grid (w) and the classical trajectory at the appropriate time ($T_t^{i,k}$), it is a straightforward matter to find $S_{0,t}^{\mathrm{HK}}$. All the details are in the propagation of the classical trajectory. The phase space variables $p_t^{i,k}$ and $q_t^{i,k}$ may be found from the initial conditions[‡] using a symplectic integrator such as the well-known velocity Verlet algorithm or the lesser known (but higher order) integrator by Ruth and Forest [FR90]. The classical action $S_t^{i,k}$ is not difficult to obtain once one has the momenta.

The HK prefactor, on the other hand, is a much more interesting quantity to calculate. Because it is defined as the square root of a complex number, we must exercise caution when deciding which branch of the square root to choose. However, that is not a tough problem to deal with so long as one is aware of it. The more pressing matter is the evaluation of the partial derivatives. If we write them in the form of a *monodromy matrix*

$$\underline{\mathbf{M}}_t = \begin{pmatrix} \dfrac{\partial p_t}{\partial p} & \dfrac{\partial p_t}{\partial q} \\ \dfrac{\partial q_t}{\partial p} & \dfrac{\partial q_t}{\partial q} \end{pmatrix} = \begin{pmatrix} m_t^{p,p} & m_t^{p,q} \\ m_t^{q,p} & m_t^{q,q} \end{pmatrix} \tag{3.23}$$

(where we have dropped the trajectory indices i and k for the time being), we may express the time evolution of this matrix as [GGT00, GL00]

$$\frac{\mathrm{d}\underline{\mathbf{M}}_t}{\mathrm{d}t} = \begin{pmatrix} 0 & -\nabla^2 V \\ \frac{1}{m} & 0 \end{pmatrix} \underline{\mathbf{M}}_t \tag{3.24}$$

with initial conditions

$$\underline{\mathbf{M}}_{t=0} = \underline{\mathbf{1}}. \tag{3.25}$$

From this, we obtain two pairs of coupled ordinary differential equations (for x either p or q):

$$\dot{m}_t^{p,x} = -(\nabla^2 V)_t m_t^{q,x} \tag{3.26a}$$

$$\dot{m}_t^{q,x} = \frac{1}{m} m_t^{p,x}. \tag{3.26b}$$

These are very similar to Hamilton's equations of motion, but the "force" is unfortunately time-dependent. In order to propagate the HK prefactor through time, we may use an integrator such as the fourth-order Runge–Kutta integrator [PTV92, pp. 710-713].

Exercise 3.1 Harmonic oscillator classical trajectory

Find the analytical expressions for the classical action and HK prefactor for a harmonic oscillator with mass m, angular frequency ω, and initial conditions p, q.

Solution on page 114.

To summarize the above discussion and to provide verification of our implementation, we provide plots of trajectories (with different time steps $\Delta t^\star$) in phase space, along with the corresponding classical action and HK prefactor, for a harmonic oscillator (shown in figs. 3.1 and 3.2). We use $m = m_\mathrm{e}$ (mass of an electron), $\omega = 1\,\mathrm{K}$, $\gamma = 0.0181\,\mathrm{nm}^{-2}$, $p = -5 \times 10^{-3}\,\mathrm{g\,nm\,ps^{-1}\,mol^{-1}}$, and $q = 50\,\mathrm{nm}$. For reference, fig. 3.3 shows the effect of neglecting to choose the correct branch for the square root in the HK prefactor.

[‡] While the initial conditions are confined to a grid, there is no such restriction placed on the time-propagated phase space variables.

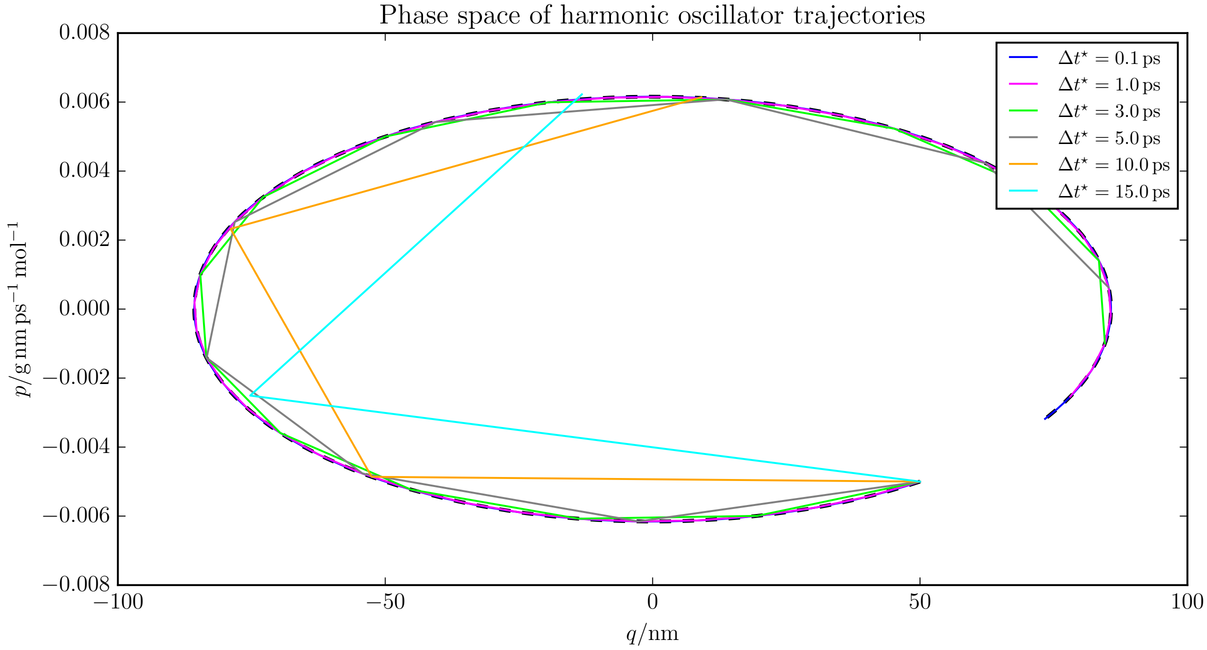

(a) Convergence of phase space variables with time step.

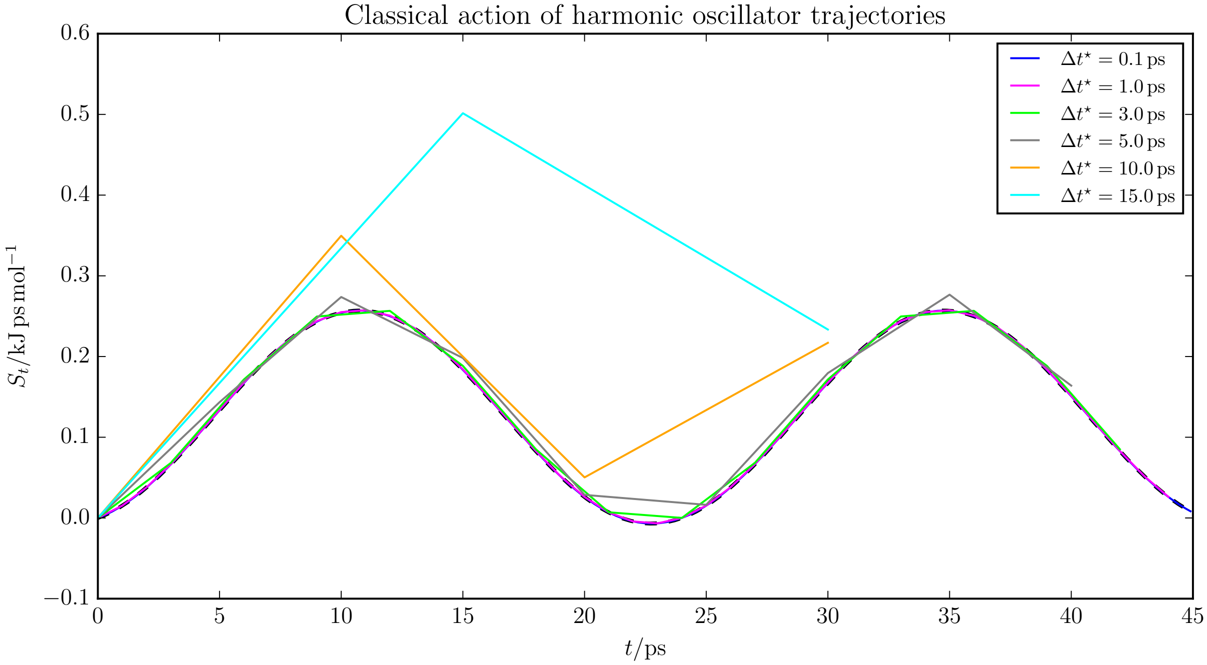

(b) Convergence of classical action with time step.

Figure 3.1: Phase space diagrams and classical actions resulting from harmonic oscillator trajectories with different time steps. Dashed curves indicate the exact answers.

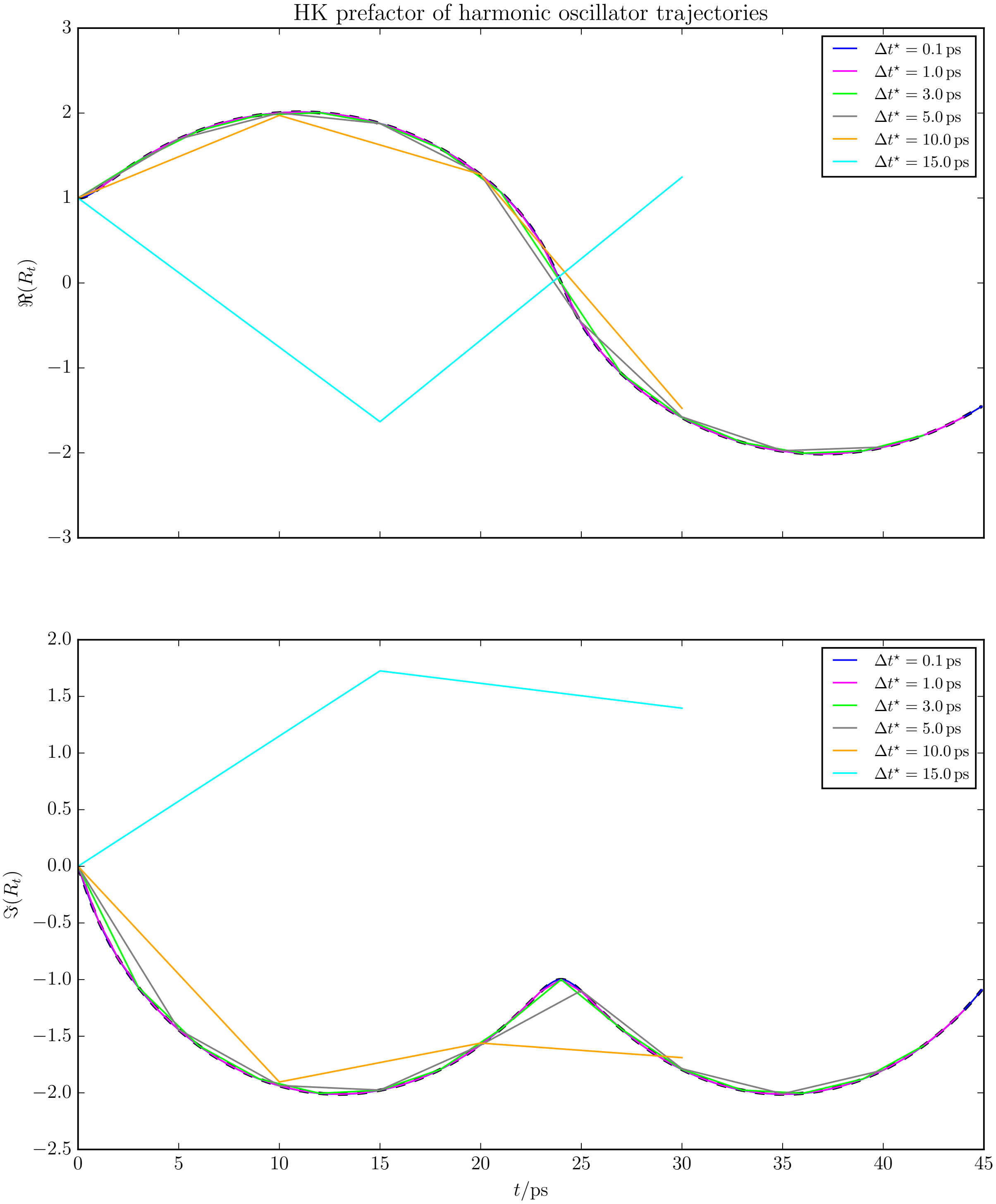

Figure 3.2: HK prefactors resulting from harmonic oscillator trajectories with different time steps. Dashed curves indicate the exact answers.

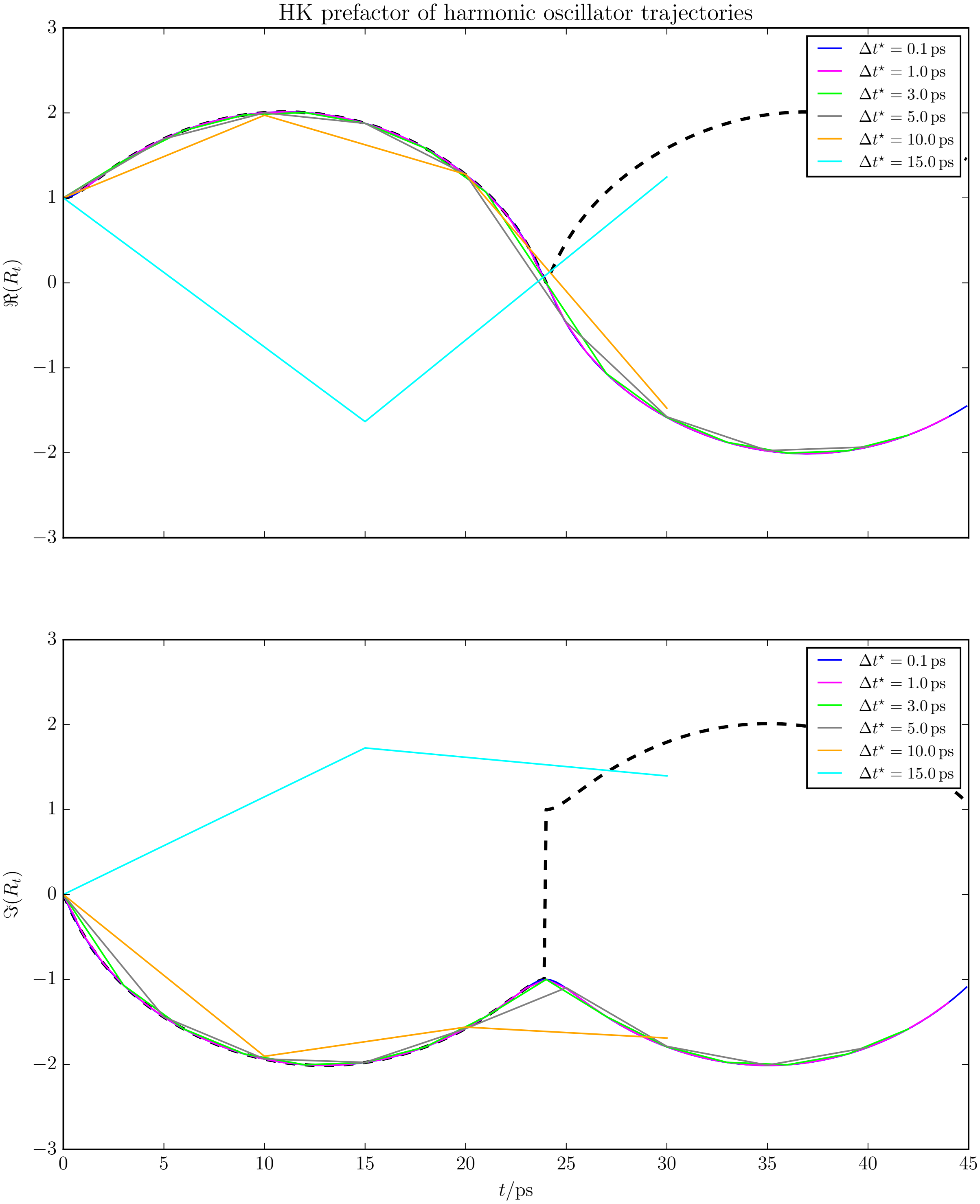

Figure 3.3: The same HK prefactors as in fig. 3.2, but the "exact" answers shown by the dashed curves neglect to take into account the branch of the square root. The result is a cusp in the real component and a discontinuity in the imaginary component at the point where the branches intersect, as well as the wrong overall sign after this point.

$\Delta t^\star$/ps	γ/nm^{-2}	$q_{\max}$/nm	Δq/nm	$q^\star_{\max}$/nm	$\Delta q^\star$/nm
1	0.001 131	300	20	80	2

Table 3.1: Selected parameters for the harmonic oscillator model system using the numerical method.

3.1.1 Harmonic oscillator

We are now prepared to find the survival amplitude for a one-dimensional system, so we start with the harmonic oscillator defined by eq. (2.28) on page 17. As elsewhere in the present work, we use $m = m_\mathrm{e}$ (mass of an electron) and $\omega = 1\,\mathrm{K}$. This still leaves us with several parameters to choose: $\Delta t^\star$, γ, $q_{\max}$, Δq, $q^\star_{\max}$, $\Delta q^\star$. Unless otherwise specified, the parameter values from table 3.1 are used for this model system.

One may wish to choose $\Delta t^\star$ to be sufficiently small so that the classical trajectories are stable, but no smaller. From figs. 3.1 and 3.2, this appears to be about 5 ps. However, since we would like to have good temporal resolution, we typically choose a shorter time step. For this system, we may cheat and choose the optimal γ, one which matches that of the system itself: $\gamma = m\omega/\hbar$; however, we want to see the effect this parameter has on the results, so we also perturb it from this value. Finally, we also need to obtain the ground state wavefunction on the $\{q^\star_{\max}, \Delta q^\star\}$ grid; because we can, we use the exact wavefunction from eq. (2.29) on page 17.

As the first step, we examine the real part of $S^{\mathrm{HK}}_{0,t=0}$, which should be exactly 1 as long as our integrals have converged. The convergence results for the position grids are shown in figs. 3.4 and 3.5. The results for $q^\star_{\max}$ are surprising: the wavefunction still has non-negligible amplitude (over 2.5 % of the maximum amplitude) when it is truncated.

As promised, we will now look at the results of increasing the p grid past the proper $p_{\max}$. Figure 3.6 shows a staircase as a function of $p'_{\max}$ (the actual extent used for the p grid) with jumps at even integer multiples of $p_{\max}$. To find the cause, in fig. 3.7 we plot the integrand which remains after the q_j and q_ℓ integrals have been performed. It seems that if we exceed the equivalent to the Nyquist frequency in momentum space, we observe aliasing!

As seen in fig. 3.8, we are able to generate ground state survival amplitudes for the harmonic oscillator system. With the parameters we have chosen by the $t = 0$ analysis above, the survival amplitudes show no deviation from the expected result for several cycles for all the γ we have used. For reference, we may also try $q_{\max} = 100\,\mathrm{nm}$, and $q^\star_{\max} = 50\,\mathrm{nm}$; the results in fig. 3.9 have the correct overall frequency, but the shape is incorrect for some γ.

3.1.2 Double well

We now move on to a more challenging, anharmonic system: a particle of mass m in a symmetric double well potential with the Hamiltonian

$$\hat{H} = \frac{\hat{p}^2}{2m} - 2\frac{d}{w^2}\hat{q}^2 + \frac{d}{w^4}\hat{q}^4, \tag{3.27}$$

where d is the depth of each minimum and w is the distance from the y-axis to the minima. We use $m = m_\mathrm{e}$ (mass of an electron), $d = 2\,\mathrm{K}$, and $w = 50\,\mathrm{nm}$. To obtain the ground state wavefunction, we use a numerical PIGS matrix multiplication method with sufficiently converged β and τ.

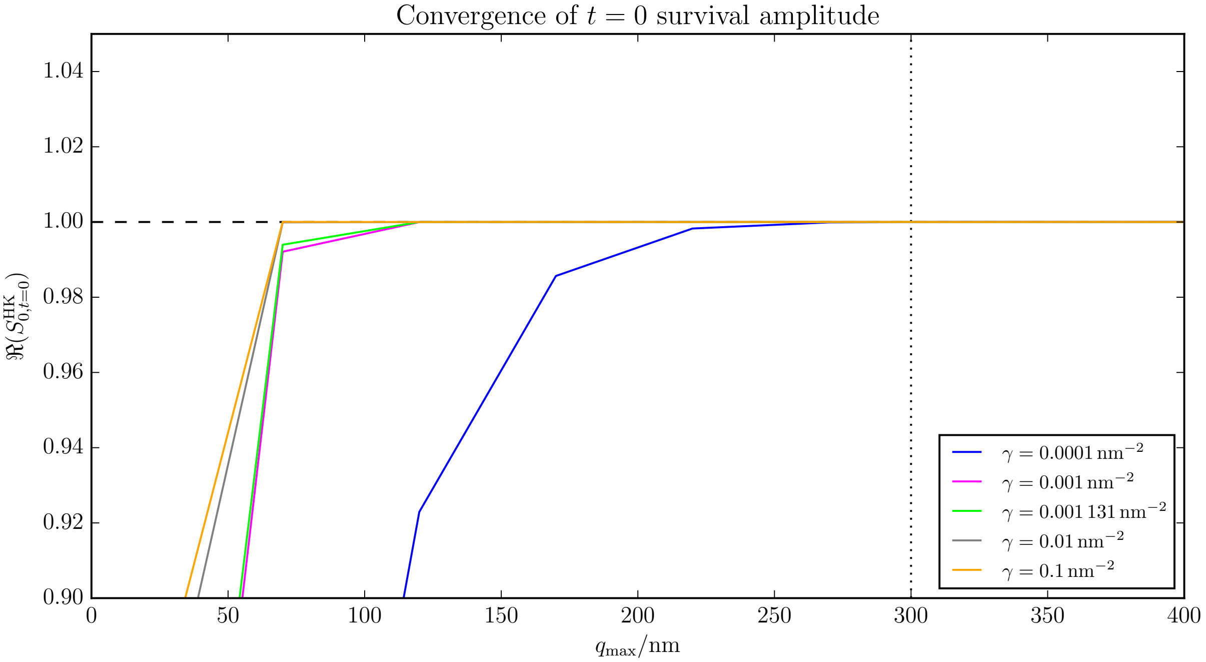

(a) Convergence of $t = 0$ survival amplitude with $q_{\max}$.

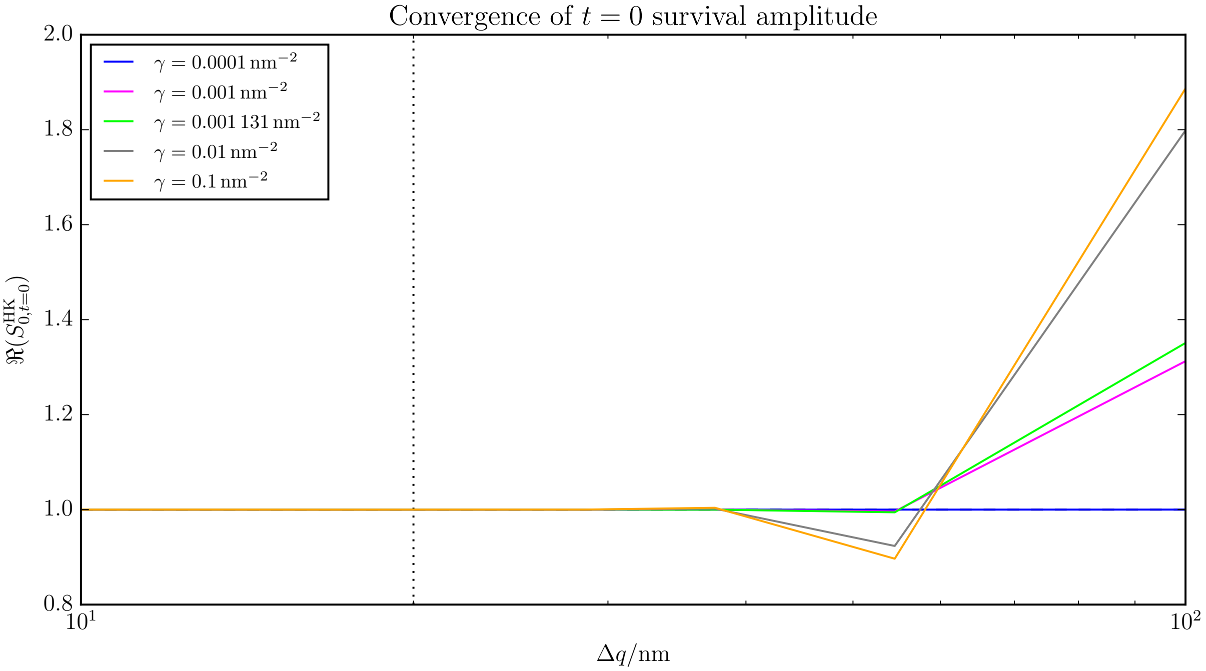

(b) Convergence of $t = 0$ survival amplitude with Δq.

Figure 3.4: Convergence of $t = 0$ survival amplitude with the $\{q_{\max}, \Delta q\}$ grid for a harmonic oscillator. Dashed lines indicate the exact answer; dotted lines mark the values in table 3.1 on page 43.

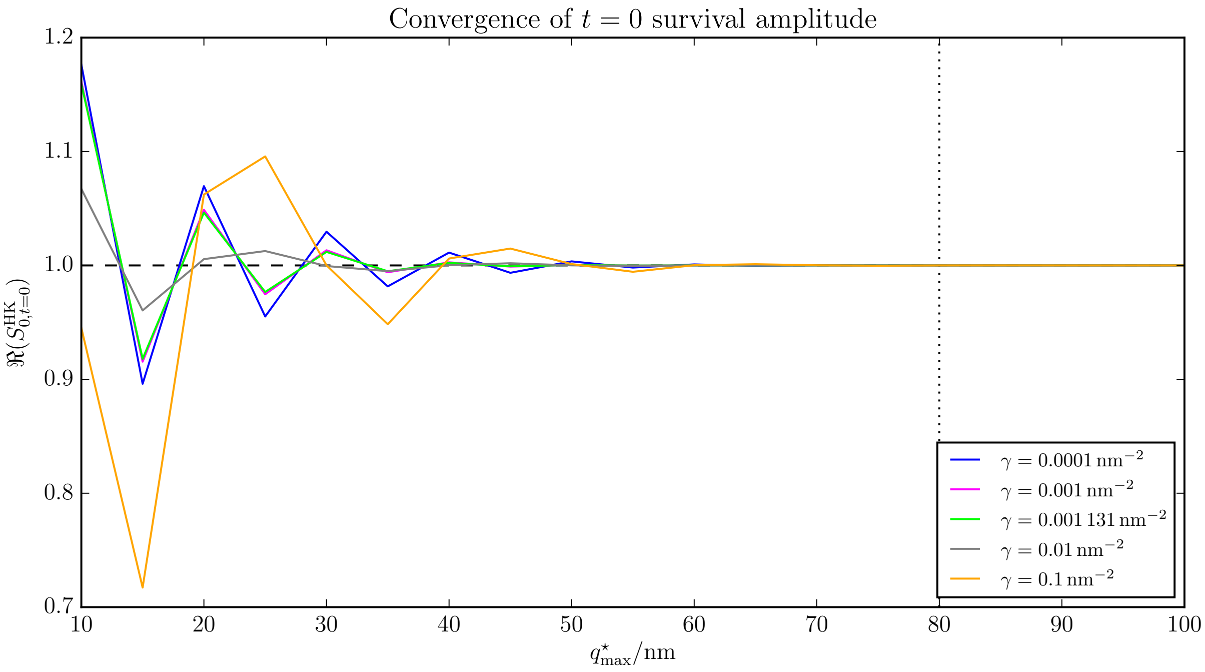

(a) Convergence of $t = 0$ survival amplitude with $q^\star_{\max}$.

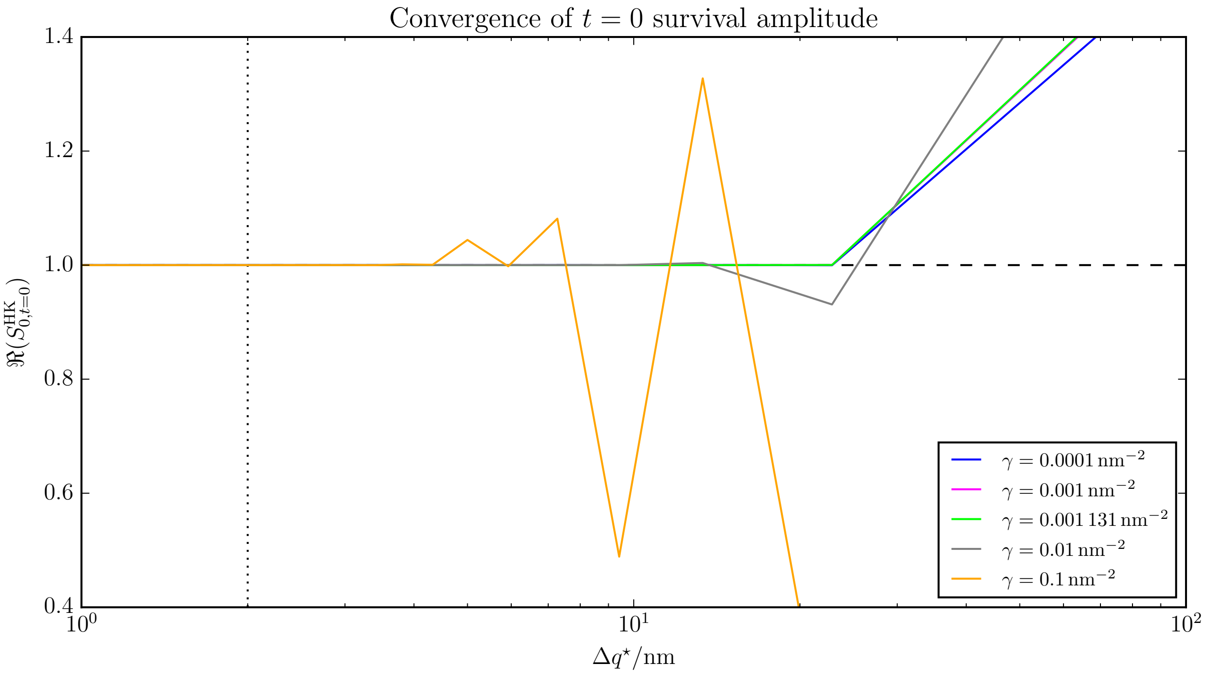

(b) Convergence of $t = 0$ survival amplitude with $\Delta q^\star$.

Figure 3.5: Convergence of $t = 0$ survival amplitude with the $\{q^\star_{\max}, \Delta q^\star\}$ grid for a harmonic oscillator. Dashed lines indicate the exact answer; dotted lines mark the values in table 3.1 on page 43.

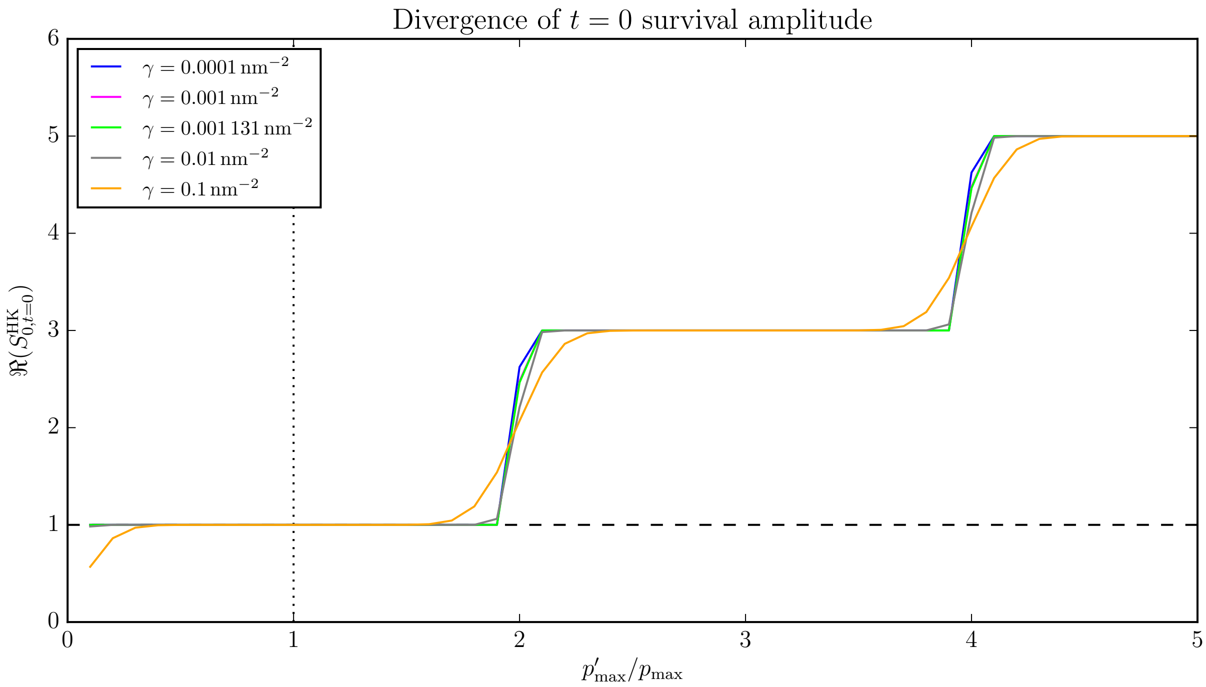

Figure 3.6: Divergence of $t = 0$ survival amplitude with p'_{max} for a harmonic oscillator. Dashed line indicates the exact answer; dotted line marks $p'_{\mathrm{max}} = p_{\mathrm{max}}$.

$\Delta t^\star/\mathrm{ps}$	γ/nm^{-2}	$q_{\mathrm{max}}/\mathrm{nm}$	$\Delta q/\mathrm{nm}$	$q^\star_{\mathrm{max}}/\mathrm{nm}$	$\Delta q^\star/\mathrm{nm}$
0.5	0.001	300	20	100	2

Table 3.2: Selected parameters for the double well model system using the numerical method.

$\Delta t^\star/\mathrm{ps}$	γ/nm^{-2}	$q_{\mathrm{max}}/\mathrm{nm}$	$\Delta q/\mathrm{nm}$	$q^\star_{\mathrm{max}}/\mathrm{nm}$	$\Delta q^\star/\mathrm{nm}$
0.1	0.001	2000	2	2000	8

Table 3.3: Improved parameters for the double well model system using the numerical method.

The results of the convergence studies in figs. 3.10 and 3.11 are shown in table 3.2. If we try to use these values to generate ground state survival amplitudes, we see in fig. 3.12 that we do a terrible job regardless of γ. In fact, the curves end where they do because the values diverge and the calculations are aborted. By changing some of the parameters, we are able to improve the shape of the curves and prolong the calculations, as shown in fig. 3.13 using the parameters from table 3.3. However, the results are still far from perfect.

We can get a feel for why the double well system is much more difficult to approach using this method by comparing figs. 3.14 and 3.15 to figs. 3.16 and 3.17. In the former, the magnitude does not change at all, and the phase changes gradually throughout. In the latter, the magnitude and phase both appear to undergo some sort of "swirling," which requires a much finer grid to resolve well at later times.

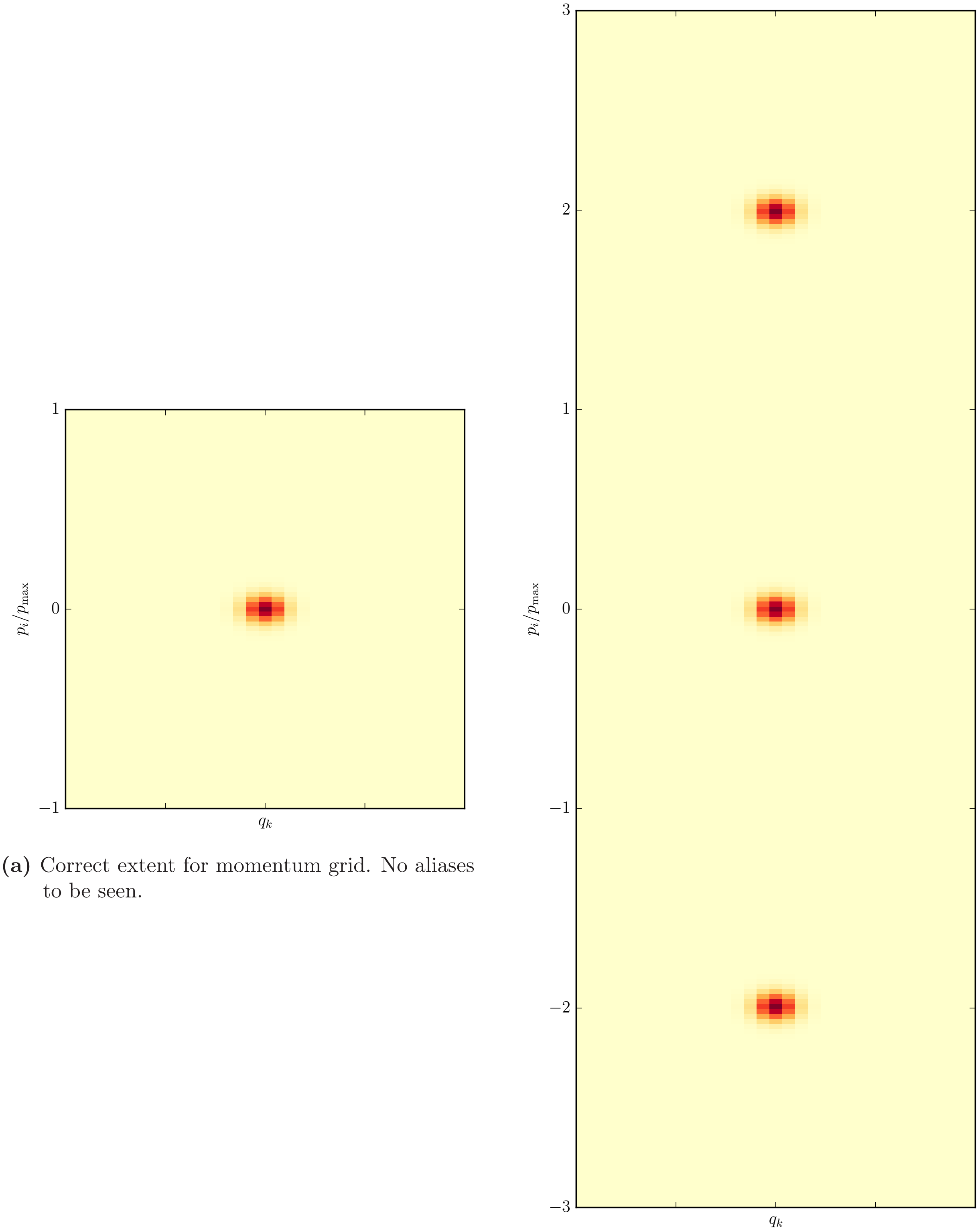

(a) Correct extent for momentum grid. No aliases to be seen.

(b) Incorrect extent for momentum grid. Two aliases are visible.

Figure 3.7: Aliasing of the magnitude of the partially integrated HK integrand in momentum space for a harmonic oscillator. Intended solely as a sketch, so no axis values or color bars are provided. For demonstration purposes, some parameters differ from the values in table 3.1 on page 43.

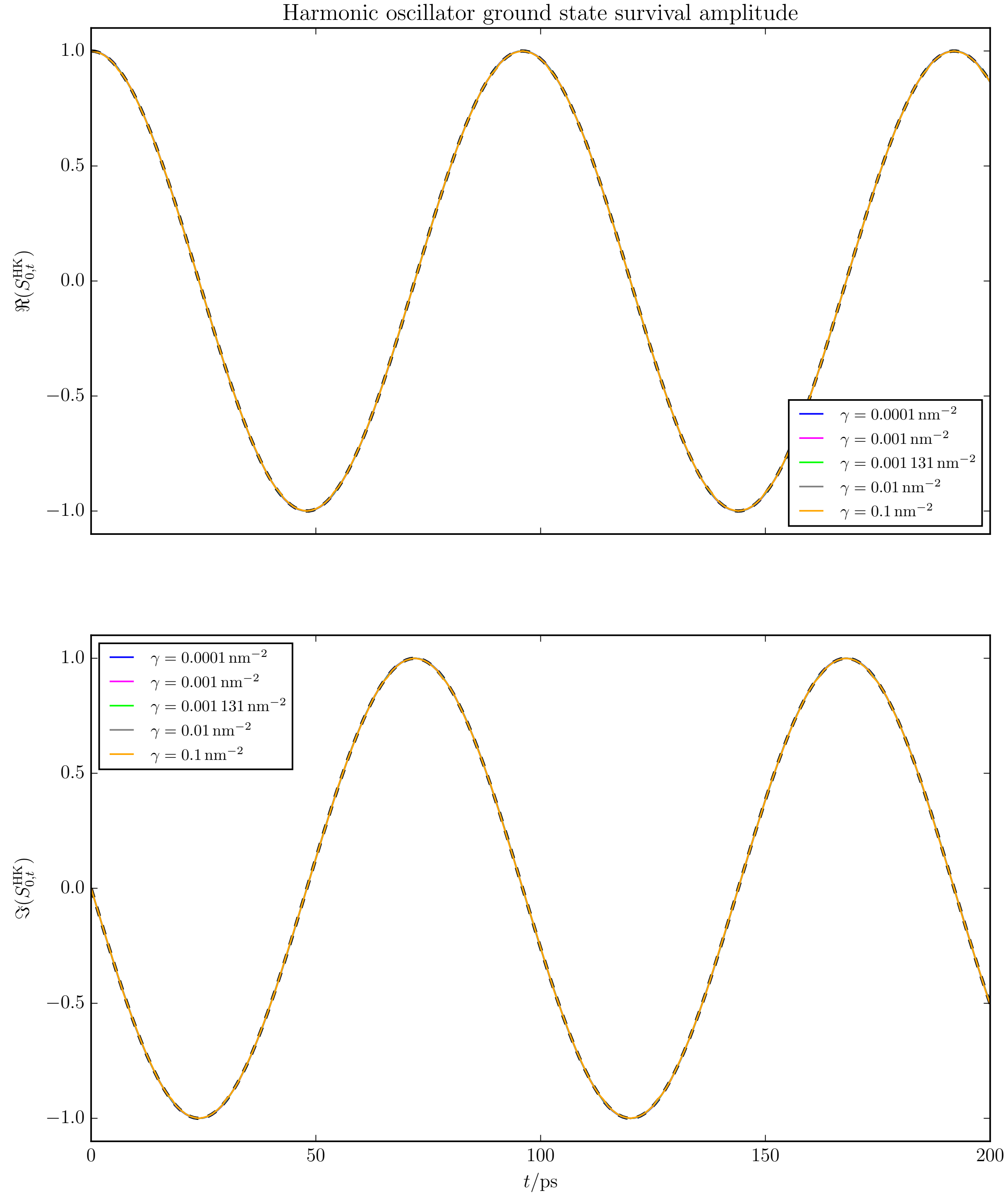

Figure 3.8: Harmonic oscillator ground state survival amplitude with converged parameters. Dashed curves indicate the exact answers.

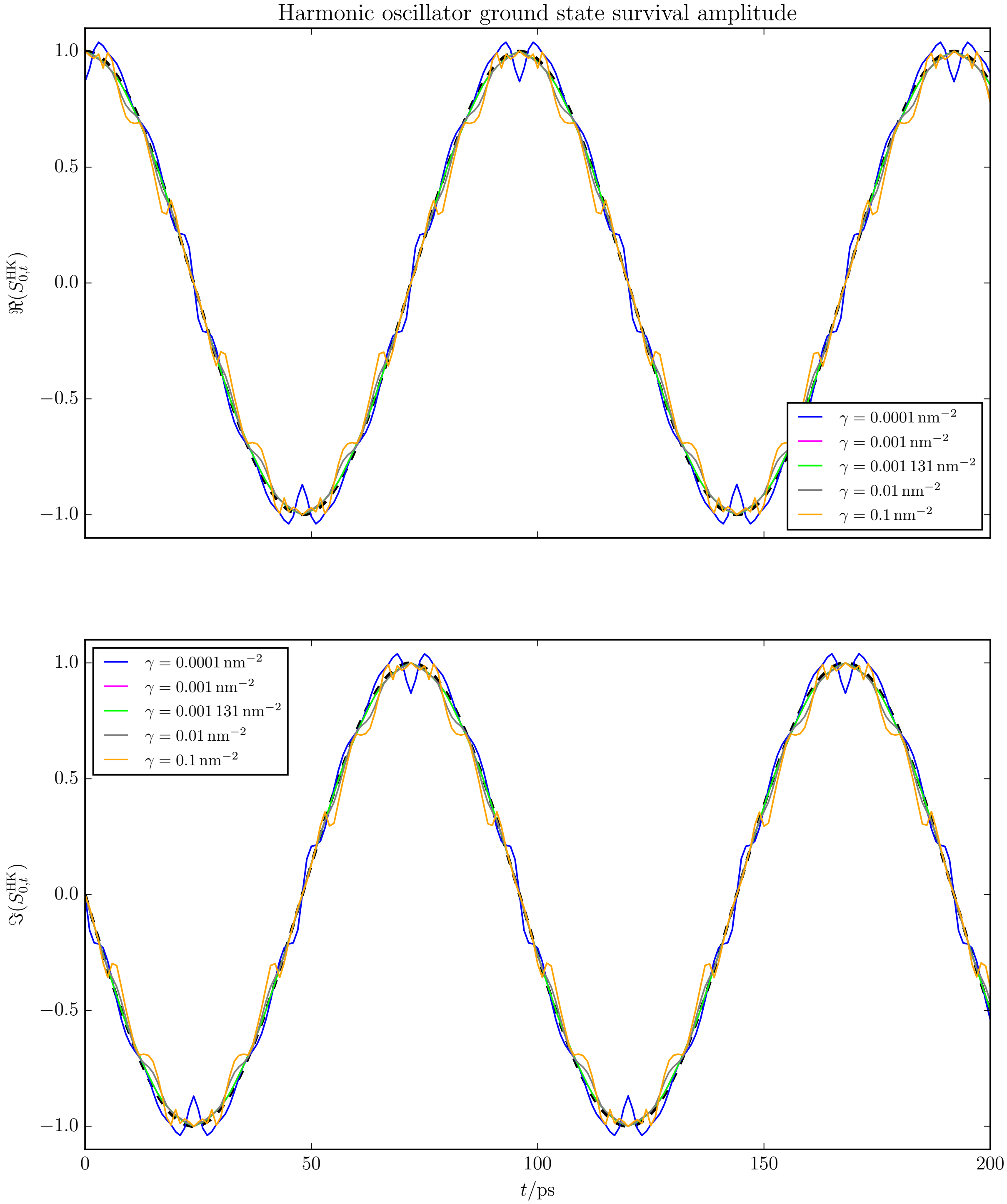

Figure 3.9: Harmonic oscillator ground state survival amplitude with unconverged parameters. Dashed curves indicate the exact answers.

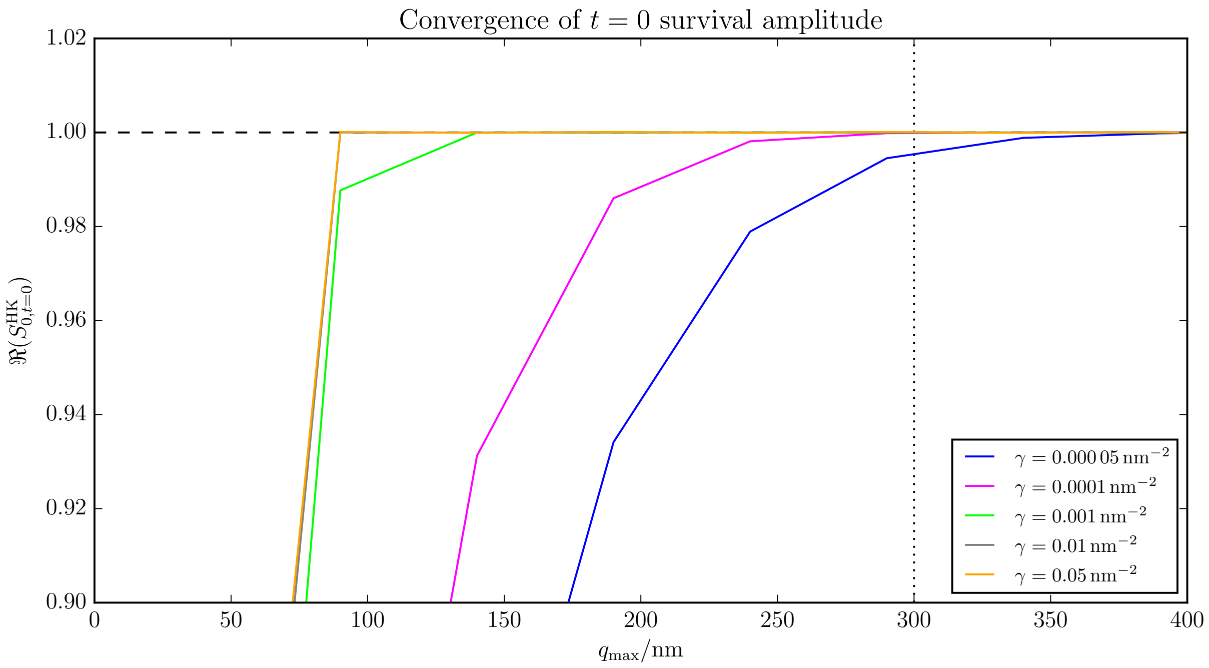

(a) Convergence of $t = 0$ survival amplitude with $q_{\max}$.

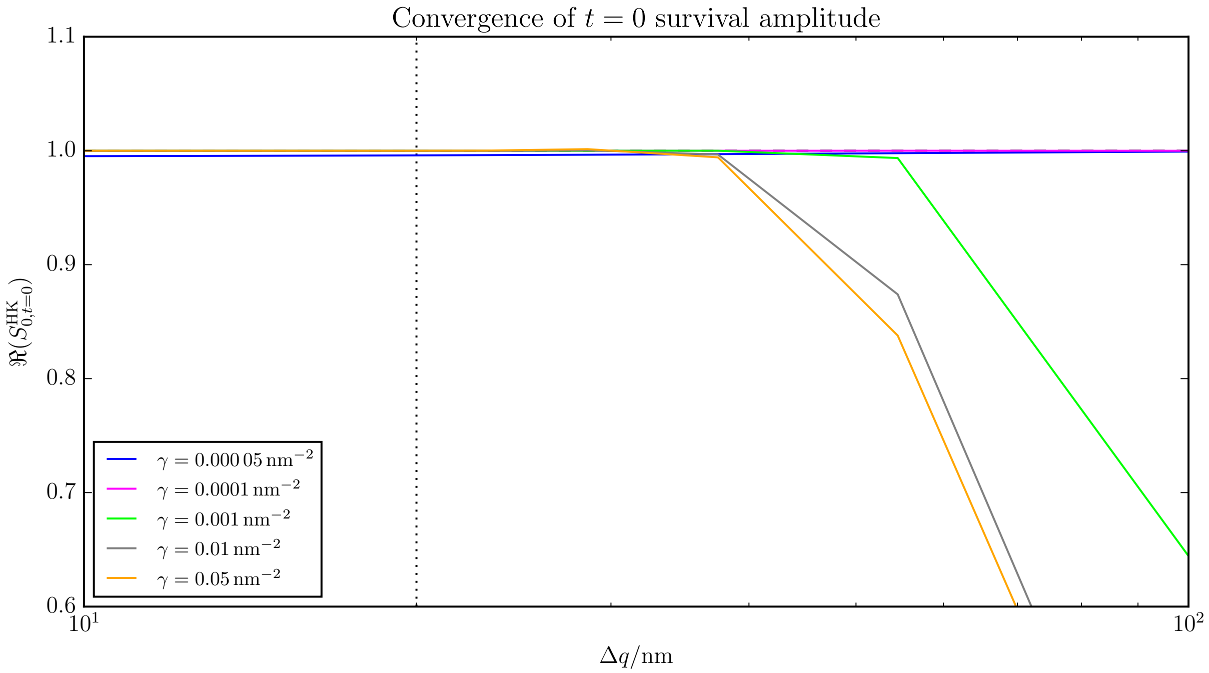

(b) Convergence of $t = 0$ survival amplitude with Δq.

Figure 3.10: Convergence of $t = 0$ survival amplitude with the $\{q_{\max}, \Delta q\}$ grid for a double well. Dashed lines indicate the exact answer; dotted lines mark the values in table 3.1 on page 43.

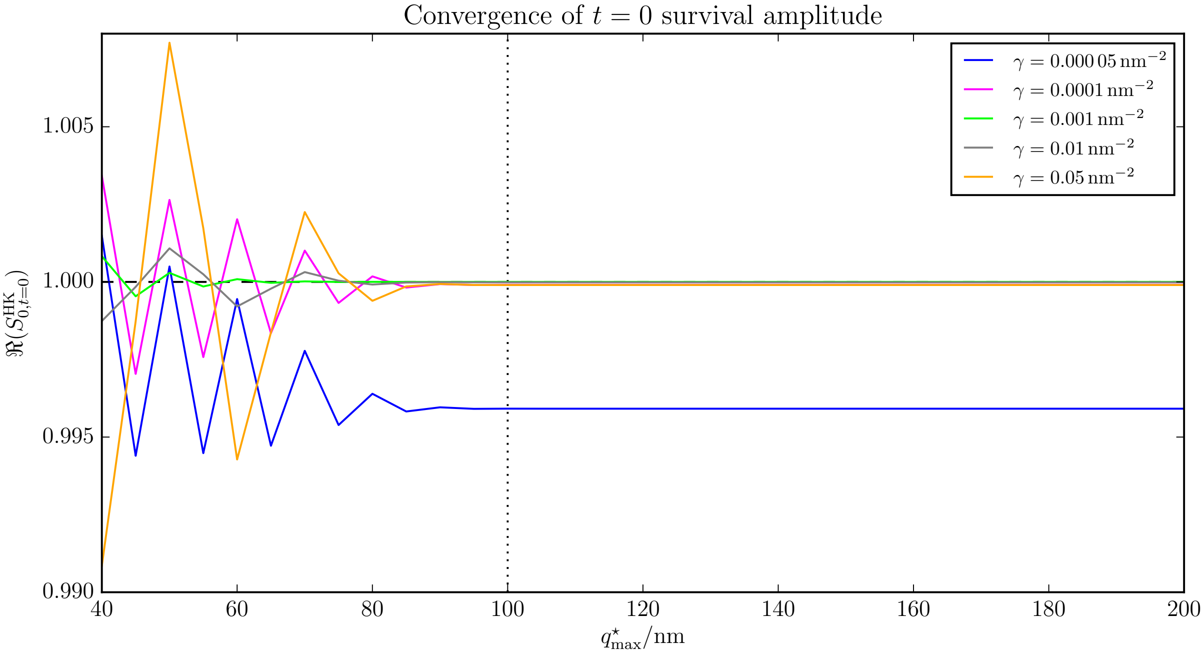

(a) Convergence of $t = 0$ survival amplitude with $q^\star_{\max}$.

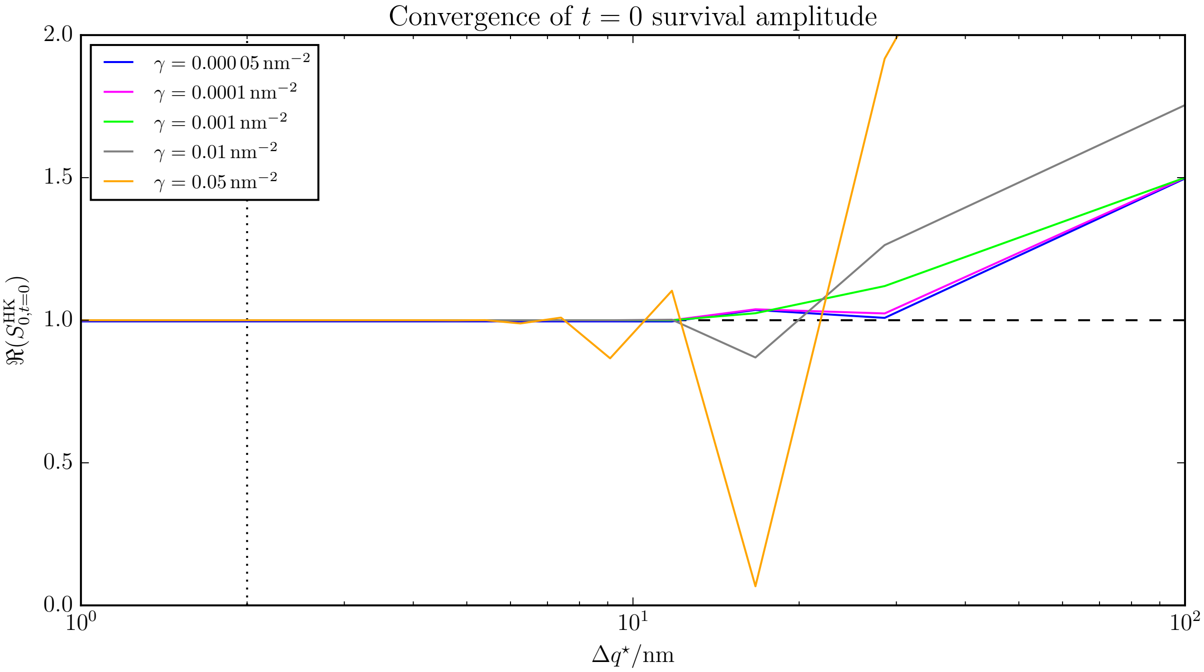

(b) Convergence of $t = 0$ survival amplitude with $\Delta q^\star$.

Figure 3.11: Convergence of $t = 0$ survival amplitude with the $\{q^\star_{\max}, \Delta q^\star\}$ grid for a double well. Dashed lines indicate the exact answer; dotted lines mark the values in table 3.1 on page 43.

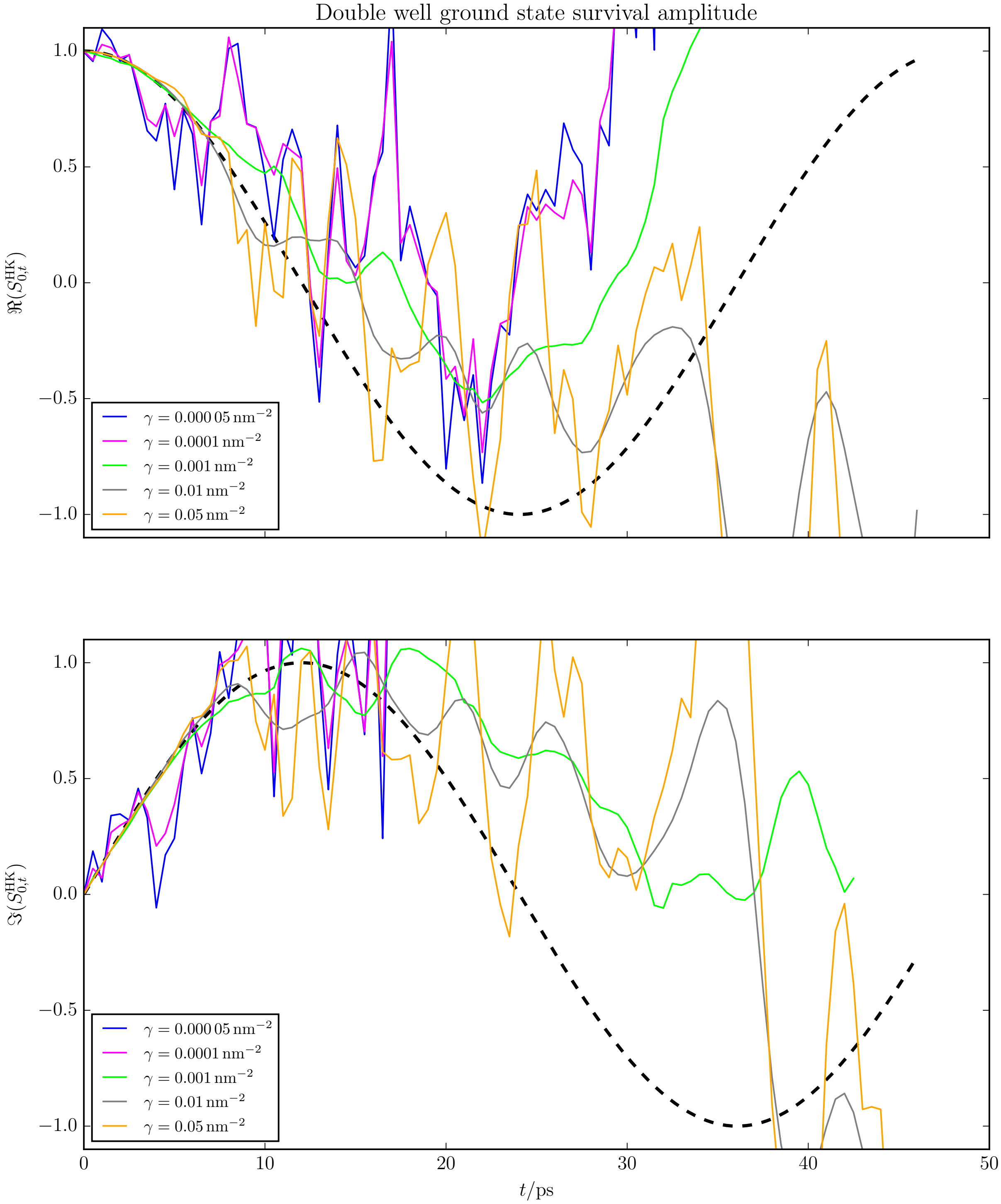

Figure 3.12: Double well ground state survival amplitude with poor parameters. Dashed curves indicate the exact answers.

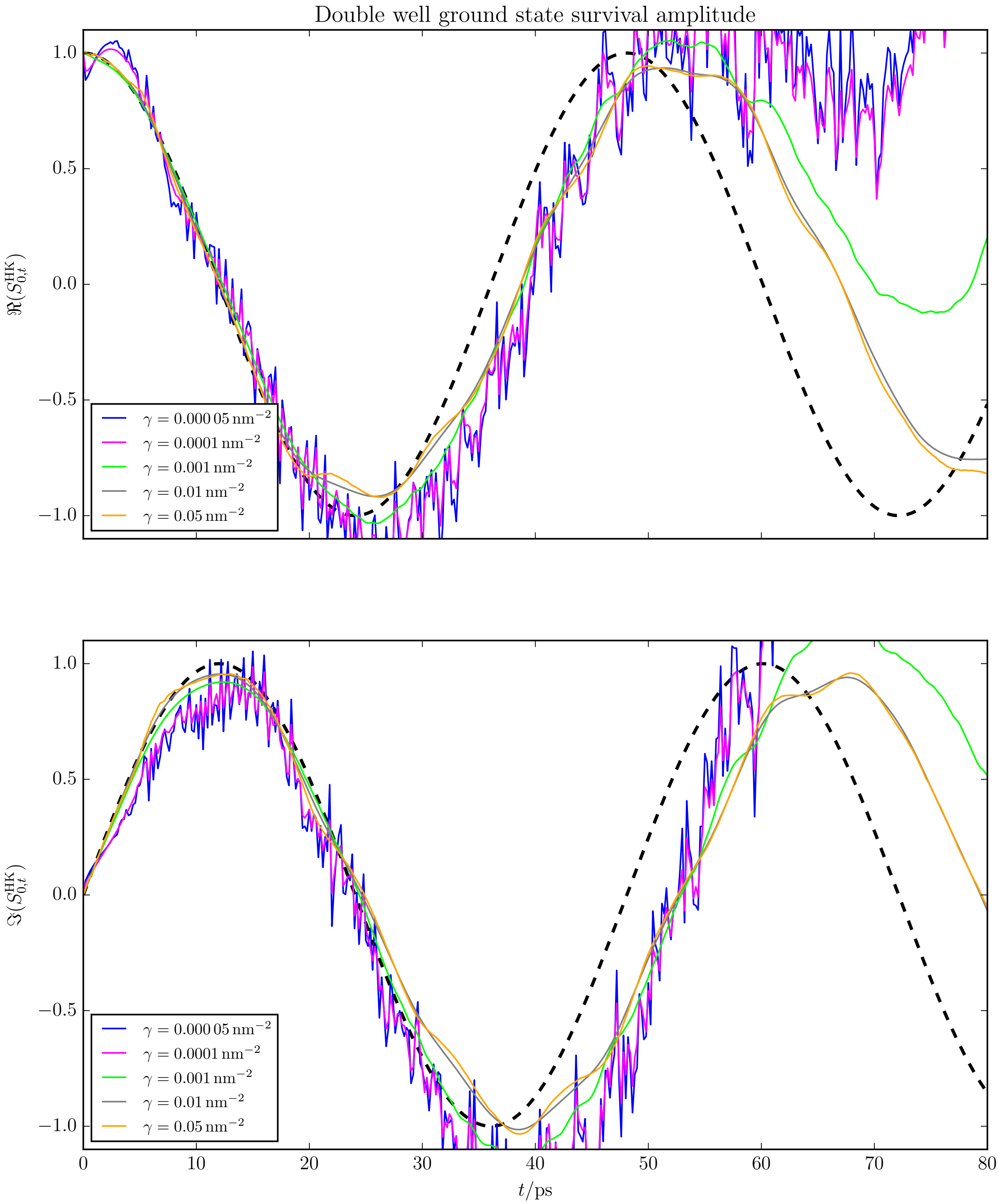

Figure 3.13: Double well ground state survival amplitude with improved parameters. Dashed curves indicate the exact answers.

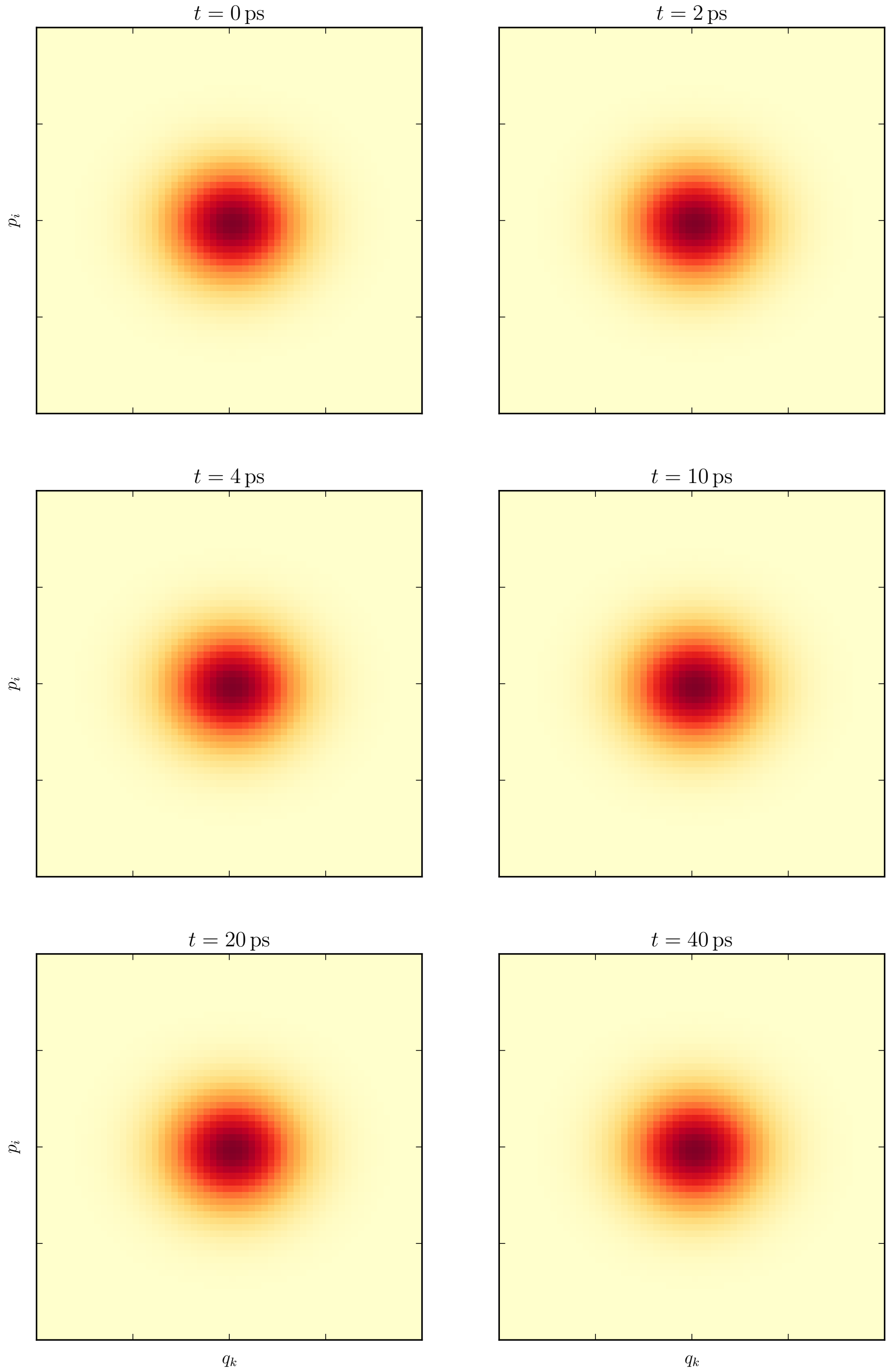

Figure 3.14: Time evolution of the magnitude of the partially integrated HK integrand for a harmonic oscillator. Intended solely as a sketch, so no axis values or color bars are provided. For demonstration purposes, some parameters differ from the values in table 3.1 on page 43.

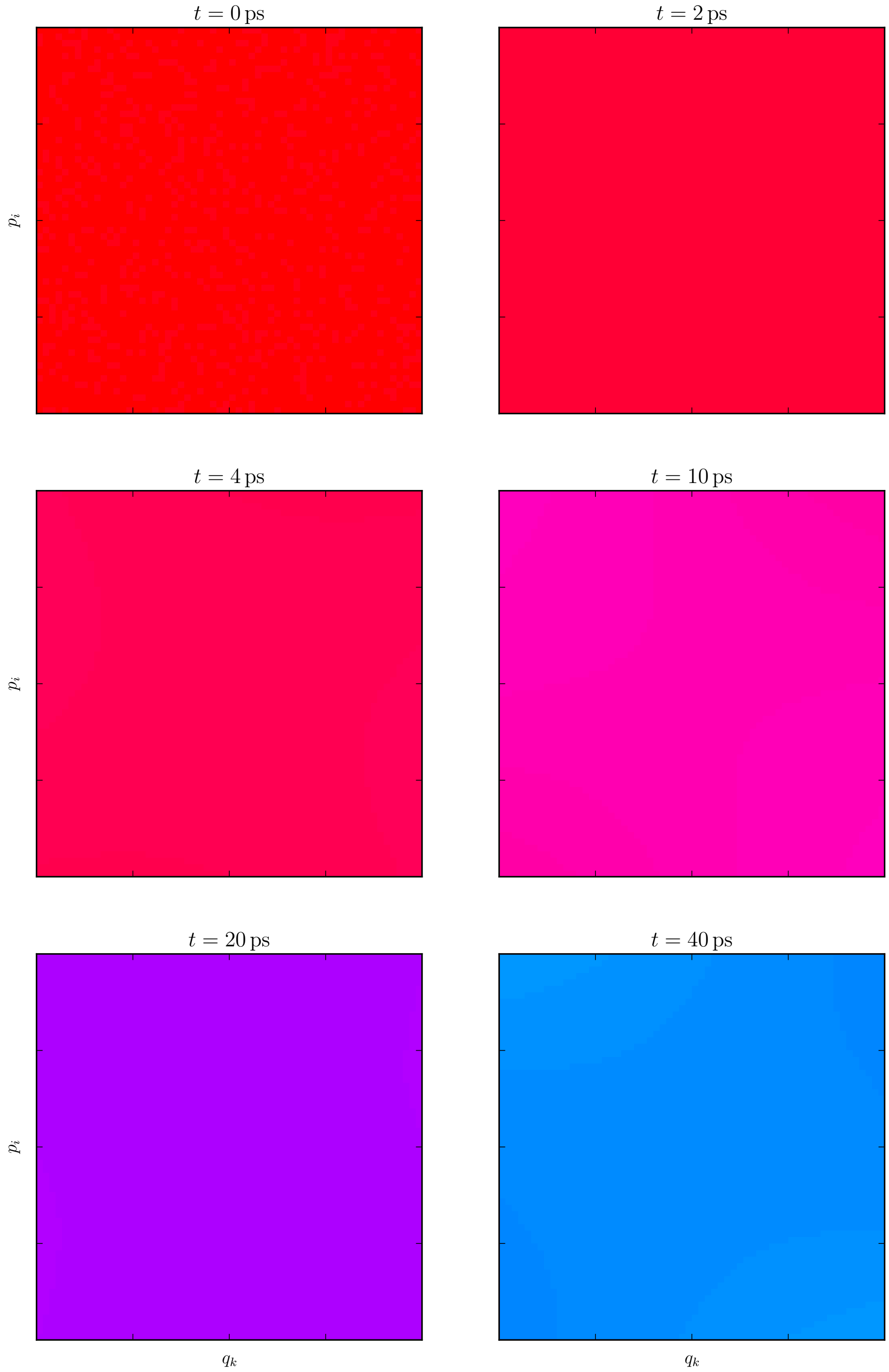

Figure 3.15: Time evolution of the phase of the partially integrated HK integrand for a harmonic oscillator. Intended solely as a sketch, so no axis values or color bars are provided. For demonstration purposes, some parameters differ from the values in table 3.1 on page 43.

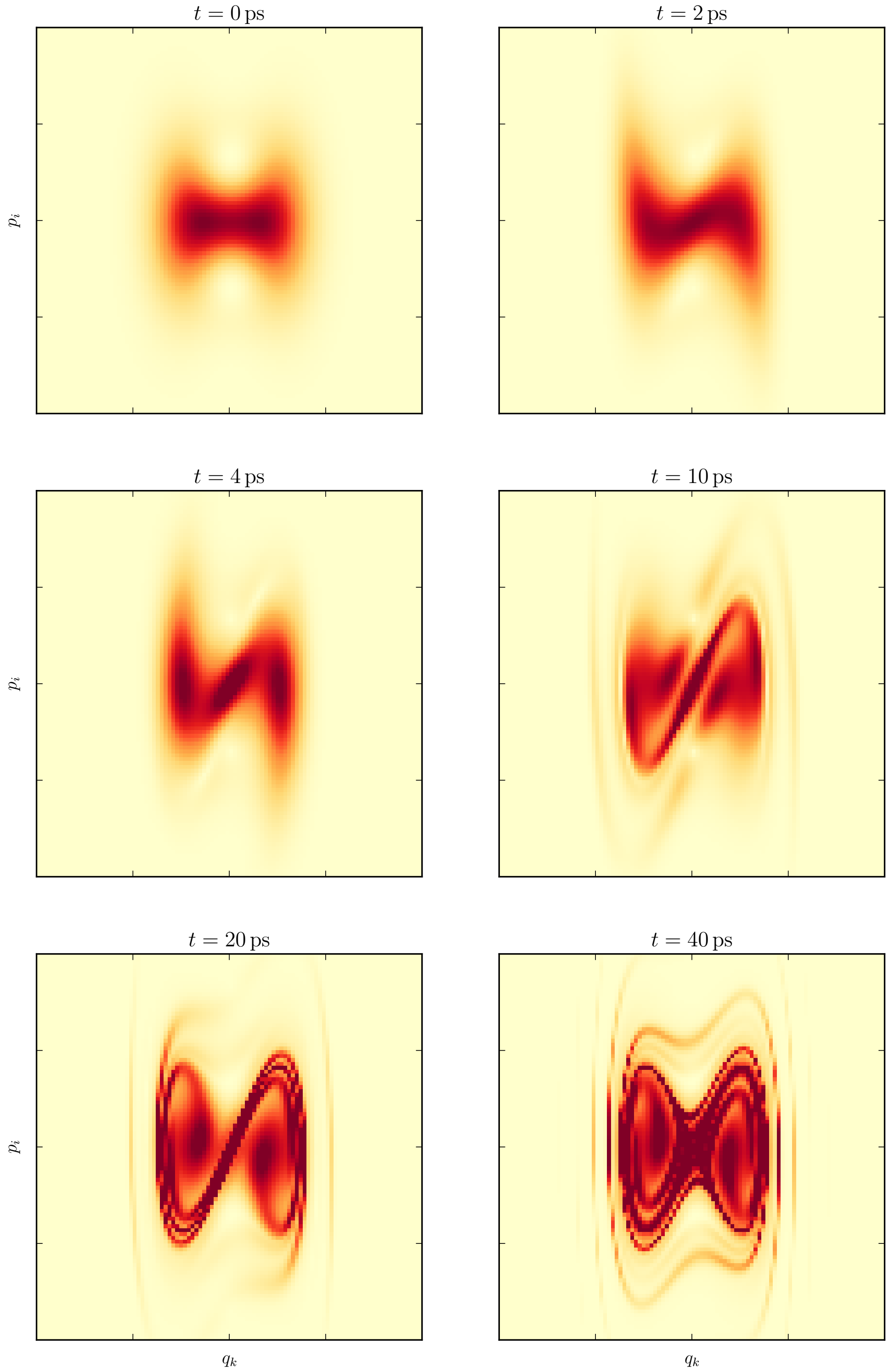

Figure 3.16: Time evolution of the magnitude of the partially integrated HK integrand for a double well. Intended solely as a sketch, so no axis values or color bars are provided. Some of the extremely large values at later times are clipped to better demonstrate the resulting shape.

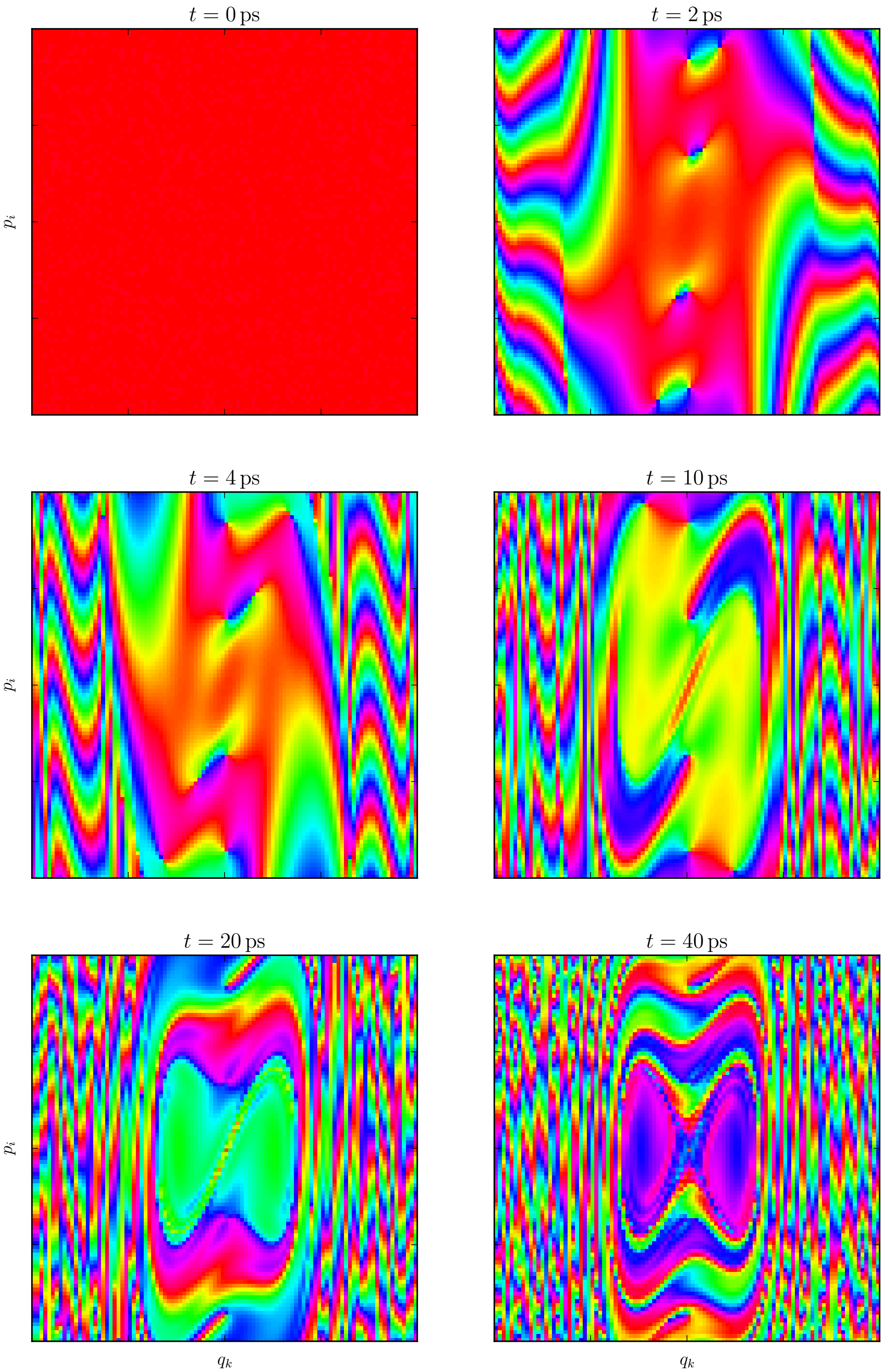

Figure 3.17: Time evolution of the phase of the partially integrated HK integrand for a double well. Intended solely as a sketch, so no axis values or color bars are provided.

3.2 Stochastic integration

The results of this section were found in collaboration with Neil Raymond.

Most interesting problems will be too large for us to find their survival amplitudes by direct integration, so we are forced to use a stochastic method. The main issue is that there is no obvious sampling distribution for the momenta. One cannot, after all, uniformly sample from $[-\infty, \infty]$! In order to remedy this problem, we introduce a Gaussian weight into the integrand.

Our goal is still to obtain the value of the integrals in eq. (3.17d) on page 37, but this time without constructing grids. Once we add the Gaussian weight, we obtain the expression

$$S_0^{\mathrm{HK,G}}(t) = \frac{1}{2\pi\hbar} \iiiint \mathrm{d}p\, \mathrm{d}q_{\mathrm{L}}\, \mathrm{d}q\, \mathrm{d}q_{\mathrm{R}}\, R_t^{p,q} \langle 0|q_{\mathrm{L}}\rangle \langle q_{\mathrm{R}}|0\rangle \exp\left[-\frac{\gamma}{2}\left((q_{\mathrm{L}} - q_t^{p,q})^2 + (q_{\mathrm{R}} - q)^2\right)\right] \\ \times \exp\left[-\frac{p^2}{2\sigma_p^2} + \frac{i}{\hbar}\left(S_t^{p,q} + p_t^{p,q}(q_{\mathrm{L}} - q_t^{p,q}) - p(q_{\mathrm{R}} - q)\right)\right]. \tag{3.28}$$

This introduces σ_p, which is yet another parameter, but that is not as bad as it might seem at first: the trade-off is that we no longer have all the grid parameters to tune. Additionally, we choose γ so that we are able to sample all three position coordinates from the same PIGS simulation.

Recall that we may evaluate integrals of the form

$$\frac{\int \mathrm{d}\mathbf{q}\, \pi(\mathbf{q})\mathcal{S}(\mathbf{q})}{\int \mathrm{d}\mathbf{q}\, \pi(\mathbf{q})} \tag{3.29}$$

by sampling from $\pi(\mathbf{q})$ and evaluating $\mathcal{S}(\mathbf{q})$ at the sampled coordinates. Consider the distribution

$$\pi_q(q^{(L)}, q^{(M)}, q^{(R)}) = \langle 0|q^{(L)}\rangle \exp\left[-\frac{m}{2\hbar^2\tau}\left(\left(q^{(L)} - q^{(M)}\right)^2 + \left(q^{(M)} - q^{(R)}\right)^2\right)\right] \langle q^{(R)}|0\rangle\,, \tag{3.30}$$

which we have written in a suggestive form (with $L = M - 1$ and $R = M + 1$). What it suggests is the path drawn in fig. 3.18, which is a complete path in the sense that its beads are all connected, but it lacks the interactions from the two links of interest.[‡] Consider also the distribution

$$\pi_p(p) = \exp\left[-\frac{p^2}{2\sigma_p^2}\right], \tag{3.31}$$

which we combine with the previous one to make the product distribution

$$\begin{aligned} &\pi(p, q^{(L)}, q^{(M)}, q^{(R)}) \\ &= \pi_p(p)\pi_q(q^{(L)}, q^{(M)}, q^{(R)}) && (3.32a) \\ &= \exp\left[-\frac{p^2}{2\sigma_p^2}\right] \langle 0|q^{(L)}\rangle \exp\left[-\frac{m}{2\hbar^2\tau}\left((q^{(L)} - q^{(M)})^2 + (q^{(M)} - q^{(R)})^2\right)\right] \langle q^{(R)}|0\rangle\,. && (3.32b) \end{aligned}$$

[‡] One subtlety here is that we must expand each of the wavefunctions $\langle q|0\rangle$ into fragments of length $(\beta - \tau)/2$ instead of the usual $\beta/2$, because the piece in the middle is of "length" 2τ and we still require the full path to be β long.

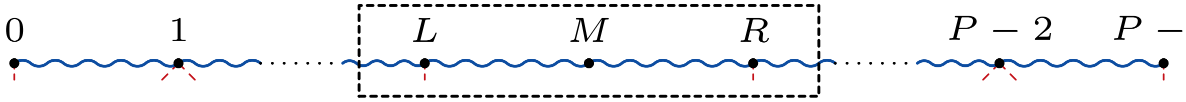

Figure 3.18: Details of the graphical notation used for the survival amplitude. Dashed box indicates the region of interest.

Because they are obtained from a LePIGS simulation, the wavefunctions $\langle q|0\rangle$ will not be normalized. However, due to the deformation, we are not interested in the normalization, so we may disregard it and write

$$\begin{aligned} S_0^{\mathrm{HK,G}}(t) \propto \iiiint \mathrm{d}p\,\mathrm{d}q^{(L)}\,\mathrm{d}q^{(M)}\,\mathrm{d}q^{(R)}\,\pi(p, q^{(L)}, q^{(M)}, q^{(R)}) R_t^{p,q^{(M)}} \\ \times \exp\left[-\frac{m}{2\hbar^2\tau}\left(\left(q^{(L)} - q_t^{p,q^{(M)}}\right)^2 - \left(q^{(L)} - q^{(M)}\right)^2\right)\right] \\ \times \exp\left[\frac{i}{\hbar}\left(S_t^{p,q^{(M)}} + p_t^{p,q^{(M)}}\left(q^{(L)} - q_t^{p,q^{(M)}}\right) - p\left(q^{(R)} - q^{(M)}\right)\right)\right]. \end{aligned} \tag{3.33}$$

We have explicitly chosen $\gamma = m/\hbar^2\tau$, and as a result our estimator is

$$\begin{aligned} &\mathcal{S}_{\mathrm{P}}(p, q^{(L)}, q^{(M)}, q^{(R)}, t) \\ &= R_t^{p,q^{(M)}} \exp\left[-\frac{m}{2\hbar^2\tau}\left(\left(q^{(L)} - q_t^{p,q^{(M)}}\right)^2 - \left(q^{(L)} - q^{(M)}\right)^2\right)\right] \\ &\qquad \times \exp\left[\frac{i}{\hbar}\left(S_t^{p,q^{(M)}} + p_t^{p,q^{(M)}}\left(q^{(L)} - q_t^{p,q^{(M)}}\right) - p\left(q^{(R)} - q^{(M)}\right)\right)\right]. \end{aligned} \tag{3.34}$$

Since this is the obvious estimator to use, we will refer to it as the *primitive estimator of the survival amplitude*, with the position distribution

$$\pi_{\mathrm{P}}(q^{(L)}, q^{(M)}, q^{(R)}) = \tag{3.35}$$

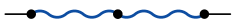

We notice that even though we have preemptively removed the extraneous potentials from the distribution, we still have a spring contribution that we remove in the estimator. If we excise it, we are left with the position distribution

$$\pi_{\mathrm{M}}(q^{(L)}, q^{(M)}, q^{(R)}) = \tag{3.36}$$

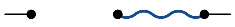

and the corresponding *minimal estimator of the survival amplitude*

$$\begin{aligned} \mathcal{S}_{\mathrm{M}}(p, q^{(L)}, q^{(M)}, q^{(R)}, t) = R_t^{p,q^{(M)}} \exp\left[-\frac{m}{2\hbar^2\tau}\left(q^{(L)} - q_t^{p,q^{(M)}}\right)^2\right] \\ \times \exp\left[\frac{i}{\hbar}\left(S_t^{p,q^{(M)}} + p_t^{p,q^{(M)}}\left(q^{(L)} - q_t^{p,q^{(M)}}\right) - p\left(q^{(R)} - q^{(M)}\right)\right)\right]. \end{aligned} \tag{3.37}$$

We hope that the reader is not biased toward or against any estimator names due to the results of chapter 2.

β/K^{-1}	τ/K^{-1}	P	$\Delta t/\mathrm{ps}$	$\gamma^{(0)}/\mathrm{ps}^{-1}$	$\Delta t^{\star}/\mathrm{ps}$	$\sigma_p/\mathrm{g\,nm\,ps^{-1}\,mol^{-1}}$
8	0.125	65	1	0.1	1	1

Table 3.4: Selected parameters for the harmonic oscillator model system using the stochastic method.

3.2.1 Harmonic oscillator

Before we try this stochastic approach with the harmonic oscillator system from section 3.1.1, we can see (using the numerical method used previously) what happens when we deform the integral with the Gaussian weight and then explicitly renormalize the survival amplitude. Unless otherwise specified, the parameter values from table 3.4 are used for this model system. The results shown in fig. 3.19 are very good over a wide range of σ_p.[‡] Thus, we may expect that performing the same deformed integral using the stochastic method would result in a smooth survival amplitude.

On the contrary, we find the disappointing result in fig. 3.20. The overall frequency appears to be correct, but the shapes of both the real and imaginary components are distorted, and the error bars are incredibly large at some points. One may suspect that this is due to a poor choice of parameters in the LePIGS simulation. However, for the harmonic oscillator system, we can sample from $\pi_q(q^{(L)}, q^{(M)}, q^{(R)})$ in eq. (3.30) directly, since it is Gaussian:

$$\pi_q(q^{(L)}, q^{(M)}, q^{(R)}) \propto \exp\left[-\frac{m\omega}{2\hbar}\left(\left(q^{(L)}\right)^2 + \left(q^{(R)}\right)^2\right)\right] \times \exp\left[-\frac{m}{2\hbar^2\tau}\left(\left(q^{(L)} - q^{(M)}\right)^2 + \left(q^{(M)} - q^{(R)}\right)^2\right)\right]. \tag{3.38}$$

This allows us to bypass PIGS altogether and see what the survival amplitude should look like given a finite number of samples. As we see in fig. 3.21, the situation was hopeless to start with.

The minimal estimator fares much better, as shown in fig. 3.22. All the error bars are fairly small and the mean values are mostly along smooth curves. Again, we get much better results if we break paths in the simulation and sample from a different sector. Perhaps surprising in this particular case is the fact that $\pi_{\mathrm{M}}(q^{(L)}, q^{(M)}, q^{(R)})$ is composed of two independent pieces!

We have not yet attempted to apply the stochastic approach to the double well system from section 3.1.2. Although we do not know of any *a priori* reasons it should fail, our efforts for that system have been focused on first improving the numerical integration results.

[‡] In fact, for the narrowest momentum distribution, we end up using only a single momentum: zero. Yet the harmonic oscillator is fine with this.

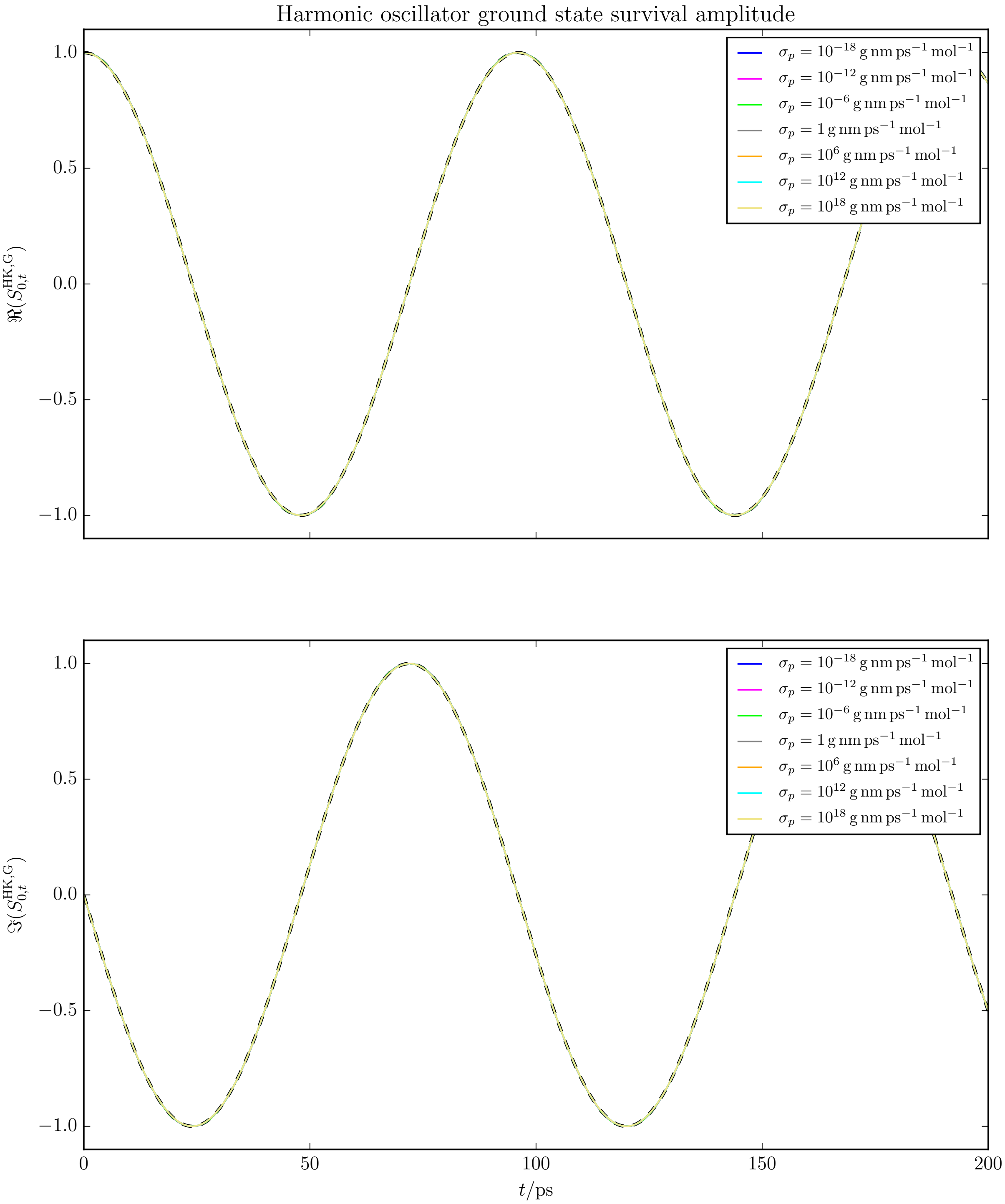

Figure 3.19: Harmonic oscillator ground state survival amplitude with added Gaussian weight and renormalization. Dashed curves indicate the exact answer.

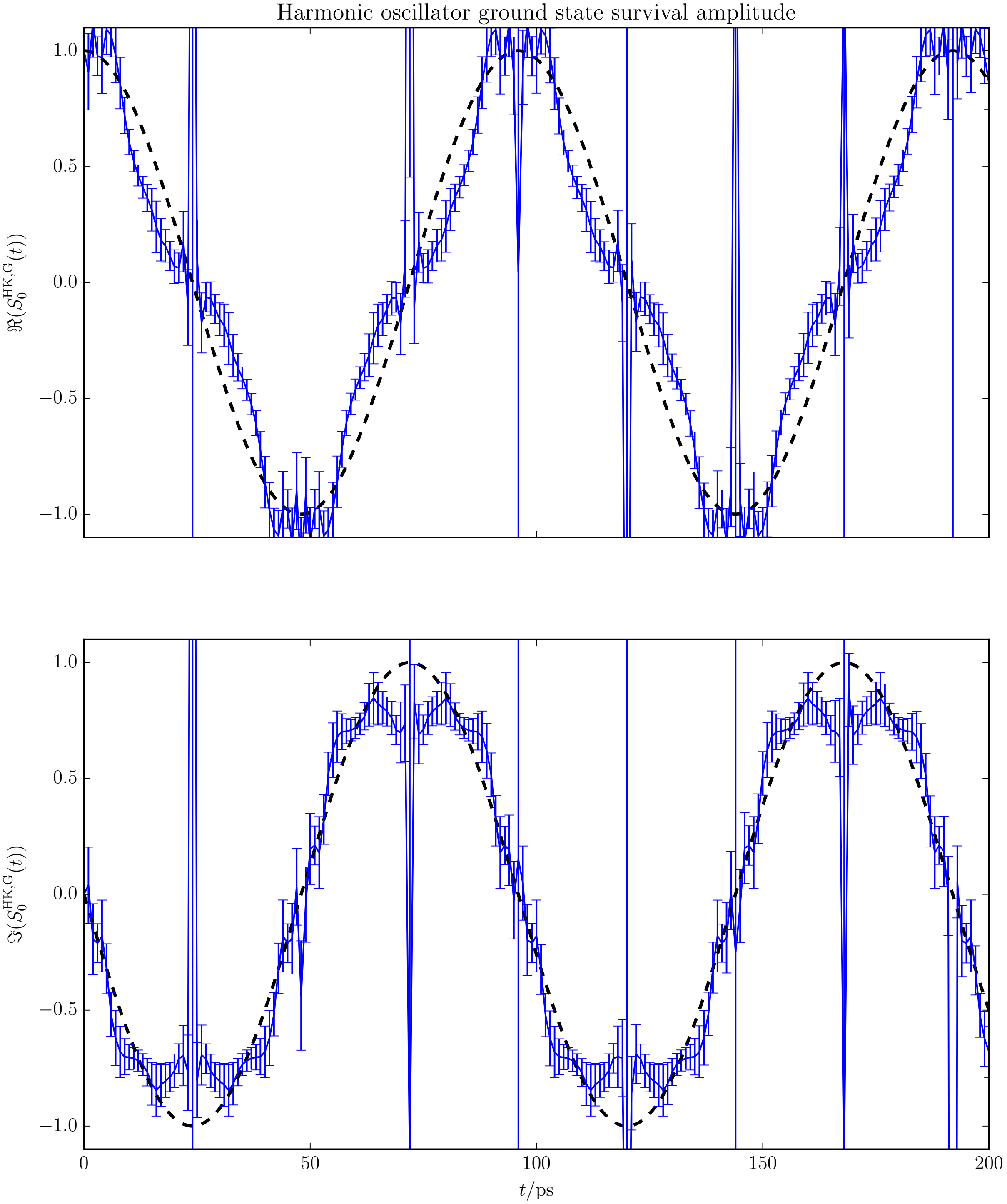

Figure 3.20: Harmonic oscillator ground state survival amplitude with stochastic sampling using the primitive estimator. Average of 16 survival amplitudes from 10^6 samples each. Dashed curves indicate the exact answer.

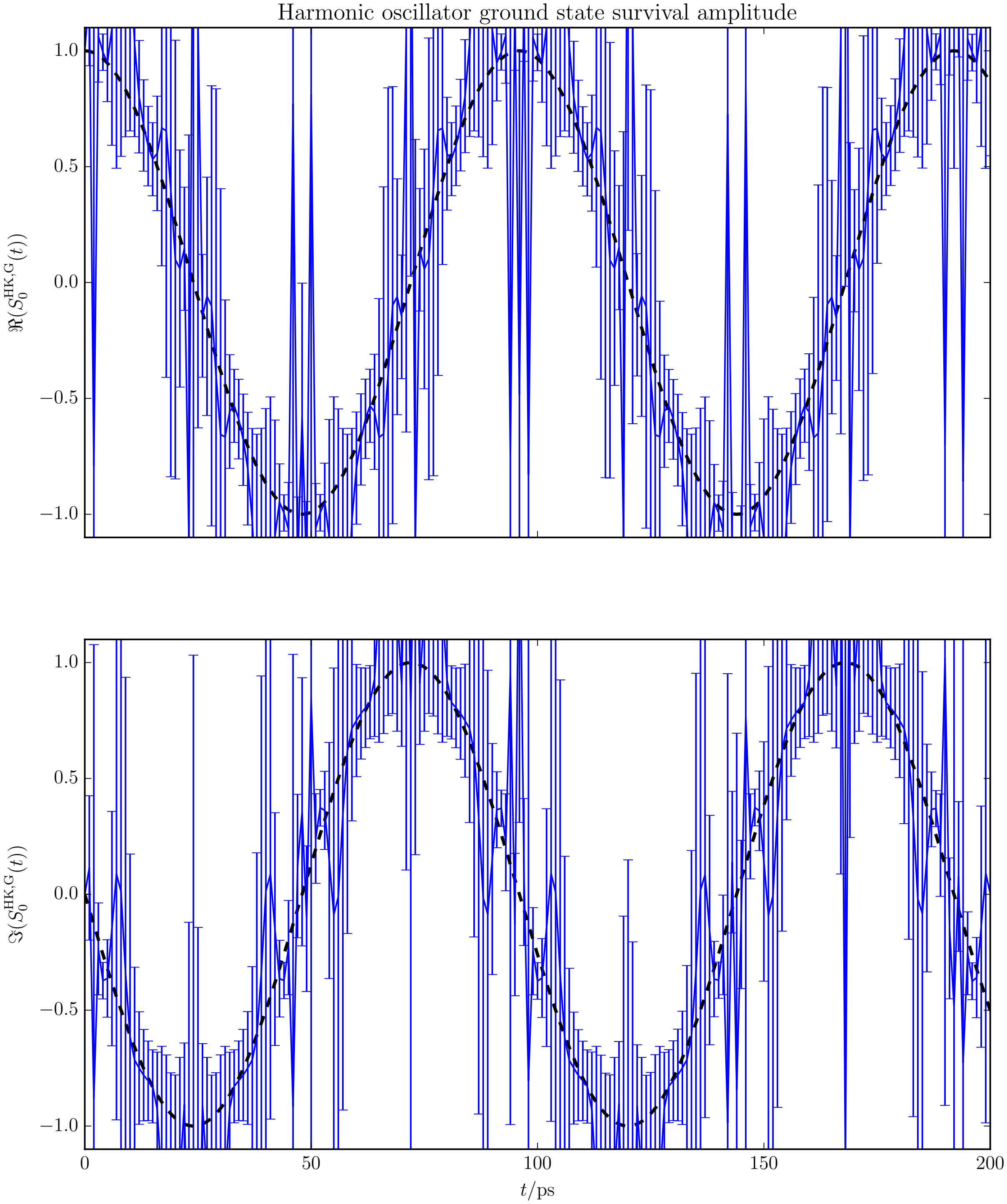

Figure 3.21: Harmonic oscillator ground state survival amplitude with exact stochastic sampling using the primitive estimator. Average of 16 survival amplitudes from 10^6 samples each. Dashed curves indicate the exact answer.

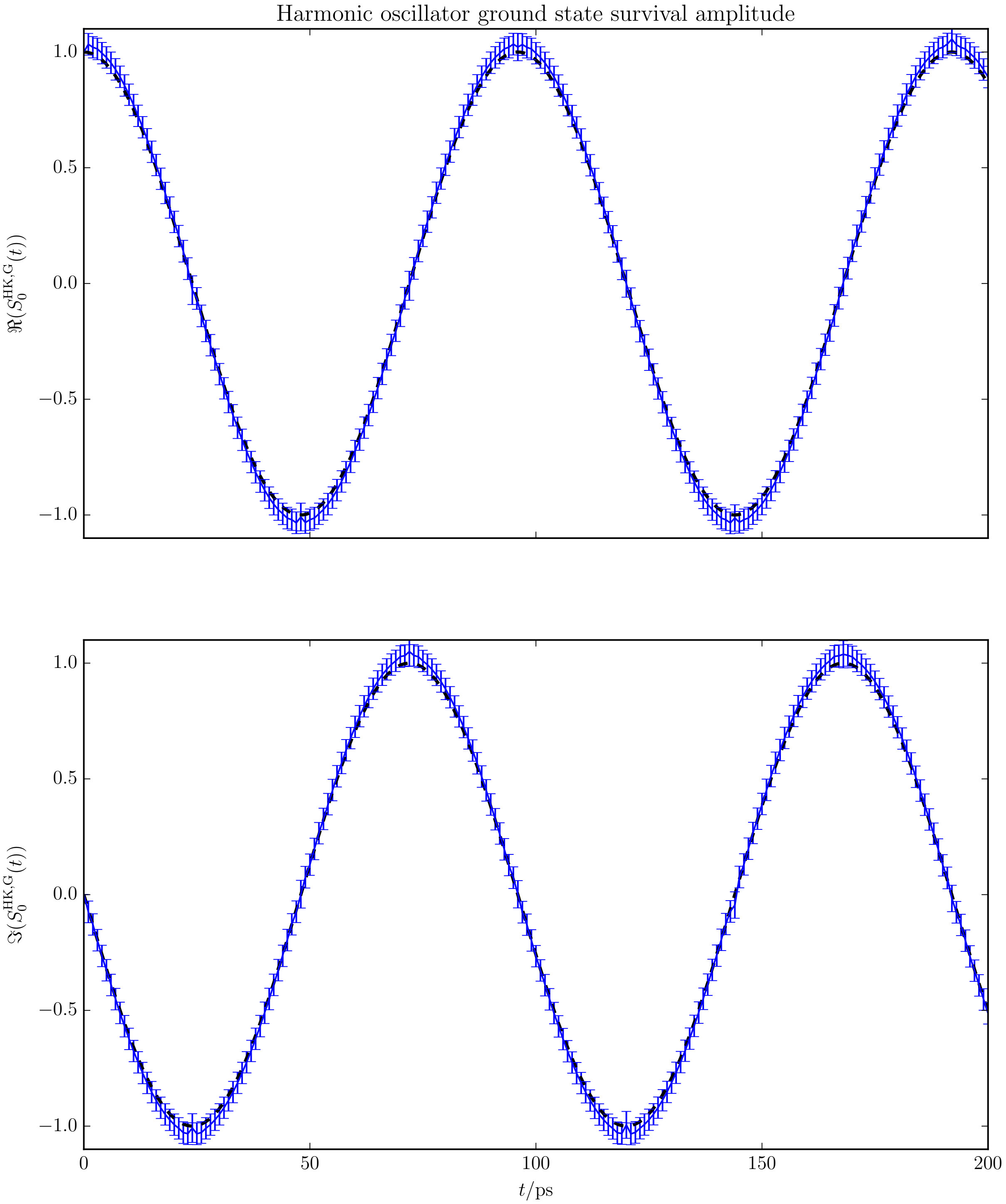

Figure 3.22: Harmonic oscillator ground state survival amplitude with stochastic sampling using the minimal estimator. Average of 16 survival amplitudes from 10^6 samples each. Dashed curves indicate the exact answer.

Chapter 4

Conclusion

4.1 Summary

We have shown that it is possible to obtain the second Rényi entropy S_2 for use as a measure of particle entanglement from PIMD simulations using LePIGS. First, we demonstrated that it is futile to attempt this with the replica trick using simulations in the Z-sector. Then we added to MMTK the capability to change sectors and successfully used the replica trick along with a modified sampling distribution to efficiently sample the entropy. So far, we have only done this for a simple model system, but the implementation should be directly applicable to more interesting systems, such as molecular clusters.

We have also combined the Herman–Kluk SC-IVR propagator with wavefunctions in the position representation to obtain ground state survival amplitudes. This worked well for the harmonic oscillator, using both direct numerical integration and the stochastic LePIGS approach. As with the entanglement entropy, we showed that improved results are possible if one is willing to move away from the Z-sector. Unfortunately, we were not able to obtain acceptable results for the double well system.

4.2 Future work

The natural next step for both methods is the application to chemical systems. Such systems include molecular dimers and trimers, as well as entire molecular clusters. For example, we would like to compare the Lindemann criterion for determining whether a cluster is “solid-like” or “liquid-like” [SCI14] to the Rényi entropy to investigate any connections between the structure of and entanglement within clusters. Since the clusters in question would be composed of bosons, we would have to add updates to our simulations in order to preserve permutation symmetry [HIR14], but the major part of the implementation for this is already in place.

4.2.1 Entanglement entropy

In addition to particle entanglement, it is also possible to partition space rather than particles and investigate *spatial entanglement* [HIR14]. Since the necessary connectivity updates for spatial entanglement are coupled to the spatial moves, they are non-trivial to implement in a molecular dynamics framework, which does not reject any updates. It may be necessary to reset the momenta after a rejected update, as described in ref. [Tuc10, p. 296].

The present work is restricted to ground state systems, but it is also interesting (perhaps more interesting) to look at finite-temperature systems. One quantity used a measure of entanglement in thermal systems is the *mutual information*, and it may be obtained from the Rényi entropy [SHK11]. Thus, there is hope that we will be able to use the replica trick in MMTK to estimate mutual information for finite-temperature systems.

4.2.2 Real-time correlation functions

Although the method for ground state survival amplitudes appears to fail for the strongly anharmonic double well system, we would like to see how effective it is for mildly anharmonic ones, such as those with quartic or Lennard-Jones interactions.

Finally, we have only considered survival amplitudes in the present work, but it should be straightforward to incorporate operators that are diagonal in the position representation in order to calculate correlation functions. It is these correlation functions which may be used to find various spectra associated with molecular systems.

Chapter 5

Bonus content

This chapter contains some results which are not related to the overall theme of the thesis, but are nevertheless interesting.

5.1 Integration of radial distribution

The simplest structural property of fluids is the *radial* (or *pair*) *distribution function* $g(r)$, which describes the local density $\varrho(r)$ relative to the bulk density ϱ at a distance r away from a fixed particle in a fluid [McQ76, pp. 257-259],[AT89, pp. 54-55]. It is obtained from the distribution $g(\mathbf{q}_1, \mathbf{q}_2, \dots, \mathbf{q}_N)$ of all N particles by integrating over all the positions except $\mathbf{q}_1$ and $\mathbf{q}_2$, giving the function $g(\mathbf{q}_1, \mathbf{q}_2)$. We assume that the fluid is homogeneous, so the absolute spatial position of the particles cannot matter, and we write simply $g(r)$, where $r = |\mathbf{q}_1 - \mathbf{q}_2|$ is the distance between the two remaining particles.

It is common to integrate radial distribution functions (perhaps together with other functions of only r) to obtain quantities such as the structure factor or virial coefficients [McQ76, pp. 260,263]. In this section, we investigate the integrals of $g(r)$ in a spherical volume and in a periodic volume.

5.1.1 Spherical volume

Consider two particles with ("space-fixed" frame) positions $\mathbf{q}_1$, $\mathbf{q}_2$ confined to a closed[‡] ball B of radius R centered at the origin. If we have some function $g(|\mathbf{q}_1 - \mathbf{q}_2|)$ that depends only on the relative distance between the two particles, it is natural to use center of mass and relative distance vectors. However, the center of mass vector is mass-weighted and we wish to avoid explicit mass dependence in our expressions. Thus, we will use the simpler vector

$$\mathbf{Q}_2 = \mathbf{q}_2 \tag{5.1}$$

along with the usual

$$\mathbf{r} = \mathbf{q}_1 - \mathbf{q}_2. \tag{5.2}$$

[‡] We could just as well work with an open ball, since a single spherical shell has no effect on the result of integration. However, if we are concrete on this matter, we can be consistent in our choice of $\leq$ or $<$ in the relevant inequalities.

The inverse transformation is

$$\mathbf{q}_1 = \mathbf{Q}_2 + \mathbf{r} \tag{5.3a}$$

$$\mathbf{q}_2 = \mathbf{Q}_2, \tag{5.3b}$$

so the Jacobian determinant for the forward transformation is conveniently

$$\begin{vmatrix} \frac{\partial \mathbf{q}_1}{\partial \mathbf{r}} & \frac{\partial \mathbf{q}_1}{\partial \mathbf{Q}_2} \\ \frac{\partial \mathbf{q}_2}{\partial \mathbf{r}} & \frac{\partial \mathbf{q}_2}{\partial \mathbf{Q}_2} \end{vmatrix} = \begin{vmatrix} \underline{\mathbf{1}} & \underline{\mathbf{1}} \\ \underline{\mathbf{0}} & \underline{\mathbf{1}} \end{vmatrix} = 1. \tag{5.4}$$

In the following, we will write $\mathbf{q}_2$ instead of $\mathbf{Q}_2$.

We want to integrate $g(r)$ over all the space of interest:

$$\mathcal{I}[g(r)] = \int_B \mathrm{d}\mathbf{q}_1 \int_B \mathrm{d}\mathbf{q}_2\, g(|\mathbf{q}_1 - \mathbf{q}_2|) = \int_{B^{(2)}} \mathrm{d}\mathbf{r}\, g(|\mathbf{r}|) \int_{V_{\mathbf{q}_2}(\mathbf{r})} \mathrm{d}\mathbf{q}_2. \tag{5.5}$$

Since the maximum possible separation between the two particles is twice the radius of the original ball, we have introduced $B^{(2)}$, the closed ball of radius $2R$ centered at the origin. We write $V_{\mathbf{q}_2}(\mathbf{r})$ for the (yet to be determined) domain of integration for the inner integral. It should be possible to reduce this integral to a simpler form, as we expect there to be redundant degrees of freedom. Unfortunately, as the expression is currently written, the two integrals are not trivially separable, since the domain of integration over $\mathbf{q}_2$ depends on $\mathbf{r}$. That is, if we allow the separation distance $\mathbf{r}$ to take on any value, then $\mathbf{q}_2$ is constrained by the spherical boundary conditions.

Thankfully, there is a great deal of symmetry in this problem. To exploit it, we represent $\mathbf{r}$ and $\mathbf{q}_2$ in spherical coordinates with radial distances $r, r_2 \in [0, \infty)$, polar angles $\theta_r, \theta_2 \in [0, \pi]$, and azimuthal angles $\varphi_r, \varphi_2 \in [0, 2\pi)$. We can then write the integral as

$$\mathcal{I}[g(r)] = \int_0^{2R} \mathrm{d}r\, r^2 g(r) \int_{-1}^{1} \mathrm{d}\cos\theta_r \int_0^{2\pi} \mathrm{d}\varphi_r \int_{V_{\mathbf{q}_2}(r,\theta_r,\varphi_r)} \mathrm{d}\mathbf{q}_2. \tag{5.6}$$

We now see that if we evaluate everything starting from the second integral sign, we remove all the extraneous degrees of freedom and compress them into an effective Jacobian for the integration over r. If we combine it with the existing Jacobian from the spherical coordinates, we get

$$J(r) = r^2 \int_{-1}^{1} \mathrm{d}\cos\theta_r \int_0^{2\pi} \mathrm{d}\varphi_r \int_{V_{\mathbf{q}_2}(r,\theta_r,\varphi_r)} \mathrm{d}\mathbf{q}_2 \tag{5.7a}$$

$$\mathcal{I}[g(r)] = \int_0^{2R} \mathrm{d}r\, J(r) g(r). \tag{5.7b}$$

It is easier to evaluate $J(r)$ if we reorder the integrals as

$$J(r) = r^2 \int_{-1}^{1} \mathrm{d}\cos\theta_2 \int_0^{2\pi} \mathrm{d}\varphi_2 \int_0^{2\pi} \mathrm{d}\varphi_r \int_{V_{\theta_r}(r)} \mathrm{d}\cos\theta_r \int_{V_{r_2}(r,\theta_r)} \mathrm{d}r_2\, r_2^2, \tag{5.8}$$

where we don't yet know the domains of integration for the last two. However, we do know that they can't depend on the variables of the first three integrals. Given some separation distance r, we are free to orient $\mathbf{q}_2$ any way we wish, which accounts for the integrals over θ_2 and φ_2. For the sake of visualization, it is convenient to fix $\mathbf{q}_2$ along the negative z-axis, as in fig. 5.1a. Then we

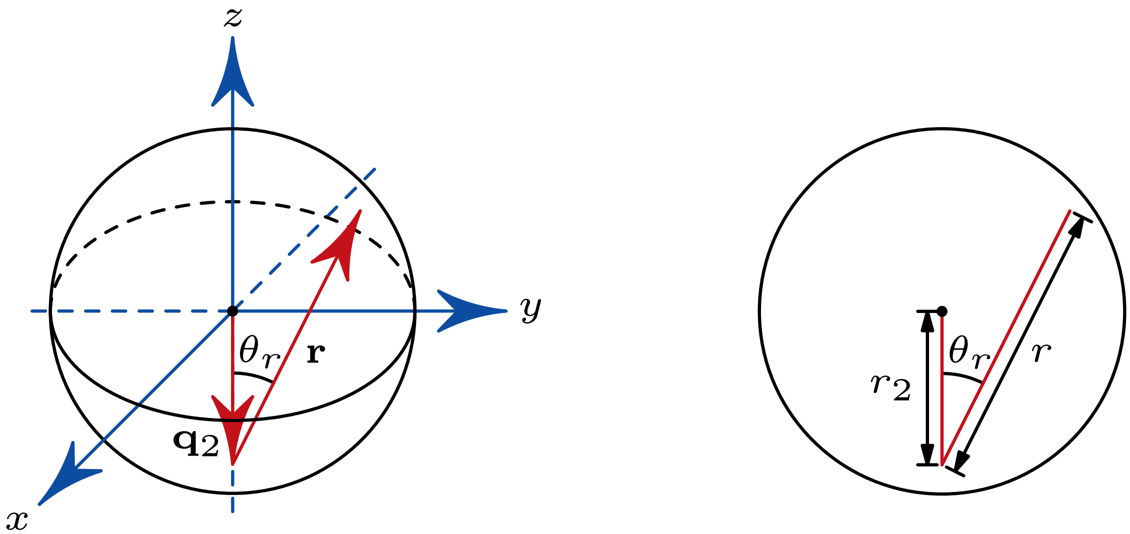

(a) Full three-dimensional problem. **(b)** Reduced two-dimensional problem.

Figure 5.1: Reduction of the spherical volume problem to a plane geometry problem.

immediately see that φ_r also has no impact on the result, leaving us with only r, r_2, and θ_r. As shown in fig. 5.1b, we have reduced our problem to a plane geometry problem! All we have left to do is find

$$J(r) = 8\pi^2 r^2 \int_{V_{\theta_r}(r)} \mathrm{d}\cos\theta_r \int_{V_{r_2}(r,\theta_r)} \mathrm{d}r_2\, r_2^2. \tag{5.9}$$

Before we can perform the integrals, we must identify the bounds of integration. The constraints that we must satisfy are

$$0 < r \leq 2R \tag{5.10a}$$
$$-1 \leq \cos\theta_r \leq 1 \tag{5.10b}$$
$$0 \leq r_2 \leq R \tag{5.10c}$$
$$0 \leq |\mathbf{q}_1|^2 \leq R^2. \tag{5.10d}$$

We have left out the trivial $r = 0$ case so that we are free to divide by r. The first three constraints are independent, but if we expand the last, we see that it couples them:

$$0 \leq |\mathbf{q}_1|^2 = |\mathbf{q}_2 + \mathbf{r}|^2 = r_2^2 + r^2 + 2\mathbf{q}_2 \cdot \mathbf{r} = r_2^2 + r^2 + 2r_2 r\cos\theta_r \leq R^2 \tag{5.11a}$$
$$r^2(\cos^2\theta_r - 1) \leq (r_2 + r\cos\theta_r)^2 \leq R^2 + r^2(\cos^2\theta_r - 1). \tag{5.11b}$$

Since

$$r^2(\cos^2\theta_r - 1) \leq 0, \tag{5.12}$$

we may write eq. (5.10d) as

$$(r_2 + r\cos\theta_r)^2 \leq R^2 + r^2(\cos^2\theta_r - 1). \tag{5.13}$$

As long as

$$1 - \left(\frac{R}{r}\right)^2 \le \cos^2\theta_r \tag{5.14}$$

so that the right-hand side is non-negative, this gives us

$$|r_2 + r\cos\theta_r| \le \sqrt{R^2 + r^2(\cos^2\theta_r - 1)} \tag{5.15a}$$

$$-r\cos\theta_r - \sqrt{R^2 + r^2(\cos^2\theta_r - 1)} \le r_2 \le -r\cos\theta_r + \sqrt{R^2 + r^2(\cos^2\theta_r - 1)}. \tag{5.15b}$$

Note that eq. (5.15b) cannot be satisfied when either $R < r$ and $0 < \cos\theta_r$, or $\sqrt{2}R < r$ and

$$-\frac{r}{2R} < \cos\theta_r < -\frac{R}{r}. \tag{5.16}$$

In anticipation of bounds we will encounter later, we define

$$L^\pm(r, \cos\theta_r) = -r\cos\theta_r \pm \sqrt{R^2 + r^2(\cos^2\theta_r - 1)}. \tag{5.17}$$

Because we get qualitatively different behaviour for different ranges of r, we will consider them separately:

$$J(r) = 8\pi^2 r^2 \begin{cases} 0 & \text{if } r = 0 \\ J_R(r) & \text{if } 0 < r \le R \\ J_{\sqrt{2}R}(r) & \text{if } R < r \le \sqrt{2}R \\ J_{2R}(r) & \text{if } \sqrt{2}R < r \le 2R \end{cases}. \tag{5.18}$$

We start with the simple case of $0 < r \le R$, where all angles θ_r are allowed and we are always permitted to set $r_2 = 0$. Both eq. (5.14) and the first inequality in eq. (5.15b) are trivially satisfied. The second inequality in eq. (5.15b) is relevant when

$$-\frac{r}{2R} < \cos\theta_r, \tag{5.19}$$

so we have

$$J_R(r) = \int_{-1}^{L_{\theta,1}(r)} \mathrm{d}\cos\theta_r \int_0^R \mathrm{d}r_2\, r_2^2 + \int_{L_{\theta,1}(r)}^{1} \mathrm{d}\cos\theta_r \int_0^{L^+(r,\cos\theta_r)} \mathrm{d}r_2\, r_2^2, \tag{5.20}$$

where

$$L_{\theta,1}(r) = -\frac{r}{2R}. \tag{5.21}$$

This simplifies (according to listing F.1 on page 119) to

$$J_R(r) = \frac{2}{3}R^3 - \frac{1}{2}R^2 r + \frac{1}{24}r^3. \tag{5.22}$$

Things get more interesting for $R < r \le \sqrt{2}R$. Now $\cos\theta_r \le 0$, but eq. (5.14) amounts to

$$\sqrt{1 - \left(\frac{R}{r}\right)^2} \le |\cos\theta_r|, \tag{5.23}$$

so

$$\cos\theta_r \leq -\sqrt{1-\left(\frac{R}{r}\right)^2}. \tag{5.24}$$

The first inequality in eq. (5.15b) must always be taken into account, and the second when $L_{\theta,1}(r) \leq \cos\theta_r$, which results in

$$J_{\sqrt{2}R}(r) = \int_{-1}^{L_{\theta,1}(r)} \mathrm{d}\cos\theta_r \int_{L^-(r,\cos\theta_r)}^{R} \mathrm{d}r_2\, r_2^2 + \int_{L_{\theta,1}(r)}^{L_{\theta,2}(r)} \mathrm{d}\cos\theta_r \int_{L^-(r,\cos\theta_r)}^{L^+(r,\cos\theta_r)} \mathrm{d}r_2\, r_2^2, \tag{5.25}$$

where

$$L_{\theta,2}(r) = -\sqrt{1-\left(\frac{R}{r}\right)^2} \tag{5.26}$$

and $L_{\theta,1}(r) \leq L_{\theta,2}(r)$. This also simplifies (according to listing F.2 on page 119) to

$$J_{\sqrt{2}R}(r) = \frac{2}{3}R^3 - \frac{1}{2}R^2 r + \frac{1}{24}r^3. \tag{5.27}$$

Finally, we consider $\sqrt{2}R < r \leq 2R$. This is the same as the previous case, but with the added restriction that one of

$$\cos\theta_r \leq L_{\theta,1}(r) \tag{5.28a}$$

$$-\frac{R}{r} \leq \cos\theta_r \tag{5.28b}$$

must always hold. The latter is impossible due to eq. (5.24), so we get just

$$J_{2R}(r) = \int_{-1}^{L_{\theta,1}(r)} \mathrm{d}\cos\theta_r \int_{L^-(r,\cos\theta_r)}^{R} \mathrm{d}r_2\, r_2^2, \tag{5.29}$$

which amazingly also simplifies (according to listing F.3 on page 120) to

$$J_{2R}(r) = \frac{2}{3}R^3 - \frac{1}{2}R^2 r + \frac{1}{24}r^3. \tag{5.30}$$

Thus, all the pieces of our piecewise Jacobian are identical and we have the compact expression

$$J(r) = 8\pi^2 r^2 \left(\frac{2}{3}R^3 - \frac{1}{2}R^2 r + \frac{1}{24}r^3\right), \tag{5.31}$$

which means our integral may be written as

$$\mathcal{I}[g(r)] = \frac{\pi^2}{3}\int_0^{2R} \mathrm{d}r\, \left(16R^3 - 12R^2 r + r^3\right) r^2 g(r). \tag{5.32}$$

We may check this result by integrating some test functions. We expect (according to listing F.4 on page 120)

$$\mathcal{I}[1] = \int_B \mathrm{d}\mathbf{q}_1 \int_B \mathrm{d}\mathbf{q}_2 = \frac{16}{9}\pi^2 R^6 \tag{5.33a}$$

$$\mathcal{I}[r^2] = \int_B \mathrm{d}\mathbf{q}_1 \int_B \mathrm{d}\mathbf{q}_2\, |\mathbf{q}_1 - \mathbf{q}_2|^2 = \frac{32}{15}\pi^2 R^8. \tag{5.33b}$$

If we use our expression, we get

$$\mathcal{I}[1] = \frac{\pi^2}{3}\int_0^{2R} \mathrm{d}r\,\left(16R^3 - 12R^2 r + r^3\right) r^2 \tag{5.34a}$$

$$= \frac{16}{3}\pi^2 R^3 \int_0^{2R} \mathrm{d}r\, r^2 - 4\pi^2 R^2 \int_0^{2R} \mathrm{d}r\, r^3 + \frac{1}{3}\pi^2 \int_0^{2R} \mathrm{d}r\, r^5 \tag{5.34b}$$

$$= \left(\frac{128}{9} - 16 + \frac{32}{9}\right)\pi^2 R^6 = \frac{16}{9}\pi^2 R^6 \tag{5.34c}$$

$$\mathcal{I}[r^2] = \frac{\pi^2}{3}\int_0^{2R} \mathrm{d}r\,\left(16R^3 - 12R^2 r + r^3\right) r^4 \tag{5.34d}$$

$$= \frac{16}{3}\pi^2 R^3 \int_0^{2R} \mathrm{d}r\, r^4 - 4\pi^2 R^2 \int_0^{2R} \mathrm{d}r\, r^5 + \frac{1}{3}\pi^2 \int_0^{2R} \mathrm{d}r\, r^7 \tag{5.34e}$$

$$= \left(\frac{512}{15} - \frac{128}{3} + \frac{32}{3}\right)\pi^2 R^8 = \frac{32}{15}\pi^2 R^8, \tag{5.34f}$$

which is what we expected.

5.1.2 Periodic volume

Consider two particles with (“space-fixed” frame) positions $\mathbf{q}_1$, $\mathbf{q}_2$ confined to the interior of a cube Q with side length L. For reasons of convenience, we position this cube with its center at the origin and align its edges with the Cartesian coordinate axes. We have a function $g(r)$ that depends only on the separation distance of the particles, and we impose periodic boundary conditions with the minimum-image convention. This gives us infinitely many particles in an infinite volume, but still with a finite density $2/L^3$.

We would like to integrate the function over the cube:

$$\mathcal{I}[g(r)] = \int_Q \mathrm{d}\mathbf{q}_2 \int_Q \mathrm{d}\mathbf{q}_1\, g(|\mathbf{q}_1 - \mathbf{q}_2|). \tag{5.35}$$

Every point in space is surrounded by a “minimal-image cube” of points, each of which has an analog in the original cube. This means that for all $\mathbf{q}_2$, the sets $\{|\mathbf{q}_1 - \mathbf{q}_2| : \mathbf{q}_1 \in Q\}$ are identical. One of these sets is $\{|\mathbf{q}| : \mathbf{q} \in Q\}$ (with $\mathbf{q}_2 = \mathbf{0}$), so we may write

$$\mathcal{I}[g(r)] = \int_Q \mathrm{d}\mathbf{q}_2 \int_Q \mathrm{d}\mathbf{q}\, g(|\mathbf{q}|) = L^3 \int_Q \mathrm{d}\mathbf{q}\, g(|\mathbf{q}|). \tag{5.36}$$

Since the result of integration is the same in each octant, we may consider only the first octant ($Q/8$), where the variables of integration are non-negative:

$$\mathcal{I}[g(r)] = 8L^3 \int_{Q/8} \mathrm{d}\mathbf{q}\, g(|\mathbf{q}|) = 8L^3 \int_0^{\frac{L}{2}} \mathrm{d}x \int_0^{\frac{L}{2}} \mathrm{d}y \int_0^{\frac{L}{2}} \mathrm{d}z\, g(\sqrt{x^2+y^2+z^2}).$$

The obvious thing to do now is change to spherical coordinates to get our hands on r, but as before that turns out to not be the simplest approach. Instead, we use

$$X = x \qquad\qquad Y = y \qquad\qquad r = \sqrt{x^2+y^2+z^2}, \tag{5.37}$$

with inverse

$$x = X \qquad y = Y \qquad z = \sqrt{r^2 - X^2 - Y^2}, \tag{5.38}$$

and Jacobian determinant

$$\begin{vmatrix} \dfrac{\partial x}{\partial X} & \dfrac{\partial x}{\partial Y} & \dfrac{\partial x}{\partial r} \\ \dfrac{\partial y}{\partial X} & \dfrac{\partial y}{\partial Y} & \dfrac{\partial y}{\partial r} \\ \dfrac{\partial z}{\partial X} & \dfrac{\partial z}{\partial Y} & \dfrac{\partial z}{\partial r} \end{vmatrix} = \begin{vmatrix} 1 & 0 & 0 \\ 0 & 1 & 0 \\ -\frac{X}{\sqrt{r^2-X^2-Y^2}} & -\frac{Y}{\sqrt{r^2-X^2-Y^2}} & \frac{r}{\sqrt{r^2-X^2-Y^2}} \end{vmatrix} = \frac{r}{\sqrt{r^2 - X^2 - Y^2}}. \tag{5.39}$$

We will use $M = L/2$ throughout. Clearly, r cannot exceed $\sqrt{M^2 + M^2 + M^2} = \sqrt{3}M$. In general, $X, Y \in [0, M]$, though there might be some constraints on them depending on the values of the other variables. We will refer to X and Y as simply x and y in the following, and we define the shorthand

$$K(r, x, y) = \frac{1}{\sqrt{r^2 - x^2 - y^2}} \tag{5.40}$$

so that the Jacobian determinant is $rK(r, x, y)$.

We choose to do the integrals in the following order (from the outside): r, then x, then y. To show what happens to the regions of the spheres confined to the cube as r is varied, some example spherical shells are displayed in fig. 5.2. If $r \le M$, the boundary of the cube does not matter, and x and y may take on their regular values: $x \le r$, $y \le \sqrt{r^2 - x^2}$.

Things become challenging when $r > M$. Now it is impossible for the contribution from x, y, or z alone to produce r; for example, we can no longer allow x and y to be zero simultaneously. We can express the constraint for z^2 in terms of the transformed variables as

$$0 \le r^2 - x^2 - y^2 = z^2 \le M^2, \tag{5.41}$$

which leads us to conclude that $y \le \sqrt{r^2 - x^2}$ always, and when $x \le \sqrt{r^2 - M^2}$, then $y \ge \sqrt{r^2 - x^2 - M^2}$. Of course, the upper bound on y is only of interest when it is less than M, which happens when $x \ge \sqrt{r^2 - M^2}$ (and $r \le \sqrt{2}M$). On the other hand, the lower bound only makes sense when it does not exceed M. If $r \le \sqrt{2}M$, this is always the case; otherwise, we need that $x \ge \sqrt{r^2 - 2M^2}$.

Thus, we may write our integral piecewise as

$$\begin{aligned} \mathcal{I}[g(r)] = {} & 8L^3 \int_0^M \mathrm{d}r\, r g(r) \int_0^r \mathrm{d}x \int_0^{\sqrt{r^2-x^2}} \mathrm{d}y\, K(r, x, y) \\ & + 8L^3 \int_M^{\sqrt{2}M} \mathrm{d}r\, r g(r) \int_0^{\sqrt{r^2-M^2}} \mathrm{d}x \int_{\sqrt{r^2-x^2-M^2}}^M \mathrm{d}y\, K(r, x, y) \\ & + 8L^3 \int_M^{\sqrt{2}M} \mathrm{d}r\, r g(r) \int_{\sqrt{r^2-M^2}}^M \mathrm{d}x \int_0^{\sqrt{r^2-x^2}} \mathrm{d}y\, K(r, x, y) \\ & + 8L^3 \int_{\sqrt{2}M}^{\sqrt{3}M} \mathrm{d}r\, r g(r) \int_{\sqrt{r^2-2M^2}}^M \mathrm{d}x \int_{\sqrt{r^2-x^2-M^2}}^M \mathrm{d}y\, K(r, x, y). \end{aligned} \tag{5.42}$$

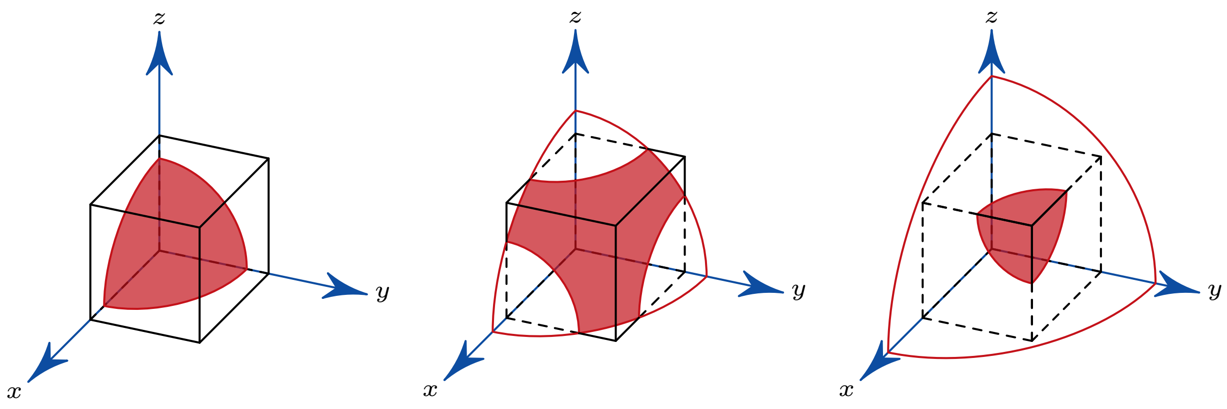

(a) $0 < r < M$ **(b)** $M < r < \sqrt{2}M$ **(c)** $\sqrt{2}M < r < \sqrt{3}M$

Figure 5.2: Representative spherical shells for different ranges of r.

Two of these are easy to do (see listing F.5 on page 120):

$$\int_0^r \mathrm{d}x \int_0^{\sqrt{r^2-x^2}} \mathrm{d}y\, K(r,x,y) = \frac{\pi}{2} r \tag{5.43a}$$

$$\int_{\sqrt{r^2-M^2}}^{M} \mathrm{d}x \int_0^{\sqrt{r^2-x^2}} \mathrm{d}y\, K(r,x,y) = \frac{\pi}{2}\left(M - \sqrt{r^2-M^2}\right). \tag{5.43b}$$

For the other two, since (by listing F.6 on page 120)

$$\int_B^M \frac{\mathrm{d}y}{\sqrt{A^2-y^2}} = \arcsin\frac{M}{A} - \arcsin\frac{B}{A} \tag{5.44}$$

for $A \geq y$, the y integrals are

$$f(M,x) = \int_{\sqrt{r^2-x^2-M^2}}^{M} \mathrm{d}y\, K(r,x,y) = \arcsin\frac{M}{\sqrt{r^2-x^2}} - \arcsin\frac{\sqrt{r^2-x^2-M^2}}{\sqrt{r^2-x^2}}. \tag{5.45}$$

We want to integrate this over x to find

$$\int_0^{\sqrt{r^2-M^2}} \mathrm{d}x\, f(M,x) \tag{5.46a}$$

$$\int_{\sqrt{r^2-2M^2}}^{M} \mathrm{d}x\, f(M,x), \tag{5.46b}$$

but we don't get anything reasonable if we integrate the arcsines directly.

What would Feynman do? Probably differentiate under the integral sign! The general expression is [Fla73]

$$\frac{\mathrm{d}}{\mathrm{d}M} \int_{a(M)}^{b(M)} \mathrm{d}x\, f(M,x) = f(M,b(M))b'(M) - f(M,a(M))a'(M) + \int_{a(M)}^{b(M)} \mathrm{d}x\, f_M(M,x). \tag{5.47}$$

This is useful for us, because the fundamental theorem of calculus states that [Ste08, p. 384]

$$f(M) = f(M_0) + \int_{M_0}^{M} \mathrm{d}M'\, f'(M'), \tag{5.48}$$

so

$$\begin{aligned}\int_{a(M)}^{b(M)} \mathrm{d}x\, f(M,x) &= \int_{a(M_0)}^{b(M_0)} \mathrm{d}x\, f(M_0,x) + \int_{M_0}^{M} \mathrm{d}M' \left[\frac{\mathrm{d}}{\mathrm{d}M}\int_{a(M)}^{b(M)} \mathrm{d}x\, f(M,x)\right]_{M=M'} \qquad (5.49\text{a})\\ &= \int_{a(M_0)}^{b(M_0)} \mathrm{d}x\, f(M_0,x) + \int_{M_0}^{M} \mathrm{d}M'\, f(M',b(M'))b'(M')\\ &\quad - \int_{M_0}^{M} \mathrm{d}M'\, f(M',a(M'))a'(M') + \int_{M_0}^{M} \mathrm{d}M' \int_{a(M')}^{b(M')} \mathrm{d}x\, f_M(M',x). \qquad (5.49\text{b})\end{aligned}$$

In our case,

$$f_M(M,x) = \frac{\partial}{\partial M}\left[\arcsin\frac{M}{\sqrt{r^2-x^2}} - \arcsin\frac{\sqrt{r^2-x^2-M^2}}{\sqrt{r^2-x^2}}\right] = \frac{2}{\sqrt{r^2-x^2-M^2}} \qquad (5.50\text{a})$$

$$\int_{a(M)}^{b(M)} \mathrm{d}x\, f_M(M,x) = 2\int_{a(M)}^{b(M)} \frac{\mathrm{d}x}{\sqrt{r^2-x^2-M^2}} = 2\arcsin\frac{b(M)}{\sqrt{r^2-M^2}} - 2\arcsin\frac{a(M)}{\sqrt{r^2-M^2}}. \qquad (5.50\text{b})$$

It doesn't look like we've achieved anything useful, but we have! If we choose $M_0 = 0$,

$$f(M=0,x) = -\frac{\pi}{2} \qquad (5.51\text{a})$$

$$\int_{a(0)}^{b(0)} \mathrm{d}x\, f(M=0,x) = \frac{\pi}{2}(a(0)-b(0)), \qquad (5.51\text{b})$$

so we can reconstruct the desired integrals as

$$\begin{aligned}\int_{a(M)}^{b(M)} \mathrm{d}x\, f(M,x) &= \frac{\pi}{2}(a(0)-b(0)) + \int_{0}^{M} \mathrm{d}M'\, f(M',b(M'))b'(M')\\ &\quad - \int_{0}^{M} \mathrm{d}M'\, f(M',a(M'))a'(M') + \int_{0}^{M} \mathrm{d}M' \int_{a(M')}^{b(M')} \mathrm{d}x\, f_M(M',x). \qquad (5.52)\end{aligned}$$

For eq. (5.46a),

$$a(M) = 0 \qquad a'(M) = 0 \qquad (5.53\text{a})$$

$$b(M) = \sqrt{r^2-M^2} \qquad b'(M) = -\frac{M}{\sqrt{r^2-M^2}} \qquad (5.53\text{b})$$

$$f(M,b(M)) = \arcsin 1 - \arcsin 0 = \frac{\pi}{2}, \qquad (5.53\text{c})$$

so

$$\begin{aligned}\int_{0}^{\sqrt{r^2-M^2}} \mathrm{d}x\, f(M,x) &= -\frac{\pi}{2}r - \frac{\pi}{2}\int_0^M \mathrm{d}M'\, \frac{M'}{\sqrt{r^2-(M')^2}} + \frac{\pi}{2}2\int_0^M \mathrm{d}M' \qquad (5.54\text{a})\\ &= \frac{\pi}{2}(2M - 2r + \sqrt{r^2-M^2}). \qquad (5.54\text{b})\end{aligned}$$

For eq. (5.46b),

$$
\begin{aligned}
a(M) &= \sqrt{r^2 - 2M^2} & a'(M) &= -\frac{2M}{\sqrt{r^2 - 2M^2}} \qquad (5.55\text{a})\\
b(M) &= M & b'(M) &= 1 \qquad (5.55\text{b})\\
f(M, a(M)) &= \arcsin\frac{1}{\sqrt{2}} - \arcsin\frac{1}{\sqrt{2}} = 0 & & \qquad (5.55\text{c})\\
f(M, b(M)) &= \arcsin\frac{M}{\sqrt{r^2 - M^2}} - \arcsin\frac{\sqrt{r^2 - 2M^2}}{\sqrt{r^2 - M^2}}, & & \qquad (5.55\text{d})
\end{aligned}
$$

so

$$\int_{\sqrt{r^2-2M^2}}^{M} \mathrm{d}x\, f(M,x) = \frac{\pi}{2}r + 3\int_0^M \mathrm{d}M' \left(\arcsin\frac{M'}{\sqrt{r^2-(M')^2}} - \arcsin\frac{\sqrt{r^2-2(M')^2}}{\sqrt{r^2-(M')^2}}\right). \tag{5.56}$$

Again it looks like we're not making any progress, but we can actually evaluate the integral over M' (see listing F.7 on page 121):

$$M\arcsin\frac{M}{\sqrt{r^2-M^2}} - M\arcsin\frac{\sqrt{r^2-2M^2}}{\sqrt{r^2-M^2}} + r\arctan\frac{r\sqrt{r^2-2M^2}}{M^2} - \frac{\pi}{2}r. \tag{5.57}$$

If we define

$$\Xi(r) = M\arcsin\frac{M}{\sqrt{r^2-M^2}} - M\arcsin\frac{\sqrt{r^2-2M^2}}{\sqrt{r^2-M^2}} + r\arctan\frac{r\sqrt{r^2-2M^2}}{M^2}, \tag{5.58}$$

then

$$\int_{\sqrt{r^2-2M^2}}^{M} \mathrm{d}x\, f(M,x) = 3\Xi(r) - \pi r. \tag{5.59}$$

The end result is

$$
\begin{aligned}
\mathcal{I}[g(r)] = 4\pi L^3 &\int_0^M \mathrm{d}r\, r^2 g(r)\\
&+ 4\pi L^3 \int_M^{\sqrt{2}M} \mathrm{d}r\, r\left(2M - 2r + \sqrt{r^2-M^2} + M - \sqrt{r^2-M^2}\right) g(r)\\
&+ 8L^3 \int_{\sqrt{2}M}^{\sqrt{3}M} \mathrm{d}r\, r(3\Xi(r) - \pi r) g(r) \qquad (5.60\text{a})\\
= 4\pi L^3 &\int_0^{\frac{L}{2}} \mathrm{d}r\, r^2 g(r) + 2\pi L^3 \int_{\frac{L}{2}}^{\frac{L}{\sqrt{2}}} \mathrm{d}r\, r(3L - 4r) g(r) + 8L^3 \int_{\frac{L}{\sqrt{2}}}^{\frac{\sqrt{3}L}{2}} \mathrm{d}r\, r(3\Xi(r) - \pi r) g(r). \qquad (5.60\text{b})
\end{aligned}
$$

The last term is distressing, but at least the entire expression is in closed form (except for the r integrals, of course). We can clean it up a bit if we introduce $\xi = r/M$ and the dimensionless piecewise Jacobian (shown in fig. 5.3)

$$J_\mathrm{d}(\xi) = \frac{\pi}{2}\xi \begin{cases} \xi & \text{if } 0 \le \xi \le 1 \\ 3 - 2\xi & \text{if } 1 < \xi \le \sqrt{2} \\ 6\Xi_\mathrm{d}(\xi)/\pi - 2\xi & \text{if } \sqrt{2} < \xi \le \sqrt{3} \end{cases}, \tag{5.61}$$

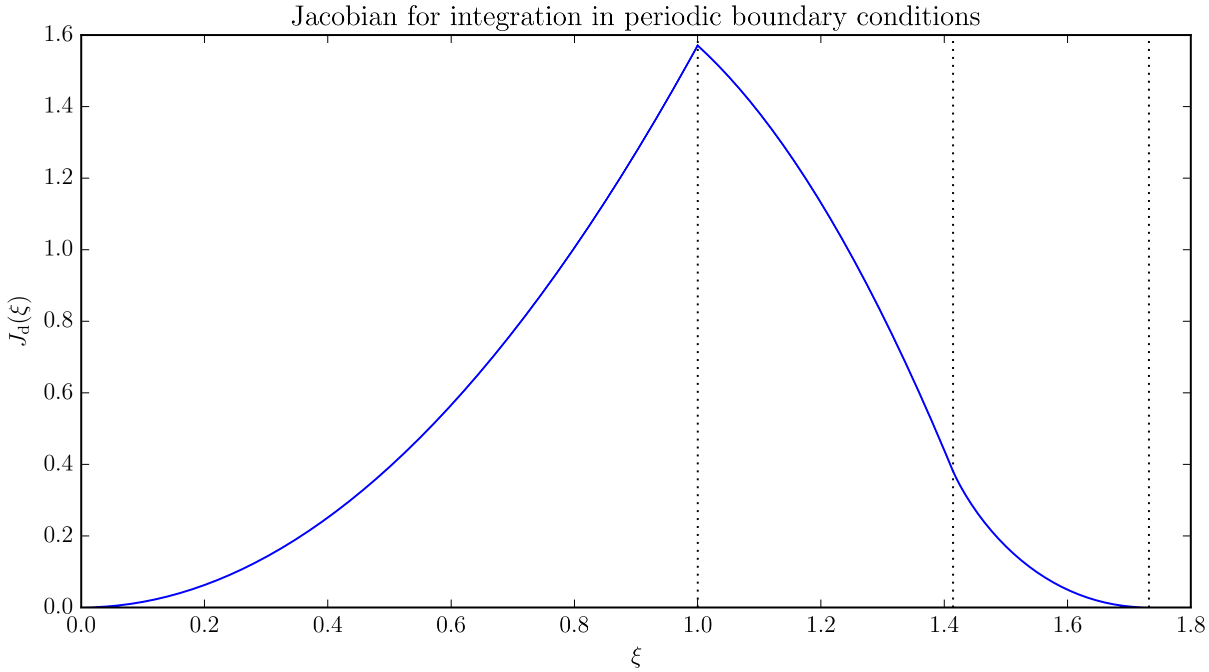

Figure 5.3: Dimensionless piecewise Jacobian from eq. (5.61) for integration in periodic boundary conditions. Dotted lines mark 1, $\sqrt{2}$, and $\sqrt{3}$. The cusp occurs when ξ begins to leave the cube.

where

$$\Xi_\mathrm{d}(\xi) = \frac{\Xi(M\xi)}{M} = \arcsin\frac{1}{\sqrt{\xi^2-1}} - \arcsin\frac{\sqrt{\xi^2-2}}{\sqrt{\xi^2-1}} + \xi\arctan\left(\xi\sqrt{\xi^2-2}\right), \tag{5.62}$$

with which we can write

$$\mathcal{I}[g(r)] = 2L^5\int_0^{\sqrt{3}M}\mathrm{d}r\, J_\mathrm{d}(r/M)g(r) = L^6\int_0^{\sqrt{3}}\mathrm{d}\xi\, J_\mathrm{d}(\xi)g(M\xi). \tag{5.63}$$

Starting from eq. (5.36) (which already takes into account the minimal image convention), we may verify the remainder of the derivation by integrating some test functions. With $L = 42$, we expect (according to listing F.8 on page 121)

$$\mathcal{I}[1] = L^3\int_Q \mathrm{d}\mathbf{q} = L^6 = 5489031744 \tag{5.64a}$$

$$\mathcal{I}[r^2] = L^3\int_Q \mathrm{d}\mathbf{q}\,|\mathbf{q}|^2 = \frac{1}{4}L^8 = 2420662999104 \tag{5.64b}$$

$$\mathcal{I}[e^{-r^2}] = L^3\int_Q \mathrm{d}\mathbf{q}\,\exp\left[-|\mathbf{q}|^2\right] \approx 412546.2847. \tag{5.64c}$$

Since we are not foolhardy enough to take on eq. (5.62) analytically, we perform the integration numerically on an evenly-spaced grid of 10^6 points. This results in relative errors of 3.49×10^{-13}, 3.43×10^{-13}, and 1.72×10^{-10}, respectively, which assures us that our expression is not entirely wrong. Note that if we ignore the particularly unpleasant bit at the end and stop integrating at $\sqrt{2}$, we get relative errors of 3.49×10^{-2}, 7.75×10^{-2}, and 1.72×10^{-10} instead. As we might have reasonably assumed, the tail is negligible for functions that decay exponentially.

5.2 PILE with odd P

When the PILE was introduced in ref. [CPM10], the transformation to normal modes was only given for even P (n in the notation of the paper). It is useful in practice to be able to apply the PILE in situations where P is odd. Since eq. (18) of ref. [CPM10] simply states the result, we perform the derivation from the beginning.

The relevant difference between the PILE and LePIGS is that the former has closed paths. This means that we may start the derivation the same way, but instead of eq. (D.30) on page 104 we use the very similar matrix

$$\underline{\mathbf{A}} = \begin{pmatrix} 2 & -1 & 0 & \cdots & 0 & -1 \\ -1 & 2 & -1 & \cdots & 0 & 0 \\ 0 & -1 & 2 & \cdots & 0 & 0 \\ \vdots & \vdots & \vdots & \ddots & \vdots & \vdots \\ 0 & 0 & 0 & \cdots & 2 & -1 \\ -1 & 0 & 0 & \cdots & -1 & 2 \end{pmatrix}. \tag{5.65}$$

This is a circulant matrix, so we may directly write the eigenvalues and eigenvectors: [KSU03]

$$\lambda_k = 2 - \left(e^{\frac{2\pi ik}{P}} + e^{-\frac{2\pi ik}{P}}\right) = 2 - 2\cos\left[\frac{2\pi k}{P}\right] = 4\sin^2\left[\frac{\pi k}{P}\right] \tag{5.66a}$$

$$s^*_{k,n} = \sqrt{\frac{1}{P}} e^{\frac{2\pi ink}{P}}. \tag{5.66b}$$

Thus, the transformation matrix $\underline{\mathbf{S}}$ is the $(P \times P)$ Discrete Fourier Transform (DFT) matrix, which makes it easy to obtain the normal mode coordinates.

This transformation matrix in general results in complex values, but we would prefer to keep things real. Unlike in the open path case, not all the eigenvalues are distinct. When $k \neq 0$ and $k \neq P/2$,

$$\lambda_k = 4\sin^2\left[\frac{\pi k}{P}\right] = 4\sin^2\left[\frac{\pi(P-k)}{P}\right] = \lambda_{P-k}. \tag{5.67}$$

We can use any linear combination of eigenvectors with the same eigenvalue, so we use (for $0 < k < P/2$):

$$s'_{k,n} = \sqrt{\frac{1}{2P}}\left(e^{\frac{2\pi ink}{P}} + e^{\frac{2\pi in(P-k)}{P}}\right) = \sqrt{\frac{1}{2P}}\left(e^{\frac{2\pi ink}{P}} + e^{-\frac{2\pi ink}{P}}\right) = \sqrt{\frac{2}{P}}\cos\left[\frac{2\pi nk}{P}\right] \tag{5.68a}$$

$$s'_{P-k,n} = i\sqrt{\frac{1}{2P}}\left(e^{\frac{2\pi ink}{P}} - e^{\frac{2\pi in(P-k)}{P}}\right) = i\sqrt{\frac{1}{2P}}\left(e^{\frac{2\pi ink}{P}} - e^{-\frac{2\pi ink}{P}}\right) = -\sqrt{\frac{2}{P}}\sin\left[\frac{2\pi nk}{P}\right]. \tag{5.68b}$$

Thus, for even P, the matrix elements are given by

$$s'_{k,n} = \begin{cases} \sqrt{\frac{1}{P}} & \text{if } k = 0 \\ \sqrt{\frac{2}{P}}\cos\left[\frac{2\pi nk}{P}\right] & \text{if } 0 < k < \frac{P}{2} \\ \sqrt{\frac{1}{P}}(-1)^n & \text{if } k = \frac{P}{2} \\ \sqrt{\frac{2}{P}}\sin\left[\frac{2\pi nk}{P}\right] & \text{if } \frac{P}{2} < k < P \end{cases}, \tag{5.69}$$

which is exactly eq. (18) of ref. [CPM10].[‡] The phase of the sine elements appears to be flipped relative to eq. (5.68b) because

$$\sin\left[\frac{2\pi n(P-k)}{P}\right] = \sin\left[2\pi n - \frac{2\pi nk}{P}\right] = -\sin\left[\frac{2\pi nk}{P}\right]. \tag{5.70}$$

Finally, we recognize that when P is odd, nothing in the derivation changes, but we no longer have to account for the $k = P/2$ case, so we may simply ignore it. This results in the matrix elements

$$s'_{k,n} = \begin{cases} \sqrt{\frac{1}{P}} & \text{if } k = 0 \\ \sqrt{\frac{2}{P}}\cos\left[\frac{2\pi nk}{P}\right] & \text{if } 0 < k < \frac{P}{2} \\ \sqrt{\frac{2}{P}}\sin\left[\frac{2\pi nk}{P}\right] & \text{if } \frac{P}{2} < k < P \end{cases}. \tag{5.71}$$

[‡] Except our matrix $\underline{\mathbf{S}}'$ happens to be the transpose of their matrix $\mathbf{C}$.

Appendix A

Useful formulas

Interpreting “Avogradro” as “Avocado”

Wolfram Alpha

A.1 Momentum-position change of basis

In a single dimension, we have [Sak85, pp. 55-56]

$$\begin{aligned}\delta\big(p-p'\big) &= \langle p'|p\rangle = \int \mathrm{d}q\,\langle p'|q\rangle\,\langle q|p\rangle && \text{(A.1a)}\\ &= \frac{1}{\hbar}\delta\bigg(\frac{1}{\hbar}(p-p')\bigg) = \frac{1}{2\pi\hbar}\int \mathrm{d}q\, e^{\frac{i}{\hbar}(p-p')q} = \frac{1}{2\pi\hbar}\int \mathrm{d}q\, e^{-\frac{i}{\hbar}p'q}e^{\frac{i}{\hbar}pq}, && \text{(A.1b)}\end{aligned}$$

from which we conclude that

$$\langle p|q\rangle = \frac{1}{\sqrt{2\pi\hbar}}e^{-\frac{i}{\hbar}pq}. \tag{A.2}$$

Since [Sak85, p. 59]

$$\delta(\mathbf{x}) = \prod_{i=0}^{F-1}\delta(x_i)\,, \tag{A.3}$$

for F-dimensional vectors $\mathbf{p}$ and $\mathbf{q}$ we instead have

$$\begin{aligned}\delta\big(\mathbf{p}-\mathbf{p}'\big) &= \langle \mathbf{p}'|\mathbf{p}\rangle = \int \mathrm{d}\mathbf{q}\,\langle \mathbf{p}'|\mathbf{q}\rangle\,\langle \mathbf{q}|\mathbf{p}\rangle && \text{(A.4a)}\\ &= \frac{1}{\hbar^F}\delta\bigg(\frac{1}{\hbar}(\mathbf{p}-\mathbf{p}')\bigg) = \frac{1}{(2\pi\hbar)^F}\int \mathrm{d}\mathbf{q}\, e^{\frac{i}{\hbar}(\mathbf{p}-\mathbf{p}')\cdot\mathbf{q}} = \frac{1}{(2\pi\hbar)^F}\int \mathrm{d}\mathbf{q}\, e^{-\frac{i}{\hbar}\mathbf{p}'\cdot\mathbf{q}}e^{\frac{i}{\hbar}\mathbf{p}\cdot\mathbf{q}}, && \text{(A.4b)}\end{aligned}$$

so the inner product is given by

$$\langle \mathbf{p}|\mathbf{q}\rangle = \left(\frac{1}{2\pi\hbar}\right)^{\frac{F}{2}} e^{-\frac{i}{\hbar}\mathbf{q}\cdot\mathbf{p}}. \tag{A.5}$$

A.2 Gaussian integrals

Gaussian integrals are quite common, and the expression for the result with real parameters is well-known. Our goal here is to generalize the result to complex parameters, so we start from the very beginning.

How do we know that

$$G(a) = \int \mathrm{d}x\, e^{-ax^2} = \sqrt{\frac{\pi}{a}} \tag{A.6}$$

for all $a > 0$? The usual squaring trick with polar coordinates is supposedly due to Poisson:[‡]

$$\begin{aligned}
(G(a))^2 &= \left(\int \mathrm{d}x\, e^{-ax^2}\right)\left(\int \mathrm{d}y\, e^{-ay^2}\right) && \text{(A.7a)}\\
&= \int_{-\infty}^{\infty} \mathrm{d}x \int_{-\infty}^{\infty} \mathrm{d}y\, e^{-a(x^2+y^2)} && \text{(A.7b)}\\
&= \int_{0}^{2\pi} \mathrm{d}\theta \int_{0}^{\infty} \mathrm{d}r\, re^{-ar^2} && \text{(A.7c)}\\
&= 2\pi \int_{0}^{\infty} \mathrm{d}r\, re^{-ar^2} && \text{(A.7d)}\\
&= 2\pi \left[-\frac{1}{2a}e^{-ar^2}\right]_{r=0}^{\infty} && \text{(A.7e)}\\
&= 2\pi \left[0 - \left(-\frac{1}{2a}\right)\right] = \frac{\pi}{a} && \text{(A.7f)}\\
\therefore G(a) &= \sqrt{\frac{\pi}{a}}. && \text{(A.7g)}
\end{aligned}$$

We need a to be positive so that $e^{-ar^2} \to 0$ as $r \to \infty$. It also helps with the division and square root.

It's then trivial to generalize this to expressions of the form

$$\int \mathrm{d}x\, e^{-ax^2+bx} \tag{A.8}$$

by completing the square:

$$\begin{aligned}
-a\left(x - \frac{b}{2a}\right)^2 + \frac{b^2}{4a} &= -a\left(x^2 - 2\frac{b}{2a}x + \frac{b^2}{4a^2}\right) + \frac{b^2}{4a} && \text{(A.9a)}\\
&= -ax^2 + bx, && \text{(A.9b)}
\end{aligned}$$

so

$$\begin{aligned}
\int \mathrm{d}x\, e^{-ax^2+bx} &= \int \mathrm{d}x\, e^{-a\left(x-\frac{b}{2a}\right)^2+\frac{b^2}{4a}} && \text{(A.10a)}\\
&= e^{\frac{b^2}{4a}} \int \mathrm{d}x\, e^{-a\left(x-\frac{b}{2a}\right)^2} && \text{(A.10b)}\\
&= \sqrt{\frac{\pi}{a}} e^{\frac{b^2}{4a}}. && \text{(A.10c)}
\end{aligned}$$

[‡] `http://www.york.ac.uk/depts/maths/histstat/normal_history.pdf`

Here we have used the fact that translation of x by a constant has no impact on the value of an improper integral, since x ranges over the entire real line:

$$\begin{aligned}
\int_{-\infty}^{\infty} \mathrm{d}x\, f(x) &= \lim_{L_1\to-\infty}\int_{L_1}^{0} \mathrm{d}x\, f(x) + \lim_{L_2\to\infty}\int_{0}^{L_2} \mathrm{d}x\, f(x) && \text{(A.11a)}\\
&= \lim_{L_1\to-\infty}\int_{L_1+\Delta x}^{\Delta x} \mathrm{d}x\, f(x-\Delta x) + \lim_{L_2\to\infty}\int_{\Delta x}^{L_2+\Delta x} \mathrm{d}x\, f(x-\Delta x) && \text{(A.11b)}\\
&= \int_{-\infty}^{\infty} \mathrm{d}x\, f(x-\Delta x). && \text{(A.11c)}
\end{aligned}$$

We still require that $a > 0$ for the same reason as before, but we impose no additional constraints on b other than $b \in \mathbb{R}$.

It turns out that the above result applies even when $b \in \mathbb{C}$, and to show this we will follow an argument similar to the one in ref. [Kwo02, pp. 132-135]. According to the Cauchy–Goursat theorem [Kwo02, p. 128],

$$\oint_C \mathrm{d}z\, f(z) = 0 \tag{A.12}$$

for a simple closed contour C when $f(z)$ is analytic on and inside C. Since $e^{-\lambda z^2}$ (with $\lambda, z \in \mathbb{C}$) is analytic everywhere [Kwo02, p. 61], if we draw any curve C in the complex plane that starts and ends at the same point and does not cross itself, we will have

$$\oint_C \mathrm{d}z\, e^{-\lambda z^2} = 0. \tag{A.13}$$

We will choose C to be the rectangle with vertices at L_1, L_2, $L_2 - i\beta$, and $L_1 - i\beta$, where $L_1, L_2, \beta \in \mathbb{R}$. We may therefore split our contour integral into simple line integrals as follows [Kwo02, p. 122]:

$$\oint_C \mathrm{d}z\, e^{-\lambda z^2} = \int_{L_1}^{L_2} \mathrm{d}x\, e^{-\lambda x^2} + \int_{0}^{\beta} \mathrm{d}x\, e^{-\lambda (L_2 - ix)^2} + \int_{L_2}^{L_1} \mathrm{d}x\, e^{-\lambda (x - i\beta)^2} + \int_{\beta}^{0} \mathrm{d}x\, e^{-\lambda (L_1 - ix)^2} = 0, \tag{A.14}$$

which implies that

$$\int_{L_1}^{L_2} \mathrm{d}x\, e^{-\lambda x^2} + \int_{0}^{\beta} \mathrm{d}x\, e^{-\lambda (L_2 - ix)^2} = \int_{L_1}^{L_2} \mathrm{d}x\, e^{-\lambda (x - i\beta)^2} + \int_{0}^{\beta} \mathrm{d}x\, e^{-\lambda (L_1 - ix)^2}. \tag{A.15}$$

We can apply the modulus inequality to the "vertical" segments to show that they vanish in the limits $L_1 \to -\infty$ and $L_2 \to \infty$ [Kwo02, p. 134]. Thus, we have (reusing the result from eq. (A.11))

$$\int_{-\infty}^{\infty} \mathrm{d}x\, e^{-\lambda x^2} = \int_{-\infty}^{\infty} \mathrm{d}x\, e^{-\lambda (x - i\beta)^2} = \int_{-\infty}^{\infty} \mathrm{d}x\, e^{-\lambda (x - \alpha - i\beta)^2} \tag{A.16}$$

for $\alpha, \beta \in \mathbb{R}$ and $\lambda \in \mathbb{C}$. This equation relies on the convergence of the integral on the left-hand side. We know that if we restrict λ to only positive real numbers, the integral *does* converge and we can generalize eq. (A.10) to

$$\int \mathrm{d}x\, e^{-ax^2 + \mu x} = \sqrt{\frac{\pi}{a}}\, e^{\frac{\mu^2}{4a}} \tag{A.17}$$

for $a > 0$ and $\mu \in \mathbb{C}$. Unfortunately, if we try to apply the above argument to complex λ with positive real part, we run into issues with choosing the branch of the square root.

A convenient shortcut (for $a, k > 0$, $\mu \in \mathbb{C}$) is

$$\int \mathrm{d}x \, e^{-k(ax^2+\mu x)} = \sqrt{\frac{\pi}{ka}} e^{\frac{k\mu^2}{4a}}. \tag{A.18}$$

For symmetrical coupled integrals (with $a, k > 0$, $b \in \mathbb{R}, |b| < 2a$), we have

$$\iint \mathrm{d}x \, \mathrm{d}y \, e^{-k(a(x^2+y^2)+bxy)} = \sqrt{\frac{\pi}{ka}} \int \mathrm{d}x \, e^{-k\left(\frac{4a^2-b^2}{4a}\right)x^2} = \frac{2\pi}{k\sqrt{4a^2-b^2}}. \tag{A.19}$$

A.3 Simple recurrence relation

Consider the homogeneous linear recurrence relation with constant coefficients

$$a_0 = 1 \tag{A.20a}$$
$$a_1 = \beta \tag{A.20b}$$
$$a_n = 2\alpha a_{n-1} - a_{n-2}. \tag{A.20c}$$

We will use ref. [Slo91, pp. 86-91] to find an explicit expression for a_n. We write the relation as

$$x^2 - 2\alpha x + 1 = 0, \tag{A.21}$$

which is trivially solved for x:

$$x = \alpha \pm \sqrt{\alpha^2 - 1}. \tag{A.22}$$

The general solution is therefore

$$a_n = c_1 \left(\alpha + \sqrt{\alpha^2-1}\right)^n + c_2 \left(\alpha - \sqrt{\alpha^2-1}\right)^n, \tag{A.23}$$

and we can determine the constants c_1 and c_2 from our initial conditions:

$$1 = c_1 + c_2 \tag{A.24a}$$
$$\beta = c_1 \left(\alpha + \sqrt{\alpha^2-1}\right) + c_2 \left(\alpha - \sqrt{\alpha^2-1}\right) = \alpha + (c_1 - c_2)\sqrt{\alpha^2-1}, \tag{A.24b}$$

so

$$c_{1/2} = \frac{1}{2}\left(1 \pm \frac{\beta - \alpha}{\sqrt{\alpha^2-1}}\right). \tag{A.25}$$

This is fine so long as $\alpha \neq \pm 1$.

Let us now handle the case when eq. (A.21) has only one degenerate root $x = \alpha = \pm 1$. In this case, the general solutions are

$$a_n = c_1^{\pm}(\pm 1)^n + c_2^{\pm} n (\pm 1)^n, \tag{A.26}$$

and

$$c_1^{\pm} = 1 \tag{A.27a}$$

$$c_2^{\pm} = \pm\beta - 1. \tag{A.27b}$$

Hence, our final answer is

$$a_n = \begin{cases} 1-(1-\beta)n & \text{if } \alpha = 1 \\ (1-(1+\beta)n)(-1)^n & \text{if } \alpha = -1 \\ \frac{1}{2}\left[\left(1+\frac{\beta-\alpha}{\sqrt{\alpha^2-1}}\right)\left(\alpha+\sqrt{\alpha^2-1}\right)^n + \left(1-\frac{\beta-\alpha}{\sqrt{\alpha^2-1}}\right)\left(\alpha-\sqrt{\alpha^2-1}\right)^n\right] & \text{otherwise} \end{cases}. \tag{A.28}$$

A.4 Roots of unity

The Nth roots of unity ($N = 1, 2, \ldots$) are given by powers of

$$\omega_N = e^{\frac{2\pi i}{N}}. \tag{A.29}$$

For any complex number $z \notin \{0, 1\}$ and any integer $N \geq 1$, we have

$$z^N + \sum_{k=0}^{N-1} z^k = 1 + \sum_{k=1}^{N} z^k = 1 + z\sum_{k=1}^{N} z^{k-1} = 1 + z\sum_{k=0}^{N-1} z^k, \tag{A.30}$$

so

$$z^N - 1 = (z-1)\sum_{k=0}^{N-1} z^k \tag{A.31}$$

and

$$\sum_{k=0}^{N-1} z^k = \frac{z^N - 1}{z - 1}. \tag{A.32}$$

If $z = 1$, $\sum_{k=0}^{N-1} z^k = N$.

For any a such that $\omega_N^a \neq 1$ (*i.e.* $a \not\equiv 0 \bmod N$),

$$\sum_{k=0}^{N-1} \omega_N^{ak} = \sum_{k=0}^{N-1} (\omega_N^a)^k = \frac{(\omega_N^a)^N - 1}{\omega_N^a - 1} = \frac{(\omega_N^N)^a - 1}{\omega_N^a - 1} = 0. \tag{A.33}$$

If $\omega_N^a = 1$, the sum is N. If we restrict a to $\{-(N-1), \ldots, -1, 0, 1, \ldots, N-1\}$, then we can write

$$\sum_{k=0}^{N-1} \omega_N^{ak} = \sum_{k=0}^{N-1} e^{\frac{2\pi i a k}{N}} = \begin{cases} N & \text{if } a = 0 \\ 0 & \text{otherwise} \end{cases}. \tag{A.34}$$

A.5 Cosine series

We would like to evaluate the series

$$S = \sum_{n=0}^{P-1} \cos^2 \left[\frac{\pi}{P} k \left(n + \frac{1}{2} \right) \right]. \tag{A.35}$$

We note that

$$\cos x = \frac{1}{2}(e^{-ix} + e^{ix}) \tag{A.36a}$$

$$\cos^2 x = \frac{1}{4}(e^{-ix} + e^{ix})^2 = \frac{1}{4}(2 + e^{-2ix} + e^{2ix}), \tag{A.36b}$$

so

$$4S = 2P + e^{-\frac{\pi ikn}{P}} \left[\sum_{n=0}^{P-1} e^{-\frac{2\pi ikn}{P}} \right] + e^{\frac{\pi ikn}{P}} \left[\sum_{n=0}^{P-1} e^{\frac{2\pi ikn}{P}} \right]. \tag{A.37}$$

By eq. (A.34),

$$4S = \begin{cases} 2P + P + P & \text{if } k = 0 \\ 2P & \text{otherwise} \end{cases}, \tag{A.38}$$

so

$$\sum_{n=0}^{P-1} \cos^2 \left[\frac{\pi}{P} k \left(n + \frac{1}{2} \right) \right] = \begin{cases} P & \text{if } k = 0 \\ \frac{P}{2} & \text{otherwise} \end{cases}. \tag{A.39}$$

A.6 Exponential derivative operator

It is stated but not proved in ref. [TBM92] that

$$e^{c\frac{\partial}{\partial x}} f(x) = f(x + c) \tag{A.40}$$

when c is independent of x. This is a contraction of

$$e^{c\frac{\partial}{\partial x}} f(x, \ldots) = f(x + c, \ldots), \tag{A.41}$$

where the other parameters are irrelevant, but we keep the partial derivative notation. To show that eq. (A.40) is true, we start with the (operator) Taylor series [Sak85, p. 48]

$$e^{\hat{A}} = \sum_{n=0}^{\infty} \frac{1}{n!} \hat{A}^n \tag{A.42}$$

and substitute our operator of choice:

$$e^{c\frac{\partial}{\partial x}} = \sum_{n=0}^{\infty} \frac{1}{n!} \left(c \frac{\partial}{\partial x} \right)^n. \tag{A.43}$$

Since we demand that c and x are independent, c and $\frac{\partial}{\partial x}$ commute, so

$$e^{c\frac{\partial}{\partial x}} = \sum_{n=0}^{\infty} \frac{1}{n!} c^n \frac{\partial^n}{\partial x^n}. \tag{A.44}$$

We can apply this to some function $f(x)$ to get

$$\left[e^{c\frac{\partial}{\partial x}} f(x)\right](x') = \sum_{n=0}^{\infty} \frac{1}{n!} c^n \left.\frac{\partial^n f}{\partial x^n}\right|_{x=x'}. \tag{A.45}$$

On the other hand, the Taylor series expansion of $f(x)$ about a is [Ste08, p. 735]

$$f(x) = \sum_{n=0}^{\infty} \frac{1}{n!} (x-a)^n \left.\frac{\partial^n f}{\partial x^n}\right|_{x=a}, \tag{A.46}$$

so the expansion of $f(x'+c)$ about x' is

$$f(x'+c) = \sum_{n=0}^{\infty} \frac{1}{n!} c^n \left.\frac{\partial^n f}{\partial x^n}\right|_{x=x'}, \tag{A.47}$$

which is exactly the same as eq. (A.45). Thus, we can claim that

$$\left[e^{c\frac{\partial}{\partial x}} f(x)\right](x') = f(x'+c), \tag{A.48}$$

or in more concise but less precise notation,

$$e^{c\frac{\partial}{\partial x}} f(x) = f(x+c). \tag{A.49}$$

In the case that we have a trivial function like $f(x) = x$, we of course find that

$$e^{c\frac{\partial}{\partial x}} x = x + c. \tag{A.50}$$

Additionally, if $\mathbf{c}$ and $\mathbf{x}$ are instead vectors (with all elements independent), then

$$e^{\mathbf{c}\cdot\frac{\partial}{\partial \mathbf{x}}} \mathbf{x} = \mathbf{x} + \mathbf{c}, \tag{A.51}$$

since all the $\frac{\partial}{\partial x_i}$ commute and we can apply the operators to each element of the vector individually.

Appendix B

Discrete cosine transform

> If your problem can be expressed as vectors and matrices, it is essentially already solved.
>
> `http://www.cl.cam.ac.uk/~sd601/papers/semirings-slides.pdf`
> Stephen Dolan

B.1 DCT normalization in FFTW

The Fastest Fourier Transform in the West (FFTW) [FJ05][‡] is a very powerful library for performing transforms in the discrete Fourier transform family, such as the Fast Fourier Transform (FFT) (a fast algorithm for the DFT) and the Discrete Cosine Transform (DCT). However, one nuance which must be kept in mind when using FFTW is that the transforms are not normalized in a way that makes them unitary.

According to the FFTW documentation[§], the matrix elements of the forward DCT (DCT-II, `REDFT10`) are

$$t^{\mathrm{f}}_{k,n} = 2\cos\left[\frac{\pi}{N}k\left(n+\frac{1}{2}\right)\right] \tag{B.1}$$

and of the reverse DCT (DCT-III, `REDFT01`) are

$$t^{\mathrm{r}}_{n,k} = C_k\cos\left[\frac{\pi}{N}k\left(n+\frac{1}{2}\right)\right] \tag{B.2}$$

with

$$C_k = \begin{cases} 1 & k=0 \\ 2 & \text{otherwise} \end{cases}. \tag{B.3}$$

[‡] `http://fftw.org/`

[§] FFTW Reference → What FFTW Really Computes → 1d Real-even DFTs (DCTs)

We would like our DCT to be orthogonal. Thus, *after* a forward transform we must be careful to scale the first element by $\sqrt{1/4N}$ and the others by $\sqrt{1/2N}$. On the other hand, *before* the reverse transform, we need to scale the first element by $\sqrt{1/N}$ and the others by $\sqrt{1/2N}$.

B.2 DCT via FFT

In some situations, it may be convenient to perform an FFT (fast DFT), but not nearly as convenient to perform a fast DCT. For example, one may be using NumPy [VCV11], which provides the `numpy.fft` package for FFTs, but no facility for DCTs. It turns out to be possible to MacGyver a length $2N$ DFT on specially-prepared input to simulate a length N DCT.

We let

$$\bar{\omega}_N = e^{-2\pi i/N} \tag{B.4a}$$

$$\omega_N = \bar{\omega}_N^* = e^{2\pi i/N}. \tag{B.4b}$$

The forward length $2N$ DFT on input $\mathbf{y}$ is defined (for $k = 0, 1, \ldots, 2N-1$) as

$$Y_k = \frac{1}{\sqrt{2N}} \sum_{n=0}^{2N-1} y_n \bar{\omega}_{2N}^{kn} \tag{B.5}$$

and the forward length N DCT on input $\mathbf{x}$ is defined (for $k = 0, 1, \ldots, N-1$) as

$$X_k = \frac{C_k}{\sqrt{N}} \sum_{n=0}^{N-1} x_n \cos\left[\frac{\pi}{N} k \left(n + \frac{1}{2}\right)\right], \tag{B.6}$$

where

$$C_k = \begin{cases} 1 & \text{if } k = 0 \\ \sqrt{2} & \text{otherwise} \end{cases}. \tag{B.7}$$

We may write the former as

$$\begin{aligned} Y_k &= \frac{1}{\sqrt{2N}} \left[\sum_{n=0}^{N-1} y_n \bar{\omega}_{2N}^{kn} + \sum_{n=N}^{2N-1} y_n \bar{\omega}_{2N}^{kn}\right] && \text{(B.8a)} \\ &= \frac{1}{\sqrt{2N}} \left[\sum_{n=0}^{N-1} y_n \bar{\omega}_{2N}^{kn} + \sum_{n=0}^{N-1} y_{(2N-1-n)} \bar{\omega}_{2N}^{k(2N-1-n)}\right] && \text{(B.8b)} \\ &= \frac{\omega_{2N}^{k/2}}{\sqrt{2N}} \left[\sum_{n=0}^{N-1} y_n \bar{\omega}_{2N}^{k(n+1/2)} + \sum_{n=0}^{N-1} y_{2N-(n+1)} \omega_{2N}^{k(n+1/2)}\right]. && \text{(B.8c)} \end{aligned}$$

If we set up $\mathbf{y}$ so that

$$y_n = \begin{cases} x_n & \text{if } 0 \le n < N \\ x_{2N-1-n} & \text{if } N \le n < 2N \end{cases}, \tag{B.9}$$

then

$$\begin{aligned}
Y_k &= \omega_{2N}^{k/2} \frac{1}{\sqrt{2N}} \sum_{n=0}^{N-1} x_n (\bar{\omega}_{2N}^{k(n+1/2)} + \omega_{2N}^{k(n+1/2)}) && \text{(B.10a)}\\
&= \omega_{2N}^{k/2} \frac{1}{\sqrt{2N}} \sum_{n=0}^{N-1} x_n (e^{-\pi i k(n+1/2)/N} + e^{\pi i k(n+1/2)/N}) && \text{(B.10b)}\\
&= \omega_{2N}^{k/2} \sqrt{\frac{2}{N}} \sum_{n=0}^{N-1} x_n \cos\left[\frac{\pi}{N} k \left(n + \frac{1}{2}\right)\right], && \text{(B.10c)}
\end{aligned}$$

which (for $k = 0, 1, \ldots, N-1$) is the same as eq. (B.6) up to a constant:

$$X_k = C'_k e^{-\frac{\pi i k}{2N}} Y_k, \tag{B.11}$$

where

$$C'_k = \begin{cases} \frac{1}{\sqrt{2}} & \text{if } k = 0 \\ 1 & \text{otherwise} \end{cases}. \tag{B.12}$$

If one is using NumPy's `numpy.fft` package, the `rfft` function is handy for this, since it only computes the first half of the transform, which is all that is necessary here.

To go in the other direction and perform an inverse DCT, we simply have to perform all the actions in the reverse order. When using NumPy's `irfft` function, one must be careful to set up the last element of the input array correctly:

$$\begin{aligned}
Y_N &= \frac{1}{\sqrt{2N}} \sum_{n=0}^{2N-1} y_n \bar{\omega}_{2N}^{Nn} && \text{(B.13a)}\\
&= \frac{1}{\sqrt{2N}} \sum_{n=0}^{2N-1} y_n e^{-\pi i n} && \text{(B.13b)}\\
&= \frac{1}{\sqrt{2N}} \sum_{n=0}^{N-1} x_n (e^{-\pi i n} + e^{-\pi i (2N-1-n)}) && \text{(B.13c)}\\
&= \frac{1}{\sqrt{2N}} \sum_{n=0}^{N-1} x_n (e^{-\pi i n} - e^{\pi i n}) && \text{(B.13d)}\\
&= \frac{1}{\sqrt{2N}} \sum_{n=0}^{N-1} x_n ((-1)^n - (-1)^n) && \text{(B.13e)}\\
&= 0. && \text{(B.13f)}
\end{aligned}$$

This is not difficult to do.

Appendix C

Coupled harmonic oscillators

The system consists of two particles of mass m, each in a harmonic trap of angular frequency ω_0, and interacting with a harmonic restraint (with zero separation distance) of angular frequency ω_{int}. In Cartesian coordinates, the Hamiltonian for this system may be expressed as

$$\hat{H} = \frac{|\hat{\mathbf{p}}_A|^2}{2m} + \frac{|\hat{\mathbf{p}}_B|^2}{2m} + \frac{1}{2}m\omega_0^2(\hat{\mathbf{q}}_A^2 + \hat{\mathbf{q}}_B^2) + \frac{1}{2}m\omega_{\text{int}}^2(\hat{\mathbf{q}}_A - \hat{\mathbf{q}}_B)^2. \tag{C.1}$$

Because this does not add any significant difficulty (since the interactions are all harmonic), we consider the more general D-dimensional case here, so that each of the momentum and positions vectors contains D scalar elements. With this in mind, we may immediately simplify the problem into D 1-dimensional problems:

$$\hat{H} = \sum_{d=0}^{D-1} \frac{\hat{p}_{A,d}^2}{2m} + \frac{\hat{p}_{B,d}^2}{2m} + \frac{1}{2}m\omega_0^2(\hat{q}_{A,d}^2 + \hat{q}_{B,d}^2) + \frac{1}{2}m\omega_{\text{int}}^2(\hat{q}_{A,d} - \hat{q}_{B,d})^2. \tag{C.2}$$

C.1 Exact ground state wavefunction

For the moment, let us consider only a single dimension, the Hamiltonian for which is

$$\hat{H}_1 = \frac{\hat{p}_A^2}{2m} + \frac{\hat{p}_B^2}{2m} + \frac{1}{2}m\omega_0^2(\hat{q}_A^2 + \hat{q}_B^2) + \frac{1}{2}m\omega_{\text{int}}^2(\hat{q}_A - \hat{q}_B)^2. \tag{C.3}$$

We use the standard approach for this situation and transform to center of mass and relative distance coordinates

$$R = \frac{q_A + q_B}{2} \qquad\qquad r = q_A - q_B \tag{C.4}$$

with total and reduced masses

$$M = 2m \qquad\qquad \mu = \frac{m}{2}. \tag{C.5}$$

This transformation has unit Jacobian determinant and the inverse transformation is

$$q_A = R + \frac{r}{2} \qquad\qquad q_B = R - \frac{r}{2}. \tag{C.6}$$

The corresponding forward transformation for the momenta may be obtained via the position representation of the momentum operator:

$$\hat{p}_R = -i\hbar\,\frac{\partial}{\partial R} = -i\hbar\left(\frac{\partial q_A}{\partial R}\,\frac{\partial}{\partial q_A} + \frac{\partial q_B}{\partial R}\,\frac{\partial}{\partial q_B}\right) = -i\hbar\left(\frac{\partial}{\partial q_A} + \frac{\partial}{\partial q_B}\right) = \hat{p}_A + \hat{p}_B \tag{C.7a}$$

$$\hat{p}_r = -i\hbar\,\frac{\partial}{\partial r} = -i\hbar\left(\frac{\partial q_A}{\partial r}\,\frac{\partial}{\partial q_A} + \frac{\partial q_B}{\partial r}\,\frac{\partial}{\partial q_B}\right) = -i\frac{\hbar}{2}\left(\frac{\partial}{\partial q_A} - \frac{\partial}{\partial q_B}\right) = \frac{\hat{p}_A - \hat{p}_B}{2}, \tag{C.7b}$$

and the inverse is therefore

$$\hat{p}_A = \hat{p}_r + \frac{\hat{p}_R}{2} \qquad\qquad \hat{p}_B = \hat{p}_r - \frac{\hat{p}_R}{2}. \tag{C.8}$$

We may now introduce

$$\omega_R = \omega_0 \qquad\qquad \omega_r = \sqrt{\omega_0^2 + 2\omega_{\text{int}}^2} \tag{C.9}$$

and write

$$\hat{H}_1 = \frac{(2\hat{p}_r + \hat{p}_R)^2}{8m} + \frac{(2\hat{p}_r - \hat{p}_R)^2}{8m} + \frac{1}{8}m\omega_0^2((2\hat{R}+\hat{r})^2 + (2\hat{R}-\hat{r})^2) + \frac{1}{2}m\omega_{\text{int}}^2\hat{r}^2 \tag{C.10a}$$

$$= \frac{\hat{p}_R^2}{4m} + \frac{2\hat{p}_r^2}{2m} + \frac{1}{2}2m\omega_0^2\hat{R}^2 + \frac{1}{2}\frac{m}{2}\omega_0^2\hat{r}^2 + \frac{1}{2}\frac{m}{2}2\omega_{\text{int}}^2\hat{r}^2 \tag{C.10b}$$

$$= \left[\frac{\hat{p}_R^2}{2M} + \frac{1}{2}M\omega_R^2\hat{R}^2\right] + \left[\frac{\hat{p}_r^2}{2\mu} + \frac{1}{2}\mu\omega_r^2\hat{r}^2\right], \tag{C.10c}$$

which is the Hamiltonian for two independent harmonic oscillators with masses M and μ and angular frequencies ω_R and ω_r. Since the total wavefunctions for a separable Hamiltonian are products of the separate wavefunctions, and we know the harmonic oscillator ground state wavefunction from eq. (2.29) on page 17, we can write the ground state wavefunction of $\hat{H}_1$:

$$\psi_1(R,r) = \left(\frac{M\mu\omega_R\omega_r}{\pi^2\hbar^2}\right)^{\frac{1}{4}} \exp\left[-\frac{M\omega_R}{2\hbar}R^2 - \frac{\mu\omega_r}{2\hbar}r^2\right] \tag{C.11a}$$

$$= \left(\frac{m^2\omega_R\omega_r}{\pi^2\hbar^2}\right)^{\frac{1}{4}} \exp\left[-\frac{4m\omega_R R^2 + m\omega_r r^2}{4\hbar}\right]. \tag{C.11b}$$

In terms of the original coordinates, and with the introduction of

$$\omega^{\pm} = \omega_R \pm \omega_r, \tag{C.12}$$

this is

$$\psi_1(q_A,q_B) = \left(\frac{m^2\omega_R\omega_r}{\pi^2\hbar^2}\right)^{\frac{1}{4}} \exp\left[-\frac{m}{4\hbar}\left(\omega_R(q_A+q_B)^2 + \omega_r(q_A-q_B)^2\right)\right] \tag{C.13a}$$

$$= \left(\frac{m^2\omega_R\omega_r}{\pi^2\hbar^2}\right)^{\frac{1}{4}} \exp\left[-\frac{m}{4\hbar}\left(\omega^+(q_A^2+q_B^2) + 2\omega^- q_A q_B\right)\right]. \tag{C.13b}$$

We may finally extend this solution back to the D-dimensional case:

$$\Psi_0(\mathbf{q}_A, \mathbf{q}_B) = \left(\frac{m^2\omega_R\omega_r}{\pi^2\hbar^2}\right)^{\frac{D}{4}} \exp\left[-\frac{m}{4\hbar}\left(\omega^+\left(|\mathbf{q}_A|^2 + |\mathbf{q}_B|^2\right) + 2\omega^-\mathbf{q}_A \cdot \mathbf{q}_B\right)\right]. \tag{C.14}$$

Since the ground state energy of a harmonic oscillator with angular frequency ω is $\hbar\omega/2$ [Mes99, p. 438] and the total energy of a separable Hamiltonian is the sum of those of its parts, the total ground state energy for the coupled harmonic oscillators in D dimensions is

$$E_0 = \frac{D\hbar}{2}(\omega_R + \omega_r). \tag{C.15}$$

C.2 Exact Rényi entropy

Now that we have the ground state wavefunction, we can find the exact expression for the second Rényi entropy S_2 in the ground state of the coupled harmonic oscillator system with the natural bipartitioning. From eq. (2.17) on page 12, we know that

$$\mathrm{Tr}\,\hat{\varrho}_A^2 = \iiiint \mathrm{d}\mathbf{q}_A\,\mathrm{d}\mathbf{q}'_A\,\mathrm{d}\mathbf{q}_B\,\mathrm{d}\mathbf{q}'_B\;\Psi_0(\mathbf{q}_A, \mathbf{q}_B)\Psi_0(\mathbf{q}'_A, \mathbf{q}_B)\Psi_0(\mathbf{q}'_A, \mathbf{q}'_B)\Psi_0(\mathbf{q}_A, \mathbf{q}'_B). \tag{C.16}$$

This $4D$-dimensional integral can be written as the product of D identical four-dimensional Gaussian integrals, so we shall first perform one of these (using eqs. (A.18) and (A.19) on page 84):

$$\iiiint \mathrm{d}q_A\,\mathrm{d}q'_A\,\mathrm{d}q_B\,\mathrm{d}q'_B\;\psi_1(q_A, q_B)\psi_1(q'_A, q_B)\psi_1(q'_A, q'_B)\psi_1(q_A, q'_B) \tag{C.17a}$$

$$\begin{aligned} = \frac{m^2\omega_R\omega_r}{\pi^2\hbar^2} \iint \mathrm{d}q_A\,\mathrm{d}q'_A\,\exp\left[-\frac{m}{2\hbar}\omega^+(q_A^2 + q_A'^2)\right] \\ \times \int \mathrm{d}q_B\,\exp\left[-\frac{m}{2\hbar}\left(\omega^+ q_B^2 + \omega^-(q_A + q'_A)q_B\right)\right] \\ \times \int \mathrm{d}q'_B\,\exp\left[-\frac{m}{2\hbar}\left(\omega^+ q_B'^2 + \omega^-(q_A + q'_A)q'_B\right)\right] \end{aligned} \tag{C.17b}$$

$$= \frac{2m\omega_R\omega_r}{\pi\hbar\omega^+} \iint \mathrm{d}q_A\,\mathrm{d}q'_A\,\exp\left[-\frac{m}{4\hbar\omega^+}\left(2(\omega^+)^2(q_A^2 + q_A'^2) - (\omega^-)^2(q_A + q'_A)^2\right)\right] \tag{C.17c}$$

$$= \frac{8\omega_R\omega_r}{\sqrt{(2(\omega^+)^2 - (\omega^-)^2)^2 - (\omega^-)^4)}} \tag{C.17d}$$

$$= \sqrt{\frac{4\omega_R\omega_r}{(\omega_R + \omega_r)^2}}. \tag{C.17e}$$

Putting the D pieces back together, we get

$$\mathrm{Tr}\,\hat{\varrho}_A^2 = \left(\frac{4\omega_R\omega_r}{(\omega_R + \omega_r)^2}\right)^{\frac{D}{2}}. \tag{C.18}$$

From this, we find

$$S_2 = -\log\left(\mathrm{Tr}\,\hat{\varrho}_A^2\right) = \frac{D}{2}\log\frac{(\omega_R + \omega_r)^2}{4\omega_R\omega_r} = \frac{D}{2}\log\left(1 + \frac{1}{4}\left(\sqrt{\frac{\omega_R}{\omega_r}} - \sqrt{\frac{\omega_r}{\omega_R}}\right)^2\right). \tag{C.19}$$

C.3 Energy convergence studies

> "When I wrestle," he told Garp, "I feel like I'm going downstairs in the dark; I don't know when I get to the bottom until I *feel* it."
>
> *The World According to Garp*
> John Irving

To verify that the force field and trial function are implemented correctly, we run convergence studies for the energy, which we can compare with eq. (C.15). The results are shown in fig. C.1. Additionally, these studies confirm that, at least as far as the energy is concerned, the values for the parameters in table 2.1 on page 23 are sufficient for convergence. The fact that the curves in fig. C.1b continue to rise as τ is decreased past the marked points indicates that we would need a shorter Δt if we wanted to run simulations with more beads.

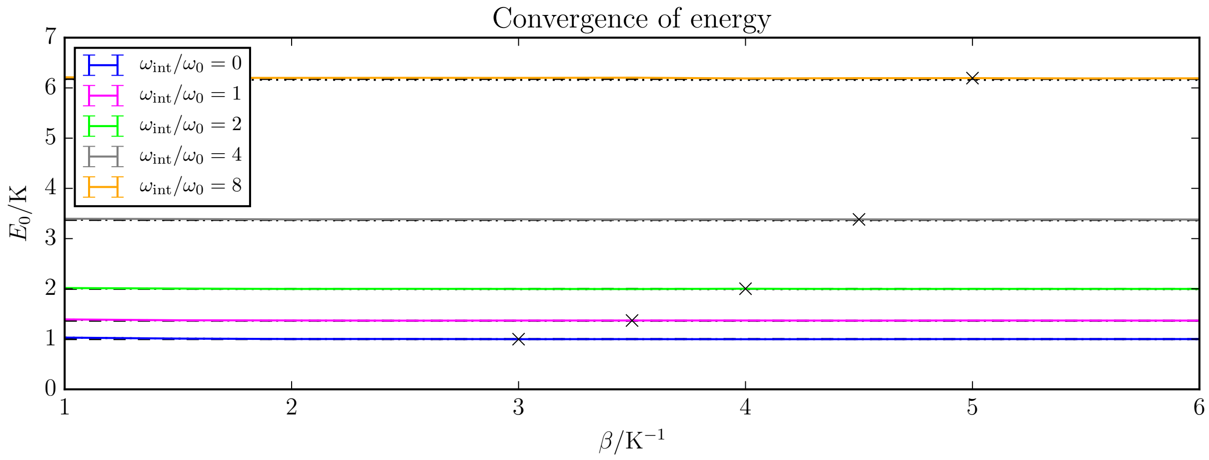

(a) Convergence of the energy with β. 10^6 steps.

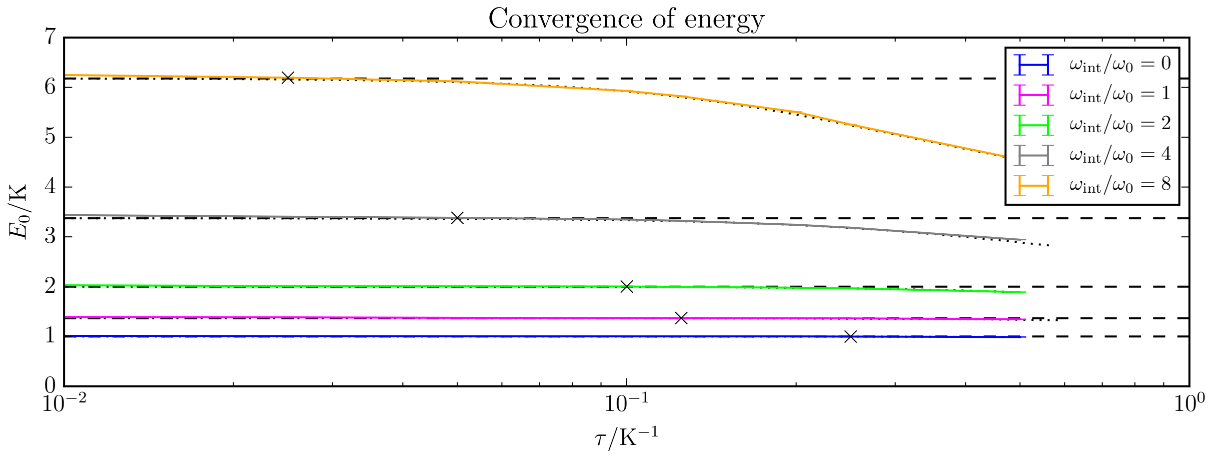

(b) Convergence of the energy with τ. 10^6 steps.

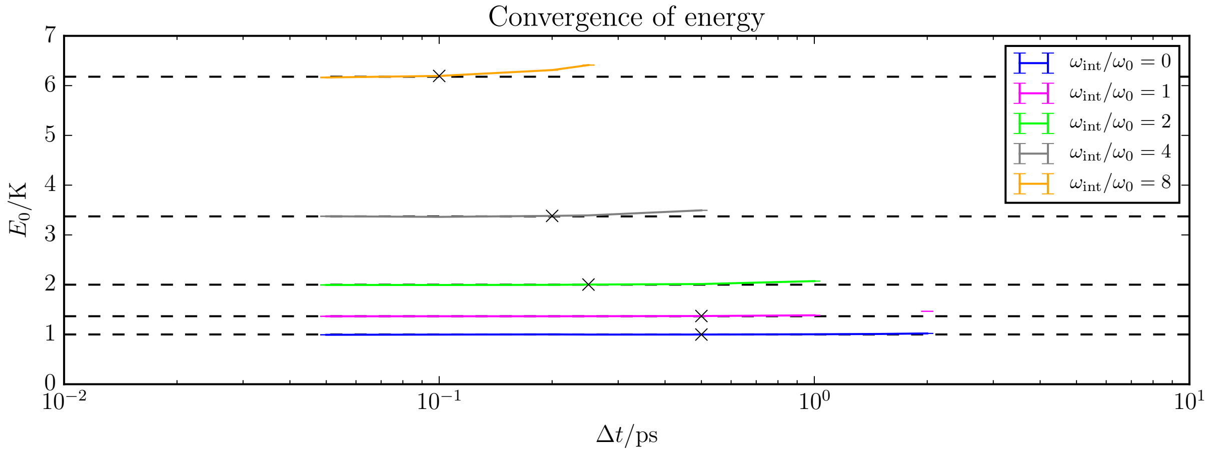

(c) Convergence of the energy with Δt. 10^6 steps.

Figure C.1: Successful convergence of the energy of the coupled oscillators with β, τ, and Δt. Dashed lines indicate the exact answer; dotted curves are the expected convergence obtained from a direct numerical method; crosses mark the values in table 2.1 on page 23.

Appendix D

Solutions to exercises

> All you need is not to be mistaken.
>
> WBaduk beginner problem BP00107

Exercise 1.1

Since

$$e^{-\beta\hat{H}}\left|\psi_{\mathrm{T}}\right\rangle = \sum_{n=0}^{\infty} e^{-\beta E_n}\left|n\right\rangle\left\langle n|\psi_{\mathrm{T}}\right\rangle \tag{D.1a}$$

$$= e^{-\beta E_0}\left[\left|0\right\rangle\left\langle 0|\psi_{\mathrm{T}}\right\rangle + \sum_{n=1}^{\infty} e^{-\beta(E_n-E_0)}\left|n\right\rangle\left\langle n|\psi_{\mathrm{T}}\right\rangle\right], \tag{D.1b}$$

all the terms in the sum after the $n = 0$ term will be exponentially suppressed with increasing β. As long as the factor $\langle 0|\psi_{\mathrm{T}}\rangle$ does not vanish, the ground state will be projected out of the trial function:

$$\lim_{\beta\to\infty} e^{-\beta\hat{H}}\left|\psi_{\mathrm{T}}\right\rangle \propto \left|0\right\rangle. \tag{D.2}$$

Exercise 1.2

We assume a Cartesian, N-particle Hamiltonian of the form

$$\hat{H} = \hat{K} + \hat{V} = \left[\sum_{n=0}^{N-1}\hat{K}_n\right] + \hat{V} = \left[\sum_{n=0}^{N-1}\frac{\left|\hat{\mathbf{p}}_n\right|^2}{2m_n}\right] + \hat{V}, \tag{D.3}$$

where the potential operator is sufficiently well-behaved that we may write

$$\hat{H} = \left[\sum_{n=0}^{N-1}\frac{\left|\hat{\mathbf{p}}_n\right|^2}{2m_n}\right] + V(\hat{\mathbf{q}}_0, \hat{\mathbf{q}}_1, \ldots, \hat{\mathbf{q}}_{N-1}). \tag{D.4}$$

We begin with the approximate pseudo partition function

$$Z_\beta = \mathrm{Tr}\,\hat{\varrho}_\beta = \langle\psi_\mathrm{T}|e^{-\beta\hat{H}}|\psi_\mathrm{T}\rangle\,. \tag{D.5}$$

Recalling that the resolution of the identity in any continuous basis is

$$\hat{1} = \int \mathrm{d}\mathbf{x}\ |\mathbf{x}\rangle\langle\mathbf{x}|\,, \tag{D.6}$$

we can introduce τ, P, and ℓ such that $\beta = (P-1)\tau = \ell\tau$[‡] and (without making any approximations) expand the Boltzmann operator as follows:

$$\begin{aligned}
Z_\beta &= \langle\psi_\mathrm{T}|e^{-\beta\hat{H}}|\psi_\mathrm{T}\rangle && \text{(D.7a)}\\
&= \langle\psi_\mathrm{T}| \left[\prod_{j=0}^{\ell-1} e^{-\tau\hat{H}}\right] |\psi_\mathrm{T}\rangle && \text{(D.7b)}\\
&= \langle\psi_\mathrm{T}| \left[\prod_{j=0}^{\ell-1} \left(\int \mathrm{d}\mathbf{q}^{(j)}\ |\mathbf{q}^{(j)}\rangle\langle\mathbf{q}^{(j)}|\right) e^{-\tau\hat{H}}\right] \left(\int \mathrm{d}\mathbf{q}^{(P-1)}\ |\mathbf{q}^{(P-1)}\rangle\langle\mathbf{q}^{(P-1)}|\right) |\psi_\mathrm{T}\rangle && \text{(D.7c)}\\
&= \int\cdots\int \left[\prod_{j=0}^{P-1} \mathrm{d}\mathbf{q}^{(j)}\right] \langle\psi_\mathrm{T}|\mathbf{q}^{(0)}\rangle \left[\prod_{j=0}^{\ell-1} \langle\mathbf{q}^{(j)}|e^{-\tau\hat{H}}|\mathbf{q}^{(j+1)}\rangle\right] \langle\mathbf{q}^{(P-1)}|\psi_\mathrm{T}\rangle && \text{(D.7d)}\\
&= \int \mathrm{d}\mathbf{q}\ \langle\psi_\mathrm{T}|\mathbf{q}^{(0)}\rangle\, \langle\mathbf{q}^{(P-1)}|\psi_\mathrm{T}\rangle \prod_{j=0}^{\ell-1} \langle\mathbf{q}^{(j)}|e^{-\tau\hat{H}}|\mathbf{q}^{(j+1)}\rangle\,. && \text{(D.7e)}
\end{aligned}$$

The integrand resembles a path of P positions (referred to as "beads") connected by ℓ "links" of a nature that is still to be determined.

We require (without loss of generality) that $\langle\mathbf{q}|\psi_\mathrm{T}\rangle = \psi_\mathrm{T}(\mathbf{q})$ be a nodeless, positive, real function. This is a perfectly reasonable demand to make, since we expect our ground state wavefunction to also be a nodeless, positive, real function. The fact that it's real implies that

$$\langle\mathbf{q}|\psi_\mathrm{T}\rangle = \langle\psi_\mathrm{T}|\mathbf{q}\rangle\,. \tag{D.8}$$

That it's also nodeless and positive means that

$$\psi_\mathrm{T}(\mathbf{q}) = e^{\ln\psi_\mathrm{T}(\mathbf{q})}, \tag{D.9}$$

so following ref. [SCI14] we can define a fictitious potential

$$V_\mathrm{T}(\mathbf{q}) = -\frac{1}{\tau}\ln\psi_\mathrm{T}(\mathbf{q}) \tag{D.10}$$

arising due to the presence of the trial function. Thus, we obtain the expression

$$Z_\beta = \int \mathrm{d}\mathbf{q}\, e^{-\tau\left[V_\mathrm{T}(\mathbf{q}^{(0)})+V_\mathrm{T}(\mathbf{q}^{(P-1)})\right]} \prod_{j=0}^{\ell-1} \langle\mathbf{q}^{(j)}|e^{-\tau\hat{H}}|\mathbf{q}^{(j+1)}\rangle\,. \tag{D.11}$$

[‡] As per the existing convention, P is the number of *beads*. At finite temperature, paths would be closed loops thanks to the additional trace operation, so the number of beads would be equal to the number of *links*. In the ground state, paths turn out to be open chains capped by a trial function, so there must be one fewer link than there are beads. As a consequence, the value $P-1$ crops up frequently, but saying $P-1$ everywhere is tedious, so instead we use ℓ.

We would like to act with the high-temperature Boltzmann operator $e^{-\tau \hat{H}}$ on the position ket, but to do so would require us to diagonalize the Hamiltonian. If we could do that, this entire work would be moot! We could try to make use of the fact that $\hat{H} = \hat{K} + \hat{V}$, but since $\hat{K}$ and $\hat{V}$ in general don't commute, we have the inconvenient inequality

$$e^{-\tau \hat{H}} = e^{-\tau \hat{K} - \tau \hat{V}} \neq e^{-\tau \hat{K}} e^{-\tau \hat{V}}. \tag{D.12}$$

However, if we are willing to live with an additional systematic error, we can apply the symmetric Trotter factorization [SL95]

$$e^{-\tau \hat{H}} = e^{-\frac{\tau}{2}\hat{V}} e^{-\tau \hat{K}} e^{-\frac{\tau}{2}\hat{V}} + \mathcal{O}\left(\tau^3\right) \tag{D.13}$$

to each factor in the product, to get

$$\begin{aligned} \langle \mathbf{q}^{(j)} | e^{-\tau \hat{H}} | \mathbf{q}^{(j+1)} \rangle &\approx \langle \mathbf{q}^{(j)} | e^{-\frac{\tau}{2}\hat{V}} e^{-\tau \hat{K}} e^{-\frac{\tau}{2}\hat{V}} | \mathbf{q}^{(j+1)} \rangle & \text{(D.14a)} \\ &= e^{-\frac{\tau}{2}\left[V(\mathbf{q}^{(j)}) + V(\mathbf{q}^{(j+1)})\right]} \langle \mathbf{q}^{(j)} | \exp\left[-\frac{\tau}{2} \sum_{n=0}^{N-1} \frac{|\hat{\mathbf{p}}_n|^2}{m_n}\right] | \mathbf{q}^{(j+1)} \rangle . & \text{(D.14b)} \end{aligned}$$

Since the potential operator is diagonal in the position representation, we were able to simply act with the potential part of the exponential. The kinetic part is not as obvious, but we can still treat it exactly. Using eqs. (A.5) and (A.17) on pages 81 and 83 we find that the matrix elements are

$$\begin{aligned} &\langle \mathbf{q}^{(j)} | \exp\left[-\frac{\tau}{2} \sum_{n=0}^{N-1} \frac{|\hat{\mathbf{p}}_n|^2}{m_n}\right] | \mathbf{q}^{(j+1)} \rangle \\ &= \int \mathrm{d}\mathbf{p} \, \langle \mathbf{q}^{(j)} | \exp\left[-\frac{\tau}{2} \sum_{n=0}^{N-1} \frac{|\hat{\mathbf{p}}_n|^2}{m_n}\right] | \mathbf{p} \rangle \langle \mathbf{p} | \mathbf{q}^{(j+1)} \rangle & \text{(D.15a)} \\ &= \int \mathrm{d}\mathbf{p} \, \langle \mathbf{q}^{(j)} | \mathbf{p} \rangle \langle \mathbf{p} | \mathbf{q}^{(j+1)} \rangle \exp\left[-\frac{\tau}{2} \sum_{n=0}^{N-1} \frac{|\mathbf{p}_n|^2}{m_n}\right] & \text{(D.15b)} \\ &= \left[\frac{1}{2\pi\hbar}\right]^{ND} \int \mathrm{d}\mathbf{p} \, \exp\left[-\frac{\tau}{2}\left[\sum_{n=0}^{N-1} \frac{|\mathbf{p}_n|^2}{m_n}\right] + \frac{i}{\hbar}\left(\mathbf{q}^{(j)} - \mathbf{q}^{(j+1)}\right) \cdot \mathbf{p}\right] & \text{(D.15c)} \\ &= \left[\frac{1}{2\pi\hbar}\right]^{ND} \prod_{n=0}^{N-1} \int \mathrm{d}\mathbf{p}_n \, \exp\left[-\frac{\tau}{2}\frac{|\mathbf{p}_n|^2}{m_n} + \frac{i}{\hbar}\left(\mathbf{q}_n^{(j)} - \mathbf{q}_n^{(j+1)}\right) \cdot \mathbf{p}_n\right] & \text{(D.15d)} \\ &= \left[\frac{1}{2\pi\hbar}\right]^{ND} \prod_{n=0}^{N-1} \prod_{d=0}^{D-1} \int \mathrm{d}p_{n,d} \, \exp\left[-\frac{\tau}{2}\frac{p_{n,d}^2}{m_n} + \frac{i}{\hbar}\left(q_{n,d}^{(j)} - q_{n,d}^{(j+1)}\right) p_{n,d}\right] & \text{(D.15e)} \\ &= \left[\frac{1}{2\pi\hbar}\right]^{ND} \prod_{n=0}^{N-1} \prod_{d=0}^{D-1} \left[\frac{2\pi m_n}{\tau}\right]^{\frac{1}{2}} \exp\left[-\frac{m_n}{2\hbar^2\tau}\left(q_{n,d}^{(j)} - q_{n,d}^{(j+1)}\right)^2\right] & \text{(D.15f)} \\ &= \prod_{n=0}^{N-1} \left[\frac{m_n}{2\pi\hbar^2\tau}\right]^{\frac{D}{2}} \prod_{d=0}^{D-1} \exp\left[-\frac{m_n}{2\hbar^2\tau}\left(q_{n,d}^{(j)} - q_{n,d}^{(j+1)}\right)^2\right] & \text{(D.15g)} \\ &= \prod_{n=0}^{N-1} \left[\frac{m_n}{2\pi\hbar^2\tau}\right]^{\frac{D}{2}} \exp\left[-\frac{m_n}{2\hbar^2\tau}\left|\mathbf{q}_n^{(j)} - \mathbf{q}_n^{(j+1)}\right|^2\right]. & \text{(D.15h)} \end{aligned}$$

Before proceeding, we define[‡]

$$\omega_\ell = \frac{\ell}{\hbar\beta} = \frac{1}{\hbar\tau} \tag{D.16}$$

and

$$V_\ell(\mathbf{q}) = \frac{1}{\ell}\left[\frac{V(\mathbf{q}^{(0)})}{2} + V_{\mathrm{T}}(\mathbf{q}^{(0)}) + \left[\sum_{j=1}^{P-2} V(\mathbf{q}^{(j)})\right] + \frac{V(\mathbf{q}^{(P-1)})}{2} + V_{\mathrm{T}}(\mathbf{q}^{(P-1)})\right]. \tag{D.17}$$

Now we can substitute everything back into the expression for the pseudo partition function (and use "=" rather than "≈", boldly disregarding the systematic error due to the Trotter factorization):

$$\begin{aligned}
Z_\beta = \int &\mathrm{d}\mathbf{q}\, e^{-\tau\left[V_{\mathrm{T}}(\mathbf{q}^{(0)})+V_{\mathrm{T}}(\mathbf{q}^{(P-1)})\right]} \\
&\times \prod_{j=0}^{\ell-1} e^{-\frac{\tau}{2}\left[V(\mathbf{q}^{(j)})+V(\mathbf{q}^{(j+1)})\right]} \prod_{n=0}^{N-1}\left[\frac{m_n}{2\pi\hbar^2\tau}\right]^{\frac{D}{2}} \exp\left[-\frac{m_n}{2\hbar^2\tau}\left|\mathbf{q}_n^{(j)} - \mathbf{q}_n^{(j+1)}\right|^2\right] && \text{(D.18a)} \\
= \left[\prod_{n=0}^{N-1}\left[\frac{m_n}{2\pi\hbar^2\tau}\right]^{\frac{\ell D}{2}}\right] &\int \mathrm{d}\mathbf{q}\, \exp\left[-\tau\left[V_{\mathrm{T}}(\mathbf{q}^{(0)}) + V_{\mathrm{T}}(\mathbf{q}^{(P-1)})\right] - \frac{\tau}{2}\sum_{j=0}^{\ell-1}\left[V(\mathbf{q}^{(j)}) + V(\mathbf{q}^{(j+1)})\right]\right] \\
&\times \exp\left[-\sum_{n=0}^{N-1}\sum_{j=0}^{\ell-1}\frac{m_n}{2\hbar^2\tau}\left|\mathbf{q}_n^{(j)} - \mathbf{q}_n^{(j+1)}\right|^2\right] && \text{(D.18b)} \\
= \left[\prod_{n=0}^{N-1}\left[\frac{m_n}{2\pi\hbar^2\tau}\right]^{\frac{\ell D}{2}}\right] &\int \mathrm{d}\mathbf{q}\, \exp\left[-\beta V_\ell(\mathbf{q}) - \beta\sum_{n=0}^{N-1}\sum_{j=0}^{\ell-1}\frac{1}{2}\frac{m_n}{\ell}\omega_\ell^2\left|\mathbf{q}_n^{(j)} - \mathbf{q}_n^{(j+1)}\right|^2\right]. && \text{(D.18c)}
\end{aligned}$$

Since we are only interested in average properties, the constant factor is irrelevant (it will disappear when we normalize), so we only need to claim that

$$Z_\beta \propto \int \mathrm{d}\mathbf{q}\, \exp\left[-\beta V_\ell(\mathbf{q}) - \beta\sum_{n=0}^{N-1}\sum_{j=0}^{\ell-1}\frac{1}{2}\frac{m_n}{\ell}\omega_\ell^2\left|\mathbf{q}_n^{(j)} - \mathbf{q}_n^{(j+1)}\right|^2\right]. \tag{D.19}$$

The only approximation we have made so far to Z_β is the Trotter factorization, and we now have what looks like a classical potential composed of: the real system potential; the potential from the trial function; the "kinetic" potential in the form of harmonic springs with force constants $m_n\omega_\ell^2/\ell$. Note that the springs connect the beads of a single particle in sequence, forming a structure similar to an open-chain polymer.

Our goal is to relate the quantum system to a classical one, so we need to make Z_β look like a classical partition function:

$$Z \propto \iint \mathrm{d}\mathbf{p}\,\mathrm{d}\mathbf{q}\, e^{-\beta H(\mathbf{p},\mathbf{q})}. \tag{D.20}$$

[‡] Our ω_ℓ is identical in spirit to the ω_n of ref. [CPM10] and ω_{P-1} of ref. [CSI13].

To this end, we introduce an integral over fictitious momenta $\mathbf{p}^\star$:

$$\int \mathrm{d}\mathbf{p}^\star \, \exp\left[-\beta \sum_{n=0}^{N-1} \frac{\left|\mathbf{p}_n^\star\right|^2}{2m_n^\star}\right]. \tag{D.21}$$

The value of this integral depends on the fictitious masses $m_n^\star$, but since we are only interested in proportionality, these masses are arbitrary. If we define

$$V_{\mathrm{spr}}(\mathbf{q}) = \sum_{n=0}^{N-1} \sum_{j=0}^{\ell-1} \frac{1}{2} \frac{m_n}{\ell} \omega_\ell^2 \left|\mathbf{q}_n^{(j)} - \mathbf{q}_n^{(j+1)}\right|^2 \tag{D.22a}$$

$$V_{\mathrm{eff}}(\mathbf{q}) = V_\ell(\mathbf{q}) + V_{\mathrm{spr}}(\mathbf{q}) \tag{D.22b}$$

$$H_{\mathrm{cl}}(\mathbf{p}^\star, \mathbf{q}) = \left[\sum_{n=0}^{N-1} \frac{\left|\mathbf{p}_n^\star\right|^2}{2m_n^\star}\right] + V_{\mathrm{eff}}(\mathbf{q}), \tag{D.22c}$$

this leads us directly to

$$Z_\beta \propto \iint \mathrm{d}\mathbf{p}^\star \, \mathrm{d}\mathbf{q} \, e^{-\beta H_{\mathrm{cl}}(\mathbf{p}^\star, \mathbf{q})}. \tag{D.23}$$

Thus, we have obtained a classical system of open-chain polymers at reciprocal temperature β which is isomorphic to the original quantum system in the sense that its partition function is an approximation to the quantum pseudo partition function.

This is useful, because it allows us to indirectly determine average properties for the quantum system. For example, consider some property

$$\hat{A} \left|\mathbf{q}\right\rangle = A(\mathbf{q}) \left|\mathbf{q}\right\rangle \tag{D.24}$$

that is diagonal in the position representation. The quantum expectation of this property with respect to the state $\hat{\varrho}_\beta$ is

$$\langle \hat{A} \rangle_{\hat{\varrho}_\beta} = \frac{\mathrm{Tr}\, \hat{\varrho}_\beta \hat{A}}{\mathrm{Tr}\, \hat{\varrho}_\beta}. \tag{D.25}$$

As demonstrated above, the denominator is Z_β, and if we repeat the above analysis with the operator $\hat{A}$ present in the expansion, we will see that the numerator is proportional to

$$\iint \mathrm{d}\mathbf{p}^\star \, \mathrm{d}\mathbf{q} \, e^{-\beta H_{\mathrm{cl}}(\mathbf{p}^\star, \mathbf{q})} A(\mathbf{q}^{(M)}), \tag{D.26}$$

where $M = \ell/2$ is the index of the middle bead. Hence, for operators that are diagonal in the position representation, the quantum average is the same as the classical phase space average for the appropriate system:

$$\langle \hat{A} \rangle_{\hat{\varrho}_\beta} = \langle A \rangle_{Z_\beta}. \tag{D.27}$$

As shown elsewhere in this work, this idea can be extended to off-diagonal operators as well, making this method a rather powerful one.

Exercise 1.3

Note that we can write the spring potential from eq. (D.22a) in quadratic form as

$$V_{\mathrm{spr}}(\mathbf{q}) = \sum_{n=0}^{N-1}\sum_{j=0}^{\ell-1}\frac{1}{2}m_n^\star\omega_\ell^2\left|\mathbf{q}_n^{(j)} - \mathbf{q}_n^{(j+1)}\right|^2 \tag{D.28a}$$

$$= \sum_{n=0}^{N-1}\sum_{j=0}^{\ell-1}\sum_{d=0}^{D-1}\frac{1}{2}m_n^\star\omega_\ell^2\left(q_{n,d}^{(j)} - q_{n,d}^{(j+1)}\right)^2 \tag{D.28b}$$

$$= \omega_\ell^2\sum_{n=0}^{N-1}m_n^\star\sum_{d=0}^{D-1}\left(\sum_{j=0}^{\ell-1}\frac{1}{2}\left((q_{n,d}^{(j)})^2 - 2q_{n,d}^{(j)}q_{n,d}^{(j+1)} + (q_{n,d}^{(j+1)})^2\right)\right) \tag{D.28c}$$

$$= \omega_\ell^2\sum_{n=0}^{N-1}m_n^\star\sum_{d=0}^{D-1}\left(\sum_{j=0}^{\ell-1}\frac{1}{2}\left((q_{n,d}^{(j)})^2 + (q_{n,d}^{(j+1)})^2\right)\right) - \left(\sum_{j=0}^{\ell-1}q_{n,d}^{(j)}q_{n,d}^{(j+1)}\right) \tag{D.28d}$$

$$= \omega_\ell^2\sum_{n=0}^{N-1}m_n^\star\sum_{d=0}^{D-1}\frac{1}{2}\mathbf{q}_{n,d}^{\mathrm{T}}\underline{\mathbf{A}}\mathbf{q}_{n,d}, \tag{D.28e}$$

where the elements of $\underline{\mathbf{A}}$ are

$$a_{i,j} = \begin{cases} 1 & i = j \in \{0, P-1\} \\ 2 & i = j \notin \{0, P-1\} \\ -1 & |i-j| = 1 \\ 0 & \text{otherwise} \end{cases}, \tag{D.29}$$

and $\underline{\mathbf{A}}$ itself is a $(P \times P)$ tridiagonal matrix that looks like

$$\underline{\mathbf{A}} = \begin{pmatrix} 1 & -1 & 0 & \cdots & 0 & 0 \\ -1 & 2 & -1 & \cdots & 0 & 0 \\ 0 & -1 & 2 & \cdots & 0 & 0 \\ \vdots & \vdots & \vdots & \ddots & \vdots & \vdots \\ 0 & 0 & 0 & \cdots & 2 & -1 \\ 0 & 0 & 0 & \cdots & -1 & 1 \end{pmatrix}. \tag{D.30}$$

If we diagonalize $\underline{\mathbf{A}}$ as

$$\underline{\mathbf{A}} = \underline{\mathbf{S}}^{\mathrm{T}}\underline{\mathbf{\Lambda}}\underline{\mathbf{S}} \iff \underline{\mathbf{\Lambda}} = \underline{\mathbf{S}}\underline{\mathbf{A}}\underline{\mathbf{S}}^{\mathrm{T}}, \tag{D.31}$$

where $\underline{\mathbf{\Lambda}}$ is diagonal and $\underline{\mathbf{S}}$ is orthogonal, then we'll get a new set of coordinates $\tilde{\mathbf{q}}$ corresponding to normal modes with frequencies that are the diagonal elements of $\underline{\mathbf{\Lambda}}$:

$$\mathbf{q}_{n,d}^{\mathrm{T}}\underline{\mathbf{A}}\mathbf{q}_{n,d} = \mathbf{q}_{n,d}^{\mathrm{T}}(\underline{\mathbf{S}}^{\mathrm{T}}\underline{\mathbf{\Lambda}}\underline{\mathbf{S}})\mathbf{q}_{n,d} \tag{D.32a}$$

$$= (\mathbf{q}_{n,d}^{\mathrm{T}}\underline{\mathbf{S}}^{\mathrm{T}})\underline{\mathbf{\Lambda}}(\underline{\mathbf{S}}\mathbf{q}_{n,d}) \tag{D.32b}$$

$$= (\underline{\mathbf{S}}\mathbf{q}_{n,d})^{\mathrm{T}}\underline{\mathbf{\Lambda}}(\underline{\mathbf{S}}\mathbf{q}_{n,d}) \tag{D.32c}$$

$$= \tilde{\mathbf{q}}_{n,d}^{\mathrm{T}}\underline{\mathbf{\Lambda}}\tilde{\mathbf{q}}_{n,d}. \tag{D.32d}$$

The existing references for LePIGS (refs. [Con12, pp. 63-66] and [CSI13]) state how to perform the transformation, but do not describe its derivation. Since the derivation is fairly straightforward, it is presented here. The characteristic equation of $\underline{\mathbf{A}}$ is

$$\det\left(\underline{\mathbf{A}} - \lambda\underline{\mathbf{1}}\right) = 0. \tag{D.33}$$

Since the matrix in question is tridiagonal, we can use the method in ref. [El04] to find the determinant. We introduce the recurrence relation

$$f_0 = 1 \tag{D.34a}$$
$$f_1 = 1 - \lambda \tag{D.34b}$$
$$f_n = (2 - \lambda) f_{n-1} - f_{n-2}, \tag{D.34c}$$

where

$$\det\left(\underline{\mathbf{A}} - \lambda\underline{\mathbf{1}}\right) = (1 - \lambda) f_{P-1} - f_{P-2}. \tag{D.35}$$

By eq. (A.28), this recurrence relation has the general solution

$$f_n = \begin{cases} 1 & \text{if } \lambda = 0 \\ (1 + 2n)(-1)^n & \text{if } \lambda = 4 \\ \frac{1}{2^{n+1}} \left[\left(1 - \frac{\lambda}{\sqrt{\lambda^2 - 4\lambda}}\right) \left(2 - \lambda + \sqrt{\lambda^2 - 4\lambda}\right)^n \right. & \\ \qquad \left. + \left(1 + \frac{\lambda}{\sqrt{\lambda^2 - 4\lambda}}\right) \left(2 - \lambda - \sqrt{\lambda^2 - 4\lambda}\right)^n \right] & \text{otherwise} \end{cases}. \tag{D.36}$$

To find the eigenvalues λ of $\underline{\mathbf{A}}$, we need to solve the characteristic equation given above, which can be phrased as

$$(1 - \lambda) f_{P-1} = f_{P-2}. \tag{D.37}$$

Clearly, $\lambda = 0$ is always an eigenvalue of $\underline{\mathbf{A}}$, while $\lambda = 4$ never is. For the others, we need to do some work. We'll need the fact that

$$\left(2 - \lambda \pm \sqrt{\lambda^2 - 4\lambda}\right)^2 = 2\left[\lambda^2 - \left(4 \pm \sqrt{\lambda^2 - 4\lambda}\right)\lambda + 2\left(1 \pm \sqrt{\lambda^2 - 4\lambda}\right)\right]. \tag{D.38}$$

Some amount of tedious (but trivial) algebra later, we arrive at

$$\left(2 - \lambda + \sqrt{\lambda^2 - 4\lambda}\right)^P = \left(2 - \lambda - \sqrt{\lambda^2 - 4\lambda}\right)^P. \tag{D.39}$$

If the square root is real ($\lambda < 0$ or $\lambda > 4$), we get nothing interesting. On the other hand, if $0 < \lambda < 4$, then

$$\sqrt{\lambda^2 - 4\lambda} = i\sqrt{4\lambda - \lambda^2}, \tag{D.40}$$

so we can write eq. (D.39) in unit polar form (the modulus being 2^P on both sides) as

$$e^{iP\theta} = e^{-iP\theta}, \tag{D.41}$$

where θ is the complex argument of $2-\lambda+i\sqrt{4\lambda-\lambda^2}$. By a simple geometrical argument in the complex plane, we must require that $P\theta$ be an integer multiple π, so θ is an integer multiple of π/P. The solutions $e^{i\theta}$ of eq. (D.41) are therefore the $(2P)$th roots of unity (for $k=0,1,\ldots,2P-1$)

$$e^{i\theta}=\exp\left[\frac{\pi ik}{P}\right]. \tag{D.42}$$

In order to satisfy (from the Cartesian form)

$$\cos\left[\frac{\pi k}{P}\right]=1-\frac{\lambda}{2} \tag{D.43a}$$

$$\sin\left[\frac{\pi k}{P}\right]=\frac{1}{2}\sqrt{4\lambda-\lambda^2}, \tag{D.43b}$$

we must restrict λ to

$$2-2\cos\left[\frac{\pi k}{P}\right]=4\sin^2\left[\frac{\pi k}{2P}\right]. \tag{D.44}$$

Since

$$\sin^2\left[\frac{\pi(2P-k)}{2P}\right]=\sin^2\left[\pi-\frac{\pi k}{2P}\right]=\sin^2\left[\frac{\pi k}{2P}\right], \tag{D.45}$$

we only get distinct eigenvalues for k up to P. Additionally, for $k=P$, we find the non-eigenvalue $\lambda=4$, so we must exclude this possibility. Thus, the eigenvalues of $\underline{\mathbf{A}}$ are (for $k=0,1,\ldots,P-1$)

$$\lambda_k=4\sin^2\left[\frac{\pi k}{2P}\right]. \tag{D.46}$$

This covers only the first quarter of the oscillation of a sine, so the eigenvalues are all between 0 and 4 (and monotonically increasing with k).

Now that we've found the eigenvalues, we need to find the transformation matrix $\underline{\mathbf{S}}$. From the way we defined $\underline{\mathbf{S}}$ and $\underline{\mathbf{\Lambda}}$ in eq. (D.31), we have

$$\underline{\mathbf{A}}\mathbf{s}_k=\lambda_k\mathbf{s}_k, \tag{D.47}$$

so $\mathbf{s}_k$ (the rows of $\underline{\mathbf{S}}$) are the eigenvectors of $\underline{\mathbf{A}}$. If we choose an eigenvalue λ and the corresponding eigenvector $\mathbf{v}$, we can write this as

$$(\underline{\mathbf{A}}-\lambda\underline{\mathbf{1}})\mathbf{v}=\mathbf{0}, \tag{D.48}$$

which in explicit form (for $i=0,1,\ldots,P-1$) is

$$\sigma_i=\sum_{j=0}^{P-1}(a_{i,j}-\lambda\delta_{i,j})v_j=0. \tag{D.49}$$

Thanks to the tridiagonal structure of $\underline{\mathbf{A}}$, none of these sums have more than three terms:

$$\sigma_i=\begin{cases}(1-\lambda)v_0-v_1 & \text{if } i=0\\ (2-\lambda)v_i-v_{i-1}-v_{i+1} & \text{if } 1\le i\le P-2\\ (1-\lambda)v_{P-1}-v_{P-2} & \text{if } i=P-1\end{cases}. \tag{D.50}$$

Since we can renormalize the eigenvectors later, we arbitrarily choose $v_0 = 1$, to find

$$v_i = \begin{cases} 1 & \text{if } i = 0 \\ 1 - \lambda & \text{if } i = 1 \\ (2-\lambda)v_{i-1} - v_{i-2} & \text{if } 2 \le i \le P-1 \end{cases} \tag{D.51}$$

with the extra constraint that $(1-\lambda)v_{P-1} = v_{P-2}$. This is exactly the same as the recurrence relation in eq. (D.34), so we can use the terms of that relation directly as the elements of the eigenvectors! We know that

$$1 \mp \frac{\lambda_k}{\sqrt{\lambda_k^2 - 4\lambda_k}} = 1 \mp \frac{\sin\left[\frac{\pi k}{2P}\right]}{\sqrt{-\cos^2\left[\frac{\pi k}{2P}\right]}} = 1 \pm i \tan\left[\frac{\pi k}{2P}\right] = \frac{e^{\pm\frac{\pi i k}{2P}}}{\cos\left[\frac{\pi k}{2P}\right]} \tag{D.52a}$$

$$\frac{1}{2^n}\left(2 - \lambda_k \pm \sqrt{\lambda_k^2 - 4\lambda_k}\right)^n = e^{\frac{\pm \pi i k n}{P}}, \tag{D.52b}$$

so

$$s_{k,n} \propto \begin{cases} 1 & \text{if } k = 0 \\ \frac{1}{2}\left[\frac{e^{\frac{\pi i k}{2P}}}{\cos\left[\frac{\pi k}{2P}\right]} e^{\frac{\pi i k n}{P}} + \frac{e^{-\frac{\pi i k}{2P}}}{\cos\left[\frac{\pi k}{2P}\right]} e^{\frac{-\pi i k n}{P}}\right] & \text{otherwise} \end{cases}. \tag{D.53}$$

We are justified in dropping the cosines in the denominators, since they are constant *within a row* (*i.e.* eigenvector) and we will renormalize those explicitly. If we introduce the normalization constants C_k, we may simplify the above to just

$$s_{k,n} = C_k \cos\left[\frac{\pi}{P} k \left(n + \frac{1}{2}\right)\right]. \tag{D.54}$$

For the normalization, we demand that

$$\sum_{n=0}^{P-1} s_{k,n}^2 = C_k^2 \sum_{n=0}^{P-1} \cos^2\left[\frac{\pi}{P} k \left(n + \frac{1}{2}\right)\right] = 1 \tag{D.55}$$

By eq. (A.39) on page 86, this becomes

$$C_k = \begin{cases} \sqrt{\frac{1}{P}} & \text{if } k = 0 \\ \sqrt{\frac{2}{P}} & \text{otherwise} \end{cases}. \tag{D.56}$$

Thus, we have rederived the open path normal mode transformation[‡] and found it to be the same Discrete Cosine Transform as in ref. [Con12].[§] The spring potential from eq. (D.28e) may be written in the new coordinates as

---

[‡] The reader may be interested in comparing this to the closed path normal mode transformation derived in section 5.2 on page 78.

[§] Some technical details relating to the DCT are discussed in appendix B on page 89.

$$V_{\mathrm{spr}}(\tilde{\mathbf{q}}) = \omega_\ell^2 \sum_{n=0}^{N-1} m_n^\star \sum_{d=0}^{D-1} \frac{1}{2} \tilde{\mathbf{q}}_{n,d}^{\mathrm{T}} \underline{\mathbf{\Lambda}} \tilde{\mathbf{q}}_{n,d} \tag{D.57a}$$

$$= \sum_{n=0}^{N-1} \sum_{k=0}^{P-1} \sum_{d=0}^{D-1} \frac{1}{2} m_n^\star \omega_\ell^2 \lambda_k (\tilde{q}_{n,d}^{(k)})^2 \tag{D.57b}$$

$$= \sum_{n,k,d} \frac{1}{2} m_n^\star \omega_k^2 (\tilde{q}_{n,d}^{(k)})^2, \tag{D.57c}$$

where we have introduced the mode-specific frequencies

$$\omega_k = 2\omega_\ell \sin\left[\frac{\pi k}{2P}\right] = \frac{2}{\hbar\tau} \sin\left[\frac{\pi k}{2P}\right], \tag{D.58}$$

whose distribution is shown in fig. D.1. In these coordinates, we have obtained NPD independent harmonic oscillators with masses $m_n^\star$ and frequencies ω_k.

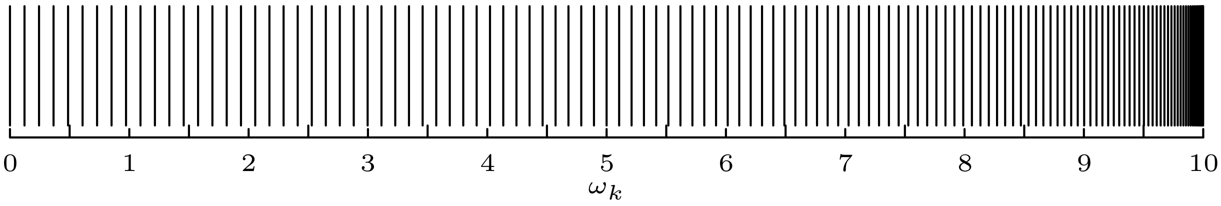

Figure D.1: Distribution of ω_k for PIGS free particle normal modes for $P = 129$. The scale is arbitrary, set by a particular choice of τ, but the general shape of the distribution is the same for any P and τ. Most of the modes are clustered at the higher frequencies.

It remains necessary to find the canonical momenta for these new coordinates. Since there are no quantum momenta with which to confuse them, we will use the label p (rather than $p^\star$) for the fictitious momenta. In terms of the Lagrangian $\mathcal{L}$, the canonical momenta are [EM08, p. 35]

$$\tilde{p}_{n,d}^{(k)} = \frac{\partial \mathcal{L}}{\partial \dot{\tilde{q}}_{n,d}^{(k)}} = \sum_{j=0}^{P-1} \frac{\partial \mathcal{L}}{\partial \dot{q}_{n,d}^{(j)}} \frac{\partial \dot{q}_{n,d}^{(j)}}{\partial \dot{\tilde{q}}_{n,d}^{(k)}} = \sum_{j=0}^{P-1} p_{n,d}^{(j)} \frac{\partial \dot{q}_{n,d}^{(j)}}{\partial \dot{\tilde{q}}_{n,d}^{(k)}}. \tag{D.59}$$

Since

$$q_{n,d}^{(j)}(\tilde{\mathbf{q}}) = (\underline{\mathbf{S}}^{\mathrm{T}} \tilde{\mathbf{q}})^{(j)} \tag{D.60}$$

and $\underline{\mathbf{S}}$ is independent of time, we have that

$$\dot{q}_{n,d}^{(j)}(\dot{\tilde{\mathbf{q}}}) = (\underline{\mathbf{S}}^{\mathrm{T}} \dot{\tilde{\mathbf{q}}})^{(j)} = \sum_{k=0}^{P-1} s_{k,j} \dot{\tilde{q}}_{n,d}^{(k)} \tag{D.61}$$

and

$$\frac{\partial \dot{q}_{n,d}^{(j)}}{\partial \dot{\tilde{q}}_{n,d}^{(k)}} = s_{k,j}. \tag{D.62}$$

Therefore,

$$\tilde{p}_{n,d}^{(k)} = \sum_{j=0}^{P-1} s_{k,j} p_{n,d}^{(j)} = (\underline{\mathbf{S}}\mathbf{p}_{n,d})^{(k)}. \tag{D.63}$$

That is, to obtain the canonical momenta, we apply the same transformation as for the coordinates.

Exercise 1.4

We wish to simulate the classical Hamiltonian given in eq. (D.22c) on page 103 at reciprocal temperature β using a Langevin thermostat. We choose the fictitious masses to be

$$m_n^\star = \frac{m_n}{\ell}. \tag{D.64}$$

Since we are not particularly interested in particles, beads, or dimensions for the time being, we will index things with a generic subscript $f \in \{0, 1, \dots, F-1\}$, signifying the fth degree of freedom, greatly reducing visual clutter. To find the simulation algorithm, we will closely follow the approach of refs. [BP07, CPM10].

For the framework of the algorithm, we want to use the Trotter-like expansion of the real-time propagator presented in ref. [TBM92], so we will need to figure out what this propagator is.[‡] Because it is more convenient for all parts of the algorithm other than application of the potential V_ℓ, we will do everything in the normal mode coordinates given by the transformation $\underline{\mathbf{S}}$ in eq. (D.54) on page 107. Since we are using Langevin dynamics, our equations of motion are [Kub66]

$$\dot{\tilde{p}}_f(t) = \tilde{F}_f(\tilde{\mathbf{q}}(t)) - \gamma_f \tilde{p}_f(t) + R_f(t) \tag{D.65a}$$

$$\dot{\tilde{q}}_f(t) = \frac{\tilde{p}_f(t)}{m_f}, \tag{D.65b}$$

where $\boldsymbol{\gamma}$ are *frictions* and $\mathbf{R}(t)$ are *random forces* (independent for each degree of freedom). In our notation, $\tilde{F}_f$ is the force applied to a normal mode degree of freedom by the total effective potential:

$$\tilde{\mathbf{F}}(\tilde{\mathbf{q}}) = -\frac{\partial V_{\text{eff}}}{\partial \tilde{\mathbf{q}}}. \tag{D.66}$$

It may seem strange that we wanted to introduce temperature, but there is no mention of temperature in these equations. However, we have not yet explained what the random force needs to be! By the fluctuation-dissipation theorem, each element of the random force vector must obey [Zwa01, pp. 5-6]

$$\langle R_f(t) \rangle = 0 \tag{D.67a}$$

$$\langle R_f(t) R_f(t') \rangle = \frac{2 m_f \gamma_f}{\beta} \delta\big(t - t'\big). \tag{D.67b}$$

It is crucial to note that $\beta = 1/k_{\mathrm{B}}T$ here is exactly the temperature we are trying to simulate, and it is only indirectly related to concepts like path length and imaginary propagation time; this distinction becomes important when the classical polymers in the simulation may have different lengths. The autocorrelation of a standard normal random number ("Gaussian number") $\xi_f(t)$ is [CPM10]

[‡] Some background on the subject is provided in ref. [EM08, pp. 44-50] and ref. [Zwa01, pp. 31-35].

$$\langle \xi_f(t) \xi_f(t') \rangle = \delta\big(t - t'\big) \,, \tag{D.68}$$

from which we deduce that

$$R_f(t) = \sqrt{\frac{2 m_f \gamma_f}{\beta}} \xi_f(t). \tag{D.69}$$

To find the time evolution operator, we need the Fokker–Planck equation corresponding to the Langevin equations in eq. (D.65). If we were dealing with Hamiltonian dynamics, this would just be the Liouville equation [Zwa01, p. 32]

$$\frac{\partial}{\partial t} \varphi = -\hat{L} \varphi \tag{D.70}$$

for the probability distribution function φ, with the Liouvillian

$$\hat{L} = -\frac{\partial}{\partial t} = \sum_f \frac{\partial H}{\partial \tilde{p}_f} \frac{\partial}{\partial \tilde{q}_f} - \frac{\partial H}{\partial \tilde{q}_f} \frac{\partial}{\partial \tilde{p}_f} \,. \tag{D.71}$$

However, eq. (D.65a) is a stochastic differential equation, so things are not as pleasant as in the case of Hamiltonian dynamics. To deal with it, we use eqs. (3.110), (3.118), (3.119), (4.96), and (4.97) from ref. [Ris84, pp. 54-55,83]. Because the force field will in general couple the degrees of freedom, we put them all together and consider a system of $2F$ Langevin equations. We introduce the shorthand $\tilde{\boldsymbol{\Gamma}}$ to mean the combined vector of momenta $\tilde{\mathbf{p}}$ and positions $\tilde{\mathbf{q}}$. The h and g functions of ref. [Ris84] are then

$$h_{\tilde{p},f}(\tilde{\boldsymbol{\Gamma}}) = \tilde{F}_f(\tilde{\mathbf{q}}) - \gamma_f \tilde{p}_f \qquad h_{\tilde{q},f}(\tilde{\boldsymbol{\Gamma}}) = \frac{\tilde{p}_f}{m_f} \tag{D.72a}$$

$$g_{\tilde{p},ff'}(\tilde{\boldsymbol{\Gamma}}) = \delta_{f,f'} \sqrt{\frac{m_f \gamma_f}{\beta}} \qquad g_{\tilde{q},ff'}(\tilde{\boldsymbol{\Gamma}}) = 0. \tag{D.72b}$$

In our case there is no explicit time dependence. The Kramers–Moyal coefficients are

$$D_{\tilde{p},f}(\tilde{\boldsymbol{\Gamma}}) = \tilde{F}_f(\tilde{\mathbf{q}}) - \gamma_f \tilde{p}_f \qquad D_{\tilde{q},f}(\tilde{\boldsymbol{\Gamma}}) = \frac{\tilde{p}_f}{m_f} \tag{D.73a}$$

$$D_{\tilde{p},ff'}(\tilde{\boldsymbol{\Gamma}}) = \delta_{f,f'} \frac{m_f \gamma_f}{\beta} \qquad D_{\tilde{q},ff'}(\tilde{\boldsymbol{\Gamma}}) = 0, \tag{D.73b}$$

with all the higher coefficients zero. From this we can construct the (backward) Fokker–Planck operator[‡]

$$\hat{L} = \sum_f D_{\tilde{p},f}(\tilde{\boldsymbol{\Gamma}}) \frac{\partial}{\partial \tilde{p}_f} + D_{\tilde{q},f}(\tilde{\boldsymbol{\Gamma}}) \frac{\partial}{\partial \tilde{q}_f} + D_{\tilde{p},ff'}(\tilde{\boldsymbol{\Gamma}}) \tfrac{\partial^2}{\partial \tilde{p}_f \partial \tilde{p}_{f'}} \tag{D.74a}$$

$$= \sum_f \tilde{F}_f(\tilde{\mathbf{q}}) \frac{\partial}{\partial \tilde{p}_f} - \gamma_f \tilde{p}_f \frac{\partial}{\partial \tilde{p}_f} + \frac{\tilde{p}_f}{m_f} \frac{\partial}{\partial \tilde{q}_f} + \frac{m_f \gamma_f}{\beta} \frac{\partial^2}{\partial \tilde{p}_f^2} \tag{D.74b}$$

$$= \sum_f \tilde{F}_f(\tilde{\mathbf{q}}) \frac{\partial}{\partial \tilde{p}_f} + \frac{\tilde{p}_f}{m_f} \frac{\partial}{\partial \tilde{q}_f} - \gamma_f \left(\tilde{p}_f \frac{\partial}{\partial \tilde{p}_f} - \frac{m_f}{\beta} \frac{\partial^2}{\partial \tilde{p}_f^2} \right) , \tag{D.74c}$$

[‡] Ref. [Ris84, p. 83] refers to this operator as $\boldsymbol{L}_{\mathrm{FP}}^{\dagger}$, while ref. [Zwa01, pp. 42-43] calls it $\mathcal{D}^{\dagger}$.

which gives us our real-time propagator $e^{\hat{L}t}$ [Zwa01, pp. 42-43].[‡]

We may now apply the factorization to this propagator. We will break the total time t into S time steps of length Δt: $t = S\Delta t$. Instead of the splitting recommended in ref. [BP07], we will group the "kinetic" spring potential (see eq. (D.22a)) with the free particle motion and use the splitting given in ref. [CPM10]. The effective potential in eq. (D.22b) is already in the form we desire, so it should be simple to split the force. However, the force we are splitting is in the transformed coordinates, so we need to be careful. We define

$$\mathbf{F}_K(\mathbf{q}) = -\frac{\partial V_{\text{spr}}}{\partial \mathbf{q}} \tag{D.75a}$$

$$\mathbf{F}_V(\mathbf{q}) = -\frac{\partial V_\ell}{\partial \mathbf{q}}. \tag{D.75b}$$

At this point we can no longer ignore the structure of the problem, and we return to the full subscripts for the degrees of freedom. Naturally,

$$F_{n,d}^{(j)}(\mathbf{q}) = -\frac{\partial V_{\text{eff}}}{\partial q_{n,d}^{(j)}} = -\frac{\partial V_{\text{spr}}}{\partial q_{n,d}^{(j)}} - \frac{\partial V_\ell}{\partial q_{n,d}^{(j)}} \tag{D.76a}$$

$$= F_{K,n,d}^{(j)}(\mathbf{q}) + F_{V,n,d}^{(j)}(\mathbf{q}). \tag{D.76b}$$

Less obviously,

$$\tilde{F}_{n,d}^{(k)}(\tilde{\mathbf{q}}) = -\frac{\partial V_{\text{eff}}}{\partial \tilde{q}_{n,d}^{(k)}} = -\sum_{j=0}^{P-1} \frac{\partial V_{\text{eff}}}{\partial q_{n,d}^{(j)}} \frac{\partial q_{n,d}^{(j)}}{\partial \tilde{q}_{n,d}^{(k)}} = -\sum_{j=0}^{P-1} \left[\frac{\partial V_{\text{spr}}}{\partial q_{n,d}^{(j)}} + \frac{\partial V_\ell}{\partial q_{n,d}^{(j)}} \right] \frac{\partial q_{n,d}^{(j)}}{\partial \tilde{q}_{n,d}^{(k)}} \tag{D.77a}$$

$$= -\sum_{j=0}^{P-1} s_{k,j} \left[\frac{\partial V_{\text{spr}}}{\partial q_{n,d}^{(j)}} + \frac{\partial V_\ell}{\partial q_{n,d}^{(j)}} \right] \tag{D.77b}$$

$$= \tilde{F}_{K,n,d}^{(k)}(\tilde{\mathbf{q}}) + \tilde{F}_{V,n,d}^{(k)}(\tilde{\mathbf{q}}). \tag{D.77c}$$

Thus, we may write

$$\hat{L}_0 = \sum_{n,k,d} \frac{\tilde{p}_{n,d}^{(k)}}{m_n^\star} \frac{\partial}{\partial \tilde{q}_{n,d}^{(k)}} + \tilde{F}_{K,n,d}^{(k)}(\tilde{\mathbf{q}}) \frac{\partial}{\partial \tilde{p}_{n,d}^{(k)}} \tag{D.78a}$$

$$\hat{L}_V = \sum_{n,k,d} \tilde{F}_{V,n,d}^{(k)}(\tilde{\mathbf{q}}) \frac{\partial}{\partial \tilde{p}_{n,d}^{(k)}} \tag{D.78b}$$

$$\hat{L}_\gamma = \sum_{n,k,d} \gamma_{n,d}^{(k)} \left(\frac{m_n^\star}{\beta} \frac{\partial^2}{\partial (\tilde{p}_{n,d}^{(k)})^2} - \tilde{p}_{n,d}^{(k)} \frac{\partial}{\partial \tilde{p}_{n,d}^{(k)}} \right), \tag{D.78c}$$

so that $\hat{L} = \hat{L}_0 + \hat{L}_V + \hat{L}_\gamma$. This leads to (for a single time step) [BP07, TBM92]

$$e^{\hat{L}\Delta t} = e^{\hat{L}_\gamma \frac{\Delta t}{2}} e^{\hat{L}_V \frac{\Delta t}{2}} e^{\hat{L}_0 \Delta t} e^{\hat{L}_V \frac{\Delta t}{2}} e^{\hat{L}_\gamma \frac{\Delta t}{2}} + \mathcal{O}\Big(\Delta t^3\Big). \tag{D.79}$$

[‡] Our expression for a single degree of freedom in eq. (D.74c) differs slightly from eq. (4) of ref. [BP07], because we have chosen a different convention for the operator (using its adjoint instead).

The last piece we need is the result of each propagator on a state $\mathbf{\Gamma}(t)$. Let us proceed from the inside out.

The propagator $e^{\hat{L}_0 \Delta t}$ describes the motion of a collection of independent harmonic oscillators with the equations of motion

$$\dot{\tilde{p}}^{(k)}_{n,d}(t) = -m^\star_n \omega_k^2 \tilde{q}^{(k)}_{n,d}(t) \tag{D.80a}$$

$$\dot{\tilde{q}}^{(k)}_{n,d}(t) = \frac{\tilde{p}^{(k)}_{n,d}(t)}{m^\star_n}. \tag{D.80b}$$

The trajectory that is the solution to these differential equations is [Zwa01, p. 31]

$$\tilde{p}^{(k)}_{n,d}(t_\mathrm{f}) = \cos{(\omega_k \Delta t)} \tilde{p}^{(k)}_{n,d}(t_\mathrm{i}) - m^\star_n \omega_k \sin{(\omega_k \Delta t)} \tilde{q}^{(k)}_{n,d}(t_\mathrm{i}) \tag{D.81a}$$

$$\tilde{q}^{(k)}_{n,d}(t_\mathrm{f}) = \frac{1}{m^\star_n \omega_k} \sin{(\omega_k \Delta t)} \tilde{p}^{(k)}_{n,d}(t_\mathrm{i}) + \cos{(\omega_k \Delta t)} \tilde{q}^{(k)}_{n,d}(t_\mathrm{i}), \tag{D.81b}$$

which may be written more compactly as

$$\begin{pmatrix} \tilde{p}^{(k)}_{n,d}(t_\mathrm{f}) \\ \tilde{q}^{(k)}_{n,d}(t_\mathrm{f}) \end{pmatrix} = \begin{pmatrix} \cos \omega_k \Delta t & -m^\star_n \omega_k \sin \omega_k \Delta t \\ \frac{1}{m^\star_n \omega_k} \sin \omega_k \Delta t & \cos \omega_k \Delta t \end{pmatrix} \begin{pmatrix} \tilde{p}^{(k)}_{n,d}(t_\mathrm{i}) \\ \tilde{q}^{(k)}_{n,d}(t_\mathrm{i}) \end{pmatrix}. \tag{D.82}$$

We need to be careful about the centroid mode, since $\omega_0 = 0$ and we'd rather not divide by that. Applying l'Hôpital's rule, we get the sinc limit:

$$\lim_{\omega_k \to 0} \frac{\sin \omega_k \Delta t}{\omega_k \Delta t} = \lim_{\omega_k \to 0} \cos \omega_k \Delta t = 1, \tag{D.83}$$

so the centroid is updated by

$$\begin{pmatrix} \tilde{p}^{(0)}_{n,d}(t_\mathrm{f}) \\ \tilde{q}^{(0)}_{n,d}(t_\mathrm{f}) \end{pmatrix} = \begin{pmatrix} 1 & 0 \\ \frac{\Delta t}{m^\star_n} & 1 \end{pmatrix} \begin{pmatrix} \tilde{p}^{(0)}_{n,d}(t_\mathrm{i}) \\ \tilde{q}^{(0)}_{n,d}(t_\mathrm{i}) \end{pmatrix}. \tag{D.84}$$

If we make use of the function

$$\operatorname{sinc} \omega_k \Delta t = \begin{cases} 1 & \text{if } \omega_k \Delta t = 0 \\ \frac{\sin \omega_k \Delta t}{\omega_k \Delta t} & \text{otherwise} \end{cases}, \tag{D.85}$$

we can write the general case as

$$\begin{pmatrix} \tilde{p}^{(k)}_{n,d}(t_\mathrm{f}) \\ \tilde{q}^{(k)}_{n,d}(t_\mathrm{f}) \end{pmatrix} = \begin{pmatrix} \cos \omega_k \Delta t & -m^\star_n \omega_k \sin \omega_k \Delta t \\ \frac{\Delta t}{m^\star_n} \operatorname{sinc} \omega_k \Delta t & \cos \omega_k \Delta t \end{pmatrix} \begin{pmatrix} \tilde{p}^{(k)}_{n,d}(t_\mathrm{i}) \\ \tilde{q}^{(k)}_{n,d}(t_\mathrm{i}) \end{pmatrix}. \tag{D.86}$$

The propagator $e^{\hat{L}_V \frac{\Delta t}{2}}$ is extremely simple, and its effect is most easily determined using eq. (A.51). Without making any additional approximations, the propagator may be written as

$$\exp\left[\hat{L}_V \frac{\Delta t}{2}\right] = \exp\left[\frac{\Delta t}{2} \sum_{n,k,d} \tilde{F}^{(k)}_{V,n,d} \frac{\partial}{\partial \tilde{p}^{(k)}_{n,d}}\right] = \exp\left[\frac{\Delta t}{2} \tilde{\mathbf{F}}_V \cdot \frac{\partial}{\partial \tilde{\mathbf{p}}}\right]. \tag{D.87}$$

Thus,

$$\begin{aligned}(\tilde{\mathbf{p}}(t_\mathrm{f}), \tilde{\mathbf{q}}(t_\mathrm{f})) &= e^{\hat{L}_V \frac{\Delta t}{2}} (\tilde{\mathbf{p}}(t_\mathrm{i}), \tilde{\mathbf{q}}(t_\mathrm{i})) && \text{(D.88a)}\\ &= \left(\tilde{\mathbf{p}}(t_\mathrm{i}) + \frac{\Delta t}{2} \tilde{\mathbf{F}}_V, \tilde{\mathbf{q}}(t_\mathrm{i}) \right). && \text{(D.88b)}\end{aligned}$$

The only potential difficulty with this result is that in practice $\mathbf{F}_V$ will most likely be expressed in Cartesian coordinates. However, this is easy to handle, since

$$\begin{aligned}\tilde{\mathbf{p}}_{n,d} + \frac{\Delta t}{2} \tilde{\mathbf{F}}_{V,n,d} &= \underline{\mathbf{S}} \mathbf{p}_{n,d} + \frac{\Delta t}{2} \underline{\mathbf{S}} \mathbf{F}_{V,n,d} && \text{(D.89a)}\\ &= \underline{\mathbf{S}} \left(\underline{\mathbf{S}}^\mathrm{T} \tilde{\mathbf{p}}_{n,d} + \frac{\Delta t}{2} \mathbf{F}_{V,n,d} \right) && \text{(D.89b)}\end{aligned}$$

means that we can update $\mathbf{p}$ in Cartesian coordinates using our regular expression for the force.

Finally, we must attack the thermostat propagator $e^{\hat{L}_\gamma \frac{\Delta t}{2}}$. Quite conveniently, the terms of $\hat{L}_\gamma$ for the different degrees of freedom commute, so we only need to solve for the generic one-dimensional case:

$$\exp \left[\frac{\Delta t}{2} \gamma \left(\frac{m}{\beta} \frac{\partial^2}{\partial \tilde{p}^2} - \tilde{p} \frac{\partial}{\partial \tilde{p}} \right) \right]. \tag{D.90}$$

This is an Ornstein–Uhlenbeck process, for which there is an exact "updating formula" [Gil92, p. 551]:

$$\tilde{p}(t_\mathrm{f}) = e^{-\gamma \frac{\Delta t}{2}} \tilde{p}(t_\mathrm{i}) + \sqrt{\frac{m}{\beta} (1 - e^{-\gamma \Delta t})} \xi(t_\mathrm{i}), \tag{D.91}$$

where $\xi(t)$ is again a Gaussian number. This result can be found by solving for the transition probability, which is a Gaussian distribution, and then applying the linear transformation theorem for a Gaussian distribution [Gil92, pp. 27-28]. It is the same result as obtained in ref. [BP07], and to be consistent we will define the same coefficients

$$\begin{aligned}c_1 &= e^{-\gamma \frac{\Delta t}{2}} && \text{(D.92a)}\\ c_2 &= \sqrt{\frac{m}{\beta} (1 - c_1^2)}. && \text{(D.92b)}\end{aligned}$$

It is then straightforward to extend this to all the degrees of freedom:

$$\begin{aligned}c_{1,n,d}^{(k)} &= e^{-\gamma_{n,d}^{(k)} \frac{\Delta t}{2}} && \text{(D.93a)}\\ c_{2,n,d}^{(k)} &= \sqrt{\frac{m_n^\star}{\beta} (1 - (c_{1,n,d}^{(k)})^2)} && \text{(D.93b)}\\ \tilde{p}_{n,d}^{(k)}(t_\mathrm{f}) &= c_{1,n,d}^{(k)} \tilde{p}_{n,d}^{(k)}(t_\mathrm{i}) + c_{2,n,d}^{(k)} \xi_{n,d}^{(k)}(t_\mathrm{i}). && \text{(D.93c)}\end{aligned}$$

We finally have a procedure for taking one time step in a LePIGS simulation. All the individual substeps are exact, and the only error we introduce is due to the factorization with a finite time step Δt. The complete procedure for a single time step Δt is as follows:

1. $\tilde{p}^{(k)}_{n,d} \leftarrow c^{(k)}_{1,n,d}\tilde{p}^{(k)}_{n,d} + c^{(k)}_{2,n,d}\xi^{(k)}_{n,d}$
2. $p^{(j)}_{n,d} \leftarrow p^{(j)}_{n,d} + \frac{\Delta t}{2} F^{(j)}_{V,n,d}(\mathbf{q})$
3. $\begin{pmatrix} \tilde{p}^{(k)}_{n,d} \\ \tilde{q}^{(k)}_{n,d} \end{pmatrix} \leftarrow \begin{pmatrix} \cos\omega_k\Delta t & -m^\star_n\omega_k \sin\omega_k\Delta t \\ \frac{\Delta t}{m^\star_n}\operatorname{sinc}\omega_k\Delta t & \cos\omega_k\Delta t \end{pmatrix} \begin{pmatrix} \tilde{p}^{(k)}_{n,d} \\ \tilde{q}^{(k)}_{n,d} \end{pmatrix}$
4. Repeat substep 2.
5. Repeat substep 1.

The following are implied:

- Each substep is performed for all degrees of freedom before moving on to the next substep. The order of updates within a substep is irrelevant.
- The coordinates and momenta are converted between Cartesian and normal mode representations between substeps as necessary.
- Each "invocation" of $\xi^{(k)}_{n,d}$ results in an independent number randomly drawn from a standard normal distribution.

Since our form of the equations of motion for a single thermostatted "free particle" degree of freedom is the same as of those in eq. (32) of ref. [CPM10], we are justified in using the same optimal frictions as those they give in eq. (36). Namely, for $k \geq 1$,

$$\gamma^{(k)}_{n,d} = 2\omega_k. \tag{D.94}$$

The centroid frictions $\gamma^{(0)}_{n,d}$ remain free parameters of the simulation.

Exercise 3.1

For a harmonic oscillator with mass m, angular frequency ω, and initial conditions p, q, the total energy is

$$H = \frac{p^2}{2m} + \frac{1}{2}m\omega^2 q^2. \tag{D.95}$$

The trajectory is given by eq. (D.81) on page 112, but is reproduced here without the extra flair on the symbols:

$$p_t = \cos(\omega t)p - m\omega\sin(\omega t)q \tag{D.96a}$$

$$q_t = \frac{1}{m\omega}\sin(\omega t)p + \cos(\omega t)q. \tag{D.96b}$$

We note that

$$p_t q_t = \big(\cos(\omega t)p - m\omega\sin(\omega t)q\big)\left(\frac{1}{m\omega}\sin(\omega t)p + \cos(\omega t)q\right) \tag{D.97a}$$

$$= \frac{1}{m\omega}\cos(\omega t)\sin(\omega t)p^2 + 2\cos^2(\omega t)pq - m\omega\cos(\omega t)\sin(\omega t)q^2 - pq. \tag{D.97b}$$

Therefore, the action is

$$\begin{aligned}
S_t &= \frac{1}{m}\int_0^t \mathrm{d}\tau\, (p_\tau)^2 - tH && \text{(D.98a)}\\
&= \frac{1}{m}\int_0^t \mathrm{d}\tau\, (\cos(\omega\tau)p - m\omega\sin(\omega\tau)q)^2 - \frac{t}{2}\frac{p^2}{m} - \frac{t}{2}m\omega^2 q^2 && \text{(D.98b)}\\
&= \frac{1}{m}\left(p^2\int_0^t \mathrm{d}\tau\, \cos^2(\omega\tau) - 2m\omega pq\int_0^t \mathrm{d}\tau\, \cos(\omega\tau)\sin(\omega\tau) + m^2\omega^2 q^2\int_0^t \mathrm{d}\tau\, \sin^2(\omega\tau)\right)\\
&\qquad - \frac{1}{m}\left(\frac{t}{2}p^2 + \frac{t}{2}m^2\omega^2 q^2\right) && \text{(D.98c)}\\
&= \frac{1}{m}\left(p^2\left[\frac{t}{2} + \frac{\sin(2\omega t)}{4\omega}\right] - mpq\sin^2(\omega t) + m^2\omega^2 q^2\left[\frac{t}{2} - \frac{\sin(2\omega t)}{4\omega}\right] - \frac{t}{2}p^2 - \frac{t}{2}m^2\omega^2 q^2\right)\\
& && \text{(D.98d)}\\
&= \frac{p^2}{2m}\frac{\sin(2\omega t)}{2\omega} - pq\sin^2(\omega t) - \frac{1}{2}m\omega^2 q^2\frac{\sin(2\omega t)}{2\omega} && \text{(D.98e)}\\
&= \frac{1}{2}\left(\frac{1}{m\omega}\cos(\omega t)\sin(\omega t)p^2 + 2\cos^2(\omega t)pq - m\omega\cos(\omega t)\sin(\omega t)q^2 - 2pq\right) && \text{(D.98f)}\\
&= \frac{1}{2}(p_t q_t - pq). && \text{(D.98g)}
\end{aligned}$$

For the HK prefactor, we need the elements of the monodromy matrix:

$$\begin{aligned}
\frac{\partial p_t}{\partial p} &= \cos(\omega t) & \frac{\partial p_t}{\partial q} &= -m\omega\sin(\omega t) && \text{(D.99a)}\\
\frac{\partial q_t}{\partial p} &= \frac{1}{m\omega}\sin(\omega t) & \frac{\partial q_t}{\partial q} &= \cos(\omega t). && \text{(D.99b)}
\end{aligned}$$

Thus, the HK prefactor is

$$\begin{aligned}
R_t &= \sqrt{\frac{1}{2}\left(\frac{\partial p_t^{p,q}}{\partial p} + \frac{\partial q_t^{p,q}}{\partial q} + \frac{i}{\hbar\gamma}\frac{\partial p_t^{p,q}}{\partial q} - i\hbar\gamma\frac{\partial q_t^{p,q}}{\partial p}\right)} && \text{(D.100a)}\\
&= \sqrt{\cos(\omega t) - \frac{i}{2}\left(\frac{m\omega}{\hbar\gamma} + \frac{\hbar\gamma}{m\omega}\right)\sin(\omega t)}. && \text{(D.100b)}
\end{aligned}$$

Note that in the case $\gamma = m\omega/\hbar$, the coherent states are on resonance with the oscillator and

$$R_t = \sqrt{\cos(\omega t) - i\sin(\omega t)}. \qquad \text{(D.101)}$$

Appendix E

Custom software

The following software was developed for the present work:

- **DrSwine** (`https://github.com/0/DrSwine`) is a minimal implementation of LePIGS written in the Racket programming language. Its focus is on the manipulation of paths as concrete objects rather than as manifestations of particles, allowing direct access to arbitrary sectors.
- **pathintmatmult** (`https://github.com/0/pathintmatmult`) is a Python 3 package for calculating wavefunctions and densities using path integrals (either finite temperature or ground state). Since it uses numerical matrix multiplication rather than Monte Carlo or molecular dynamics, it is limited to very low-dimensional systems. However, it provides numerically exact results, with systematic error but no statistical error.
- **realtimepork** (`https://github.com/0/realtimepork`) is a Python 3 package for finding real-time correlation functions for 1-dimensional systems using the approximate Herman–Kluk real-time propagator and PIGS ground state wavefunctions. It takes care of propagating the classical trajectories and combining the results using numerical integration. Some of the computation may be performed on a Graphics Processing Unit (GPU), leading to a significant increase in speed.

Appendix F

Code listings

The following listings show the Maple™ scripts (followed by their outputs) used for some of the calculations performed in the present work.[‡] Maple is a trademark of Waterloo Maple Inc.

Listing F.1: Integration of eq. (5.20) on page 70.

```
interface(showassumed=0):
assume(R >= 0, r > 0, r <= R):

Ltheta1 := r -> -r / (2 * R):
Lplus := (r, x) -> -r * x + sqrt(R^2 + r^2 * (x^2 - 1)):

int1 := int(int(r2^2, r2=0..R), x=-1..Ltheta1(r)):
int2 := int(int(r2^2, r2=0..Lplus(r, x)), x=Ltheta1(r)..1):
simplify(int1 + int2);
```

```
     3        2           3
2/3 R  - 1/2 R  r + 1/24 r
```

Listing F.2: Integration of eq. (5.25) on page 71.

```
interface(showassumed=0):
assume(R >= 0, r > 0, r^2 <= 2 * R^2):

Ltheta1 := r -> -r / (2 * R):
Ltheta2 := r -> -sqrt(1 - (R/r)^2):
Lminus := (r, x) -> -r * x - sqrt(R^2 + r^2 * (x^2 - 1)):
Lplus := (r, x) -> -r * x + sqrt(R^2 + r^2 * (x^2 - 1)):

int1 := int(int(r2^2, r2=Lminus(r, x)..R), x=-1..Ltheta1(r)):
int2 := int(int(r2^2, r2=Lminus(r, x)..Lplus(r, x)), x=Ltheta1(r)..Ltheta2(r)):
simplify(int1 + int2);
```

```
     3          2         3
2/3 R  - 1/2 r R  + 1/24 r
```

[‡] Maple 17. Maplesoft, a division of Waterloo Maple Inc., Waterloo, Ontario.

Listing F.3: Integration of eq. (5.29) on page 71.

```
interface(showassumed=0):
assume(R >= 0, r > 0, 2 * R^2 - r^2 <= 0):

Ltheta1 := r -> -r / (2 * R):
Lminus := (r, x) -> -r * x - sqrt(R^2 + r^2 * (x^2 - 1)):

int1 := int(int(r2^2, r2=Lminus(r, x)..R), x=-1..Ltheta1(r)):
simplify(int1);
```

```
     3         3          2
2/3 R  + 1/24 r  - 1/2 r R
```

Listing F.4: Integration of eq. (5.33) on page 71.

```
with(VectorCalculus):

S := Sphere(<0, 0, 0>, R):

int(int(1, [x1, y1, z1]=S), [x2, y2, z2]=S);
int(int((x1-x2)^2 + (y1-y2)^2 + (z1-z2)^2, [x1, y1, z1]=S), [x2, y2, z2]=S);
```

```
     2  6
16 Pi  R
---------
    9

     2  8
32 Pi  R
---------
   15
```

Listing F.5: Integration of eq. (5.43) on page 74.

```
int(1/sqrt(r^2 - x^2 - y^2), y=0..sqrt(r^2 - x^2), x=0..r);
int(1/sqrt(r^2 - x^2 - y^2), y=0..sqrt(r^2 - x^2), x=sqrt(r^2 - M^2)..M);
```

```
Pi r
----
 2

           2    2 1/2
Pi (M - (-M  + r )   )
----------------------
          2
```

Listing F.6: Integration of eq. (5.44) on page 74.

```
interface(showassumed=0):
assume(A >= 0, A >= y, B >= 0, M >= 0):

int(1/sqrt(A^2 - y^2), y=B..M);
```

```
-arcsin(B/A) + arcsin(M/A)
```

Listing F.7: Integration of eq. (5.56) on page 76.

```
interface(showassumed=0):
assume(r >= 0, M >= 0, r >= sqrt(2) * M):

simplify(int(arcsin(x/sqrt(r^2 - x^2)), x=0..M));
simplify(int(-arcsin(sqrt(r^2 - 2 * x^2)/sqrt(r^2 - x^2)), x=0..M));
```

```
                                                   2    2 1/2
               M          r Pi                (-2 M  + r )    r
M arcsin(-------------) - ---- + 1/2 r arctan(-----------------)
            2    2 1/2     4                         2
         (-M  + r )                                 M

                       2    2 1/2                      2    2 1/2
  r Pi            (-2 M  + r )                    (-2 M  + r )    r
- ---- - M arcsin(---------------) + 1/2 r arctan(-----------------)
   4                  2    2 1/2                          2
                   (-M  + r )                            M
```

Listing F.8: Integration of eq. (5.64) on page 77.

```
with(VectorCalculus):

P := Parallelepiped(-L/2..L/2, -L/2..L/2, -L/2..L/2):

L^3 * int(1, [x, y, z]=P);
L^3 * int(x^2 + y^2 + z^2, [x, y, z]=P);

L := 42:

L^3 * int(1, [x, y, z]=P);
L^3 * int(x^2 + y^2 + z^2, [x, y, z]=P);
evalf(L^3 * int(exp(-(x^2 + y^2 + z^2)), [x, y, z]=P));
```

```
 6
L

  8
 L
----
 4

5489031744

2420662999104

412546.2847
```

References

[AT10] V. Ambegaokar and M. Troyer, "Estimating errors reliably in Monte Carlo simulations of the Ehrenfest model", American Journal of Physics **78**, 150–157 (2010) `10.1119/1.3247985`.

[AT89] M. P. Allen and D. J. Tildesley, *Computer simulation of liquids* (Oxford University Press, 1989), ISBN: 0-19-855645-4.

[Bal07] S. Balibar, "The discovery of superfluidity", Journal of Low Temperature Physics **146**, 441–470 (2007) `10.1007/s10909-006-9276-7`.

[BP07] G. Bussi and M. Parrinello, "Accurate sampling using Langevin dynamics", Physical Review E **75**, 056707 (2007) `10.1103/PhysRevE.75.056707`.

[BPS06] M. Boninsegni, N. Prokof'ev, and B. Svistunov, "Worm algorithm and diagrammatic Monte Carlo: a new approach to continuous-space path integral Monte Carlo simulations", Physical Review E **74**, 036701 (2006) `10.1103/PhysRevE.74.036701`.

[Cep95] D. M. Ceperley, "Path integrals in the theory of condensed helium", Reviews of Modern Physics **67**, 279 (1995) `10.1103/RevModPhys.67.279`.

[Con12] S. J. Constable, "Path integral approaches and graphics processing unit tools for quantum molecular dynamics simulations" (University of Waterloo, 2012), `10012/6866`.

[CPM10] M. Ceriotti, M. Parrinello, T. E. Markland, and D. E. Manolopoulos, "Efficient stochastic thermostatting of path integral molecular dynamics", Journal of Chemical Physics **133**, 124104 (2010) `10.1063/1.3489925`.

[CR08] J. E. Cuervo and P.-N. Roy, "On the solid- and liquidlike nature of quantum clusters in their ground state", Journal of Chemical Physics **128**, 224509 (2008) `10.1063/1.2938369`.

[CSI13] S. Constable, M. Schmidt, C. Ing, T. Zeng, and P.-N. Roy, "Langevin equation path integral ground state", Journal of Physical Chemistry A **117**, 7461–7467 (2013) `10.1021/jp4015178`.

[CW81] D. Chandler and P. G. Wolynes, "Exploiting the isomorphism between quantum theory and classical statistical mechanics of polyatomic fluids", Journal of Chemical Physics **74**, 4078–4095 (1981) `10.1063/1.441588`.

[De05] R. de la Madrid, "The role of the rigged Hilbert space in quantum mechanics", European Journal of Physics **26**, 287 (2005) `10.1088/0143-0807/26/2/008`.

[Dir81] P. A. M. Dirac, *The principles of quantum mechanics* (Oxford University Press, 1981), ISBN: 0-19-852011-5.

[El04] M. E. El-Mikkawy, "On the inverse of a general tridiagonal matrix", Applied Mathematics and Computation **150**, 669–679 (2004) `10.1016/S0096-3003(03)00298-4`.

[EM08] D. J. Evans and G. Morriss, *Statistical mechanics of nonequilibrium liquids* (Cambridge University Press, 2008), ISBN: 978-0-521-85791-8.

[FBK96] E. Fattal, R. Baer, and R. Kosloff, "Phase space approach for optimizing grid representations: the mapped Fourier method", Physical Review E **53**, 1217 (1996) `10.1103/PhysRevE.53.1217`.

[FJ05] M. Frigo and S. G. Johnson, "The design and implementation of FFTW3", Proceedings of the IEEE **93**, 216–231 (2005) `10.1109/JPROC.2004.840301`.

[Fla73] H. Flanders, "Differentiation under the integral sign", American Mathematical Monthly **80**, 615–627 (1973) `10.2307/2319163`.

[FR90] E. Forest and R. D. Ruth, "Fourth-order symplectic integration", Physica D **43**, 105–117 (1990) `10.1016/0167-2789(90)90019-L`.

[GGT00] R. Gelabert, X. Giménez, M. Thoss, H. Wang, and W. H. Miller, "A log-derivative formulation of the prefactor for the semiclassical Herman-Kluk propagator", Journal of Physical Chemistry A **104**, 10321–10327 (2000) `10.1021/jp0012451`.

[Gil92] D. T. Gillespie, *Markov processes: an introduction for physical scientists* (Academic Press, Inc., 1992), ISBN: 0-12-283955-2.

[GL00] S. Garashchuk and J. C. Light, "Simplified calculation of the stability matrix for semiclassical propagation", Journal of Chemical Physics **113**, 9390–9392 (2000) `10.1063/1.1321032`.

[GST00] S. Grebenev, B. Sartakov, J. P. Toennies, and A. F. Vilesov, "Evidence for superfluidity in para-hydrogen clusters inside helium-4 droplets at 0.15 kelvin", Science **289**, 1532–1535 (2000) `10.1126/science.289.5484.1532`.

[GTV98] S. Grebenev, J. P. Toennies, and A. F. Vilesov, "Superfluidity within a small helium-4 cluster: the microscopic Andronikashvili experiment", Science **279**, 2083–2086 (1998) `10.1126/science.279.5359.2083`.

[GZ04] C. Gardiner and P. Zoller, *Quantum noise: a handbook of Markovian and non-Markovian quantum stochastic methods with applications to quantum optics* (Springer, 2000), ISBN: 3-540-66571-4.

[HGK10] M. B. Hastings, I. González, A. B. Kallin, and R. G. Melko, "Measuring Renyi entanglement entropy in quantum Monte Carlo simulations", Physical Review Letters **104**, 157201 (2010) `10.1103/PhysRevLett.104.157201`.

[Hin00] K. Hinsen, "The molecular modeling toolkit: a new approach to molecular simulations", Journal of Computational Chemistry **21**, 79–85 (2000).

[HIR14] C. M. Herdman, S. Inglis, P.-N. Roy, R. Melko, and A. Del Maestro, "Path-integral Monte Carlo method for Rényi entanglement entropies", Physical Review E **90**, 013308 (2014) `10.1103/PhysRevE.90.013308`.

[HRD14] C. M. Herdman, A. Rommal, and A. Del Maestro, "Quantum Monte Carlo measurement of the chemical potential of ^{4}He", Physical Review B **89**, 224502 (2014) `10.1103/PhysRevB.89.224502`.

[HRM14] C. M. Herdman, P.-N. Roy, R. G. Melko, and A. Del Maestro, “Particle entanglement in continuum many-body systems via quantum Monte Carlo”, Physical Review B **89**, 140501 (2014) `10.1103/PhysRevB.89.140501`.

[IR07] B. B. Issack and P.-N. Roy, “Semiclassical initial value representation treatment of a hydrogen bonded complex of rigid water molecules from a single trajectory in Cartesian coordinates”, Journal of Chemical Physics **127**, 144306 (2007) `10.1063/1.2786456`.

[KSU03] H. Karner, J. Schneid, and C. W. Ueberhuber, “Spectral decomposition of real circulant matrices”, Linear Algebra and Its Applications **367**, 301–311 (2003) `10.1016/S0024-3795(02)00664-X`.

[Kub66] R. Kubo, “The fluctuation-dissipation theorem”, Reports on Progress in Physics **29**, 255 (1966) `10.1088/0034-4885/29/1/306`.

[Kwo02] Y. K. Kwok, *Applied complex variables for scientists and engineers* (Cambridge University Press, 2002), ISBN: 0-521-00462-4.

[LLR10] H. Li, R. J. Le Roy, P.-N. Roy, and A. McKellar, “A molecular superfluid: non-classical rotations in doped *para*-hydrogen clusters”, Physical Review Letters **105**, 133401 (2010) `10.1103/PhysRevLett.105.133401`.

[McQ76] D. A. McQuarrie, *Statistical mechanics* (Harper & Row, 1976), ISBN: 06-044366-9.

[Mes99] A. Messiah, *Quantum mechanics, two volumes bound as one* (Dover Publications, Inc., 1999), ISBN: 0-486-40924-4.

[Mil02] W. H. Miller, “An alternate derivation of the Herman–Kluk (coherent state) semiclassical initial value representation of the time evolution operator”, Molecular Physics **100**, 397–400 (2002) `10.1080/00268970110069029`.

[PST98] N. Prokof’ev, B. Svistunov, and I. Tupitsyn, ““Worm” algorithm in quantum Monte Carlo simulations”, Physics Letters A **238**, 253–257 (1998) `10.1016/S0375-9601(97)00957-2`.

[PTV92] W. H. Press, S. A. Teukolsky, W. T. Vetterling, and B. P. Flannery, *Numerical recipes in C* (Cambridge University Press, 1992), ISBN: 0-521-43108-5.

[Ren61] A. Rényi, “On measures of entropy and information”, in Fourth Berkeley symposium on mathematical statistics and probability (1961), pp. 547–561.

[Ris84] H. Risken, *Fokker-Planck equation* (Springer, 1984), ISBN: 3-540-13098-5.

[RJL12] P. Raston, W. Jäger, H. Li, R. Le Roy, and P.-N. Roy, “Persistent molecular superfluid response in doped para-hydrogen clusters”, Physical Review Letters **108**, 253402 (2012) `10.1103/PhysRevLett.108.253402`.

[Sak85] J. J. Sakurai, *Modern quantum physics* (Benjamin/Cummings Publishing Company, Inc., 1985), ISBN: 0-8053-7501-5.

[Sch95] B. Schumacher, “Quantum coding”, Physical Review A **51**, 2738 (1995) `10.1103/PhysRevA.51.2738`.

[Sch96] L. S. Schulman, *Techniques and applications of path integration* (Wiley-Interscience, 1996), ISBN: 0-471-16610-3.

[SCI14] M. Schmidt, S. Constable, C. Ing, and P.-N. Roy, “Inclusion of trial functions in the Langevin equation path integral ground state method: application to parahydrogen clusters and their isotopologues”, Journal of Chemical Physics **140**, 234101 (2014) `10.1063/1.4882184`.

[SCK91] P. Sindzingre, D. M. Ceperley, and M. L. Klein, “Superfluidity in clusters of p-H_2 molecules”, Physical Review Letters **67**, 1871 (1991) `10.1103/PhysRevLett.67.1871`.

[Sha48] C. E. Shannon, “A mathematical theory of communication”, Bell System Technical Journal **27**, 379–423, 623–656 (1948) `10.1002/j.1538-7305.1948.tb01338.x`.

[SHK11] R. R. Singh, M. B. Hastings, A. B. Kallin, and R. G. Melko, “Finite-temperature critical behavior of mutual information”, Physical Review Letters **106**, 135701 (2011) `10.1103/PhysRevLett.106.135701`.

[SL95] K. Schmidt and M. A. Lee, “High-accuracy Trotter-formula method for path integrals”, Physical Review E **51**, 5495 (1995) `10.1103/PhysRevE.51.5495`.

[Slo91] A. Slomson, *Introduction to combinatorics* (Chapman and Hall, 1991), ISBN: 0-412-35360-1.

[SMP12] J.-M. Stéphan, G. Misguich, and V. Pasquier, “Rényi entanglement entropies in quantum dimer models: from criticality to topological order”, Journal of Statistical Mechanics: Theory and Experiment **2012**, P02003 (2012) `10.1088/1742-5468/2012/02/P02003`.

[SSM00] A. Sarsa, K. Schmidt, and W. Magro, “A path integral ground state method”, Journal of Chemical Physics **113**, 1366–1371 (2000) `10.1063/1.481926`.

[Ste08] J. Stewart, *Calculus: early transcendentals*, 6th ed. (Thomson Brooks/Cole, 2008), ISBN: 978-0-495-01166-8.

[TBM92] M. Tuckerman, B. J. Berne, and G. J. Martyna, “Reversible multiple time scale molecular dynamics”, Journal of Chemical Physics **97**, 1990–2001 (1992) `10.1063/1.463137`.

[Tuc10] M. Tuckerman, *Statistical mechanics: theory and molecular simulation* (Oxford University Press, 2010), ISBN: 978-0-19-852526-4.

[TWM01] M. Thoss, H. Wang, and W. H. Miller, “Generalized forward–backward initial value representation for the calculation of correlation functions in complex systems”, Journal of Chemical Physics **114**, 9220–9235 (2001) `10.1063/1.1359242`.

[VCV11] S. van der Walt, S. C. Colbert, and G. Varoquaux, “The NumPy array: a structure for efficient numerical computation”, Computing in Science & Engineering **13**, 22–30 (2011) `10.1109/MCSE.2011.37`.

[VPR97] V. Vedral, M. B. Plenio, M. A. Rippin, and P. L. Knight, “Quantifying entanglement”, Physical Review Letters **78**, 2275–2279 (1997) `10.1103/PhysRevLett.78.2275`.

[Wil13] M. Wilde, *Quantum information theory* (Cambridge University Press, 2013), ISBN: 978-1-107-03425-9.

[ZGC13] T. Zeng, G. Guillon, J. T. Cantin, and P.-N. Roy, “Probing the superfluid response of *para*-hydrogen with a sulfur dioxide dopant”, Journal of Physical Chemistry Letters **4**, 2391–2396 (2013) `10.1021/jz401188j`.

[ZLR12] T. Zeng, H. Li, and P.-N. Roy, “Simulating asymmetric top impurities in superfluid clusters: a *para*-water dopant in *para*-hydrogen”, Journal of Physical Chemistry Letters **4**, 18–22 (2012) `10.1021/jz3017705`.

[Zwa01] R. Zwanzig, *Nonequilibrium statistical mechanics* (Oxford University Press, 2001), ISBN: 0-19-514018-4.